Modelling Water and Solute Transport in *Chara*: A Numerical Study of the Effects of Unstirred Layers on Membrane Parameter Estimation

Sharon Koh, B.A/B.Sc (Hons)

Submitted in fulfillment of the requirements for the degree of Doctor of Philosophy

School of Mathematics and Physics
The University of Tasmania

May, 2008

Declarations

This thesis contains no material that has been accepted for a degree or diploma by the University of Tasmania or any other institution. To the best of my knowledge and belief this thesis contains no material previously published or written by another person except where due acknowledgement is made in the text of the thesis.

Sharon Koh

This thesis may be made available for loan and limited copying in accordance with the Copyright Act 1968.

Sharon Koh

Abstract

The cell pressure probe (CPP) is an apparatus used to measure membrane parameters of cells, namely the hydraulic conductivity which indicates the permeability of the membrane to water, the permeability coefficient which indicates the permeability of the membrane to solutes, and the reflection coefficient which indicates the extent to which water and solute transport across the membrane is coupled. This thesis is a numerical exploration of the impact of unstirred layers on the measurement of these parameters. Unstirred layers alter the effective concentration across the membrane, and hence influence the calculation of the membrane parameters which are usually obtained using the concentration value in the external bulk solution and assume a homogeneous internal cell solution.

In CPP experiments, cell pressure dynamics are changed by imposing either: a) a hydrostatic perturbation, where cell sap is injected into or removed from the cell, or b) an osmotic perturbation, where permeable solutes are added to or removed from the external solution. Outputs are pressure-time curves which are termed relaxation curves.

Much of the CPP data has been obtained for *Chara*, a large-celled algae. The model developed here will be applied to two sets of *Chara* data: one previously published, and one unpublished and obtained from collaborators who freely contributed their data to this study. Data from two types of CPP experiments were used to estimate membrane parameters by fitting both the classical and unstirred layer (UL) models. These were: hydrostatic pressure pulse experiments, and osmotic pressure pulse experiments using permeable solutes.

This thesis comprises five chapters. Chapter 1 provides an introduction to the research area, and gives an overview of the cell system, CPP experiments, and membrane transport theory. In Chapter 2 an analysis of predictions and limitations using the classical (i.e. usual) method of parameter estimation is made by applying it to published data. This classical model makes simple assumptions about the system,

allows analytical solutions to the membrane transport equations, and does not include unstirred layers. In Chapter 3, a model based upon the classical model but incorporating unstirred layers, is outlined and its behaviour and predictions examined. In Chapter 4, the unstirred layer model is applied to unpublished CPP data, its predictions compared with those from the classical model, and the overall predictions and behaviour of the unstirred layer model evaluated. Finally, in Chapter 5 an assessment of usual practices and assumptions made in the parameter estimation process using the CPP is carried out, and recommendations for future research are given.

The UL model was found to reproduce the observed CPP data to a high degree of accuracy, and reproduced subtle details in the observed data better than the classical model. Estimated parameters from the two models differed significantly; the relative difference in the parameters with respect to the UL model was up to 50% for osmotic experiments and 5% for hydrostatic experiments. This shows that unstirred layers have a significant impact on estimated parameters, and that the membrane parameters commonly estimated using the classical model may be in error by up to 50%.

Data from three *Chara* cells were fit in Chapter 4. Significant inter-cell variation in estimated parameters was found. Estimated parameters for experiments carried out within the same cell were quite consistent, indicating that the UL model is predicting the membrane parameters well since parameters are expected to characterise a cell and its membrane. The behaviour of the UL model was also consistent with expectations from the Kedem and Katchalsky theory for membrane transport, suggesting that the UL model affects the estimated membrane parameters but not the overall behaviour predicted by the membrane transport equations.

Cell pressure dynamics were found to be very sensitive to the thickness of the unstirred layers in the system, so that estimated membrane parameters are dependent on knowledge of the UL thicknesses. In Chapter 4, the UL model was used to estimate the external UL thickness together with the membrane parameters, while the internal UL thickness was fixed at a value effectively equivalent to assuming the whole cell interior is a UL. The model estimated the external UL thickness to be in the range of 30-50 μm for fits to the unpublished data. Some variation in estimated

parameters between types of CPP experiments (e.g. hydrostatic or osmotic experiments; experiments with positive or negative pressure perturbations) were found, but the sample size was not sufficiently large for definite conclusions to be made. The UL model did not predict polarity in the membrane parameters (i.e. differences in parameters between positive and negative pressure perturbations). This suggests that evidence of polarity found in the parameters is likely due to effects of a composite membrane (e.g. presence of a tonoplast) or of dehydration of the membrane, and not due to the presence of ULs.

Data were also available from osmotic experiments where bubbles were used to separate the new and old external solutions during the solution changeover. Fits to experiments where bubbles are present were found to be more straightforward and to give more accurate estimates of membrane parameters, as the time for solution exchange was significantly shortened. Where bubbles were not present, the time for solution exchange could not be as effectively incorporated into the model due to lack of experimental data regarding the duration and shape of the solution changeover.

Results clearly showed that some common assumptions regarding the effects of ULs on CPP experiments are incorrect. External ULs are often assumed to primarily influence only the first few seconds of the relaxation curve, but the UL model shows that internal and external ULs influence the cell dynamics throughout the entire course of a CPP experiment. Furthermore, the extent of the influence on ULs on CPP data can only be quantified numerically. Previous attempts at using solutions to steady-state diffusion equations, or using steady-state equations relating permeability across the membrane to permeability in the ULs to predict the impact of ULs on estimated membrane parameters, are shown to be inaccurate. Published estimates of membrane parameters for *Chara* are deemed to be in error, because even where effects of ULs have been claimed to be taken into account, this has not been done numerically. In addition, it is shown that relaxation curves can be fit using the classical model (which does not incorporate ULs) despite the presence of unstirred layers, because ULs do not change the fundamental shape of the relaxation curves, and therefore the true effects of ULs are hidden.

It is recommended that the classical model no longer be used for parameter estimation, and a more realistic model incorporating ULs be applied. This will lead to a more accurate estimation of membrane parameters. The model developed in this thesis, by taking into account effects of unstirred layers, can help to resolve the extent to which ULs impact on estimated membrane parameters, and also the extent to which ULs influence parameter variation among different types of experiments or experimental conditions. Currently, further experimental data is necessary for a wider application of the UL model and fuller assessment of its predictions. The UL model may also be extended in the future for application to more complicated systems such as root tissues.

Acknowledgements

I sincerely thank the following people for their valued contributions to this thesis:

Dr. Peter Sands, my supervisor (CSIRO Forestry), for providing continual guidance and support, for discussions regarding aspects of the thesis, and for thorough reviewing of all chapters, even after retirement. I acknowledge his valuable contribution in writing the Excel programs used to evaluate some model results;

Prof. Mel Tyree, my associate supervisor (USDA Forest Service), for providing expertise in this topic, for guidance in the modelling approach and numerical algorithms, for providing experimental data, for his support and the opportunity to work with him in the U.S.A;

Prof. Larry Forbes, my academic supervisor (University of Tasmania), for providing assistance in the applied mathematics and modelling approaches, his financial assistance for my trip to the U.S.A and Matlab maintenance license, and for his general support throughout my candidature;

Dr. Helen Bramley (University of Adelaide) for providing experimental data and assistance with the experimental knowledge required for this thesis;

Dr. Tobias Henzler (Beyreuth University), for providing the raw data for Chapter 2;

Dr. Chris Beadle (CSIRO Forestry - Ensis), for providing personal support and financial assistance throughout my candidature;

Dr. Des Fitzgerald (University of Tasmania) for his help with the statistics and data analyses, and people at Matlab support, who helped me with the Matlab code;

Judy Sprent (CSIRO Forestry) who obtained references for me, Jean Richmond (CRC-SPF), Dr. Marie Yee (University of Tasmania), Brynne Lazarus (University of Vermont, USDA Forest Service) for personal support and friendship, Kelly Baggett (USDA Forest Service) for helping me move and settle into Vermont.

This project was funded by a CRC-Sustainable Production Forestry scholarship. Additional funding was provided by the Wilf Crane Award for the trip to the U.S.A to work with Prof. Mel Tyree.

Table of Contents

1 Introduction

1.1 Background to membrane transport parameters

Understanding cell membrane transport properties is central to our understanding of water and pressure dynamics in cells and entire organisms. Physical properties of cell membranes and walls can be described by parameters such as hydraulic conductivity and solute permeability, which describe the extent to which water and solutes permeate the cell membrane. These parameters govern the passive transport of water and solutes into and out of cells, and thus control changes in cell pressure and volume. Solutes also cross membranes via active transport of ions, however active transport is beyond the scope of this study.

Determining and characterising membrane transport parameters, and understanding what factors affect and influence them, aids in our understanding of how cells regulate the transport of water and solutes into and out of their system, and how these dynamics may be affected by changes in their environment. Understanding how a plant or animal cell grows and interacts with its surroundings is fundamental to our understanding of biology and all living organisms.

An accurate measurement of membrane transport parameters has, however, proven difficult. Most of this research in plant cells has been carried out on *Chara,* a large-celled pond water algae with typical length 30-130 mm and diameter 0.7-1 mm (Hertel and Steudle, 1997). Membrane parameters in giant algal cells were originally determined using intracellular perfusion and transcellular osmosis techniques, which were developed in the 1950's (Zimmermann and Steudle, 1978). Today, most current techniques for measuring cell pressure and volume are either pressure relaxation or pressure clamp methods (Ortega, 1993). In the former the volume is held constant while the cell pressure change is measured, in the latter the pressure is held constant while changes in cell volume are measured. Pressure relaxation experiments yield a plot of pressure with time,

while the pressure clamp yields a plot of sap volume in the pipette with time (Murphy and Smith, 1998).

The cell pressure probe (CPP) is an instrument designed to measure hydrostatic pressure (turgor pressure) in cells. It uses a pressure relaxation technique which was developed in the 1970's to determine membrane transport parameters (hydraulic conductivity, solute permeability, and reflection coefficient) and elasticities of plant cell walls (Steudle and Zimmermann, 1974; Hüsken *et al*. 1978; Steudle and Tyerman, 1983; Steudle *et al.* 1987; Steudle, 1993; Henzler and Steudle, 1995; Ye *et al.* 2004). A related technique, the root pressure probe, performs similar experiments on roots and the methods of parameter estimation are also similar to that for the CPP (Steudle, 1994; Steudle, 1993).

The CPP is a widely used technique. However, unstirred layers (ULs) adjacent to the cell wall or membrane have not adequately been taken into account in CPP analyses. The importance of ULs on membrane transport have been well documented (Dainty, 1963; Barry and Diamond, 1984; Kargol, 2000). Consideration of the impact of ULs on membrane parameters in CPP experiments has been more qualitative than quantitative, and calculations have largely been performed by applying transport equations on the basis that the effects of ULs can be considered negligible (Heidecker *et al.* 2003). Therefore, membrane parameters estimated by the CPP may, in fact, not reflect the true membrane parameters of the cells.

Variations in measured membrane parameter values may be due to changes in the system outside the membrane (e.g. effects of ULs, and external concentration levels), changes in the system inside the membrane (effects of ULs, or more than one membrane in the cell affecting the pressure dynamics), or changes in the physical properties of the membrane caused by water and solute flow interaction (Zimmermann and Steudle, 1978; Kiyosawa and Tazawa, 1973; Dainty and Ginzburg, 1964a). Most of these changes are not directly observable by the CPP, and without proper quantitative analysis reasons for observed parameter behaviour and identification of the variables affecting parameter estimation can only be inferred.

The determination of membrane parameters with the CPP is based on a conceptual two-compartment model of the cell, which shall be referred to here as the 'classical model' (Wendler and Zimmermann, 1985a). This views the system as a single membrane separating two compartments, namely the inner and outer regions of the cell. These compartments are sharply defined by the membrane, and are assumed to be homogeneous with uniform solute concentrations, so that a step change in concentration occurs across the membrane. In many plants cells, however, the vacuole occupies a large portion of the interior so that the cell contains two membranes: the plasmalemma and the tonoplast, and three compartments: the external region, the cytoplasm, and the vacuole. The compartments are not homogeneous since ULs are present. The anatomy of a simple cell, such as is exhibited in *Chara*, is illustrated in Fig. 1.1.

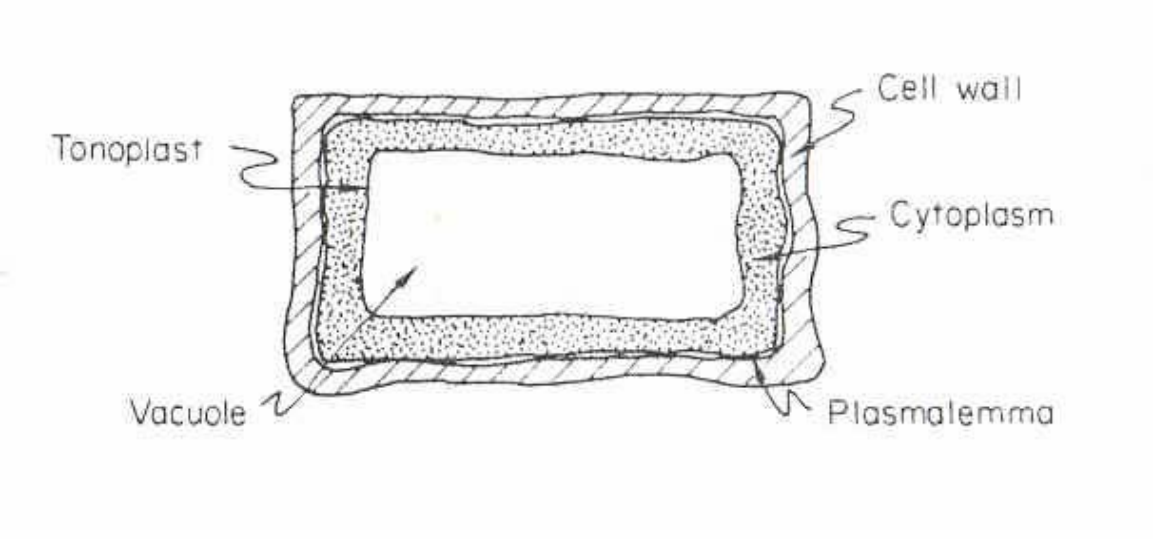

Fig. 1.1 Diagram of a simple cell, showing cell wall, plasmalemma (plasma membrane), cytoplasm, tonoplast and vacuole (Molz and Ferrier, 1982).

Quantitative analysis of CPP experiments based on the classical model uses analytical solutions of the transport equations to estimate the membrane parameters. It is argued here that these analyses are limited by those assumptions in the model required for the development of analytical solutions, and especially the assumption that there are no ULs. Further knowledge can be gained by using process-based numerical models which implement differential equations to explore more complex conceptual models of the

system. To my knowledge no process-based numerical work on the classical model and CPP experiments has been done, prior to Tyree *et al.* (2005). The aim of this study is to develop a more realistic numerical model than the classical model, where the model developed here has non-homogeneous compartments, with ULs adjacent to the membrane. The well-known Kedem-Katchalsky (KK) equations for membrane transport (Kedem and Katchalsky, 1963a,b,c; Katchalsky and Curran, 1967) on which current CPP experimental analyses are based, and diffusional processes in the ULs, will be the foundation for this model. This model will be used to examine the validity of the classical model, by fitting real data with both models and comparing estimated parameters between the two models.

A numerical study of measurements from a CPP experiment and the impact of ULs on these is timely in light of the renewed interest in aquaporin (water channel) research, and research into pathways of water and solute movement. Inhibition of water channel activity and the resulting changes in the membrane parameters in the presence of certain solutes have shown that some solutes pass through water channels and that water channels are less selective than previously thought (Henzler and Steudle, 1995; Hertel and Steudle, 1997; Ye *et al.* 2004). Experimental conclusions and the accuracy with which parameter measurements reflect membrane pathways depend on understanding those factors that may affect parameter measurements. For example, ULs may contribute to low values for the reflection and permeability coefficients (Henzler and Steudle, 1995; Henzler and Steudle, 2000). Hertel and Steudle (1997) and Henzler and Steudle (2000) have considered various possible effects of ULs on their measurements and claimed that the effects of ULs should not be significant. However, Hertel and Steudle (1997) admitted that for conclusive results more precise parameter measurements are required and the effects of ULs should be eliminated, which they added is difficult to carry out experimentally. Numerical models that explore the effects of ULs more fully, therefore, can be an important aid in the interpretation of these experimental results.

Application of the model in this thesis will be limited to data from CPP experiments on *Chara*. *Chara* data is readily available, and the focus of the thesis is on development of the model rather than the model's general application.

However, the model developed in this thesis could be applied to experimental data from other membrane systems to examine the impact of unstirred layers. For example, in stopped flow spectrofluorimetry experiments on wheat root membrane vesicles, carried out to examine the role and function of aquaporins (e.g. Niemietz and Tyerman, 1997), effects of unstirred layers on the estimated parameters are predicted to be small. The model in this thesis could be applied to these data to aid in the examination of the effects of unstirred layers.

The model in this thesis could also be applied to experiments which have tried to estimate the relative permeabilities of the tonoplast and the plasma membrane. Niemietz and Tyerman (1997) measured the hydraulic conductivity of isolated membrane vesicles with and without a plasma membrane, and found that the water permeability of the tonoplast was higher than that of the plasma membrane. Zhang and Tyerman (1999) applied the CPP to intact wheat root cells, and modelled pressure changes using the coupled differential equations by Wendler and Zimmermann (1985) for a double membrane (three-compartment) system. In contrast to Niemietz and Tyerman (1997), they found that the water flow was dominated mostly by flow across the plasma membrane. Application of the model in this thesis to these data could aid in the interpretation of these results, as the CPP experiments are more likely to be affected by unstirred layers.

1.2 Cell Pressure Probe Experiments

The CPP measures the change in cell turgor pressure over time following a perturbation of the cell from an equilibrium state. Turgor pressure is easily measured and is one of the variables that describe the state of a cell. Cell volume also changes with pressure, but by less than 1% of the total cell volume during a typical experiment, as the cell wall is fairly rigid (Henzler and Steudle, 2000).

The CPP (Fig. 1.2) comprises a pressure chamber, at one end of which is a micrometer device attached to a metal rod to adjust pressure in the chamber, and at the other a micropipette which inserts into the cell. The pressure chamber and micropipette contain silicon oil, which transmits cell pressure to the pressure transducer in the middle of the chamber. The transducer consists of a membrane containing a wheatstone bridge which, when the membrane is distorted, converts pressure into a voltage. The cell sits in a separate chamber containing artificial pond water (APW, a nutrient solution comprised of a mixture of impermeant solutes with an osmotic pressure of about 0.01 MPa) (Hüsken *et al.* 1978; Steudle, 1993).

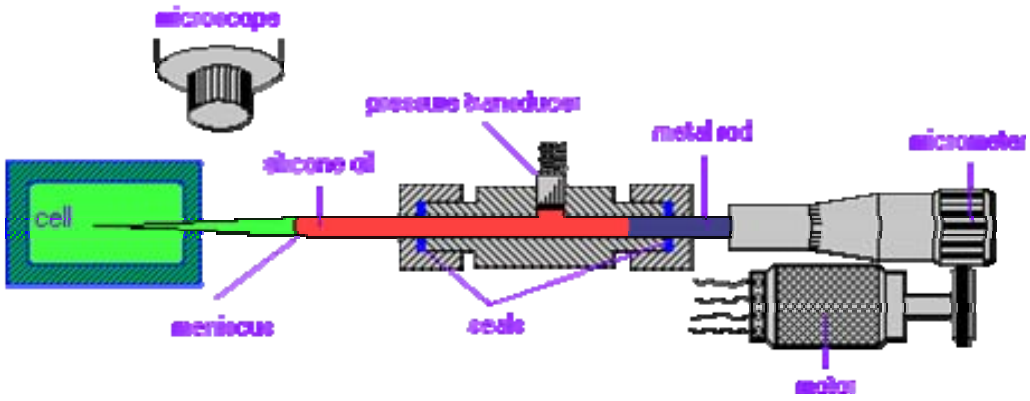

Fig. 1.2 The cell pressure probe (E. Steudle's webpage).

During an experiment the micropipette is pushed into the cell. This causes sap to escape from the cell into the micropipette, from which it is assumed that the tip of the pressure probe is located in the vacuole of the cell (Zhang and Tyerman, 1999). Since the silicon oil is immiscible with water a meniscus forms between the cell sap and the oil. The bathing solution (APW) is kept flowing at a constant rate around the cell, and a constant temperature is usually maintained throughout the experimental procedure.

The experimental procedure is slightly different for small and large cells. Since a slight compressibility of the chamber exists, which is mostly due to the rubber seals and partly

due to the silicon oil, changes in the volume and pressure of small cells are not sufficient to register a pressure in the transducer. Therefore, when measuring pressure changes in small cells, the position of the meniscus is kept fixed during the course of an experiment, and the volume of the chamber changed by adjusting the metal rod via a compensation method. For a large cell, such as *Chara*, the meniscus does not need to be fixed (Hüsken *et al.* 1978; Steudle, 1993; Tomos, 2000).

Two kinds of experiments (perturbations) are performed with the CPP. In a hydrostatic pressure pulse (HPP) experiment cell sap is injected into (a positive pulse) or removed from the cell (a negative pulse) via the micropipette. When the probe is first pushed into the cell some sap escapes into the probe, and so a positive HPP experiment is first performed, followed by a negative HPP experiment, and so on with positive and negative pulses alternating. In an osmotic pressure pulse (OPP) experiment the external concentration is changed via a rapid changeover of bathing solution, where a test solute has been added to (a positive pulse) or omitted from (a negative pulse) the new solution. Only one test solute is used at a time. Positive and negative OPP experiments are usually carried out alternately.

The changeover of bathing solution in an OPP experiment does not occur instantaneously, and it takes a few seconds for the external concentration to reach the maximum perturbation level. The external concentration is said to “ramp up” (or “ramp down”). A more rapid changeover can be made by inserting an air bubble between the solutions, which will be described in more detail in Chapter 4. In the experiments of Henzler *et al.* (2004), whose data is modelled in Chapters 2 and 3, no bubbles were used intentionally during the solution changeover but occasionally bubbles were accidentally present (Tyree, *pers. comm.*; Henzler, *pers. comm.*).

Different solutes with varying permeabilities have been used in CPP experiments. However, those using very slow permeating solutes are less common. Full details of the CPP technique can be found in Hüsken *et al.* (1978), Steudle and Tyerman (1983), and Steudle (1993).

Outputs from the CPP are plots of pressure over time (*P*-*t* curves), termed pressure relaxations, for they chart the behaviour of the cell's return to equilibrium pressure after a perturbation. For both an HPP and for osmotic flows with impermeant solutes, the pressure relaxation is an exponential increase or decrease to a new equilibrium (Fig. 1.3a). The rate of return to equilibrium is described by the halftime, which is inversely proportional to the slope of a suitably log-transformed curve. In theory, the *P*-*t* curve is exponential such that a semilog plot of the *P*-*t* curve will give a straight line, however in reality only part of the curve is exponential and only a portion of the curve is log-transformed (see §2.5.1a). Since some cell sap is added to or removed from the cell, the osmotic pressure and concentration in the cell changes only very slightly following perturbation, but the number of mol of solute changes more. Therefore the final equilibrium pressure will be slightly different from the initial pressure.

For an OPP with permeant solutes, the pressure-time curves are biphasic (Fig. 1.3b). Following perturbation a rapid water flow across the membrane occurs in the 'water phase' bringing the pressure to a maximum or minimum, and thereafter a slow return to equilibrium occurs due to both solute and water crossing the membrane in the 'solute phase'. Two halftimes, that of the water and solute phases, are associated with osmotic flows. In theory, the equilibrium pressure should be equal to the initial pressure, however experimentally this is often not the case. Although one expects that after a positive-negative set of experiments the pressure should also return to its equilibrium value at the start of the set, this is also not always observed.

The halftimes are determined from the relaxation curves, and from these the membrane transport parameters are obtained.

Prior to applying pressure pulses, a separate set of experiments are also carried out to determine the bulk elastic modulus ε of the cell wall, which controls how volume of the cell changes with cell pressure. The parameter ε is directly measurable, in contrast to the membrane parameters, and is required for the determination of these. To measure ε, a few pressure change steps are made in the cell in both positive and negative directions, and

covering the expected range of pressure change in the pressure pulse experiments (Fig. 1.4). This is done by moving the metal rod (Fig. 1.2) by various increments. From the size of each increment and the rod diameter, the corresponding volume change ΔV_{rod} in the pressure chamber can be inferred.

The associated pressure changes of the system (recorded by the pressure transducer) are plotted as a *P*-*V* graph. The slope of the *P*-*V* curve changes with pressure, however as ε is determined using small pressure intervals locally the *P*-*V* curve tends to be linear (Steudle *et al.* 1977). The slope of this line gives ε according to the formula $\Delta P / \Delta V_{rod} = \varepsilon / V_0$ (where V_0 is the volume of the cell at equilibrium). If ΔV_{rod} is the volume change of the pressure chamber, ε combines the elasticity of the cell wall and that of the CPP rubber seals. However, if ΔV_{rod} is the volume swept out by the meniscus during the measurement of ε then ε is that of the cell wall.

In addition to exhibiting a pressure-dependence, ε has been shown to exhibit hysteresis such that the value of ε may differ depending on whether the cell is swelling or shrinking, when measured over the same range of cell osmotic pressure. The cell wall has also been shown to exhibit viscoelastic properties, where the value of ε is not constant over time and the measured value due to an 'instantaneous' volume change (as measured by the CPP) is larger than the 'stationary' value measured following relaxation in the cell. The instantaneous value of ε also depends on the time it takes for the pressure and volume change to be induced (Zimmermann and Hüsken, 1979; Tyerman, 1982).

Electrical noise in the CPP limits the accuracy of pressure measurements for all experiments to around ± 0.0005 MPa (Tyree, unpublished data). The hydraulic conductivity of the probe tip, which is usually high, is temperature dependent due to the dependence of water viscosity on temperature, and the electrical noise can often be related to a lower than ideal conductivity of the probe tip. Some operator error due to vibrations during insertion of the micropipette would also be present, and may cause leaking around the probe tip. However, Zimmermann and Hüsken (1979) found that the

cell forms an effective seal around the tip of the pipette and there is no loss of cell pressure due to leakage during a typically successful experiment. They also found no dependence of L_p and ε measurements on the size of the cell puncture.

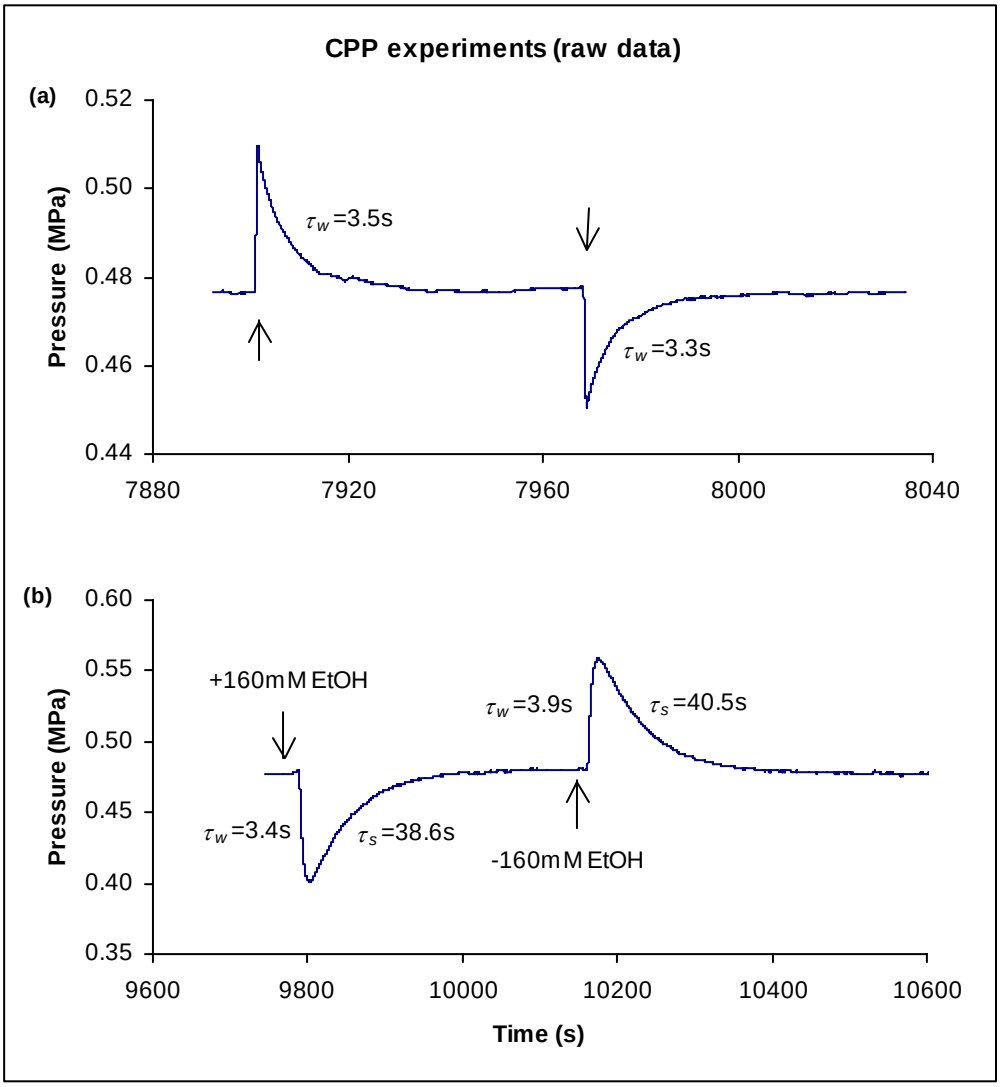

Fig. 1.3 Relaxation curves for (a) a HPP experiment showing halftimes τ_w, and (b) a OPP experiment with permeant solute ethanol showing halftimes τ_w for the water phase and τ_s for the solute phase. Arrows indicate approximate points where a perturbation (a HPP or OPP) is made. Data from Tyree (unpublished).

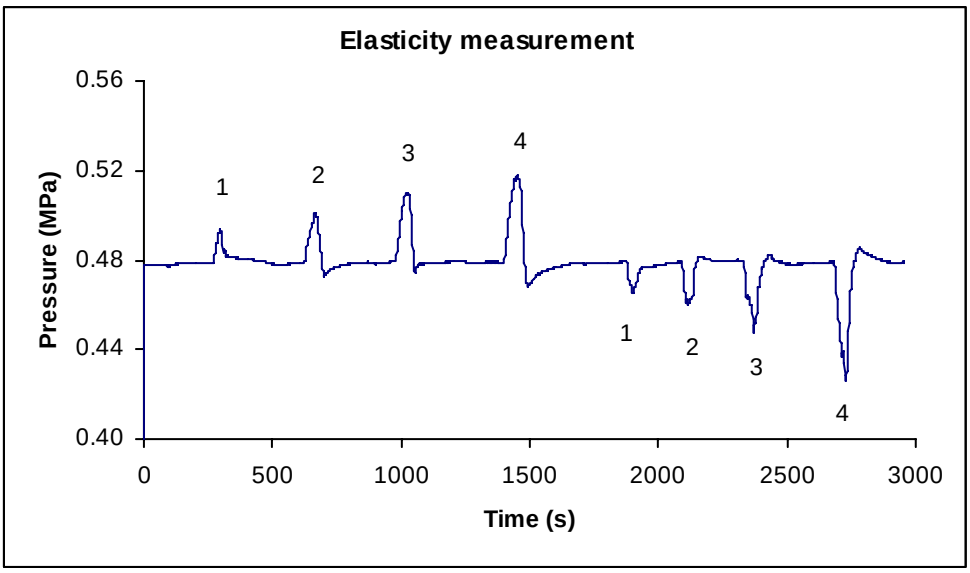

Fig. 1.4 Experimental curves for determining membrane elasticity. In this experiment 4 pressure change steps are taken in each direction. Data from Tyree (unpublished).

1.3 Membrane transport theory

1.3.1 The KK equations

Three main quantities can be used to describe the pressure and water dynamics in a cell: the cell turgor pressure, internal cell volume, and quantity of solutes in the cell. Turgor pressure refers to the hydrostatic pressure difference between the inside and outside of the cell (Zimmermann and Steudle, 1978), and is due to a balance between hydrostatic and osmotic pressure gradients. Flows across the cell membrane can be described by the volume flow (made up of water and some solute flow, and otherwise known as 'bulk' flow), and the solute flow. These flows have been expressed as a pair of coupled differential equations known as the Kedem-Katchalsky or KK equations (Kedem and Katchalsky, 1963). The behaviour of these equations are governed by 3 main membrane parameters, namely: the hydraulic conductivity L_p, reflection coefficient σ, and solute permeability p_s. An additional parameter, the elastic modulus ε, also governs cell wall extensibility. These are discussed further below.

The KK equations describe water and solute flows for a system of two aqueous solutions separated by a homogeneous membrane. They have been one of the main tools in the study of transport across biological and artificial membranes (Kargol, 2001). For passive (non-electrolyte) transport, where the solutions contain impermeant solutes and a single permeating uncharged solute, the KK equations for the volume flux density J_v (m s^{-1}) and solute flux density J_s (mol m^{-2} s^{-1}) are (Dainty, 1963; Kedem and Katchalsky, 1963; Katchalsky and Curran, 1967):

$$J_V = -\frac{1}{A}\frac{dV}{dt} = L_P(\Delta P - \Delta\pi_i - \sigma\Delta\pi_s) \tag{1.1}$$

$$J_s = -\frac{1}{A}\frac{dn_s}{dt} = (1-\sigma)\overline{C}_s J_V + p_s\Delta C_s, \tag{1.2}$$

where n_s = amount of a particular permeant solute in the cell (mol), V = cell volume (m^3), A = cell surface area (m^2), t = time (s), P = hydrostatic pressure (MPa), π = osmotic pressure (MPa) , C_s = solute concentration (mol m^{-3}), $\overline{C_s}$ = mean solute concentration across the membrane (mol m^{-3}), L_p = hydraulic conductivity (m s^{-1} MPa^{-1}), σ = reflection coefficient for a particular solute (dimensionless), p_s = solute permeability (m s^{-1}), and Δ = difference across the membrane. Fluxes are defined as positive for flows out of the cell. The subscripts '*i*' and '*s*' indicate for an impermeant and permeant solute respectively. The equations assume isothermal conditions.

The KK equations describe a linear relationship between forces and flows across a membrane. They describe 4 processes: filtration ($L_p \Delta P$) and osmosis ($L_p \sigma \Delta\pi$) in Eq. (1.1), and convection $(1-\sigma)\overline{C}_s J_V$ and passive diffusion ($p_s \Delta C_s$) in Eq. (1.2) (Kargol and Kargol, 2003). These processes are due to the simultaneous action of pressure and osmotic gradients (forces), and the 3 membrane parameters (i.e. L_p, p_s, σ) govern the behaviour of the volume and solute fluxes (flows) in response to these gradients. It is assumed that the membrane parameters are independent of the driving forces.

The hydraulic conductivity L_p and solute permeability p_s denote how permeable the membrane is to water and solutes respectively. The reflection coefficient σ describes the extent to which permeable solute flow is coupled to bulk water flow, and how much the permeant solutes contribute to the osmotic pressure difference $\Delta\pi$. The convection term is also known as the solvent drag term, because solutes are dragged along with water flow arising from friction between the two. The case σ=1 for a particular solute indicates that the solute cannot significantly permeate the membrane or at most at a rate several orders of magnitude less than water (i.e. the solute is effectively impermeant), and that the solute contributes maximally to osmotic pressure and there is no water-solute coupling. The case σ=0 for a particular solute indicates the solute permeates the membrane as efficiently as water, does not contribute to osmotic pressure, and there is complete water-solute coupling. The solvent drag is usually small, comprising about 2% of total solute flow (Henzler and Steudle, 2000). The value of σ can also be negative, e.g. when solutes are more permeant than water across cell membranes.

Although the membrane parameters are measured independently, experimental data suggests there is some correlation between them. For example, a higher (lower) p_s tends to be related to a lower (higher) σ (Kargol and Kargol, 2000). This is also predicted to be correlated with a lower (higher) L_p by the so-called frictional pore theory (Henzler and Steudle, 1995).

All three membrane parameters are membrane-specific, and values of σ and p_s are also solute-specific. A detailed interpretation of the KK equations can be found in Kedem and Katchalsky (1961), Kargol and Kargol (2000), and Kargol and Kargol (2003).

1.3.2 Non-ideal behaviour of membrane parameters

Application of the KK equations assumes the membrane is ideal, in the sense that the membrane parameters are constant, independent of the driving forces such as pressure and concentration changes, and independent of temperature. However, in reality membranes are not ideal.

Measured values of the membrane parameters change a little with temperature (Barry and Diamond, 1984; Hertel and Steudle, 1997). Attempts are usually made to maintain the CPP apparatus at a constant temperature, and in this study the temperature of the CPP is assumed to be uniform and constant.

Significant changes in L_p with P have been found for low pressures ($P < 0.2$MPa; Zimmermann and Hüsken, 1979; Steudle and Zimmermann, 1974). This should not be an issue here since cell pressures in CPP experiments do not drop below 0.2MPa. Experiments have also found a slight dependence of membrane parameters on pressure and concentration (and hence osmotic pressure) in higher pressure ranges (Dainty and Ginzburg, 1964a,b; Steudle and Zimmermann, 1974; Zimmermann and Steudle, 1974a,b). However, this should also not impact greatly on the estimated parameters here since the osmotic driving force is the same for each experiment, and hydrostatic pressure perturbations involve small pressure changes. A theoretical study of how estimated parameters may be influenced by changes in cell pressure and external concentration will be conducted in Chapter 3.

The dependence of membrane parameters on pressure and concentration may also be due to the fact that we are in reality dealing with a composite membrane (Kedem and Katchalsky, 1963c). A composite membrane is where the membrane system comprises components in series (e.g. there is more than one membrane in the system) or in parallel (e.g. there is more than one pathway in the system). This will be discussed further in §2.1.

1.3.3 Application of the KK equations

The KK equations are based on the principles of ‘irreversible’ or ‘non-equilibrium’ thermodynamics. The system is described in terms of external macroscopic variables, and the equations do not depend on the microscopic structure or internal workings of the membrane (Zemansky and Dittman, 1981; Kargol *et al.* 2005). Direct use of the above equations is confined to two-compartment membrane systems, for flows of solutions

which are sufficiently diluted and well-stirred, and close to steady state (Katchalsky and Curran, 1967; Kargol and Kargol, 2003).

The KK equations, however, have been adapted and applied to a wide range of membrane transport problems. They have been applied to systems in non-steady state, for thermodynamic theory assumes ideal quasi-static processes where “the system is at all times infinitesimally near a state of thermodynamic equilibrium”, which does not mean the processes must necessarily be in steady state (Zemansky and Dittman, 1981). The equations have been adapted and generalised for systems where unstirred layers are considered to be additional compartments (Kargol, 2000).

More interestingly, the equations have been applied to porous membranes, for although the KK equations treat the membrane as a black box, the transport coefficients can nevertheless provide information about the membrane porous structure (Kargol, 2001; Kargol *et al.* 2005). In the formulation by Kargol *et al.* (2005), J_V is the volume flow per unit effective area of the pores, L_p depends on the ratio of the membrane surface area to the total effective area of the pores, σ is related to the ratio of the total cross-sectional area of the semi-permeable pores (for which σ=1, i.e. permeable only to water) to the total cross-sectional area of the permeable pores (for which σ=0), and p_s is expressed in terms of L_p and σ. Lipid-pore models involving frictional coefficients between solutes and water in the pores have also been developed (Kedem and Katchalsky, 1961; Dainty and Ginzburg, 1963).

1.4 Aims and motivation

The principal aims of this study are to develop a more realistic model of membrane transport which incorporates ULs, and use this model to examine the classical model and its associated method for estimating membrane parameters. The study is based on numerical models developed from established membrane transport theory. This theory also forms the backbone of the classical CPP model and experimental analyses. Raw data

provided by experimentalists, as well as data taken from the literature, are used for analysing the models.

In this study, models of water and solute transport into and out of a *Chara* cell are formulated as coupled differential equations, and solved numerically using Matlab (Version 7, MathWorks, Inc.). Model behaviour is explored, including the relative effects of internal and external ULs, and different UL thicknesses, on cell water relations and parameter calculations. Model predictions are also analysed, in particular how well the models fit the data, and what they estimate the membrane parameters to be. Model behaviours, predictions, and limitations are compared, in particular to assess the adequacy of current CPP methods to draw conclusive statements about membrane parameters when ULs may be present.

Motivation for this study includes the following questions: Does a more comprehensive model give a better fit to data than the classical model? What are the implications for current methods of parameter determination and experimental analyses based on the classical model? Are there alternative methods of parameter estimation?

In Chapter 2, the classical model is described and applied to data using an analytical solution for the pressure relaxation, and its behaviour and predictions are analysed. Chapter 3 gives the theory of and background to ULs, reviews previous numerical models with and without ULs, describes the new model developed in this study and outlines its numerical implementation, applies the new model to data, and compares its behaviour and predictions to that of the classical model. Chapter 4 builds on Chapter 3 by applying the UL model to recently obtained data by Prof. Mel Tyree and Dr. Helen Bramley at Adelaide University. The applicaton and analysis take into consideration sampling error, and include further information regarding the time of impact of the pressure perturbation. Chapter 5 concludes the findings of this study, discusses the implications of these on parameter estimation using the CPP and the conduct of CPP experiments, and gives various recommendations for further research.

2 Classical model

2.1 Scope and assumptions of the model

2.1.1 Assumption of single membrane

The Classical two-compartment cell model outlined in §1.1, with a single membrane, is the simplest possible model for a cell. The advantage of this simple conception is that it allows transport equations to be easily applied to the membrane, and since these equations are based on thermodynamic processes the internal structure of the membrane can be ignored. However, the cell is actually a "composite membrane", that is a system comprised of an array of membranes either in series or parallel (Kedem and Katchalsky, 1963b,c). The two membranes in series are the tonoplast surrounding the vacuole, and the plasmalemma at the cell wall (see Fig 1.1). With the exception of the studies by Wendler and Zimmermann (1985a,b), Niemietz and Tyerman (1997) and Zhang and Tyerman (1999), quantitative effects of the tonoplast and plasmalemma on CPP experiments seem to have largely been ignored, and the classical model makes no provision for composite membrane effects.

Within the framework of the Classical model, the tonoplast and plasmalemma are treated as a single membrane, and the measured parameters can be regarded as those of the combined membranes (Heidecker *et al.* 2003). However, a problem with this interpretation is that the KK equations would be applying across both membranes, implying there must be a pressure difference across both membranes which is not possible, since a hydrostatic pressure difference cannot occur across the tonoplast (Wendler and Zimmermann, 1985a). This is due to the fact that a membrane has no mechanical strength, the pressure difference across the plasmalemma being due to the presence of the cell wall, which supports the plasmalemma which is pushed against it during nonzero turgor pressures. The two-compartment model, then, can only work if the

tonoplast has very little effect on the pressure dynamics observed by the CPP, i.e. if it has a low resistance and high permeability to water and solute flow (*ibid.* 1985a).

Properties of the tonoplast, however, have been difficult to determine. Kiyosawa and Tazawa (1973) removed the tonoplast of *Chara* cells, and concluded that the tonoplast is much more permeable to water than the plasmalemma. This finding is supported by Niemietz and Tyerman (1997) and Henzler and Steudle (2000). However, Wendler and Zimmermann's (1985a,b) theoretical study of the effects of the tonoplast on CPP experiments found that the relative hydraulic conductivities of the tonoplast and plasmalemma differed depending on the pressure range, and concluded that the tonoplast L_p is not large enough that its influence on relaxation curves can be neglected. Generally, parameter estimation methods in CPP experiments (with the exception of Zhang and Tyerman, 1999) do not explicitly take effects of the tonoplast into account, but simply neglect the influence of the tonoplast on the hydraulic conductivity and account for only the plasmalemma component in the analysis.

Other regions in the cell are not considered significant sites of resistance. Although the cell wall in large algal cells is also a barrier to water and solute movement, studies indicate that it has a higher hydraulic conductivity than the plasmalemma (Kiyosawa and Tazawa, 1977). Since the two components can't be separated experimentally, measured properties of the plasmalemma may be considered properties of the plasmalemma/ cell wall complex (Wendler and Zimmermann, 1985b). The cytoplasm, a solution of salts, carbohydrates and proteins, has an osmotic concentration of about 250mM, and a relatively high hydraulic conductivity (Wendler and Zimmermann, 1985a; Raven *et al.*, 1992; Tyree, *pers. comm.*). It moves slowly around the cell at a rate of about 4cm/hour (Tyree *et al.* 1974) in "cytoplasmic streaming". The vacuole typically occupies about 90% of the cell volume in a mature cell and contains a solution of the same osmolality as the cytoplasm (since the tonoplast cannot support a pressure difference), but is richer in salts and poorer in organic solutes (Raven *et al.* 1992).

Although the numerical model developed in this thesis is limited to a two-compartment model based on the *Chara* cell, this conceptual model is relevant to other cell systems and the numerical model can certainly be applied to other cell systems (see §1.1).

2.1.2 Other assumptions

The *Chara* cell is assumed to exhibit cylindrical symmetry, and the flow across the membrane to be in the radial direction only. The cell is assumed to contain impermeant (i.e. non-permeating) solutes only (Tyerman and Steudle, 1982). Although a cell contains both permeant and impermeant solutes (solutes are continually being exchanged with the environment), the permeability of test solutes are usually much higher than those of the natural internal cell solutes so that these can be considered effectively impermeant. Artificial pond water (APW) outside the cell is assumed to have a pressure equal to atmospheric pressure. The volume external to the cell is considered to be of infinite size in relation to the cell volume, and so for all intents and purposes the external region is unchanging. The solute concentrations on either side of the membrane are assumed to be uniform with space, and unstirred layers and influence of the expanding/ contracting membrane on adjacent solute concentrations are assumed to be absent. The temperature of the whole system is assumed to be uniform and constant.

The cell is assumed to be at equilibrium (i.e. $J_v = 0$, $J_s = 0$) for $t<t_0$. At $t= t_0$ a hydrostatic or osmotic perturbation to the system is made. The perturbations are assumed to impact on the cell instantaneously.

2.2 Transport equations and their solution

2.2.1 Transport equations

The KK equations Eqs. (1.1) & (1.2) can be written in the more detailed form (assuming the external solution is at atmospheric pressure):

$$J_V = -\frac{1}{A}\frac{dV}{dt} = L_P[P - R_gT(C_i - C_{ie}) - \sigma R_gT(C_s - C_{se})] \quad (2.1)$$

$$J_s = -\frac{1}{A}\frac{dn_s}{dt} = (1-\sigma)\overline{C}_s J_V + p_s(C_s - C_{se}), \quad (2.2)$$

where the subscripts '*i*' denote impermeant solutes, '*s*' permeant solutes, and '*e*' external to the cell (Steudle and Tyerman, 1983). Eq. (2.1) uses the Van't Hoff equation for ideal dilute solutions (Katchalsky and Curran, 1967):

$$\pi = qCR_gT, \quad (2.3)$$

where π = osmotic pressure, R_g = universal gas constant (8.3144 x 10^{-6} m^3 MPa mol^{-1} K^{-1}), T = temperature (K), and q = sum of cation and anion valencies of a completely dissociated salt (Dalton *et al.*, 1975), which is assumed to behave ideally. For non-electrolytes (which we are assuming here) q = 1. Note also that $C = n/V$, where n is the molar quantity of solutes in the cell.

For a full description of passive membrane transport, further expressions for π and P (the internal hydrostatic or turgor pressure of the cell) are required. The number of mol of impermeant solutes inside the cell remain a constant so that:

$$\pi_i = \frac{\pi_{i0}V_0}{V}. \quad (2.4)$$

The rate of change of cell volume with respect to a change in turgor pressure P is described by the bulk elastic modulus ε (Dainty, 1963), given by:

$$\frac{dP}{dV} = \frac{\varepsilon}{V}. \quad (2.5)$$

In Eq. (2.5) it is often assumed that $V=V_0$, where V_0 (m^3) is a constant reference volume taken at equilibrium (Molz and Ferrier, 1982; Steudle and Tyerman, 1983). It has been found that the increase of ε with P is generally greater at low pressures of less than about

0.3MPa (Steudle *et al.* 1977), and greater for larger cells where the ε-P relation is typically hyperbolic (Zimmermann and Steudle, 1974b). For some smaller cells ε has been found to be constant over a large pressure range, and volume-dependent (*ibid.* 1974b). Experiments on other small cells have found that the value of ε changes with pressure depending on the direction of the pressure change, and that the value of ε also changes over time (Zimmermann and Hüsken, 1979; Tyerman, 1982; see §1.2). However, the time-dependence of ε has largely been ignored in the water-relations literature. In CPP experiments, ε is usually assumed to be constant over the small pressure range used in the experiments (see §1.2), and assumed to be constant over time.

Eqs. (2.1)–(2.5) enable the KK equations to be solved numerically and, under certain assumptions, analytically. It can be shown that the same equations apply irrespective of the presence or absence of impermeant solutes in the external solution.

2.2.2 Analytical solution

The KK equations have been solved analytically by Steudle and Tyerman (1983) and Steudle *et al.* (1987) to give the temporal variation of P. The analytical solution forms the basis of the classical method of parameter estimation. It is summarized here, but for full details refer to these papers.

In the derivation of the analytical solution the following assumptions are made:

- cell surface area, A, is a constant
- cell volume, V, in Eq. (2.5) is a constant
- elastic modulus, ε, is a constant
- the convection term in Eq. (2.2) is negligible compared to the diffusion term
- solute concentrations on either side of the membrane are uniform with space.

The second assumption regarding V is not a necessary condition for the attainment of an analytical solution, however it is an assumption made in the analytical solution used by CPP experimenters. The assumptions will be examined in §2.7.2.

For the case of impermeant solutes only (in either a hydrostatic or osmotic experiment), the analytical solution is:

$$P = P_E + (P_1 - P_E)e^{-k_w(t-t_0)} \tag{2.6}$$

where P_E = final equilibrium turgor pressure and P_1 = turgor pressure at time of perturbation (when $t=t_0$). As noted in §1.2, $P_E \neq P_0$ where P_0 is the initial equilibrium turgor pressure. k_w is the rate constant given by:

$$k_w = \frac{A_0 L_P}{V_0}(\varepsilon + \pi_{i0}), \tag{2.7}$$

where the subscript '0' denotes an initial equilibrium value. The halftime τ_w is related to k_w by:

$$\tau_w = \frac{\ln 2}{k_w}. \tag{2.8}$$

If permeant solutes are present (in an osmotic experiment), the analytical solution is a sum of two exponentials:

$$\frac{V - V_0}{V_0} = \frac{P - P_0}{\varepsilon} = \frac{L_p A_0 \sigma R_g T \Delta C_{se}}{V_0(k_w - k_s)}[e^{-k_w(t-t_0)} - e^{-k_s(t-t_0)}], \tag{2.9}$$

where P_0 = initial equilibrium pressure (= pressure at time of perturbation), k_w is the rate constant for the water phase, given by Eq. (2.7), and k_s is the rate constant for the solute phase given by:

$$k_s = \frac{p_s A_0}{V_0}. \tag{2.10}$$

The halftime τ_s is related to k_s by:

$$\tau_s = \frac{\ln 2}{k_s}. \qquad (2.11)$$

Eq. (2.9) shows that as $t \to \infty$, $V \to V_0$ and $P \to P_0$; that is the system returns to its initial equilibrium state. When permeant solutes are present the curve is biphasic, with the first term in Eq. (2.9) dominating in the water phase and the second dominating in the solute phase. If permeant solutes are not present then the relaxation curve is a single exponential with a halftime given by k_w. It is important to note that in Eqs. (2.6) & (2.9), k_w and k_s are always positive and the equations remain the same irrespective of the sign of the pressure perturbation. This is clear by the definition of k_w and k_s given above. According to the analytical solution, *P-t* curves due to similar positive and negative perturbations should be symmetrical about the line $P = P_0$.

2.3 Parameter estimation methods

2.3.1 Characteristics of observed data

Relaxation curves for HPP and OPP observed data are shown in Fig. 1.3. The curves begin at an initial equilibrium pressure, reach a maximum or minimum, and return to a final equilibrium pressure. The following values can thus be obtained from the observed data: the maximum or minimum point of the data (t_m, P_m), and the initial and final equilibrium pressures P_0 and P_E. The halftimes τ_w and τ_s can also be obtained (by methods discussed in §2.3.2 and §2.3.3). These 4 sets of values partly characterise or describe the shape of the curve, and we may call them *curve characteristics.*

Let (t_0, P_1) denote the time and pressure at perturbation for an HPP, and (t_0, P_0) denote the time and pressure at perturbation for an OPP. Relaxation curves for an HPP begin at the maximum or minimum of the data, for the model assumes the pressure perturbation occurs instantaneously. The curve characteristics of an HPP curve are therefore: {t_0, P_1, τ_w, P_E,}. The curve characteristics of an OPP curve are: {t_0, P_0, t_m, P_m, τ_w, τ_s, P_E}.

Values of the curve characteristics depend on the membrane parameters, and are important quantities in the parameter estimation process. The analytical solution to the transport equations illustrates the relationship. For the HPP, increasing L_p decreases τ_w by Eqs. (2.7) & (2.8), and makes the *P*-*t* curve steeper. For the OPP, increasing L_p similarly decreases τ_w, and makes the slope of the water phase steeper so that t_m decreases. Increasing p_s decreases τ_s by Eqs. (2.10) & (2.11), and makes the slope of the solute phase steeper. Increasing σ also decreases P_m. Changes in any parameter also has smaller effects on the other curve characteristics.

2.3.2 Classical method of parameter estimation

The classical (traditional) method of parameter estimation utilizes the curve characteristics and analytical solution to apply appropriate transforms and equations to the observed data. The theory and equations given here are taken from Steudle and Tyerman (1983), Steudle *et al.* (1987), and Zhu and Steudle (1991).

(a) Determination of $\mathbf{L_p}$

The hydraulic conductivity L_p is most often obtained from hydrostatic experiments. Occasionally it may be obtained from osmotic experiments using impermeant solutes. A log transform of Eq. (2.6) gives:

$$\ln(P - P_E) = K - k_w(t - t_0), \tag{2.12}$$

where the constant $K = \ln(P_1 - P_E)$. A semilog plot of $(P\text{-}P_E)$ vs. t then gives k_w and hence L_p, since from Eq. (2.7):

$$L_p = \frac{V_0 k_w}{A_0(\varepsilon + \pi_0)}. \tag{2.13}$$

This is the expression for L_p based on the analytical solution to the KK equations. Note that for a negative pulse, $P_E > P$, so a semilog plot of $(P_E\text{-}P)$ must be used in place of Eq. (2.12).

Although Eq. (2.12) is linear, the semilog plot for the observed data is nonlinear, the slope being generally steeper for smaller *t* values. The nonlinearity may be due to errors in determining *P* and P_E, nonlinear properties of the plasmalemma, the dependence of ε on *P* (as expressed by Eq. (2.5)), presence of permeating solutes inside the cell, the contribution of the vacuole and tonoplast to the pressure relaxation, or effects of unstirred layers and solvent drag (Tyree *et al.* 2005; Wendler and Zimmermann, 1985b).
It is generally not clear from the literature which region of the semilog plot is used to find L_p. However, since it has been observed here that for low values of *t* the semilog plot is usually steeper, and theory predicts that only the plasmalemma L_p should be important around t=0 (Wendler and Zimmermann, 1985a), it may be assumed that in CPP experiments only this initial steeper, almost-linear portion is used to give a value for k_w. Since the semilog plot of this region still displays a slight nonlinearity, the calculated value of L_p is dependent upon the portion of the semilog plot used, as well as the value of P_E.

(b) Determination of $\mathbf{p_s}$

The permeability coefficient p_s is obtained from the solute phase of an osmotic experiment using permeant solutes. Since it is usually the case that $k_s << k_w$ (i.e. the halftime of the solute phase is much larger than that of the water phase) we may assume the response for large *t* is dominated by k_s, with $e^{-k_w t} \to 0$ very rapidly. Under this assumption a log transform of Eq. (2.9) gives:

$$\ln(P - P_0) = K' - k_s(t - t_0), \tag{2.14}$$

where the constant $K' = \ln\left(\frac{\varepsilon L_p A_0 \sigma R_g T C_{se}}{V_0(k_w - k_s)}\right)$. The semilog plot for observed data rises rapidly to a maximum value (corresponding to the time when P_m occurs) then decreases linearly. The slope of this linear portion taken at some time after the maximum gives k_s. The parameter p_s is then calculated using Eq. (2.10). This semilog plot is usually very

linear and the value of p_s quite precise. As for L_p, a semilog plot of ln(P_0-P) must be used for a negative pulse.

(c) Determination of σ

The reflection coefficient σ can be calculated directly from the osmotic experiment using permeant solutes. It requires the observed extreme values (t_m, P_m). When $dP/dt = 0$ we have:

$$(t_{\mathrm{m}} - t_0) = \frac{1}{(k_w - k_s)} \ln\left(\frac{k_w}{k_s}\right). \tag{2.15}$$

P_m can then be found using Eq. (2.9), from which we also obtain an equation for σ:

$$\frac{P_0 - P_{\mathrm{m}}}{R_g T \Delta C_{se}} = \frac{\varepsilon\sigma}{(\varepsilon + R_g T C_{i0})} e^{-k_s (t_{\mathrm{m}} - t_0)}, \tag{2.16}$$

where k_s is given by Eq. (2.10). The value of σ can usually be determined quite precisely, provided that values for P_m and t_m are accurate.

(d) Determination of $\mathbf{L_p}$ from biphasic experiments

It has been shown that all three parameters L_p, σ, and p_s, can be obtained by carrying out a hydrostatic and an osmotic experiment in conjunction. It is desirable to obtain all three parameters from the one (osmotic) experiment, however the method of calculating L_p from biphasic OPP experiments is not clearly stated in the literature. It is not definite whether it can be determined by this means, and appears that L_p is usually only obtained from HPP experiments, as this is regarded as the most direct and accurate measurement of L_p (T. Henzler, *pers. comm*). However, L_p for a biphasic osmotic experiment can be determined from the analytical solution by first determining k_s and t_m, and then numerically solving for k_w in Eq. (2.15), and using Eq. (2.13) to calculate L_p.

The value of L_p should be the same for both hydrostatic and osmotic experiments (being a physical property of the membrane), but it has been found that in osmotic experiments it is strongly dependent on external stirring rates, suggesting its measurement is more affected by ULs than with hydrostatic experiments (Steudle and Tyerman, 1983). Measurements of L_p with the two types of experiments give similar results at high external stirring rates.

The Classical method was applied by implementing the equations in Excel.

2.3.3 Optimization methods

More modern methods of calculating the membrane parameters use optimization methods to fit the observed data. This involves minimizing the residuals between observed and simulated data. Numerical algorithms are used to fit the relaxation curves to single or double exponential functions, and the rate constants k_w and k_s are obtained as results of the procedure. From the rate constants the membrane parameters can be calculated using the appropriate analytical solution equation. Optimization techniques have been used in recent years by CPP experimenters (Henzler and Steudle, 2000; Henzler *et al*. 2004).

The optimization used here is to minimize the overall root-mean-square (RMS) error of the whole curve. The RMS is defined as:

$$RMS = \sqrt{\frac{\sum_{i=1}^{N} (P_i - P_i^*)^2}{N}} \qquad (2.17)$$

where P_i are the predicted P values, P_i^* are the corresponding observed P values, N is the number of observations, and the summation is over all observations. Least-squares fitting is a maximum likelihood estimation of the fitted parameters, when the measurement errors are independent of each other, and normally distributed with constant standard deviations. These assumptions may be considered to hold here. In the case that standard

deviations for each measurement are not constant, a weighted least-squares formula called the *chi-square* is often used as a maximum likelihood estimate.

For convenience, this method will be termed the 'RMS method'. The minimization of the RMS was carried out using Excel Solver.

2.4 Preliminary to results

2.4.1 Determination of curve characteristics

The curve characteristics are obtained for both the Classical and RMS methods of parameter estimation. Although curve characteristics are not required to fit the data in the RMS method, they are used as either inputs into the model or in an analysis of goodness of fit. Curve characteristics of the simulated data, where calculated, are done so using the same method as for the observed data.

The halftimes τ_w and τ_s are obtained from the slopes k_w and k_s of semilog plots of the observed data. For τ_w in a HPP, semilog plots are taken during the initial portion of the curve. For τ_s, semilog plots are taken over the region $t>2t_m$.

Extreme values (t_m, P_m) can be obtained by reading off the discrete data (t,P) values, or by interpolating between the data values to give a more accurate value. Here interpolation was used by fitting a second degree polynomial to a window around the extremum. The initial equilibrium pressure P_0 and the final equilibrium pressure P_E were obtained by averaging 10 or more observed values of P.

The simulated relaxation curves are very sensitive to the time t_0 at which the perturbation occurs. It is therefore important to determine an accurate value for t_0, however this is not always possible. For an HPP, P_1 was taken to be the maximum change in P from P_0. The time t_0 when this occurs can be read from the data, or chosen to be a point near that time

since there is often some noise around this point. For an OPP, there is some freedom in choosing t_0 since it is unknown when exactly the perturbation pulse impacts on the cell.

For an OPP, theory dictates that $P_0 = P_E$. Therefore in Eqs. (2.14) & (2.16) either the observed P_0 or observed P_E value can be used for P_0 in the equations. However, in many data sets there is some variation from this, as the experiment may not have been run for long enough for a steady equilibrium to be attained, a long-term pressure drift was present in the data, or changes in the external solution occurred around t_0. Therefore, using P_0 in the equations will mean that P_E may not be predicted well by the model, and using P_E will mean that P_0 may not be predicted well by the model. Here it was chosen to use the observed P_0 value.

2.4.2 Error analysis

The error in the estimation of each parameter or curve characteristic must be calculated for the model fits. The error is comprised of: a) numerical error in the model or optimization method, and b) experimental error in the observed data due to the measurement precision of the CPP. The experimental noise in the CPP has been found to have a standard deviation of ± 0.0003 MPa and a maximum of 0.0008MPa, so the error in P is taken to be about ± 0.0005 MPa (M. Tyree, unpublished). The experimental error in t is taken to be the time-resolution of the data (about ± 0.05s in Henzler *et al*. 2004). There may also be some error in the exact size of the pressure perturbation, however the magnitude of this error is unknown and should not be large, so is ignored in the present study.

In the Classical method of parameter estimation, Eqs. (2.12)–(2.16) are used to determine the membrane parameters that reproduce the curve characteristics obtained from the observed data. The accuracy of this method depends on the accuracy of the analytical solution, and the accuracy to which the curve characteristics can be determined from observed data. Standard errors (SE) in the calculated parameters are derived from the errors in the curve characteristics of the observed data. The standard errors in the

estimated parameters were determined using a formula for propagation of errors (Young, 1962). If $Q = f(a,b,c)$, then the error δQ in Q is:

$$\delta Q^2 = \left(\frac{\partial Q}{\partial a}\right)^2 \delta a^2 + \left(\frac{\partial Q}{\partial b}\right)^2 \delta b^2 + ... \ , \qquad (2.18)$$

where δa is the error in a, etc. For the HPP experiment, the error in the slope of the semilog plot of the observed data, $k_{w,}$ can be obtained from the linear regression. From this, the error in L_p is calculated using Eq. (2.13), and the SE in τ_w calculated using Eq. (2.18). The error in P_E was derived by calculating the standard deviation of the last 10 values of P of the observed data.

For the OPP experiment, the error in k_s was obtained from the error in the regression of the semilog plot of the solute phase. From the measurement error in t_m and the error in k_s, the error in k_w can be determined using Eqs. (2.15) & (2.18). The errors in L_p, p_s and σ can be determined using Eq. (2.18) and the previous parameter definitions given by Eqs. (2.10), (2.13) & (2.16).

Standard errors in optimized or fitted parameters using the RMS method were calculated using the NonlinXL toolbox in Excel (P. Sands, unpublished). For the HPP, the SE in τ_w was also calculated from the SE in L_p by using Eqs. (2.7), (2.8) & (2.18). For the OPP, the percentage departure of the model curve characteristics from the data curve characteristics were also calculated.

2.5 Application of model: Results

The analytical solution for the classical model (i.e. Eqs. (2.1)–(2.5)) was implemented in Excel, and applied to simulate raw data obtained from Dr. Henzler and Mr. Ye, corresponding to published data in Henzler *et al.* (2004). The membrane parameters were obtained using both the Classical method and RMS method, and for comparison purposes curve characteristics and RMS values are given for results from both methods. Assumptions of the Classical model given in §2.2.2 apply.

The model was applied to data for a positive and negative hydrostatic pressure pulse (HPP), and a positive and negative osmotic pressure pulse (OPP) in the presence of permeant solutes (160mM acetone was added or removed from the external solution). The data corresponds to Fig. 2A in Henzler *et al*. (2004). The data is extracted for use in the model starting at a chosen value, and the time scale is then adjusted so that this value becomes 0. An optimized value of t_0 is expressed relative to this zero value.

2.5.1 HPP experiment

(a) Application of Classical method

The negative HPP data was fit first using Eqs. (2.6) & (2.7). As mentioned in §2.3.1, the curve characteristics for an HPP curve are $\{t_0, P_1, \tau_w, P_E,\}$. In order to determine L_p, a value for τ_w must be obtained from the observed data. The semilog plot of the observed P-P_E was found to be very slightly nonlinear (see Fig. 2.1, and refer to Tyree *et al.* 2005 for a discussion of possible reasons). The determination of k_w was indeterminate since using the slope from different regions of the semilog plot would give different values for k_w, resulting in different values of τ_w which is very sensitive to k_w. Accordingly, slopes from 2 different regions were trialed. A regression over 0-3 s gave τ_w = 1.62s, which corresponds to a value near to that quoted by Henzler *et al.* (2004) (τ_w = 1.6s). A regression over 0-8 s gave τ_w = 1.99s, which corresponded to values of P where (P-P_E) > 0.002MPa. This critical value was used because Steudle and Tyerman (1983) state that "the relaxation curves were well fitted by a single exponential down to pressure differences...of about 0.02bar ($R^2 > 0.98$)", suggesting a good fit for values where (P-P_E) > 0.002MPa.

As mentioned in §2.4.1 the quality of the fits are sensitive to the value of (t_0, P_1). A value of t_0 = 0 was first chosen near to, but not equal to, that when P_1 occurs, and then in order to obtain the best fit t_0 was further adjusted by optimizing its value using Excel Solver (refer to Table 2.1, where t_0 values are relative to the chosen point t_0 = 0). The adjusted

value of t_0 did not affect L_p (since L_p is obtained using a constant τ_w and P_E obtained from the data, and the adjustment in t_0 was very small), but was found to affect the RMS value from the fit (by up to 20%). This justified the optimization of t_0 instead of taking t_0 as the point at which P_1 occurs.

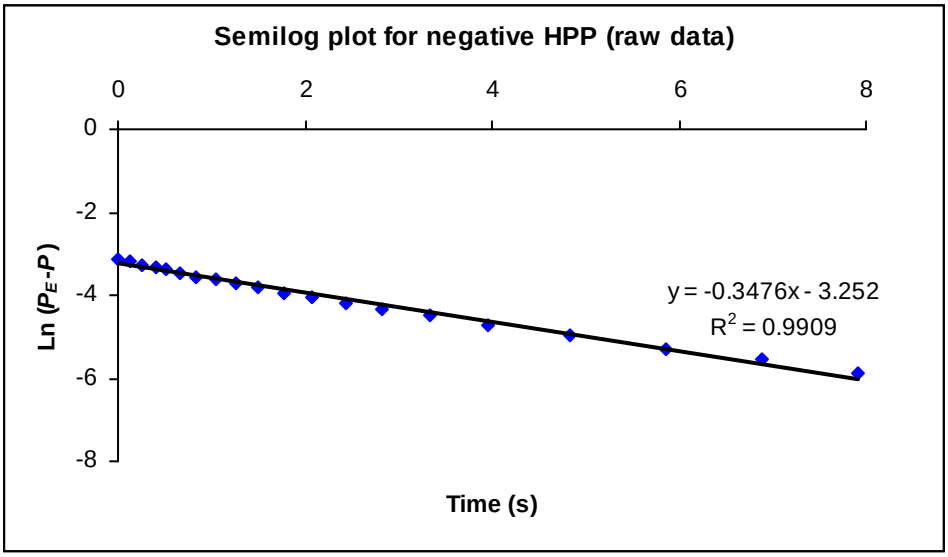

Fig. 2.1 Semilog plot for 0-8 s of the negative HPP data from Henzler *et al.* (2004), with trendline.

It was found that using τ_w = 1.62s to fit the negative HPP curve simulated the earlier data points better (up to 4s, Fig. 2.2) and gave a lower RMS value (first column in Table 2.1). Fitting to τ_w = 1.99s simulated the later data points better (after about 10s, Fig. 2.2b), and gave a higher RMS value (second column in Table 2.1). An L_p based on a semilog plot regression over 0-3 s gave the best fit for the Classical method, which concurs with the inference that only the beginning parts of the semilog plots are used in the derivation of L_p when using the classical model.

A determination of the curve characteristics for the positive HPP curve found that it was symmetrical to the negative HPP curve, with a data halftime τ_w =1.67s lying within 1.62s ± 2SE of the negative HPP. A semilog regression over 0-3 s, same as for the negative

pulse, was used to derive τ_w. When the data was fit, it was found that the estimated L_p was not significantly different between the negative and positive HPP curves, the values agreeing to within 2SE (Table 2.1).

Table 2.1 Model results for a HPP experiment using the Classical method of parameter estimation. Errors are standard errors.

	Negative HPP				Positive HPP	
	*0-3 s		*0-8 s		*0-3 s	
t_0 (s)	-0.08	±0.02	-0.08	±0.02	0.11	±0.03
L_p (x 10^6 m s^{-1} MPa^{-1})	3.02	±0.05	2.46	±0.05	2.94	±0.04
τ_w (s)	1.62	±0.03	1.99	±0.04	1.67	±0.02
P_E (MPa)	0.6409	±0.0001	0.6409	±0.0001	0.6421	±0.0001
RMS (x10^4)	7.6		15.8		8.3	

* Time period over which regression of semilog plot was taken.

(b) Application of RMS method

The negative and positive HPP curves were fit by minimizing the RMS value given by Eq. (2.17). Although the RMS values were lower than those obtained with the Classical method, the estimated values of L_p were within 2SE of each other (Table 2.1 & Table 2.2). The main difference was in the values of P_E, where the RMS method underpredicted P_E by 0.0005 MPa (compare Fig. 2.2 & Fig. 2.3; see Table 2.2). Considering the measurement error of ± 0.0005 MPa, however, this difference is not significant. For the positive HPP, the fits and residuals between the Classical and RMS methods were also similar, with the RMS method overestimating P_E by 0.0004 MPa.

Averaging results in Table 2.1 and Table 2.2 gives $L_p = 3.03 \pm 0.01$ m s^{-1} MPa^{-1} for the negative HPP, and $L_p = 2.96 \pm 0.02$ m s^{-1} MPa^{-1} for the positive HPP, where errors are standard deviations. These L_p values, although lying outside 2 standards deviations of each other, do not differ significantly since the standard errors from the model estimations are quite large (Table 2.1 and Table 2.2). This is in agreement with the analytical solution to the KK equations, which predicts that the positive and negative experiments should be symmetric about the *t*-axis.

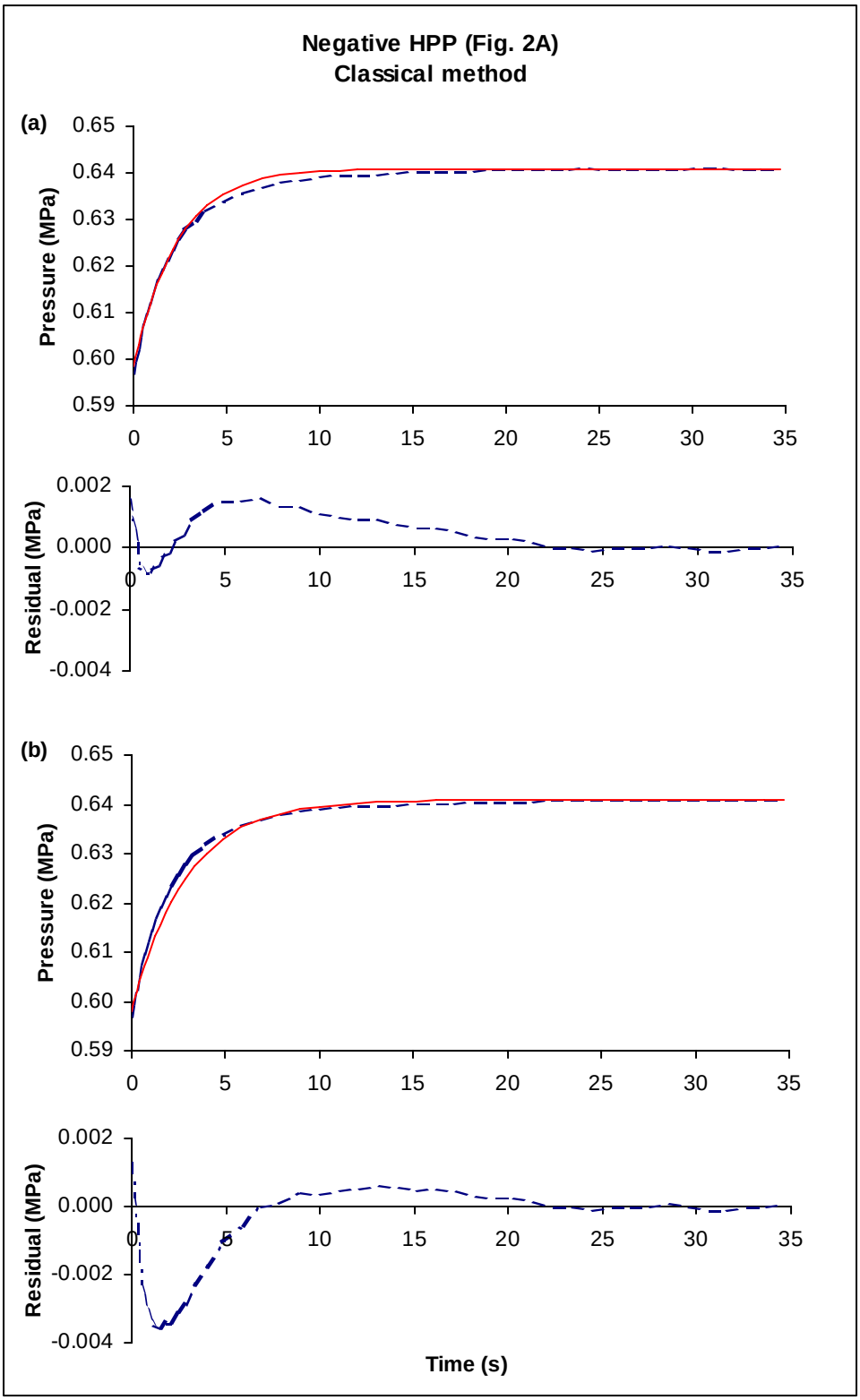

Fig. 2.2 *P-t* curves and residuals for a negative HPP, using the Classical method. Showing raw pressure data (-----) and model fit (——). (a) Using τ_w = 1.62s, (b) using τ_w = 1.99s.

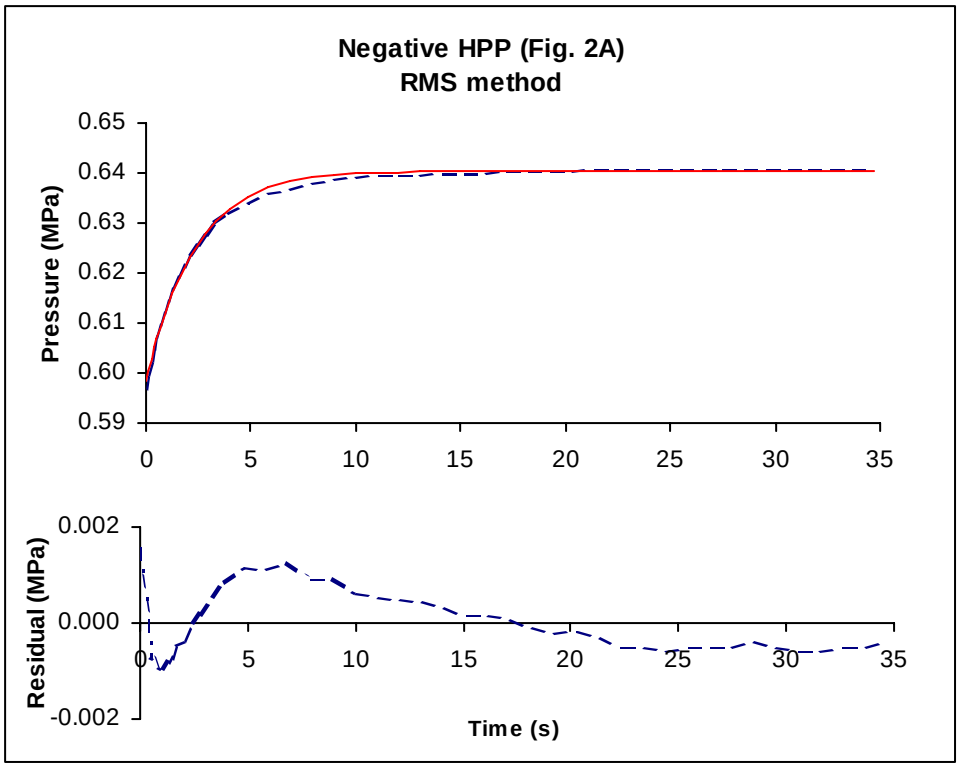

Fig. 2.3 *P-t* curves and residuals for a negative HPP, using the RMS method. Showing raw pressure data (----) and model fit (——).

Table 2.2 Model results for a HPP experiment using the RMS method of parameter estimation. Errors are standard errors.

	Negative HPP		Positive HPP	
t_1 (s)	-0.08	±0.02	0.11	±0.03
L_p (x 10^6 m s $^{-1}$ MPa^{-1})	3.04	±0.06	2.97	±0.07
τ_w (s)	1.62	±0.03	1.65	±0.04
P_E (MPa)	0.6404	±0.0001	0.6425	±0.0001
RMS (x 10^4)	6.5		7.6	

Agreement of L_p and τ_w values between the two fitting methods, where a semilog regression period of 0-3 s was used for the Classical method and the RMS method is based on all the data (not just the points for t<3s), confirms the practice of using only the initial region of the semilog plot of the observed data for fitting with the Classical method.

2.5.2 OPP experiment

(a) Application of Classical method

As mentioned in §2.3.1, the curve characteristics of an OPP curve are: $\{t_0, P_0, t_m, P_m, \tau_w, \tau_s, P_E\}$. Of these, P_E is not important for fitting since the analytical solution gives $P_0 = P_E$, and τ_w is also not important since τ_w can be derived from t_0, t_m and k_s through Eq. (2.15). Thus the curve characteristics required for fitting an OPP curve are: $\{t_0, P_0, t_m, P_m, \tau_s\}$. These were obtained from the observed data by the methods described in §2.4.1.

The negative OPP was fit first using Eqs. (2.9) and (2.10). A regression of the semilog plot over the period 20-125 s was used for determining τ_s. P_0 and P_E were found to be the same within experimental error (0.6361 MPa and 0.6360 MPa respectively) for this data set.

A slight curvature was present in the data near $t = 0$, before P rises steeply (Fig. 2.4a). We may call this period of curvature a "time-delay", referring to a delay in the response of P to the pressure perturbation, since the classical model supposes that the response time is immediate and the perturbation instantaneous. The time-delay is usually of the order of a few seconds at most, and is not evident when the full P-t curve is plotted (Fig. 2.4b). Because the Classical model does not predict a time-delay, the estimated parameters and model fits will clearly depend on the choice of t_0.

In order to examine the impact of t_0 on the estimated parameters, the negative OPP data was fit using different values of t_0. In addition to $t_0 = 0$ the data was fit to: a) $t_0 = 0.73$s, obtained by fitting a piecewise linear continuous function ("broken stick" regression) to points around $t_0 = 0$; b) $t_0 = 1.14$s, the optimized value obtained by Excel Solver using the analytical solution; c) $t_0 = 1.5$s, a manually adjusted value made after the optimized t_0 was obtained, which seemed to give the best fit and smallest residuals (Fig. 2.4c).

A comparison of how the estimated parameters vary with the choice of t_0 is given in Table 2.3. L_p increased with increasing t_0, σ decreased slightly with increasing t_0, and p_s

was independent of the choice of t_0. These behaviours are as expected, since: a) L_p governs the water phase, which is relatively steeper for a smaller t_m - t_0; b) p_s governs the solute phase, for which the slope is not affected by a time-delay; c) σ is calculated from the analytical solution for P (Eq. (2.9)), from which we see that as t_m - t_0 decreases, σ decreases slightly for a constant P_0 - P_m and k_s. The RMS values were lower, as expected, when the time-delay in the observed data was better taken into account (i.e. RMS values were lower for higher values of t_0). The RMS errors were comparable for t_0 in the range 1.14–1.5 s. The choice of t_0 mainly affected L_p and the RMS error.

Table 2.3 Estimated parameters for the negative OPP curve, using the Classical method, for four different values of t_0. Errors are standard errors.

	Negative OPP					Positive OPP	
t_0 (s)	0	0.73	1.14	1.5		0.37	
L_p (x 10^6 m s^{-1} MPa^{-1})	2.01	2.25	2.40	2.56	(±0.02)*	2.30	±0.02
p_s (x 10^6 m s^{-1})	4.43	4.43	4.43	4.43	(±0.01)	4.54	±0.02
σ	0.132	0.129	0.128	0.127	(±0.001)	0.121	±0.001
RMS (x 10^{-4})	19.5	10.6	6.1	6.5		8.5	

* standard errors for the model fits to t_0 = 1.5s, t_0 = 0.1s.

The positive OPP data was noisier than the negative OPP data in the first half of the experiment, especially around the extremum (Fig. 2.5). τ_s was derived by taking a regression of the semilog plot in the period 20-125 s, the same as for the negative pulse.

The data could not be fit using the value of P_0 derived from the data. The experiment had been run for a shorter period of time and the pressure did not return to its initial equilibrium value of 0.6384 MPa. A problem may have occurred during the experiment, since the pressure had an upward trend prior to the perturbation and so was not at true equilibrium. Since this value of P_0 is suspect an optimized value of P_0 = 0.6362 MPa, obtained using Excel Solver for the classical model, was used for curve-fitting. This value of P_0 is close to the values of P_0 and P_E for the negative OPP, and is likely to be what P_0 should have been in the positive OPP experiment.

Due to the adjustment of P_0 there was an absence of a real time-delay in the data. The data was fit with an optimized value of t_0 = 0.37s, obtained using the RMS method. The fit was found to be poorer than the fit for the negative OPP (with t_0 = 1.14s), with a higher RMS error. This is probably due to the greater presence of noise in the data.

(b) Application of RMS method

The negative OPP was also fit to different values of t_0 using the RMS method. A similar trend in the parameters with varying t_0 was observed as for the Classical method (Table 2.4), but with p_s decreasing slightly with increasing t_0, due to t_m decreasing with higher values of t_0. (The value of t_m does not change in the Classical method, since it is made to equal t_m of the observed data.) The changes in L_p due to t_0 were greater with the RMS method than with the Classical method of fitting. As with the Classical method, the RMS values were lower when the time-delay in the observed data was better taken into account, and the time-delay mainly affected values of L_p and the RMS value.

It is useful to examine what sort of information the RMS value gives about the fits. Within the Classical method, although the fit with t_0 = 1.14s gave the same RMS value as the fit with t_0 = 1.5s (Table 2.3), it was found that the water phase was not fit as well, and the similar RMS values were a consequence of different distributions of the residuals in the water phase where they are dependent on the value of t_0. Within the RMS method, the fit with t_0 = 1.14s gave the lowest RMS value (Table 2.4), but it was found that data points around the extremum were not fit as well as the fit for t_0 = 1.5s.

The fits with t_0 = 1.5s had the most evenly distributed residuals, and on the basis of this was deemed to be the best fit for both methods. The residuals were similar between the fitting methods, with only a slight difference in the water phase and around the extremum where the RMS method did not fit the points as well. The fits were not so good for small t, but this is a natural consequence of using a larger value of t_0. For this value of t_0, the estimated parameters (Table 2.3 & Table 2.4) agreed closely between the two fitting methods.

The residuals for the second half of the solute phase were similar for all the fits, and were larger in this region as more relative noise was present in the data for larger t (Fig. 2.4b,c). These larger residuals do not affect the fit of the curve since it was chosen to fit to a τ_s value based on 20-125 s of the semilog plot. Using this value of τ_s emphasises fitting regions of the curve where the cell dynamics are faster, i.e. the water phase, around the extremum, and the first half of the solute phase.

Table 2.4 Estimated parameters for the OPP curve, using the RMS method, for four different values of t_0. Errors are standard errors.

	Negative OPP					Positive OPP	
t_0 (s)	0	0.73	1.14	1.5		0.37	±0.02
L_p (x 10^6 m s^{-1} MPa^{-1})	1.41	1.83	2.19	2.59	(±0.04)*	2.82	±0.06
p_s (x 10^6 m s^{-1})	4.66	4.54	4.47	4.41	(±0.03)	4.35	±0.03
σ	0.132	0.129	0.127	0.126	(±0.001)	0.120	±0.001
τ_w (s)	3.49	2.68	2.25	1.90	(1.6%)***	1.74	(18.5%)
τ_s (s)	29.7	30.6	31.0	31.5	(0.4%)	31.89	(4.3%)
P_m (MPa)	0.6738	0.6749	0.6756	0.6761	(0.1%)	0.5977	(0.1%)
t_m (s)	12.2	11.0	10.3	9.7	(1.0%)	8.09	(11.9%)
P_E (MPa)	0.6361	0.6361	0.6361	0.6361	(0.0%)	0.6362	(0.0%)
RMS (x 10^{-4})	11.9	6.5	4.5	6.3		5.7	

* standard errors (for a particular value of t_0) obtained using SolverStat in Excel.
** relative % difference between model and data curve characteristics, for a particular value of t_0.

The positive OPP was fit with an optimized value of t_0 (Table 2.4). There was a significant difference in the estimated values of L_p and σ, and in the residuals, between fits using the two fitting methods (Fig. 2.5). The difference was larger compared to the two negative OPP fits using the optimized value of t_0 (Table 2.3 & Table 2.4). This was due to the two methods fitting points around the noisy extremum differently (Fig. 2.5).

Averaging results from the two methods (for t_0 = 1.5 s) in Table 2.3 & Table 2.4 gives estimated parameters ± SD for the negative OPP of : L_p = 2.58 ± 0.02 x 10^{-6} m s^{-1} MPa^{-1}, p_s = 4.42 ± 0.01 x 10^{-6} m s^{-1}, and σ = 0.127 ± 0.001. Estimated parameters ± SD for the positive OPP are: L_p = 2.56 ± 0.37 x 10^{-6} m s^{-1} MPa^{-1}, p_s = 4.45 ± 0.13 x 10^{-6} m s^{-1}, and σ = 0.121 ± 0.001. These parameters do not differ significantly from each other. The

difference in σ can be explained by the fact that P_0 was adjusted for, so that $P_0 - P_m$ for the positive pulse was less than for the negative pulse, resulting in a lower σ by Eq. (2.16).

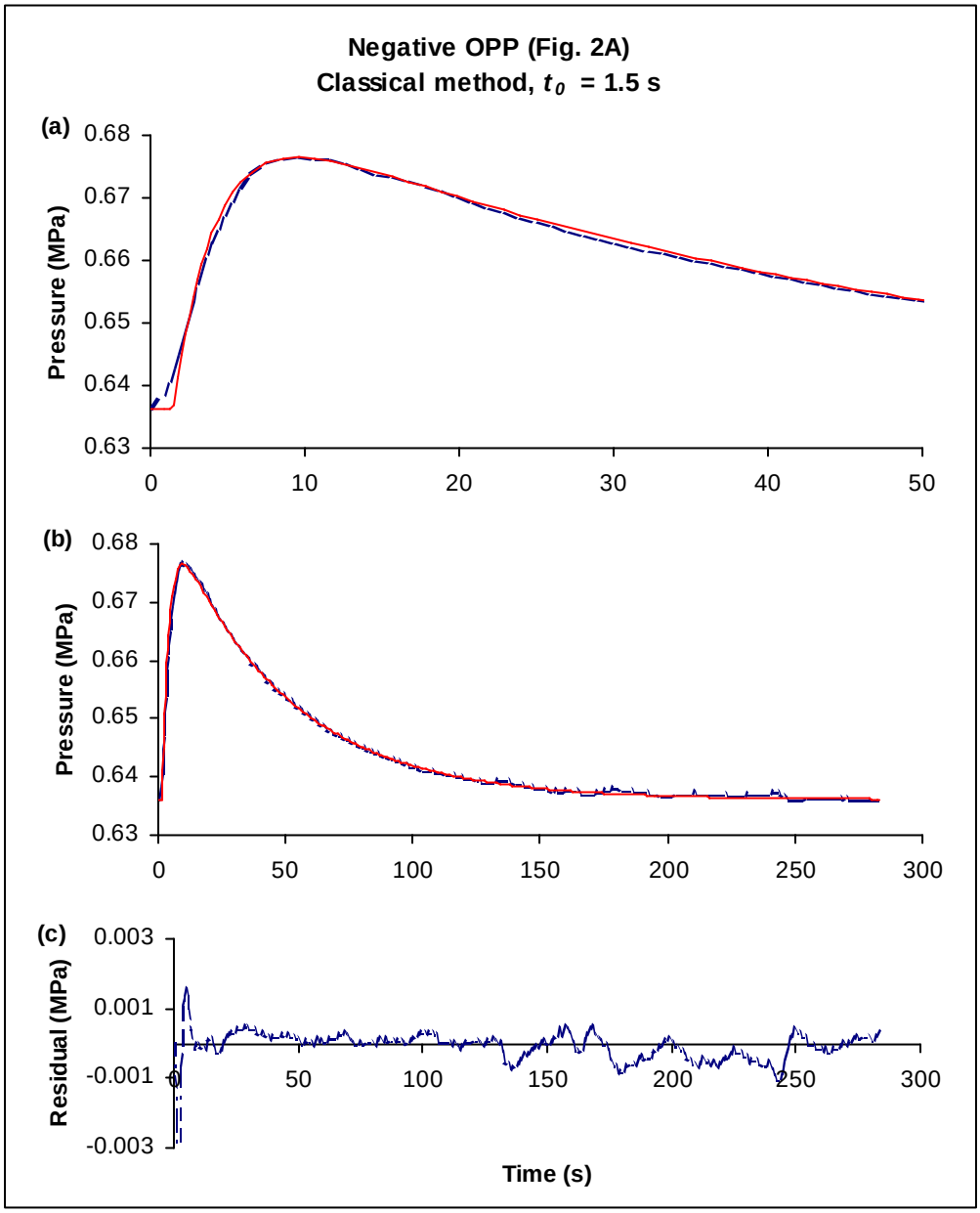

Fig. 2.4 *P-t* curve and residuals for a negative osmotic pressure pulse, showing raw pressure data (----) and model fit (——). Using Classical method with t_0 = 1.5s. (a) *P-t* curve for 0-50 s; (b) full *P-t* curve; (c) residuals for full *P-t* curve. Data from Henzler *et. al.* (2004).

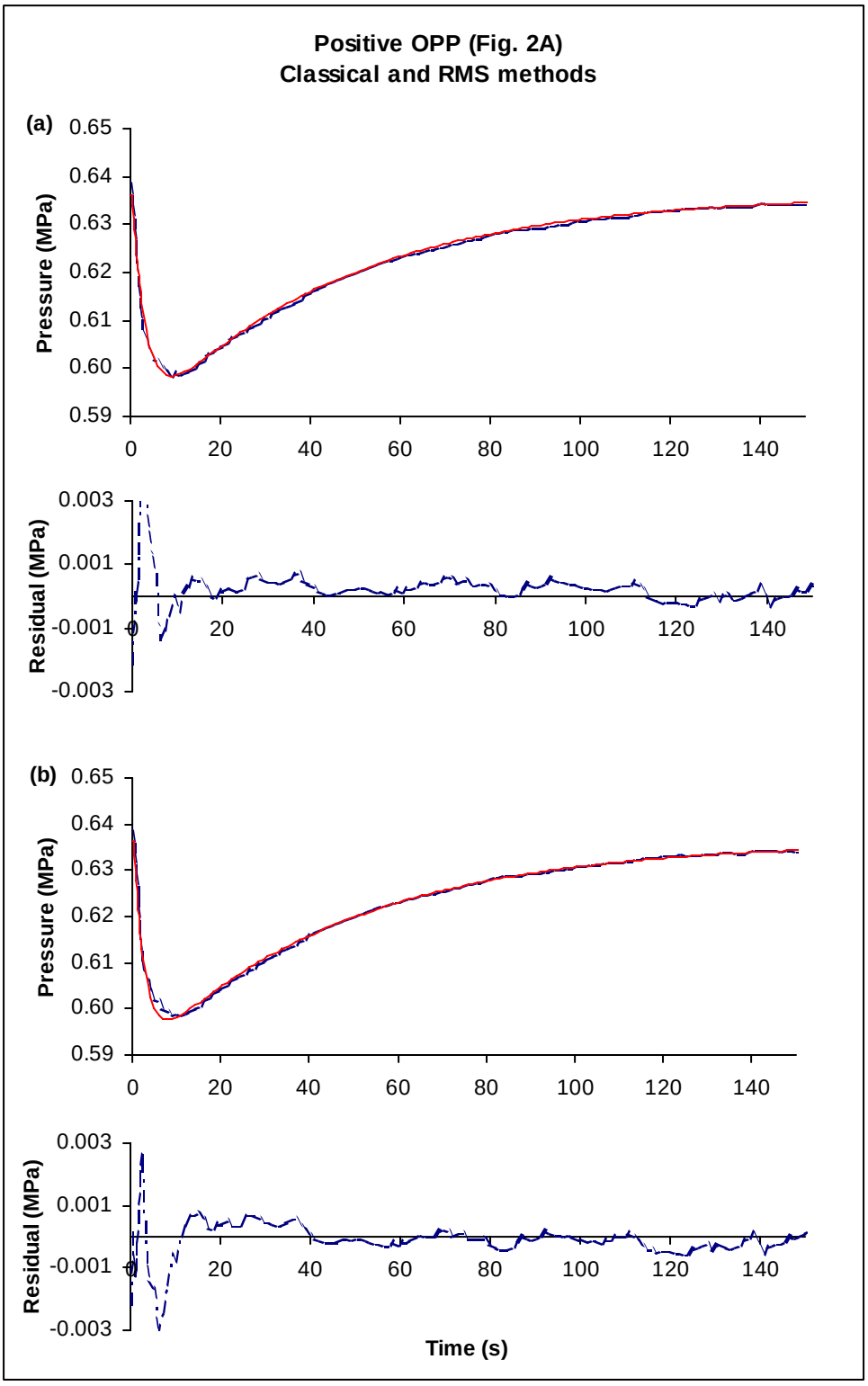

Fig. 2.5 *P-t* curves and residuals for a positive osmotic pressure pulse, showing raw pressure data (----) and model fit (——). (a) Using Classical method with t_0 = 0.37s, (b) using RMS method with t_0 = 0.37s.

Averaging results across the 4 fits to the positive and negative pulses, gives L_p = 2.99 ± 0.05 m s^{-1} MPa^{-1} for the HPP experiment, and L_p = 2.57 ± 0.21 m s^{-1} MPa^{-1} for the OPP experiment. These results show that the estimated L_p for the OPP experiments is significantly lower than L_p for the HPP experiments.

2.6 Analysis of results

2.6.1 Correlation of parameters

Correlation tables between optimized parameters were obtained by NonlinXL for fits to a negative HPP and negative OPP experiment. Table 2.5 shows that for the HPP experiment, L_p is strongly correlated with t_0 and less so with P_E. This means small changes in t_0 will affect the value of L_p, so it is important to optimize t_0 for the fits, and that fits using the RMS method are likely to change P_E along with L_p.

Table 2.5 Parameters correlation table for a fit to a negative HPP experiment, with the RMS method.

	P_E	L_p	t_0
P_E	1	-0.41	-0.14
L_p	-0.41	1	0.69
t_0	-0.14	0.69	1

Table 2.6 Parameters correlation table for a fit to a negative OPP experiment, with the RMS method. t_0 = 1.14s.

	L_p	p_S	σ	t_0
L_p	1	-0.52	-0.58	0.69
p_S	-0.52	1	0.81	-0.18
σ	-0.58	0.81	1	-0.21
t_0	0.69	-0.18	-0.21	1

Table 2.6 shows that for the OPP experiment, p_s and σ are strongly correlated. This is consistent with theory and the literature. L_p is also correlated with p_s and σ, showing that

all 3 membrane parameters are correlated. L_p is strongly correlated with t_0 whilst p_s and σ aren't, which is consistent with the results in §2.5.2.

2.6.2 Comparison of fitting methods

Results show that the Classical and RMS methods are both useful for fitting the data. Fitting the OPP curve was a more a complex task than fitting the HPP curve, due to the greater number of curve characteristics involved, and the greater impact of t_0 on the model fits. The two fitting methods give different parameter estimates for the OPP experiment, since they emphasise fitting different regions of the data. The Classical method gives more weight to errors in t_m, P_m, and τ_s; the RMS method gives equal weight to errors in the observed P distributed across the whole data set. The difference between the methods is highlighted by fits to the OPP experiment (Table 2.3 and Table 2.4).

The RMS method is an average error over all the data points, and therefore a large error in predicting a few data points may not alter the overall RMS error by a significant amount. Although this is an advantage as it balances a few erroneous data points with many good ones, it is also a drawback when fitting OPP data since the period during which the data returns to equilibrium is much longer than the period during which the data reaches a maximum or minimum. This effectively gives a large weight towards fitting values near the final equilibrium pressure compared to fitting values in the earlier regions where the cell dynamics are changing rapidly or significantly. The RMS method may fail to fit these earlier regions (such as points in the water phase and around the extremum) if a long tail in the solute phase of OPP data is subject to relatively more significant error. The earlier regions of the data may be fit better by weighting the RMS value in these regions (so that minimising the residuals between observed and simulated data in these regions is emphasised), although which points are given more weight is subjective.

A drawback of the Classical method is that where there is significant noise in the data around the curve characteristics, the latter cannot be determined very precisely, making it

difficult to determine a good fit. This was seen in fits to the positive OPP (Fig. 2.5), which had significant noise around the extremum. Another factor affecting the fits and adding to variability in the estimated parameters, is the regions of the curve used to derive the halftimes for fitting. However, if the RMS error is reasonably low, and the data is fit well with low overall residuals, we may conclude with some confidence that the estimated parameters are the ones which govern the cell dynamics, insofar as the classical model is correct.

Parameters estimated by the two methods may agree for a certain value of t_0 to give a single set of estimated parameters. However this would not always be the case, and one method should be chosen. Here the RMS method is chosen to fit subsequent data sets, with t_0 an optimized parameter. This is because it is a more flexible method than the Classical method, as it avoids issues of noisy locations in the data, and fits to specific regions of the data can be improved by weighting the RMS value around these points.

The quality of the fit cannot be determined by the value of the RMS error alone, since it does not uniquely characterise the quality of the fit. It merely serves as a guide to a good fit, as better fits generally have lower RMS errors. The RMS value must be used in conjuction with the overall residuals between the model and data, in order to judge quality of fit. The “best fit” will be the fit with the lowest mean residual, most even distribution of residuals, and a low bias and trend in the residuals. The RMS value may be weighted around the extremum or other regions of the curve to give more even residuals.

Estimated parameters for the positive and negative OPP curves may differ when the curves are fit separately. If consistency is desired, i.e. it is decided a priori that parameters estimated for both the positive and negative pulses should be the same, both curves can be simultaneously fitted using the RMS method. As an exercise, this was attempted with the positive OPP. However, since the fits to each curve were clearly a compromise in this instance, and fell far short of the best fit, the resulting estimated parameters added little knowledge to the likely parameters for these curves.

2.7 Discussion and limitations of the classical model

2.7.1 Full numerical model

The full transport equations for the classical model were solved numerically by implementing the model in Matlab. A numerical solution was required to provide more flexibility than the analytical solution, to analyse assumptions of the analytical solution, and to explore different perturbation conditions. Unstirred layers were also added to the model in Chapter 3. The implementation was verified by: (a) direct comparison with the analytical solution, where the results agreed to a high degree of accuracy, (b) demonstrating that the parameter values were recovered by applying the parameter estimation techniques of §2.3.2, and (c) application of the model to observed data from the literature.

2.7.2 Numerical consequences of simplifying assumptions

The numerical consequences on the *P-t* curve of the model assumptions listed in §2.2.2 were explored using the Matlab implementation. That is, effects of incorporating variable *A*, variable *V* in Eq. (2.5), and variable ε on the solution were analysed, as well as the relative influence of the convection term in Eq. (2.2) compared to the diffusion term.

ε was modelled as a function of *P* using the slope in ε vs. *P* taken from data published in Steudle *et al*. (1982). For the pressure range in the current data, this slope was calculated to be 33.3 (dimensionless). Taking the constant value of ε = 27.6 MPa used in the model fits of §2.5 as the median ε value, a variable ε over the *P* range of the data was obtained.

For both HPP and OPP data, the incorporation of variable *A*, *V* and ε into the model was found to give relative errors of < 1% for the estimated parameters, and very small errors of <0.1% for the predicted *P(t)*. The relative influence of the convection term in Eq. (2.2) was found to be negligible compared to the diffusion term (Fig. 2.6).

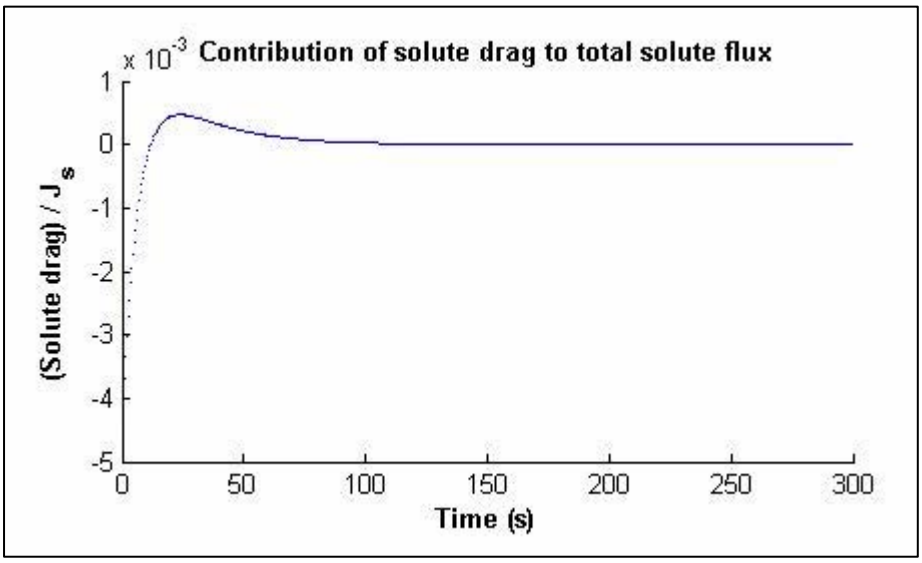

Fig. 2.6 Showing the contribution of solute drag to the total solute flux for simulated OPP data.

2.7.3 Model fits

Model fits to the HPP curves were generally good except for the region where P begins to level off (the bend or "shoulder" of the curve). This region could not be fit well by either of the fitting methods for the Classical model. Model fits to the OPP curves were generally good except for the initial curvature near t_0, which could not be fit by the Classical model. In this section, explanations for these failings of the model, and methods for improving the model fits, are explored.

(a) Fitting the HPP curve with a double exponential

In §2.5.1 it was shown that HPP data could be fit with the Classical model only by using the initial region of the semilog plot of the observed data. This reveals a failure of the Classical model to fit data away from the initial portion, and indicates that the classical model is not incorporating some aspects of the cell dynamics. For example, it may be failing to taking into account the presence of the tonoplast, effects of which could be incorporated by expressing the cell pressure as a double rather than a single exponential (Wendler and Zimmermann, 1985a,b; Zhang and Tyerman, 1999).

To explore this, the negative and positive HPP curves were fit using 2 exponential terms, according to the equation:

$$P = P_0 + p_1\left(1 - e^{-k_1(t-t_0)}\right) + p_2\left(1 - e^{-k_2(t-t_0)}\right) \tag{2.19}$$

where p_1 and p_2 represent general coefficients and k_1 and k_2 represent rate constants. These 4 parameters plus t_0 were optimized using Excel Solver (i.e. the RMS method). It was found that the fits were much better than using Eq. (2.6) of the classical model, with RMS = 1.5 x 10^{-4} (compared to 6.5 x 10^{-4}) for the negative HPP, and RMS = 6.5 x 10^{-4} (compared to 7.6 x 10^{-4}) for the positive HPP (compare Fig. 2.2 & Fig. 2.7; refer to Table 2.2). For both fits the first rate constant, k_1, was found to be about 3 times larger than k_2.

(b) Effect of shape of input pulse on the OPP curve

The failure of the Classical model to fit the curvature near t=0 in the OPP curve suggests something is missing from the model. One thing missing is the shape of the perturbation pulse, i.e. when and in what form the perturbation impacts on the cell. As mentioned in §1.2, it is known that the external concentration takes a short period of time to reach the maximum perturbation level (which is known as “ramping”). This is due to two effects: the shape of the front of the changeover solution, and the time it takes for the front to traverse the length of the cell.

The time the external concentration takes to ramp up may be measured by electrical resistance methods (see §4.2.1). These measurements are not available for the present data set and therefore this ramp time is unknown. The spatial distribution of the external concentration during the ramp could be modelled on the basis of fluid dynamics for flow through a pipe (the pipe being the pressure chamber in the CPP, see Fig. 1.2). Since we are assuming radial and axial symmetry here, this is beyond the scope of the model. However, the change in external concentration at a point along the cell can be modelled for by making the simple assumption that it changes linearly over time to reach the

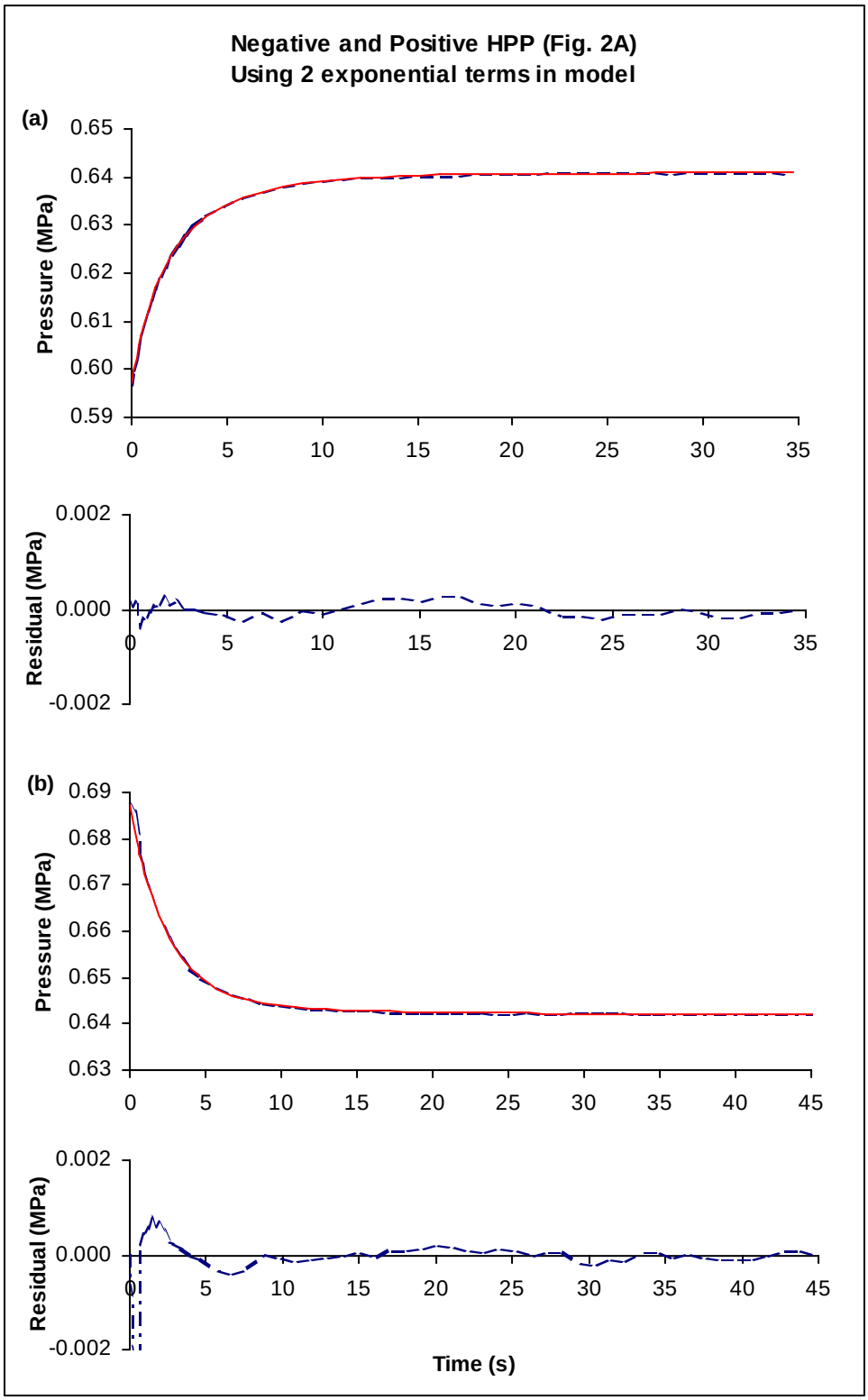

Fig. 2.7 *P-t* curves and residuals for fits to the HPP data, using 2 exponential terms. Showing raw pressure data (----) and model fit (——). (a) Negative HPP, RMS = 1.5 x 10^{-4}, (b) positive HPP, RMS = 6.5 x 10^{-4}.

perturbation level. This simple function does not necessarily reflect the true shape of the pulse and concentration distribution along the length of the cell following perturbation. However, it is easy to implement, and as a first approximation represents how inclusion of a ramp may affect the model fits.

The time over which ramping occurs may be gauged from flow rates in the CPP. In Henzler *et al.* (2004) the flow rates were 0.15-0.2 m s^{-1} for cells of 50-150 mm in length, so that for a cell length of 50mm (which was used for the models in this chapter) the time for the exchanged solution to traverse the length of the cell is 0.25-0.33 s. The ramp time can then be said to be around 0.33s, which is somewhat shorter than the time-delay determined from the observed negative OPP data (at least 0.73s; see §2.5.2a). However, mixing between solutions during the changeover would cause the ramp time to be longer, and also since the time of impact of the osmotic perturbation on the cell is unknown, uncertainty in t_0 has to be included in the uncertainty in the ramp time.

The numerical model was fit to the negative OPP experiment, using the Classical method where t_m is fit to within ± 0.05s. Two linear ramps (where the concentration in the external solution changes linearly with time) were included, both centered around 1.5s as this time-delay gave the best fit with the classical model. A ramp of 3s with $t_0 = 0$ (where t_0 is the start of the perturbation) was found to give a better fit than a ramp of 1.5s with $t_0 = 0.75$s. The model with a ramp fits the data extremely well, reproducing the time-delay, and giving a very low overall RMS error of 4.0×10^{-4} (Table 2.7; compare Fig. 2.4a & Fig. 2.8). This model may be considered a “perfect fit” to the data within experimental and model error. Estimated parameters were similar to the previous fit with no ramp and $t_0 = 1.5$s (Table 2.3).

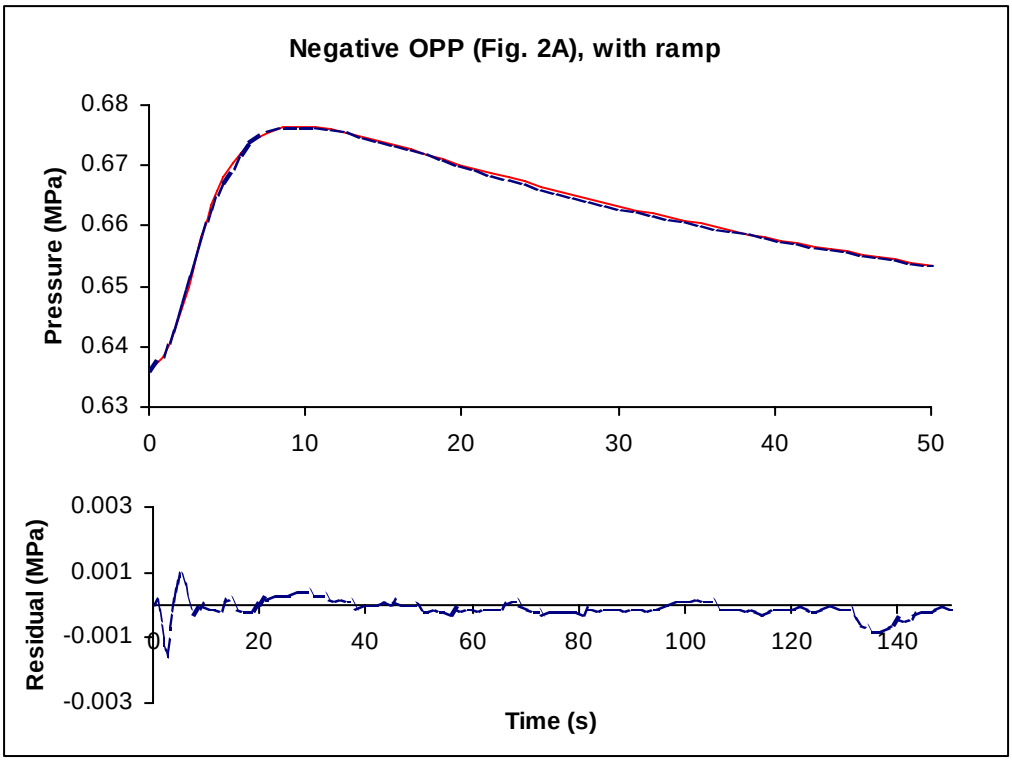

Fig. 2.8 *P-t* curve and residuals for a classical model + ramp fit to a negative OPP curve. Showing raw pressure data (----) and model fit (——). Note that the time scale for the *P-t* curve and residuals are different.

Table 2.7 Results for a fit to the negative OPP (Fig. 2A), using the classical model with external ramping (linear ramp) included. Errors are standard errors.

	Negative OPP	
ramp time (s)	3	
t_0 (s)	0	
L_p (x 10^6 m s^{-1} MPa^{-1})	2.63	±0.25
p_s (x 10^6 m s^{-1})	4.50	±0.005
σ	0.1274	±0.0016
RMS (x 10^{-4})	4.0	

(c) Role of unstirred layers

Unstirred layers (ULs) also contribute to the time-delay, since it takes some time for the solutes to diffuse through the external UL (ULe) to the membrane. Unstirred layers in general would slow down the diffusion of solutes through the membrane, and affect the whole relaxation curve. Since both external ramping and ULs contribute to the time-delay, it is not possible to determine to what extent each factor contributes to the time-delay unless there is an experimental method of determining the time it takes for the external solution to ramp up, or the time it takes for the solutes to move through the ULe. The latter is dependent on knowing the ULe thickness. However, a method of determining the ULe thickness in CPP experiments has not been reported in the literature. Due to the lack of experimental knowledge on ramping and ULs, and the fact that the shape of the input pulse and the shape of the ULe are modelled simplistically in this study, the impact of ramping and ULs can at present only be studied theoretically. Accordingly, the classical model with the addition of ULs will be the subject of Chapter 3.

2.8 Conclusions

The classical model, based on the analytical solution, has been analysed and applied to raw CPP data obtained from Dr. Henzler and Mr. Ye. The analytical solution was validated, and the necessary simplifying assumptions were shown to be numerically justified. The model was implemented in Excel, and Excel Solver used as a tool to estimate membrane parameters from observed *P*-*t* data. Membrane parameters were estimated using 2 methods: (a) the Classical method, which uses curve characteristics to fit the data, and (b) the RMS method, which optimizes the parameters such that the overall RMS error is minimized.

Results show that quite a good fit to observed *P*-*t* data can be obtained for the classical model with both fitting methods, for both HPP and OPP experiments. Although the methods are not mutually exclusive, they emphasise fitting different regions of the curve

and give different estimated parameters. The Classical method gives more weight to certain characteristics of the curve. Drawbacks are that its accuracy depends on how well curve characteristics from the data can be determined, and it does not fit noisy data well. The RMS method gives equal weight to all data points. A potential drawback is that regions where the cell dynamics are changing rapidly may not be fit well. However, this problem can be overcome by differentially weighting points in the minimized function (the RMS value) to improve the fit to the less well-fitted regions. The RMS method, therefore, will be used for subsequent data fits in this study. For comments on further use of curve characteristics, see §A.1 in appendix. While a low RMS error will be used as a guide to "best" fit, the RMS error does not uniquely determine a best fit, and the final decision will be made by making an analysis of the overall residuals between the model and data.

Fits with the Classical method confirmed that only a short initial period of the semilog plot should be used to calculate τ_w for the HPP curve (0-3 s for the data set used). This is due to the non-linearity in the semilog plot. Although Ye *et al.* (2006) state that this non-linearity is "an artefact" arising from measurement errors, using 2 additional values of P_E (0.001 MPa above and 0.001 MPa below the calculated P_E of the observed data) to calculate the slope of the semilog plot still revealed a slight nonlinearity (R^2=0.997). Although this is statistically very close to linear, the semilog plot slopes for the 3 different values of P_E still differed by about 10%, and the fact remains that L_p is very sensitive to the slope of the semilog plot. The results in §2.5.1 gave halftimes of 1.62s and 1.99s for semilog plot slopes which differed by 23%.

The method by which L_p from OPP experiments is estimated in other studies has not been described in the literature. In this study, L_p was determined numerically using an equation from the analytical solution to the KK equations. Using this method, it was found that the average L_p for the HPP experiments was 17% higher than L_p for the OPP experiment (L_p = 2.99 ± 0.05 m s^{-1} MPa^{-1} and L_p = 2.57 ± 0.21 m s^{-1} MPa^{-1} respectively). A higher L_p for HPP experiments agrees with results from Steudle and Tyerman (1983), who suggest that this behaviour is due to an external unstirred layer influencing the pressure dynamics

in OPP experiments. Estimated parameters for positive and negative pulses for both the HPP and OPP experiments did not differ significantly, although differences in the estimated L_p between positive and negative pulses have been observed in the literature (*ibid.* 1983).

The classical model was found to predict the cell dynamics very well, despite the simplifying assumptions in the theory. The main drawbacks of the model are its inability to properly fit the shoulder of HPP relaxation curves, and the initial curvature and time delay in OPP relaxation curves. It was found that the first could be solved by fitting the HPP data with a double exponential, and the second could be solved by assuming a gradual rather than an instantaneous change in the external concentration.

These results suggest that a single exponential does not accurately represent the cell dynamics in a HPP experiment. A likely explanation is that the influence of the tonoplast on cell dynamics is being ignored, thus illustrating the limitations to viewing the cell as a single membrane rather than a composite membrane. Models of HPP pressure relations in wheat root cells (Zhang and Tyerman, 1999) revealed that a double exponential function fit the data better when aquaporins were blocked, showing the inadequacy of using a single exponential function when the influence of the tonoplast and plasma membrane are both significant. The blocking of aquaporins may impact the hydraulic conductivity of the tonoplast and plasma membrane differently depending on the amount of aquaporins in each.

A double exponential representation would mean that the expression for the hydraulic conductivity L_p in Eq. (2.13) no longer applies. This will not be explored here, but merely pointed out that the expression for L_p used in current practice may be incorrect, and impact on the accuracy to which L_p can be determined by current means.

Although the ramp change in external concentration assumed in an OPP is unrealistic, the resulting improvement to the classical model shows that the time and form in which the external perturbation impacts on the cell is an important consideration. If ramping is not

included, t_0 must be adjusted or optimized to obtain a good fit to the data. L_p in particular is very sensitive to the value of t_0.

The time-delay observed in the OPP data may, however, be attributed to a combination of ramping in the external concentration (see §1.2), and effects of an external unstirred layer which would delay the external solute from reaching the membrane. The classical model may be made more realistic by the incorporation of ULs, which would impact on the parameter estimation. (It may also be made more realistic by including the effects of the tonoplast, but that is beyond the scope of this study.) In Chapter 3 we will incorporate UL effects into the models, and explore their impact on the model fits and parameter estimation.

3 Model with Unstirred Layers: Description of model and analysis of behaviour

3.1 Introduction to unstirred layers

3.1.1 What is an unstirred layer?

An unstirred layer (UL) is a still or slow-moving region of laminar flow adjacent to a solid boundary (in this case the membrane), within which there is no significant mixing of the solution (Dainty, 1963). For a cell there exist external (ULe) and internal (ULi) ULs (see schematic diagram in Fig. 3.1). The internal ULi may be considered to be the entire cell interior (Barry and Diamond, 1984), however in this study the possibility is allowed for a homogeneous region within the cell beyond the ULi. The dynamics in the region inside the cell, including the ULi, are governed only by the membrane and change in concentration across the membrane. The bulk solution which lies beyond the ULe is a region in which a constant flow of solution maintains the concentration at a constant value, and this region can be considered to be well-mixed and homogeneous.

Although in the absence of stirring some mixing in the ULs may occur because of solute, water density, or temperature gradients, a UL may effectively be modelled as a region where solutes primarily move by diffusion (Barry and Diamond, 1984). A smaller convective component due to volume flow across the membrane also exists in the UL, which has been discussed in Barry and Diamond (1984), and included in equations by Kargol (2000).

Fig. 3.1 depicts a positive osmotic perturbation, where the concentration in the bulk solution has been increased. As solutes diffuse through the ULe from the bulk solution, the concentration decreases toward the membrane, encounters a drop across the membrane due to the membrane resistance, and continues to decrease as the solutes move further inside the cell. Over a sufficient length of time an equilibrium level will be reached where the solute concentration is equal in all regions inside and outside the cell.

In Fig. 3.1 the non-membrane ULe and ULi boundaries are shown and treated as distinct entities. The model ignores mixing at these boundaries, and assumes that the concentration in the homogeneous regions remain constant so that there is a discontinuity in the concentration gradient at the outer ULe boundary. The concentration gradient is the same either side of the membrane.

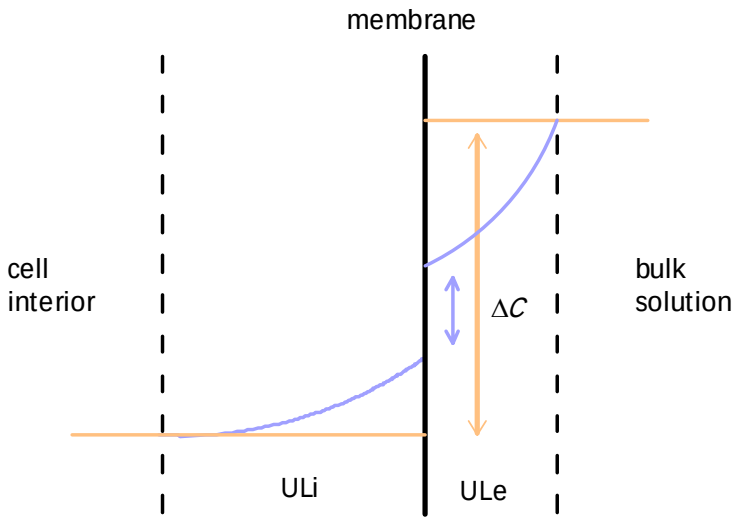

Fig. 3.1 Schematic diagram showing a system with 1 membrane and an internal (ULi) and an external (ULe) unstirred layer. In the absence of unstirred layers the concentration inside and outside the cell are constant in time and space (orange line); with unstirred layers the concentration varies with time and space within the ULs (blue line). Unstirred layers change the concentration difference (ΔC) at the membrane.

3.1.2 Significance of ULs to CPP experiments

ULs significantly affect the measurement of membrane-specific parameters. This is because solute movement across a membrane may be partly rate-controlled by ULs and not solely governed by the membrane (Barry and Diamond, 1984; Verkman, 2000). The solute concentrations governing transport across a membrane are those immediately adjacent to the membrane. These are not observable and are determined in part by the dynamics of the ULs. Also, they are not equal to those in the bulk solution which are the directly observed and measurable quantities (Dainty, 1963; Barry and Diamond, 1984;

Kargol, 2000). UL effects also depend on the membrane geometry and surface area (Verkman, 2000), and on the orientation of the membrane relative to the moving solution.

Direct effects of ULs cannot be observed. However, there is experimental evidence from observed behaviour of the measured (classically-estimated) membrane parameters L_p, p_s, and σ that ULs may be affecting fluxes of solutes and water across cell membranes. This evidence includes:

(a) A dependence of the classically-estimated parameters on external flow rate. In osmotic experiments, the classically-estimated L_p and p_s have been found to increase with increasing flow rates (Steudle and Tyerman, 1983). This behaviour can be explained by examining the impact of ULs on the KK equations. Increasing the external flow rate increases mixing in the external solution which in turn reduces the size of external ULs. Eq. (2.1) expresses a direct linear response between the volume flow J_V and the pressure gradients across the membrane, related to each other by the constant L_p. If ULs are present, J_V may change linearly with the pressure gradients across the membrane but not with the pressure gradients in the bulk solution. Since the classical method uses pressure gradients in the bulk solution to approximate those at the membrane, the classically-estimated L_p derived using Eq. (2.1) may no longer be constant if the external UL thickness and thus pressure gradients at the membrane are changed. As Eq. (2.2) is coupled to Eq. (2.1), this would affect the values of p_s and σ also.

(b) A dependence of the classically-estimated parameters on external solute concentration. In osmotic experiments (and hydrostatic experiments in the case of L_p), the classically-estimated L_p and σ have been found to decrease with increasing external solute concentration (Steudle and Tyerman, 1983; Steudle and Zimmermann, 1974). ULs may be expected to have a greater effect on membrane parameters in the presence of higher external solute concentrations. This is because, similar to (a), the classical method uses the concentrations in the bulk solution to approximate the concentrations at the membrane in Eqs. (2.1) & (2.2).

(c) An observed polarity in the classically-estimated membrane parameters, where the parameters differ in magnitude between positive and negative perturbation pulses. A polarity in L_p has been observed in both hydrostatic and osmotic experiments, which is more marked at higher external solute concentrations (Zimmermann and Steudle, 1978; Steudle and Tyerman, 1983; Steudle, 1993). Polarity is where a change in direction of a pressure gradient (of the same magnitude) causes not only a change in direction but a change in magnitude of the flow as well (Kedem and Katchalsky, 1963c). If the ULi and ULe are of unequal thickness, the cell pressure may respond differently to opposite flow directions across the membrane.

Although the above observations may be explained by the presence of ULs, this explanation in itself does not seem sufficient. In particular, the subject of polarity in L_p has been much debated, and the general consensus is that it is probably partly due to ULs and partly due to properties of the membrane. Dainty (1963) has stated that a polar permeability to water is not surprising in biological membranes, but also "the influence of unstirred layers...[can] produc[e] a certain degree of apparent polar permeability to water". Polarity may also be related to the presence of a tonoplast, as Kedem and Katchalsky (1963c) have predicted that polarity and non-linearity between forces and flows should arise in composite membranes (and that therefore polarity in p_s and σ should also arise, although there seems to be little mention of this in the experimental literature). There is general agreement that ULs should cause an under-estimation of p_s and σ in CPP experiments (Henzler and Steudle, 1995; Barry and Diamond, 1984), however to what extent is unclear. A numerical study on the effects of ULs, using a simple membrane model, may therefore shed light on contributing factors to these experimental observations.

3.1.3 How ULs affect cell pressure dynamics and the measurement of membrane parameters

Diffusion in unstirred layers contributes a resistance in series with the membrane, and slows the flow of solutes through the membrane (Barry and Diamond, 1984). Convection (solvent drag) in the UL and the movement of the membrane also affect the concentration

distribution by causing solutes to build up on one side of the membrane and decrease on the other. ULs affect overall solute transport by reducing the effective concentration gradient across the membrane, and by causing the solute concentration in the UL to change with time and space (Dainty, 1963). The classical model outlined in Chapter 2 assumes complete mixing of the bulk solution and hence a uniform concentration with space on either side of the membrane. By corollary this implies ULs are absent.

A detailed review of ULs has been written by Barry and Diamond (1984), in which they identified two main effects of ULs on membrane parameters for systems in steady state flux:

(a) A 'gradient-dissipation effect'. This may occur when a significant fraction of the concentration gradient occurs across a UL (such as occurs with thick ULs), so that the UL's diffusional resistance is comparable to or greater than the membrane resistance. As a result, classically-estimated values of p_s and σ tend to underestimate the actual membrane parameters (Barry and Diamond, 1984), as is the case for L_p (Wendler and Zimmermann, 1985b).

(b) A 'sweep-away effect' (or 'concentration polarization', 'convective-flow effect'). This may occur due to convection (solvent drag) in the UL, sweeping away solutes from the membrane surface downstream from the water flow, and concentrating solutes on the upstream side of the membrane. This reduces the volume flow J_v because the flow perturbs the solutes in a direction that opposes J_v, i.e. the outward convective solute movement is opposed by inward diffusion in the UL. In steady state this can be described by the following equation from Fick's first law (Dainty, 1963):

$$J_v C + D\frac{dC}{dr} = 0 . \qquad (3.1)$$

Since there is a large diffusive component in the UL, these opposing flows cause J_v to be lower than that in the absence of a UL, leading to an underestimation of L_p, p_s and σ (Dainty, 1963; Barry and Diamond, 1984; Steudle, 1993). ULs can

give rise to what has been termed ‘pseudo solvent drag’, where the measured or observed solvent drag is not purely solvent drag (see Barry and Diamond, 1984).

In CPP experiments, gradient-dissipation (diffusional) effects in the UL are thought to be more important than sweep-away effects, since volume flows through the cell membrane are small (Henzler and Steudle, 2000; Hertel and Steudle, 1997; Steudle, 1993; Steudle and Tyerman, 1983; Zimmermann and Steudle, 1978). Analysis of the classical model in §2.7.2 confirmed this. The gradient-dissipation effect can be analysed by noting that $1/p_s$ is a resistance, and exploring effects on p_s due to diffusion.

Forming an analogy with Kirchoff’s law for electrical circuits, which says that resistances in series are additive, the total permeability p_T across the membrane-UL system for the cylindrical case can be expressed as:

$$\frac{1}{p_T} = \frac{1}{p_m} + R\left(\frac{1}{D_1}\ln\frac{R}{a} + \frac{1}{D_2}\ln\frac{b}{R}\right) \tag{3.2}$$

(Steudle and Frensch, 1989; see also §A.3 in appendix). In Eq. (3.2) D_1 is the diffusivity for the region inside the cell, D_2 is the diffusivity for the region outside the cell, p_m is the membrane permeability, b is the radial distance to the boundary of the ULe, a is the radial distance to the boundary of the ULi, and R is the radius of the cell.

If $D_1 = D_2 = D$, as is often assumed, then Eq. (3.2) becomes:

$$\frac{1}{p_T} = \frac{1}{p_m} + \frac{R}{D}\ln\left(\frac{b}{a}\right),$$

which can be re-arranged as:

$$p_T = \frac{p_m}{1 + \frac{p_m R}{D}\ln(b/a)}\ . \tag{3.3}$$

Eq. (3.3) shows that for large values of p_m,

$$p_T \cong \frac{D}{R\ln(b/a)},$$

where the apparent (measurable) permeability p_T is dominated by diffusion in the ULs.

For small values of p_m, where $p_m \to 0$,

$$p_T \to p_m .$$

The above analysis shows that for rapidly permeating solutes (with high p_m), the apparent membrane permeability is partially rate-controlled by the ULs, so that the classically measured permeability will underestimate p_m. For slowly permeating solutes, the apparent permeability approaches the actual membrane permeability. That is, depending on the size of p_m, the overall resistance of the membrane-UL system may be dominated by either the diffusional resistance of the membrane itself, or the diffusional resistance of the ULs (Dainty, 1963; Barry and Diamond, 1984). ULs are predicted to have more effect on the observed, total solute permeability p_T for larger values of the membrane permeability p_m. Dainty (1963) considers a permeability "greater than a few times 10^{-7} m s^{-1} suspect" to UL errors. When no ULs are present, we have $b \to R$, $a \to R$, and $p_T \to p_m$.

It is important to note that Eq. (3.2) is strictly valid only for systems in steady state. The equations may not hold for the models here since they deal with systems not in a steady state.

3.1.4 Taking into account effects of ULs

In CPP experiments external ULs are minimized by vigorous stirring (Henzler *et al.* 2004, Henzler and Steudle, 2000; Tyerman and Steudle, 1984). Parameter measurements from OPP experiments are dependent on the external flow rate, reflecting the presence of ULs since the actual permeability of the membrane should not depend on stirring rates (Steudle and Tyerman, 1983; Verkman, 2000). Steudle and Tyerman (1983) varied the

external flow rate between 5 and 44 cm s^{-1}, and found that their estimated membrane parameters increased rapidly at first and then less rapidly at the higher rates. They guessed the ULe in *Chara corallina* to be 50-100 μm thick, and probably no more than 50μm for a vigorously stirred system. Although some authors have described the external flows as turbulent (Ye *et al.* 2006), the external flow is most likely laminar even for flow rates of 44 cm s^{-1} or more (Tyree *et al.* 2005).

The internal UL cannot be minimized, and has been guessed to be a few hundred micrometers thick (Hertel and Steudle, 1997), and as large as the entire cell radius (Barry and Diamond, 1984). Although the ULi thickness is significant, Hertel and Steudle (1997) and Henzler and Steudle (2000) have claimed that since the interior of *Chara* is "relatively well-stirred" by cytoplasmic streaming, and the cell has a cylindrical geometry, effects of internal ULs should be minimal. However, a comprehensive study of ULs by Barry and Diamond (1984) has shown that internal ULs may be more important than external ULs, more problematic to deal with, and that the diffusional resistance of the cytoplasm may be a dominating factor when measuring L_p and other transport parameters. It is doubtful that cytoplasmic streaming would contribute much to the radial convection or diffusion of solutes, since it has a low velocity (~4 cm hr^{-1} = 0.0011 cm s^{-1}, Tyree *et al.* 1974) and is parallel to the membrane surface. This flow rate is much slower than the flowrates of > 15-20 cm s^{-1} commonly used in CPP experiments to minimize external ULs (Henzler *et al.* 2004). The vacuole is also largely water and is unstirred, so that the entire cell interior could in fact be considered an unstirred compartment, with the size and effects of internal ULs increasing with cell size (Barry and Diamond, 1984).

CPP experimenters have attempted to take ULs into account by correcting for UL effects in parameter calculations (Steudle and Zimmermann, 1974; Steudle and Tyerman, 1983; Henzler and Steudle, 1995; Hertel and Steudle, 1997). It is not clear, however, that parameters determined by the above experimenters have actually been corrected for UL effects. Firstly, the classical model on which calculations are based makes no provision for this, and secondly, corrections have not been rigorous since claims regarding the impact of ULs have mostly been qualitative. Hertel and Steudle (1997), and Henzler and Steudle (2000), considered possible impacts of ULs and, by various arguments, declared they are not "dominating" transport. Henzler and Steudle (2000) argued that diffusion is

not a big limiter to solute permeation, since pressure-time curves could be "nicely fitted" by single exponentials. They observed a wide range in permeability values for different solutes with similar diffusion coefficients, which they concluded meant the parameters should reflect the permeability of the membrane. Yet, even if it was the case that effects of ULs are not "dominating" transport, this does not mean the effects of ULs are negligible or do not have a hidden, systematic impact on permeability measurements. A proper, quantitative study of the effects of ULs on CPP measurements does not appear to have been carried out.

Some quantitative studies of the effects of diffusion in ULs on permeability coefficients have been carried out for radioactive tracer and transcellular osmosis techniques in *Chara*. In these experiments the effects of ULs were found to be considerable for very permeant solutes (Dainty and Ginzburg, 1964c,d). Various CPP experimenters have inferred that since results from both CPP and transcellular osmosis experiments appear to be consistent, ULs in CPP experiments have a low impact (Dainty, 1976; Zimmermann and Steudle, 1978; Henzler and Steudle, 1995; Henzler and Steudle, 2000). Yet this is hardly conclusive, since it assumes the corrected values in Dainty and Ginzburg (1964c,d) are the true values for the membrane, but Dainty and Ginzburg (1964c) state that their analysis underestimates the impact of ULs. Steudle and Tyerman (1983) state that while "a rather good agreement with Dainty and Ginzburg's (1964c) values" may indicate that effects of ULs in their experiments are small, at the same time they concede that "unstirred layers are a problem" and that p_s is "almost certainly underestimated as a result of unstirred layers." Any attempt to compare CPP results to that of transcellular osmosis only reveals the shortcomings of existing analyses of CPP measurements. In general, an objective analysis of the effects of ULs in CPP experiments is lacking, and efforts have largely concentrated on dismissing the effects of ULs. However, there are other experimenters who have little doubt that ULs affect parameter determinations, and must be considered (Dainty, 1963; Dainty, 1976; Heidecker *et al.* 2003).

Apart from the lack of rigor, another disadvantage of previous "quantitative" studies which have attempted to correct for the impact of ULs in CPP measurements, is that the analyses have been valid only for systems in steady state. For example, using Eq. (3.3) Steudle and Frensch (1989) derived an equation for the apparent reflection coefficient in

the presence of ULs, however the equation only holds for a system in steady state. Hertel and Steudle (1997) assumed an upper limit to the ULe of 50μm, and argued that since the time it takes for solutes to diffuse through the ULe is much smaller than the halftime τ_s of equilibration of solutes, the influence of external ULs can be discarded. However, Hertel and Steudle (1997) have failed to consider the temporal behaviour of ULs and its possible impact on membrane transport, so their argument is not necessarily valid, as will be shown in the present study.

In the present study the system is assumed to be in non-steady state. The result is a model which more accurately reflects reality and thus should more accurately reflect the impact of ULs on CPP measurements. This is an important difference between the present study and previous studies of UL effects in the CPP.

It is argued here that ULs have an important impact on parameter measurements, and that effects of ULs in CPP experiments require close examination. Although external ULs may be minimized by stirring, neither external or internal ULs can be eliminated. Due to the difficult nature of experimentally identifying the precise effects of ULs, modelling can make a significant contribution by making a quantitative assessment of these impacts. In this study a numerical approach is taken to examine the impact of ULs. There are two main questions to answer, namely:

(a) How do the presence of ULs affect the pressure-change dynamics in the cell?
(b) How do the presence of ULs affect the parameter values determined by the classical method?

3.2 The present model in the context of previous models

3.2.1 Brief review of numerical models

Many numerical models of membrane-UL systems have been developed by researchers in various fields, where KK equations are applied across a membrane, and Fick's equations applied to the ULs. However, only a few models have been developed for plant

cell or plant tissue systems. A couple of those relevant to the model or system in this study are reviewed here.

Kargol (2000) derived generalised KK equations for transport through a planar membrane-UL system. Expressions for concentration in the ULs were derived using Fick's diffusion-convection equations, and substituted into Kedem-Spiegler equations (similar to the KK equations) for local fluxes at the membrane. The final linearized equations express fluxes across the membrane-UL system in terms of the membrane parameters, bulk concentration values, and UL thicknesses. The equations are for steady state where fluxes are constant with space and time, and concentration profiles linear with space. The equations do not solve for concentration at the membrane surface. In contrast to Kargol (2000), the present study applies the much simpler classical KK equations at the membrane. Concentration at the membrane surface is determined using Fick's diffusion-convection equation in the ULs, which is coupled to the KK equations at the membrane. The cell is assumed to be cylindrical, and the equations are solved under non-steady state conditions. Fluxes change over time, and concentration profiles in the ULs are nonlinear with space.

Devireddy (2005) modelled water and solute transport in human ovarian tissue sections, applying the KK equations in the membrane regions and Fick's laws in the vascular regions. Axial convection and radial diffusion were assumed, and outputs were solute concentration vs. time in a tissue segment. The model was fit to data using nonlinear least squares curve fitting, and membrane parameters and diffusion coefficients predicted at different temperatures. In contrast to Devireddy (2005), in the present study transport is assumed to be in the radial direction only, and outputs are pressure vs. time in a cell.

Murphy (1999) developed a model in the context of pressure clamp experiments. He developed a numerical 2-compartment model of the root without ULs and examined the response of the model to a pressure clamp. Equations for the overall volume flux across the root were based on the KK equations. In contrast to Murphy (1999) the model presented here is applied to pressure probe experiments on plant cells, and includes ULs.

The model in the present study combines elements of the above models. KK equations and Fick's equations are used in conjunction, and solved for non-steady state conditions. Cell membrane parameters are estimated by fitting the model to data using nonlinear least squares curve fitting. Pressure vs. time is predicted for a membrane-UL system in a cylindrical cell where flow is assumed to be in the radial direction. The model is applied to the conditions of a cell pressure probe experiment, and water dynamics in response to a pressure probe are examined.

3.2.2 Description of present model

The *Chara* system is the same as described previously, with the addition of internal or external ULs. The UL thicknesses δ_{ULe} and δ_{ULi} are unknown, and are varied to examine the effects of different UL thicknesses on the pressure dynamics. The δ_{ULe} is chosen to be in the range 0-200 μm, and the ULi is permitted to occupy the entire internal cell volume. Standard diffusion theory, and Fick's diffusion-advection equations, are applied to the UL regions. The diffusivity D is assumed to be constant and the same for both ULs, and equal to D for the solute in pure water taken from published chemistry tables.

It is assumed that standard KK theory applies to the cell membrane in the presence of ULs, and that at the membrane the flow in the ULs equals the flow across the membrane as given by the KK equations. The full KK equations, Eqs. (2.1) & (2.2), are used in all the models here so solute drag in the J_s equation is not neglected, in contrast to the classical model used in Chapter 2. Further, the cell volume V in the P-V equation (Eq. (2.5)), and the cell surface area A, are assumed to be variable (c.f. §2.2.2) and determined from the cell radius R. ε is assumed to be a constant.

It is assumed that in a CPP experiment the external solution flows past the cell in the axial direction only. Although the cell does not usually lie such that its axis is parallel to the walls of the CPP chamber, for modelling purposes it shall be assumed that this is so. Following this, it is assumed that there is no flow of the external solution in the radial direction and no flow into the cell, for although there is some flow into the ends of the cell, the area of these regions comprises <1% of the total cell surface area and can therefore be ignored. Flow of the solution into the ends of the cell could be significant if

the hydraulic conductivity L_p of these regions is larger than the L_p of the rest of the cell membrane, however, in this model L_p is assumed to have a single value for the entire cell membrane.

Water flow into and out of the cell is caused by hydrostatic and osmotic pressure gradients across the membrane, and not by an external flow of solution into the cell. Since both cell sap and APW are assumed to be incompressible, water flux across the membrane does not give rise to convective movement inside or outside the cell. However, a *relative* convection is present in the radial direction due to radial movement of the system (the membrane and ULs) through the external solution which is not moving with *r*. That is, in the frame-of-reference of the cell membrane, the external solution is "seen" to be moving with *r*, and therefore there exists a radial flow velocity which is variable in space.

As the membrane moves due to cell expansion or contraction, conditions in the ULs change accordingly. It is unknown whether the ULs move with the membrane, or whether the UL boundaries remain stagnant as the membrane moves. Both scenarios, therefore, will be modelled. However, it is important to note that the total radial movement of the membrane is a very small fraction of the UL thickness, e.g. typically less than 5μm during a CPP experiment.

3.3 Derivation and interpretation of diffusion equations

The movement of the cell membrane, which forms one boundary of the ULe and ULi, is a moving boundary problem for diffusion in the ULs. This has important implications for the application and solution of the diffusion equations. The ULs are divided into grids which facilitate finite difference approximations to differentials, and since the membrane moves volume elements in the ULs are variable in time and space.

Either Fick's first or second law can be used to model diffusion in the ULs. For theoretical interest both are given in this section, but for practical reasons only the first law is used for the numerical solution in §3.5.

3.3.1 Fick's first law

We consider a cylindrical system with flux in the radial direction only. Fick's first law for the flux *J(r,t)* at any point is given by:

$$J(r,t) = -D\frac{\partial C}{\partial r} + \nu C \qquad (3.4)$$

where r = radial distance from the centre of the cell, D = diffusion coefficient (which depends on the solute and solvent), C = solute concentration, and $\nu = \nu(r)$ is a radial flow velocity (convection) at that point.

The radial flow velocity v across the membrane is defined as:

$$v = J_V / \varphi \qquad (3.5)$$

where the flow-constriction factor φ denotes the fraction of the membrane area available for volume flow (Barry and Diamond, 1984; Kargol, 2000). Since pores or water channels in the membrane are not included in the model here, it is assumed the entire membrane area is available for volume flow so that $\varphi = 1$, and $v = J_V$. It can readily be shown that $v = J_V = -dR/dt$, where R is the radius of the cell, and reflects the fact that v is a relative velocity due to the movement of the membrane, and not bulk flow of a solution. The radial flow velocity in the ULs is given by:

$$v = -dr/dt \qquad (3.6)$$

where r is a radial point in the ULs.

3.3.2 Fick's second law

We consider a cylindrical shell with volume V and total surface area S. Let the flux *J(r,t)* be in the radial direction through S, and *C(r,t)* the concentration at any point inside V. The conservation of mass equation for the cylindrical shell is:

$$\frac{d}{dt}\iiint_V C(r,t)dV = -\iint_{S(r,t)} \boldsymbol{J}(r,t).\boldsymbol{n}\, dS \quad , \tag{3.7}$$

where $\boldsymbol{n}$ is an outward normal vector.

If $C(t)$ is the average concentration inside V, the mean value theorem can be applied to the L.H.S to give:

$$\frac{d}{dt}(CV) = -\iint_{S(r,t)} \boldsymbol{J}(r,t).\boldsymbol{n}\, dS \quad . \tag{3.8}$$

Let $A_1(r_1,t)$ and $A_2(r_2,t)$ be the outer and inner surface areas of S respectively. If J_1 is the flux across A_1 and J_2 is the flux across A_2, integrating the R.H.S of Eq. (3.8) gives:

$$\frac{d}{dt}(CV) = -(J_1A_1 - J_2A_2)\,, \tag{3.9}$$

$$\boxed{\frac{dC}{dt} = -\frac{J_1A_1 - J_2A_2}{V} - \frac{C}{V}\frac{dV}{dt}} \tag{3.10}$$

where C is the average concentration inside the cylindrical shell.

From Fick's first law we have for the fluxes across areas A_1 and A_2:

$$J_1 = -D\left.\frac{\partial C}{\partial r}\right|_{r+\Delta r} + \left(\nu C\right)_{r+\Delta r}, \tag{3.11}$$

$$J_2 = -D\left.\frac{\partial C}{\partial r}\right|_{r} + \left(\nu C\right)_{r}. \tag{3.12}$$

Taylor's expansion of J_1 to first order gives:

$$J_1 = -D\left(\frac{\partial C}{\partial r} + \frac{\partial^2 C}{\partial r^2}\Delta r\right)_r + \left(\nu + \frac{\partial \nu}{\partial r}\Delta r\right)_r \left(C + \frac{\partial C}{\partial r}\Delta r\right)_r$$

$$= -D\frac{\partial C}{\partial r}\bigg|_r - D\frac{\partial^2 C}{\partial r^2}\bigg|_r \Delta r + (\nu C)_r + \left(\nu\frac{\partial C}{\partial r}\Delta r\right)_r + \left(C\frac{\partial \nu}{\partial r}\Delta r\right)_r + O(\Delta r^2)$$

$$= J_2 - D\frac{\partial^2 C}{\partial r^2}\bigg|_r \Delta r + \frac{\partial}{\partial r}(\nu C)_r \Delta r + O(\Delta r^2). \qquad (3.13)$$

Applying Eqs. (3.12) & (3.13), the first term in Eq. (3.10) is:

$$-\frac{J_1 A_1 - J_2 A_2}{V} = -\frac{J_1 2\pi L(r+\Delta r) - J_2 2\pi L r}{\pi((r+\Delta r)^2 - r^2)L}$$

$$= \frac{-J_1(r+\Delta r) + J_2 r}{\Delta r(r + \Delta r/2)}$$

$$= -\frac{-(r+\Delta r)\left(J_2 - D\frac{\partial^2 C}{\partial r^2}\Delta r + \frac{\partial}{\partial r}(\nu C)\Delta r\right) + rJ_2}{\Delta r(r+\Delta r/2)}$$

$$= \frac{-J_2 + D\frac{\partial^2 C}{\partial r^2}(r+\Delta r) - \frac{\partial}{\partial r}(\nu C)(r+\Delta r) - \frac{\partial \nu}{\partial r}\frac{\partial C}{\partial r}\Delta r(r+\Delta r)}{r + \Delta r/2}. \qquad (3.14)$$

In the limit as $\Delta r \to 0$, the variables and derivatives which strictly applied at values of *r* on the shell boundaries apply in the middle of the shells. Eq. (3.10) becomes:

$$\frac{dC}{dt} = D\frac{\partial^2 C}{\partial r^2} - \frac{\partial}{\partial r}(\nu C) - \frac{J_2}{r} - \frac{C}{V}\frac{dV}{dt}$$

$$= D\frac{\partial^2 C}{\partial r^2} - \frac{\partial}{\partial r}(\nu C) + \frac{1}{r}D\frac{\partial C}{\partial r} - \frac{\nu C}{r} - \frac{C}{V}\frac{dV}{dt},$$

$$\therefore \quad \boxed{\frac{dC}{dt} = \frac{1}{r}\frac{\partial}{\partial r}(rD\frac{\partial C}{\partial r}) - \frac{1}{r}\frac{\partial}{\partial r}(vrC) - \frac{C}{V}\frac{dV}{dt}} \qquad (3.15)$$

using Eq. (3.12). Eq. (3.15) is the same as the usual Fick's 2nd law in polar coordinates, but with an additional term *dV/dt* due to the moving boundaries of the volume elements. Analytical solutions to the usual form of Fick's 2nd law, subject to different boundary conditions, are detailed comprehensively in Crank (1975). Some solutions are also given by Dworecki *et al.* (2000) and Dworecki *et al.* (2003) in their analysis of concentration profiles in membrane boundary layers.

These expressions for Fick's second law are of little advantage in the present model, and therefore the application of Fick's first law will be focussed on.

3.4 Numerical approach to solving the diffusion equations

3.4.1 Numerical approach

There are three ways the model can be numerically implemented:

1. Assume the outer ULe and inner ULi boundaries are fixed relative to the cell axis, and the thickness of the ULs (δ_{UL}) and numerical grids change over time as the cell expands or contracts;

2. Assume the outer ULe and inner ULi boundaries move in space with the membrane, and the thickness of the ULs and numerical grids remain constant over time;

3. Assume that the outer ULe and inner ULi boundaries are fixed, and all the numerical grids in the ULs are also fixed, except for the two immediately adjacent to the membrane which change width over time.

The first two are more mathematically rigorous than the third, since the numerical scheme should place no conditions on the relative width of the grids, for which $\Delta r \to 0$ in the limit. However, as the third approach has been used elsewhere (Tyree *et al.* 2005) this model is included here to check its results with a more rigorous approach. All three schemes should give the same results, since the membrane moves only slightly during the course of a CPP experiment and the change in volume of the cell (and UL) at any one

time step is small relative to the total cell volume. However, a limitation of the second approach is that the ULi thickness is only able to come close to but not equal the entire cell volume, for the center of the cell is fixed and cannot move. A limitation of the third approach is that it may become numerically unstable when Δr is made sufficiently small such that the membrane moves further than the width of a grid.

All three approaches were implemented, and found to give the same quantitative results. Runtimes for a simple simulation of CPP dynamics were the same to within 3%. Runtimes for parameter estimations, involving many simulation runs, varied between the methods by differing amounts depending on the model conditions.

Implementation of the first 2 methods is described in §3.5. For ease of reference the first method is named the "Varying δ_{UL} method", and the second method named the "Fixed δ_{UL} method". Characteristics of each are that:

1. **Varying δ_{UL} method:** Non-membrane UL boundaries are fixed, δ_{UL} changes over time. dr_j / dt differs for each radial point r_j in the UL. The shell spacing Δr is dependent on t. Radial points r_j, the surface area A_j, and volume V_j of the shells change with time.

2. **Fixed δ_{UL} method:** Non-membrane UL boundaries move with the membrane, and δ_{UL} remains constant over time. $dr_j / dt = dR / dt$ where R is the cell radius. In the frame-of-reference of the membrane the shells are fixed so that the shell spacing Δr remains constant over time. Radial points r_j, the surface area A_j, and volume V_j of the shells change with time.

3.4.2 Indexing

Let R be the radial distance to the membrane, R_a be the radial distance to the inner ULi boundary, and R_b the radial distance to the outer ULe boundary. The ULs are segmented into concentric shells of width Δr (i.e. denotes shell spacing), and which have the same

cylindrical geometry as the cell. Let the number of shells in the ULe be *m-1* and the number of shells in the ULi be *n-1*.

The indexing was chosen to step inwards from the bulk solution towards the cell axis, in both the ULe and ULi, since in an OPP the perturbation occurs outside the cell and propagates inwards. The midpoint of each ULe shell is at a distance r_j from the center of the cell, where $j = 1{:}m$. The index 1 corresponds to a point outside the ULe (in the bulk solution), and the index m corresponds to the midpoint of the shell externally adjacent to the membrane. This is illustrated in Fig. 3.2. Similarly, the midpoint of each ULi shell is at a distance r_j from the center of the cell, where $j = 1{:}n$. The index 1 corresponds to the midpoint of the shell internally adjacent to the membrane, and the index n corresponds to a point outside the ULi in the central region of the cell.

The j^{th} shell has volume V_j, and inner and outer surface areas A_{j+1} and A_j respectively. The indexing of V_j corresponds to that of r_j. The volume of the bulk solution is assumed to be infinite. The total number of A_j values is *m-1* for the ULe and *n-1* for the ULi, 1 less than that for r_j and V_j in each of the ULe and ULi regions.

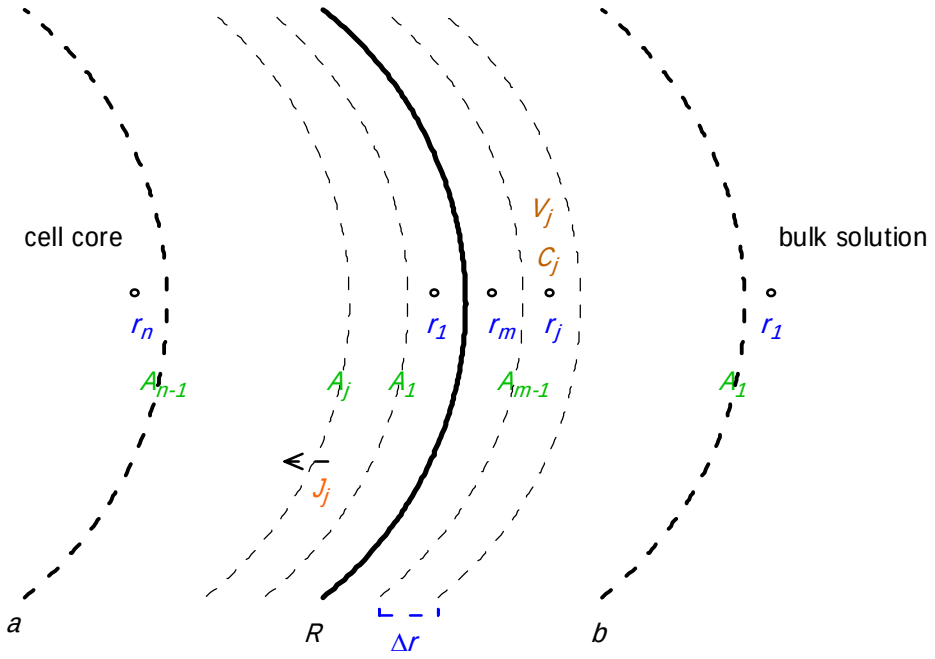

Fig. 3.2 Indexing for the numerical UL model

The distance between the midpoint of 2 adjacent shells is equal to the width of a shell. C_j is the concentration at the midpoint of the shells (at each r_j), and J_j is the flux across the shell boundaries (at each A_j).

The numerical code was made compatible with the no-ULs case, by making m=1 when no ULe is present, and n=1 when no ULi is present.

3.5 Numerical solution of the diffusion equations

Transport in the ULs may be solved by applying either Eqs. (3.10) & (3.4), or Eq. (3.15), since the latter is derived from the former. It was chosen to use Eqs. (3.10) & (3.4), as this avoids second derivatives, and the method of solution is more straightforward and more numerically stable. Explicit finite differences based on Euler's method (Ames, 1977) were used for the equations, and found to be sufficiently stable and accurate for the problem.

The areas A_j, fluxes J_j, and velocities v_j are solved at the UL shell boundaries, and the concentrations C_j and shell volumes V_j are solved at the middle of the shells (see Fig. 3.2). A point at the center of a shell has radial coordinate r_j, and a point on a shell boundary has radial coordinate r_{Bj}. Time steps are denoted by the superscript 'k'.

3.5.1 Main equations

For each j^{th} shell in the UL, the flux J_j across a shell boundary is given by:

$$J_j = -D\frac{\partial C_{Bj}}{\partial r_{Bj}} + vC_{Bj} \tag{3.16}$$

where C_{Bj} is the concentration at the shell boundary and determined by averaging the concentration across 2 adjacent shells.

From Eq. (3.9), the mass balance equation for a shell is:

$$\frac{d}{dt}(C_j V_j) = J_j A_j - J_{j-1} A_{j-1}, \tag{3.17}$$

where C_j is determined at the center of the shells.

Eq. (3.17) can be expanded and then finite-differenced, however the indexing is clearer when finite differences are made directly. This gives:

$$C_j^{k+1} V_j^{k+1} - C_j^k V_j^k = (J_j^k A_j^k - J_{j-1}^k A_{j-1}^k)\Delta t$$

$$\therefore \boxed{C_j^{k+1} = \frac{1}{V_j^{k+1}}\left[(J_j^k A_j^k - J_{j-1}^k A_{j-1}^k)\Delta t + C_j^k V_j^k\right]} \tag{3.18}$$

where:

$$A_j^k = 2\pi L r_{Bj}^k;$$

$$V_j^k = \pi L(r_{Bj-1}^{k\,2} - r_{Bj}^{k2});$$

and from Eq. (3.16):

$$J_j^k = -D\frac{(C_{j-1}^k - C_j^k)}{\Delta r} + v_j^k \frac{(C_{j-1}^k + C_j^k)}{2}.$$

The shell width, Δr, equals the thickness of the UL at each time step, divided by the number of shells (which is a constant). For the Varying δ_{UL} method, Δr and r are time-dependent and $v = v(r)$, so these values will change with the new cell radius R at each time-step. We have:

$$\Delta r^{k+1} = \frac{R^{k+1} - R_a}{n-1} \qquad \text{in the ULi;}$$

$$\Delta r^{k+1} = \frac{R_b - R^{k+1}}{m-1} \qquad \text{in the ULe;}$$

$v_j^k = -\dfrac{(r_{Bj}^{k+1} - r_{Bj}^{k})}{\Delta t}$, except at R_a and R_b where v^k=0 for all k.

For the Fixed δ_{UL} method, Δr and r values are time-independent. As r moves together with the cell radius R, v depends on R only. Therefore we have:

$$\Delta r^{k+1} = \Delta r^{k};$$

$$v_j^k = -\frac{R^{k+1} - R^k}{\Delta t}.$$

For both methods,

$$r_{Bj}^{k+1} = r_{Bj+1}^{k+1} - \Delta r^{k+1}.$$

The ends of the cylindrical shells have been ignored in the equations for A_j, since these contribute a very small component to the area. In the expression for cell area the ends of the cell have also been ignored.

3.5.2 Boundary equations

a) At the membrane

The boundary condition at the membrane is that the flux across the membrane due to the KK equations equals the flux into or out of the UL due to diffusion-advection. For the fluxes in the ULi shell adjacent to the membrane:

$J_1^k = J_s^k$ for permeant solutes; and

$J_1^k = 0$ for impermeant solutes.

For the fluxes in the ULe shell adjacent to the membrane:

$J_m^k = J_s^k$ for permeant solutes; and

$J_m^k = 0$ for impermeant solutes.

b) At the inner ULi and outer ULe boundaries

The boundary condition at the outer ULe boundary is that the concentration in the external solution is a constant. I.e.:

$C = C_o$ at $r = r_1$,

where C_0 is a constant bulk concentration value.

In the homogeneous cell core, C_j=C_n, and as there is no flux across an inner shell boundary, the mass balance equation becomes:

$$\frac{d}{dt}(C_n V_n) = -J_{n-1} A_{n-1}. \tag{3.19}$$

Finite differencing Eq. (3.19) gives

$$C_j^{k+1} V_j^{k+1} - C_j^k V_j^k = -J_{n-1}^k A_{n-1}^k \Delta t$$

$$\boxed{C_n^{k+1} = \frac{1}{V_n^{k+1}}\left(-J_{n-1}^k A_{n-1}^k \Delta t + C_n^k V_n^k\right)} \tag{3.20}$$

where:

$A_{n-1}^k = 2\pi L r_{Bn-1}^k$;

$V_n^{k+1} = \pi (r_{Bn-1}^k)^2 L$;

and r_{Bn-1}^k = *constant* for the Varying δ_{UL} method,

$r_{Bn-1}^{k+1} = r_{Bn-2}^{k+1} - \Delta r^{k+1}$ for the Fixed δ_{UL} method.

c) At the membrane in the absence of ULs

When no ULs are present, the concentration C inside the cell is given by an equation with the same form as Eq. (3.20) but with A, V, and J $(=J_s)$ determined at the membrane. This is because mass balance is now for a complete cylinder rather than a cylindrical shell.

3.5.3 Numerical stability and internal consistency

a) Numerical stability

For stability, a numerical solution of the diffusion equations with Euler's method requires that (Ames, 1977; also see §A.2 in appendix):

$$\Delta t < (\Delta r)^2 / (2D) . \qquad (3.21)$$

A numerical analysis was performed to determine values for Δr and Δt which optimized runtime and accuracy. Simulated OPP data were generated using: a) a few values of Δr ranging between 0.2-1.0 x 10^{-5} m, and b) a small value of Δr (0.15×10^{-5} m) for which it was assumed numerical errors would be small. The data from (b) was used as a reference for evaluating the accuracy of data from (a). Runtimes for each of these runs, and RMS errors between data from (a) compared with data from (b), were calculated. The analysis was carried out using two criteria for Δt: $\Delta t = (\Delta r)^2 / (2D)$ and $\Delta t = (\Delta r)^2 / (4D)$, and for 2 systems: 1 ULi = 5×10^{-5} m, and 2 ULs where ULi = 3.6×10^{-4} m and ULe = 1.0×10^{-4} m, all with D = 1.15×10^{-9} m^2 s^{-1}, the diffusion coefficient for acetone in water.

It was verified that $\Delta t < (\Delta r)^2 / (2D)$ was required for numerical stability, as when $\Delta t = (\Delta r)^2 / (2D)$ the results were unstable and the simulated curve did not return to equilibrium for the system with 2 ULs and small values of Δr. The runtimes for the 1 ULi and 2UL systems were found to decrease exponentially with increased Δr, and the RMS values (as defined in the previous paragraph) increase linearly with Δr (Fig. 3.3). A value for Δr of 0.5×10^{-5} m, corresponding to Δt = 0.005s, was considered a good choice which

minimized the runtime without loss of numerical precision. The residual plot between the corresponding *P-t* curve, and the *P-t* curve using $\Delta r = 0.15 \times 10^{-5}$m and $\Delta t = 0.0005$s, is shown in Fig. 3.4. Residual values are well within the measurement error in *P* of 0.0005 MPa.

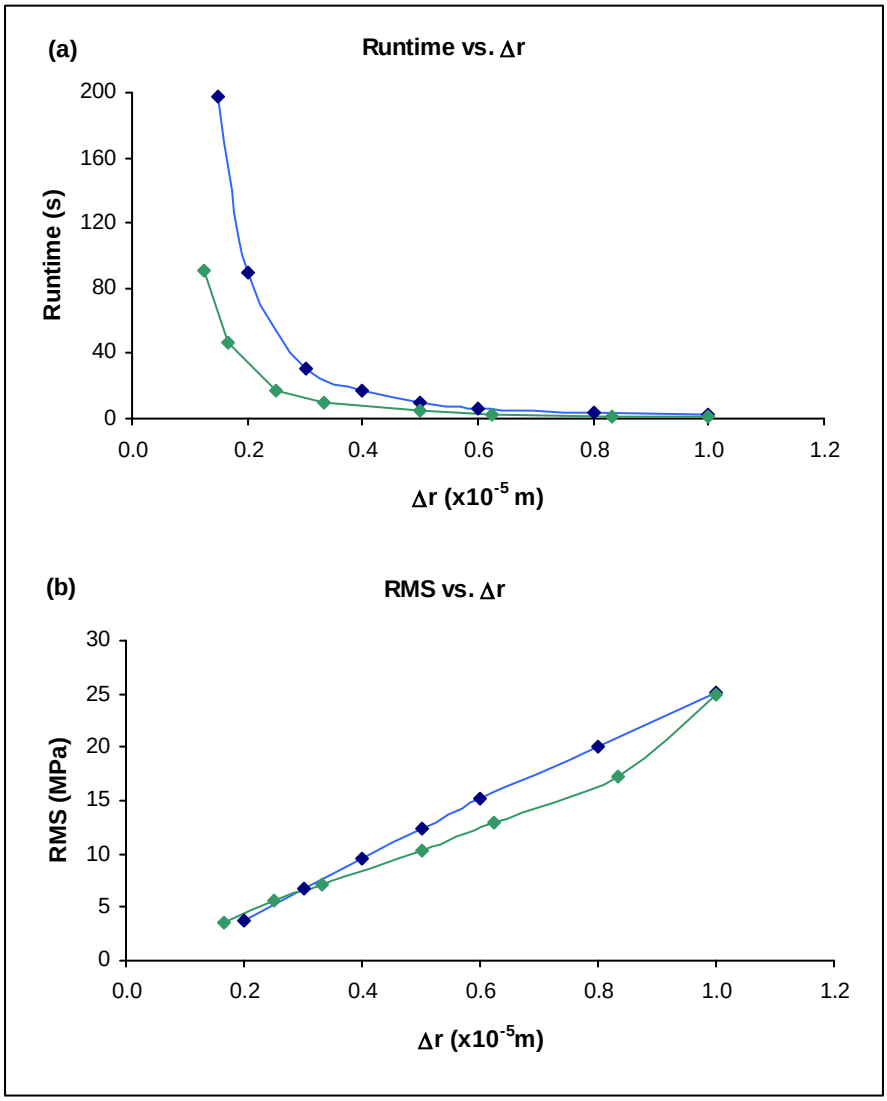

Fig. 3.3 Showing how runtime and RMS values (using simulated data) vary with Δr. Using $\Delta t = \Delta r^2/(4D)$ for: a) 1 ULi = 5×10^{-5}m (——), and b) 2 ULs with ULi = 3.6×10^{-4}m and ULe = 1.0×10^{-4}m (——).

As the size of Δt is very small, simulated *P* values were output at time intervals larger than Δt (e.g. every few Δt) and these values were in turn interpolated to give *P* values

corresponding to each data time *t*. These output intervals had to be small enough for the interpolation to be accurate. An output interval was determined using the same method detailed above, based on minimizing RMS errors between runs using a particular interval

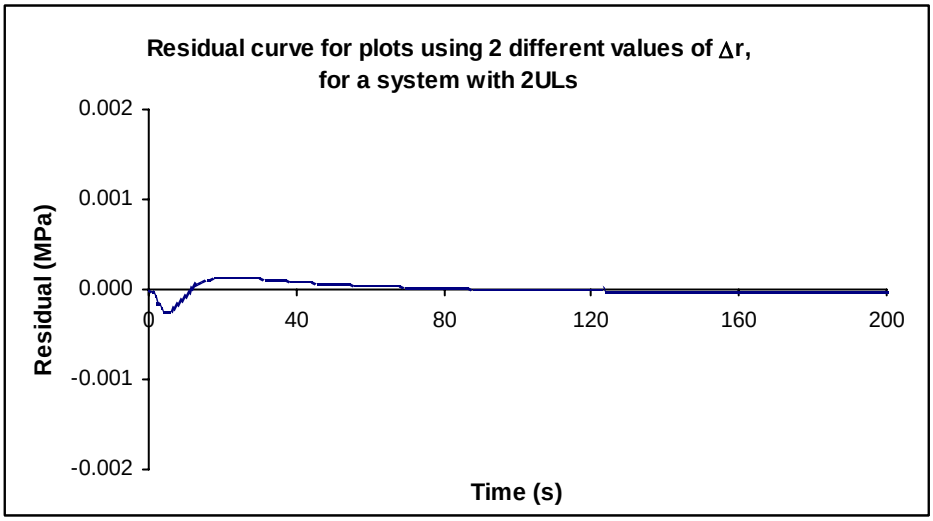

and runs using a small output interval. This analysis was carried out for an HPP experiment, since HPP data is more sensitive to the size of the output interval. Storing *P* at every $\tau_w/10$ was found to be sufficient. However, as the size did not appear to affect the runtime of the code a smaller output interval of $\tau_w/30$ was used.

Fig. 3.4 Residual plot for 2 simulated *P*-*t* curves, using $\Delta r = 0.5\text{x}10^{-5}$m and $\Delta r = 0.15\text{x}10^{-5}$m.

b) Internal consistency

The numerical solution of the model must satisfy conservation of mass across the membrane-UL system. For the permeant solutes this requires:

$$\sum_k \sum_j C_{sj}^k V_j^k - \sum_k J_1^k A_1^k \Delta t = 0 . \qquad (3.22)$$

The first term is across the whole membrane-UL system (with one or two ULs), and C_{sj} and V_j are the concentrations of permeant solutes and volumes of the j^{th} shell in the ULs, including the central core of the cell. The second term is the number of mol of solute entering the system up to any time *t*, where J_1 and A_1 are, respectively, the solute flux across and surface area of the outermost shell (either the ULe or the cell membrane).

The number of mol of impermeant solutes inside the cell remains constant, so that:

$$n_{i0} - \sum_k \sum_j C_{ij}^k V_j^k = 0, \tag{3.23}$$

where n_{i0} is the number of mol of impermeant solutes in the cell at $t=0$, and C_{ij} and V_j are the concentrations of impermeant solutes and volumes of the j^{th} shell in the ULi, including the central core of the cell. For the impermeant solutes outside the cell, Eq. (3.22) is used with the first term summed over all the shells in the ULe only.

Where no ULs are present, the number of mol of permeant solutes in the cell must equal the sum of the number of mol of permeant solutes crossing the membrane up to any time *t*. The concentration of impermeant solutes in the cell changes with cell volume, according to Eq. (2.4). The concentration of impermeant and permeant solutes outside the cell remain constant.

From the principle of conservation of mass, the concentration gradient of permeant solutes should also be the same on either side of the membrane – otherwise mass would accumulate in the membrane, which should not happen. The gradients should be exactly equal in steady state and approximately equal in non-steady state. That is, one should have:

$$\frac{\Delta C_{sem}^k}{\Delta r_m^k} - \frac{\Delta C_{s1}^k}{\Delta r_1^k} = 0 \qquad \text{for all } k, \tag{3.24}$$

which says that the difference in the concentration gradients on either side of the membrane (at the m^{th} shell in the ULe and the 1^{st} shell in the ULi) should be zero at all times.

3.6 Examination of model behaviour

Fitting of the CPP data to obtain the membrane parameters will be carried out in Chapter 4. In this chapter the model is not fit to observed data, but different aspects of the model are varied in order to analyse the behaviour of the model.

3.6.1 Implementation of model

The model was coded in Matlab such that modifications to the model could be made through changing appropriate switches. Depending on the system and experiment:

- an external UL may or may not exist
- an internal UL may or may not exist
- the pressure perturbation is hydrostatic or osmotic
- the pressure perturbation is positive or negative
- permeant solutes are present or not present in the external solution
- an external ramp (where the external concentration reaches the final perturbation value over a period of time, see §2.7.3b) does or does not exist.

It was verified that when δ_{ULe} and δ_{ULi} were set to 0 in the model, the relaxation curves and RMS errors for observed vs. predicted data were the same as those for the classical model and analytical solution. In addition, mass was conserved to within 1 part per billion. This illustrated that the equations for a system without ULs were implemented correctly.

When ULs were present in the model, the *P*-*t* curves were found to be log-linear and exhibit the same shape as the data relaxation curves. This verified that the KK equations still represent the cell dynamics in the presence of ULs, and that the classical method of parameter determination may still be applied. Mass was conserved to within 1 ppb.

The relative difference in the concentration gradient of permeant solutes on either side of the membrane was plotted against time for the first 15s, using the normalized form of Eq. (3.24) given by:

$$\left(\frac{\Delta C_{sem}^{k}}{\Delta r_{m}^{k}}-\frac{\Delta C_{s1}^{k}}{\Delta r_{1}^{k}}\right)\Bigg/\left((\frac{\Delta C_{sem}^{k}}{\Delta r_{m}^{k}}+\frac{\Delta C_{s1}^{k}}{\Delta r_{1}^{k}})/2\right)=0 \quad \text{for all } k. \tag{3.25}$$

The relative difference became close to zero after the first few seconds, and decreased when Δr was decreased (Fig. 3.5). The non-zero value during the first few seconds is a numerical manifestation due to possible inconsistencies in the initialization of the system of equations, due to the largely arbitrary assignment of values within the finite difference shells.

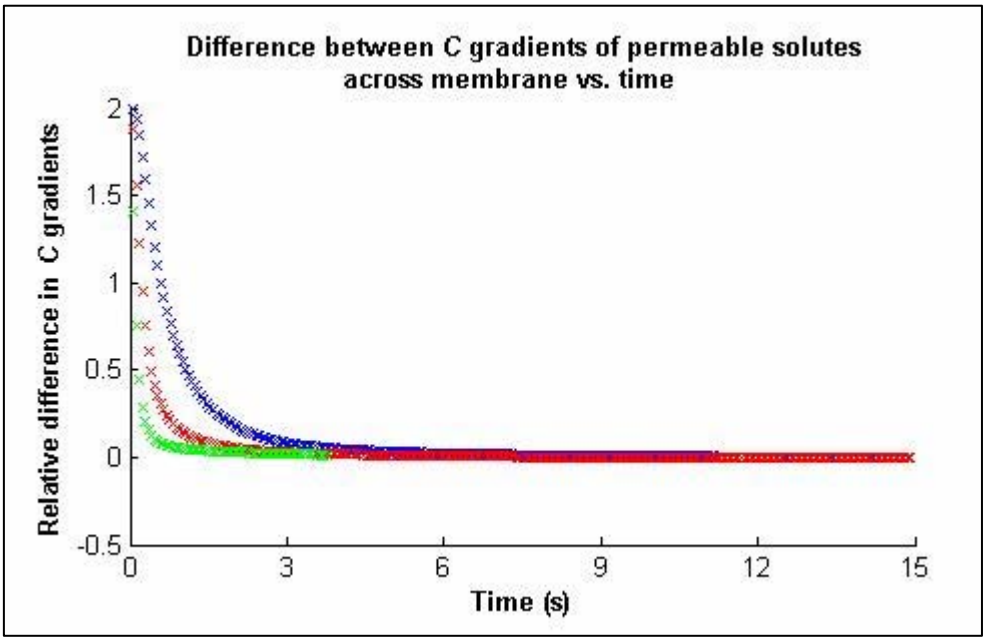

Fig. 3.5 Relative difference in the concentration gradients of permeant solutes on either side of the membrane, vs. time. Relative difference is calculated using Eq. (3.25). 'x': with $\Delta r=5\text{x}10^{-6}$m, 'x': with $\Delta r=1\text{x}10^{-6}$m, 'x': with $\Delta r=2\text{x}10^{-7}$m.

Validation of the model with ULs will be carried out in Chapter 4 when the model is applied to real data.

3.6.2 Effects of ULs on the relaxation curve

The model was run using initial and perturbation conditions consistent with the HPP and OPP data from Henzler *et al*. (2004) fitted in §2.5. A constant set of membrane parameters were used with the ULe and ULi thicknesses varying, namely: $L_p = 2.0 \times 10^{-6}$ m s^{-1} MPa^{-1}, $p_s = 5.0 \times 10^{-6}$ m s^{-1}, and $\sigma = 0.15$.

P-t curves for a negative OPP experiment were plotted for 4 different ULe thicknesses and 4 different ULi thicknesses (Fig. 3.6). The plots show that ULs have a clear effect on the relaxation, damping the range of pressure changes, and slowing down the rate of return to equilibrium and decreasing the gradient of the curves. Further examination of effects of ULs on the *P-t* curves was performed by analysing changes in the curve characteristics (identified later in Fig. 3.8). These were calculated using the same method by which curve characteristics were derived for the observed data (see §2.4.1), with t_m interpolated from the simulated values. It was found that as δ_{ULe} increases, P_m decreases, while t_m, τ_w and τ_s increase (Fig. 3.7a). As δ_{ULi} increases, P_m decreases, τ_s increases, while t_m and τ_w change little (Fig. 3.7b). The effect of a ULi on the *P-t* curve is less pronounced than the effect of a ULe. Most of the influence of a ULi occurs within 1×10^{-4} m from the membrane, and for $\delta_{ULi} > 2 \times 10^{-4}$ m the curve characteristics reach a stable value.

The ULe also causes a time-delay in the curve (Fig. 3.6c), due to the time taken for solutes to pass through the ULe and reach the cell membrane. This effect is not observed when only a ULi is present. The time-delay was calculated by fitting a straight line regression through a few initial points (Fig. 3.8), with the time-delay given by the time at which this line intersects the line $P=P_0$. The time-delay was found to increase non-linearly with δ_{ULe} **(**Fig. 3.9**)**.

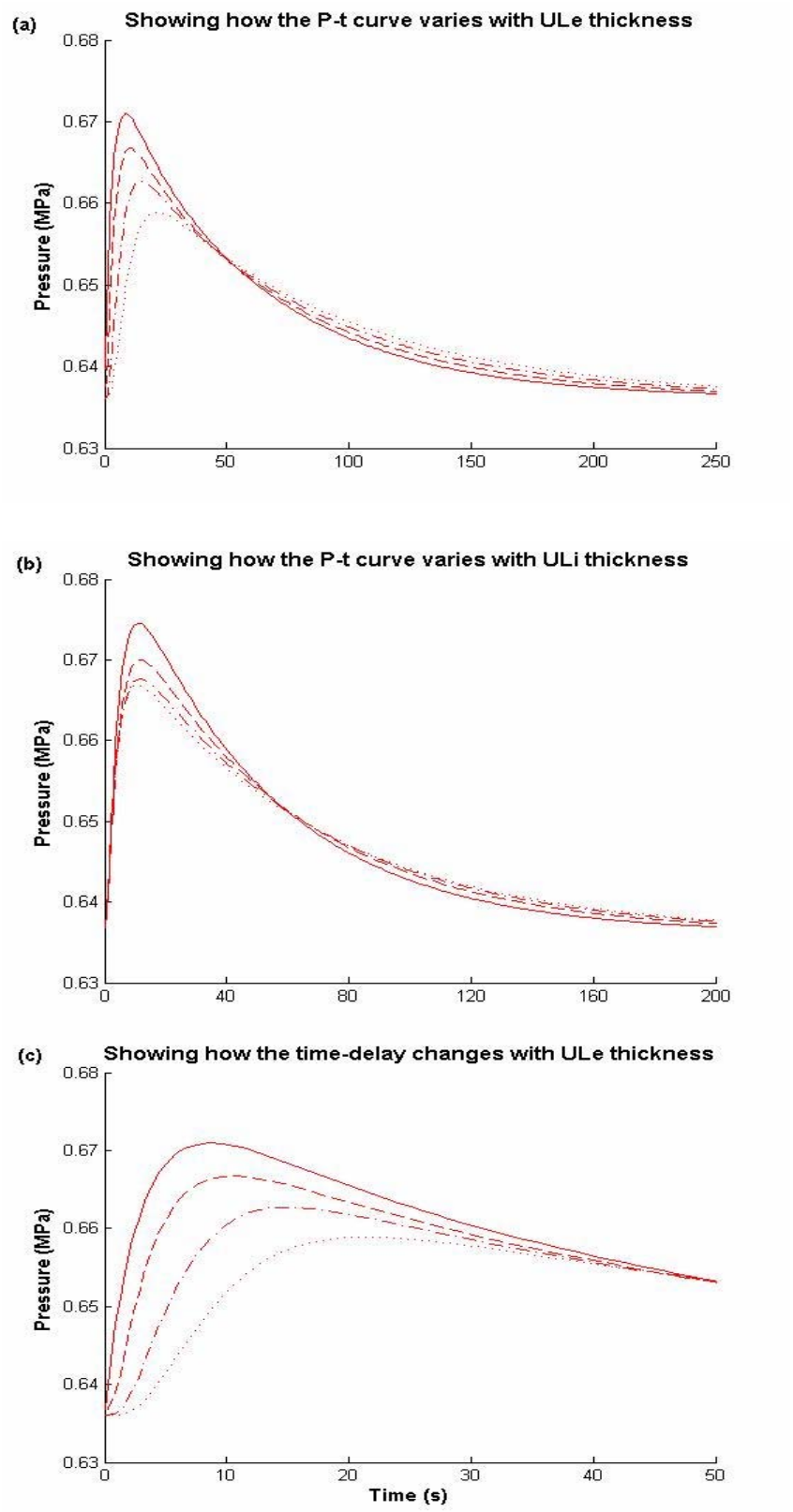

Fig. 3.6 Showing how the simulated OPP curve varies with UL thickness. (a) With δ_{ULi} = 350μm, and δ_{ULe} = 0 (——), 50μm (— —), 100μm (—. —), 150μm (-----). (b) With δ_{ULe} = 50μm, and δ_{ULi} = 0 (——), 100μm (— —), 200μm (—. —), 300μm (-----). (c) Close-up of (a) illustrating the time-delay in the curve.

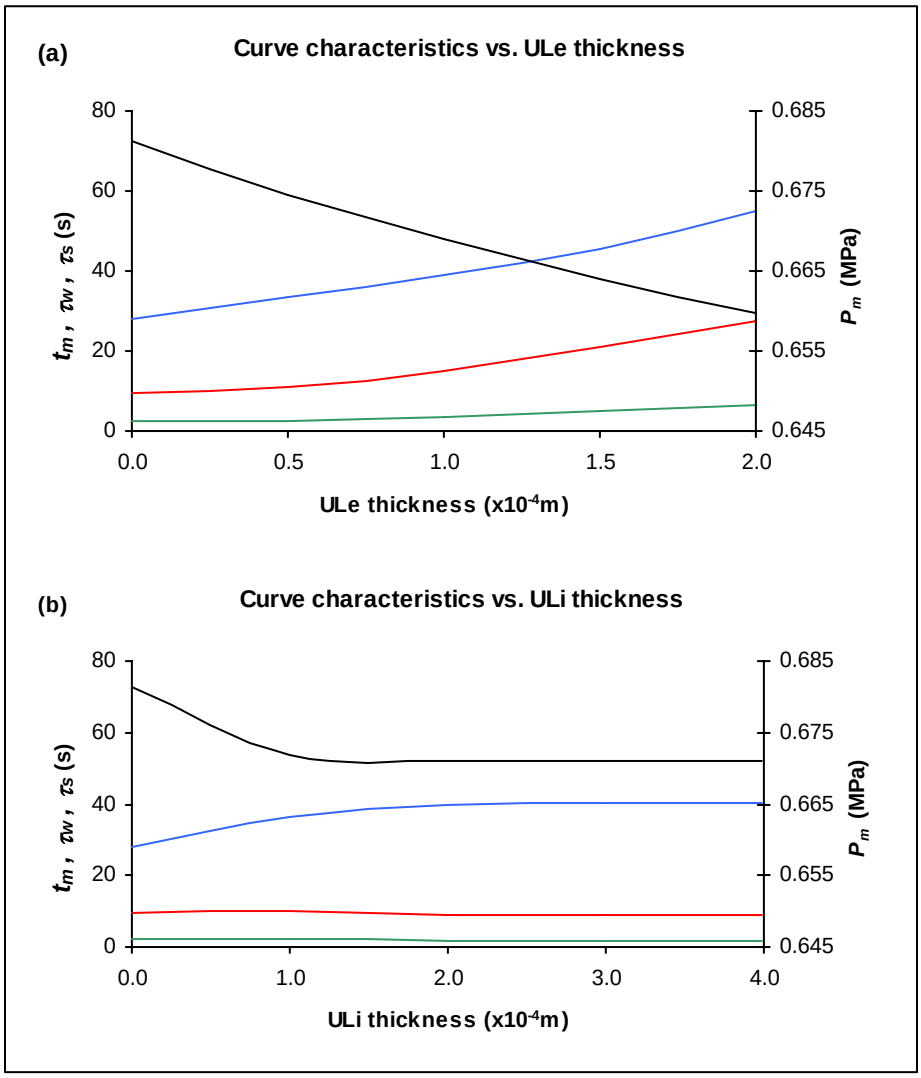

Fig. 3.7 Showing how curve characteristics of the simulated OPP relaxation curve changes with UL thickness, for: a) 1 ULe present, and b) 1 ULi present. Curve characteristics: P_m (——), t_m (——), τ_w (——), τ_s (——). Calculation of τ_w, L_p, and σ include the time-delay.

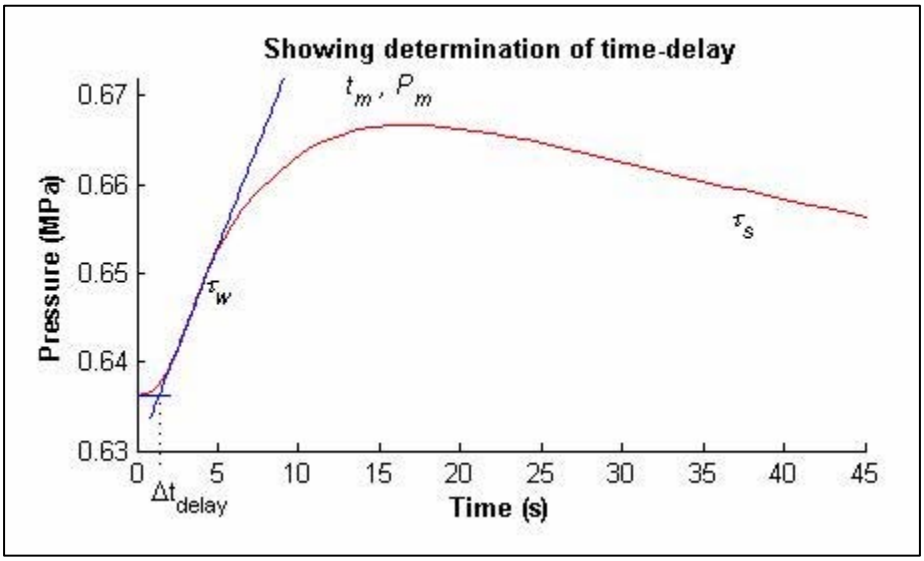

Fig. 3.8 Illustrating method for calculation of the time-delay, and showing locations of curve characteristics, for a negative OPP (Fig. 2A) with 2 ULs.

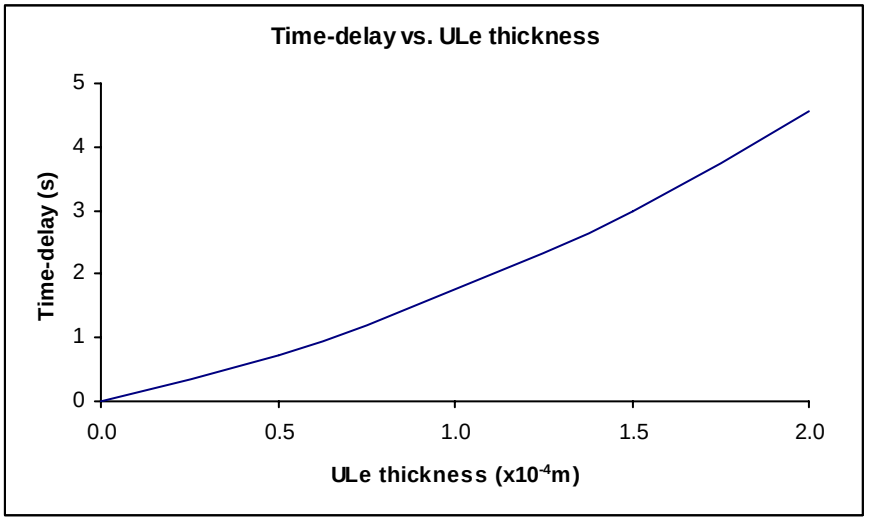

Fig. 3.9 Time-delay vs. ULe thickness for simulated OPP data.

For an HPP experiment, a ULi also slows down the rate of return to equilibrium, and hence increases τ_w (Fig. 3.10). After a certain value of δ_{ULi} the ULi has little additional influence. The ULe has negligible effect since the external concentration of impermeant solutes is very low. The effects of ULs are much smaller for an HPP experiment compared to an OPP experiment.

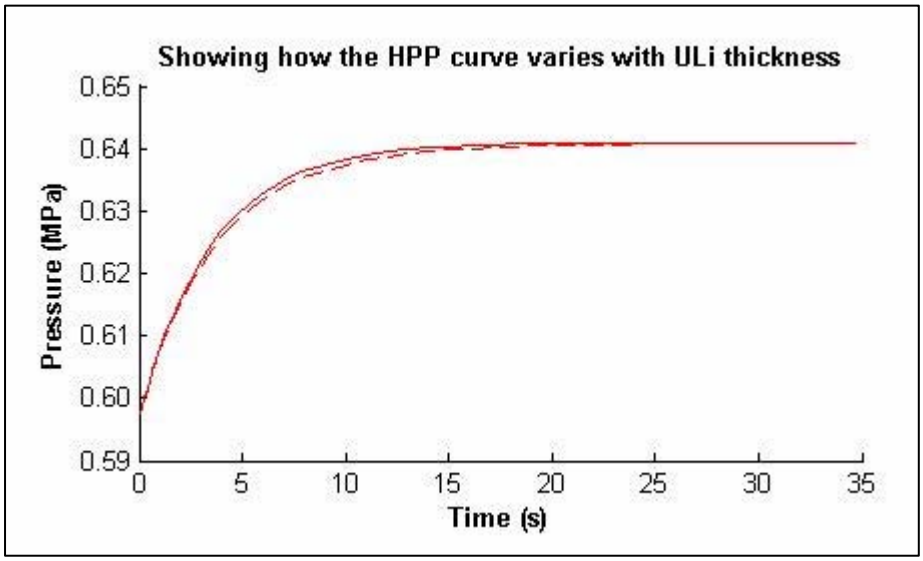

Fig. 3.10 Showing how the simulated HPP curve varies with ULi thickness. With δ_{ULe} = 50μm and: a) δ_{ULi} = 0 (——), b) $\delta_{ULi} \geq$ 100μm (— —).

While ULs slow the rate of return to equilibrium, they do not change the final equilibrium pressure. In accordance with the analytical solution to the KK equations, the model predicts that for an HPP, $P_E < P_0$ for a negative pulse and $P_E > P_0$ for a positive pulse, and $P_E = P_0$ for an OPP experiment.

3.6.3 Concentration profiles in the ULs

The concentration of permeant solutes C_s in the ULs was plotted against r for a positive OPP experiment (Fig. 3.11), using the same parameters and initial conditions as in §3.6.2. It was chosen to plot concentration profiles for a positive pulse as concentration profiles in the literature are often shown for this case. Concentration profiles for a negative pulse take the form of those for the positive pulse reflected about the r-axis.

The profiles in Fig. 3.11 are similar to those in Crank (1975) for non-steady-state diffusion through a cylinder, where the concentration profiles in the ULi correspond to the case of variable surface concentration (the surface being the membrane), and the concentration profiles in the ULe correspond to the case of constant surface concentration (the "surface" being the outer boundary of the ULe). When ramps are present in the model, concentration profiles in the ULe have a flatter gradient since the concentration at the outer ULe boundary decreases from 160mM at t=0 to 0 during the period of the ramp (Fig. 3.12).

The profiles in Fig. 3.11 are consistent with the diagram in Fig. 3.1 which shows how ULs affect the concentration gradient at the membrane. Fig. 3.1 corresponds to the concentration profiles given in Pedley (1983) for the steady-state solution to Fick's convection-diffusion equation (Eq. (5.1)) for transport in two ULs separated by a membrane, subject to the boundary conditions that beyond the ULs the concentrations are constant. These profiles differ from the common diagram given in the literature (Fig. A.1 in appendix) for how ULs affect the concentration gradient at the membrane.

The profiles in Fig. 3.1 and Fig. 3.11 are a consequence of having a discontinuous concentration difference both at the membrane and at the outer boundary of the ULe. The latter arises because it is assumed that at t=0 the concentration in the bulk solution changes instantaneously while the concentration in the ULe remains as it was, and then changes due to diffusion when t>0. Only if the concentration in the ULe changes together with the bulk solution at t=0, will the concentration profiles then look like Fig. A.1. This

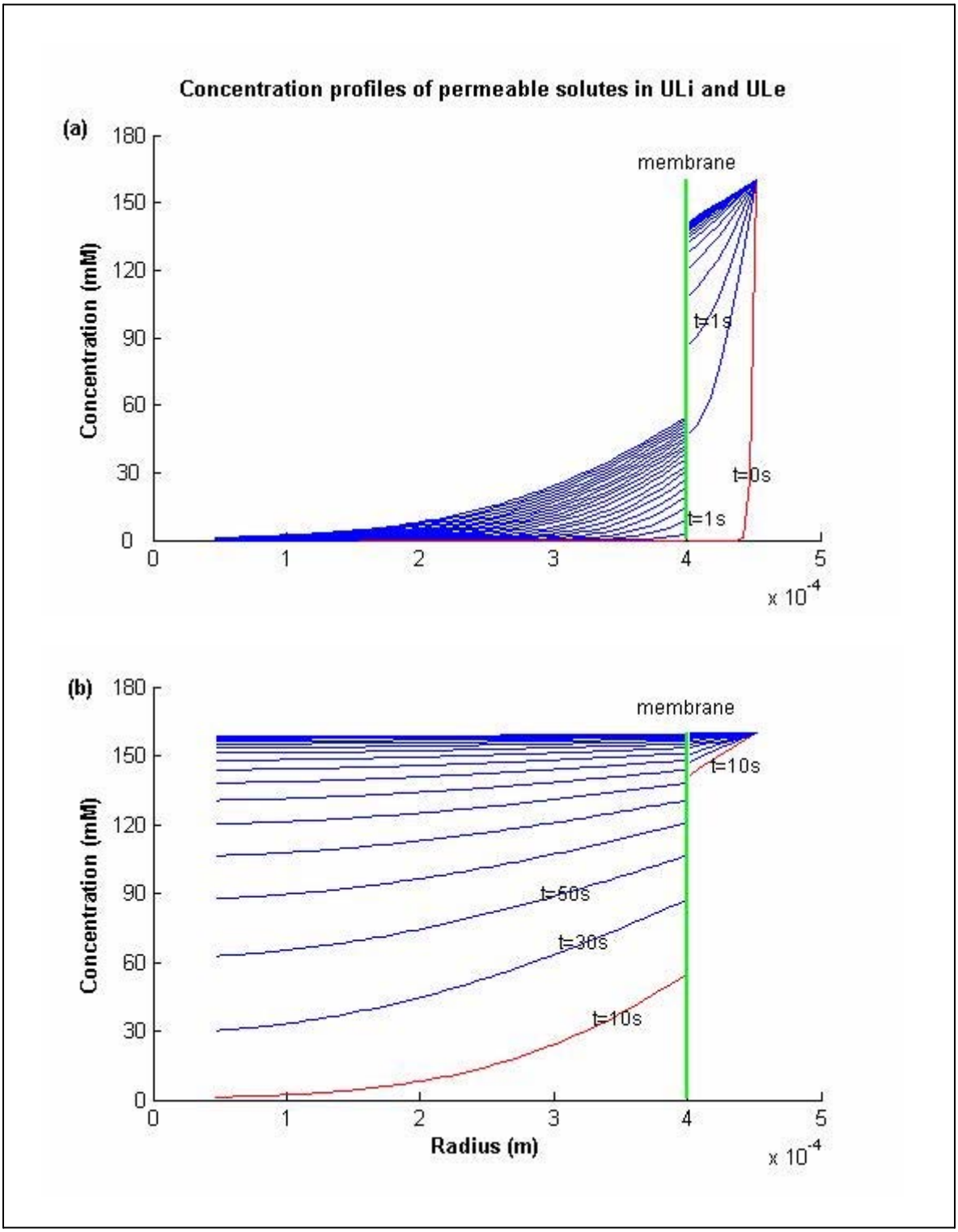

Fig. 3.11 Concentration profiles in the ULi and ULe for OPP data. Showing: a) a period of 0-10 s, lines at 0.5s intervals; b) a period of 10-330 s, lines at 20s intervals. Red lines indicate the initial concentration profile at the beginning of the plot.

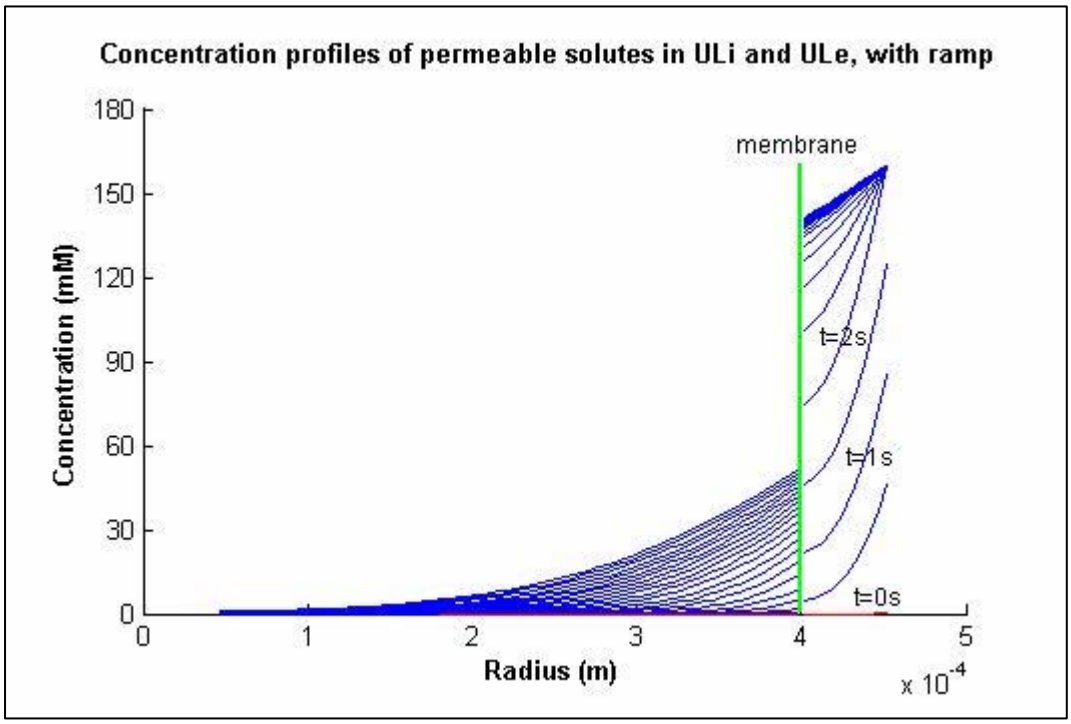

Fig. 3.12 Concentration profiles in the ULi and ULe for OPP data, when a 2s ramp is present in the external solute concentration. Showing a period of 0-10 s, with lines at 0.5s intervals. Red lines indicate the initial concentration profile at the beginning of the plot.

perturbation condition, however, is akin to having no ULe but diffusion occurring in the bulk solution. Fig. A.1, therefore, does not accurately reflect the concentration profiles across the membrane under the conditions of a CPP experiment.

The true concentration profiles are probably a combination of those in Fig. A.1 and those in Fig. 3.11 or Fig. 3.12. This is because in the present model radial transport is modelled at one axial point only, which can be taken to be a point mid-way along the length of the cell, so that t=0 is when the external solution reaches this point. However, in reality as the new solution traverses the length of the cell, the ULe concentration is perturbed at the leading edge of the cell first, so that at t=0 in the model the ULe concentration mid-way along the length of the cell has already changed.

3.6.4 Effects of convection on pressure dynamics

The convective component to transport in the ULs can be removed by making v=0 in Fick's diffusion-advection equation (Eq. (3.4)), and keeping the areas A and volumes of the UL shells constant (dV/dt=0) in the mass-balance equation (Eq. (3.10)). This was done in a HPP and an OPP experiment, in order to explore the relative contribution of convection to the pressure dynamics.

a) HPP experiment

In an HPP experiment there are no solutes permeating the membrane, and concentration profiles in the ULs will be constant with r unless the concentration is perturbed due to the membrane moving into the UL regions. The membrane increases the solute concentration on the upstream side of the flow, and decreases it on the downstream side. In the frame-of-reference of the cell a flow into the cell (for example) sweeps away the solutes from the membrane, reducing the concentration at the inner membrane surface. Solutes are concentrated at the outer membrane surface. This "sweep-away effect" (see §3.1.3b) due to solute-drag is the main effect of ULs in an HPP experiment. When the terms contributing to convection are removed, no effect of the ULs are seen because the concentration distribution in the ULs have not been perturbed, and no fluxes due to diffusion or convection are present.

b) OPP experiment

The presence or absence of convection in an OPP experiment makes a negligible difference to the relaxation curves, concentration profiles in the ULs, and concentration difference across the membrane. With permeant solutes, the convective component which gives rise to the sweep-away effect is a much smaller component than diffusion which gives rise to the gradient-dissipation effect (see §3.1.3). The convective component is therefore relatively larger in an HPP than in an OPP experiment.

3.6.5 Effects of ULs on measured membrane parameters

a) Estimation of membrane parameters

Since ULs affect the simulated relaxation curves, the classically-estimated parameters are also affected. To examine how much ULs cause the classically-estimated membrane parameters to differ from the actual parameters, the ratios of the classically-estimated parameters ($parameter_c$) over the corresponding membrane parameters ($parameter_m$), were plotted against UL thickness (Fig. 3.13). In this analysis $parameter_m$ represents the "true" membrane parameter (i.e. used in the KK equations to produce the simulated data), and $parameter_c$ represents the "observed" membrane parameter (i.e. calculated from the simulated data using the same technique as that applied to CPP data). A parameter ratio ξ can be defined as:

$$\xi = \frac{parameter_c}{parameter_m}. \tag{3.26}$$

It was found that for an OPP curve, a ULe causes the classically-estimated parameters to underestimate the true parameters (Fig. 3.13a), and this effect increases with increasing δ_{ULe}. This underestimation of the true parameters is consistent with Fig. 3.6 where it was shown that a UL "flattens" the *P-t* curve. The effect is much more marked for L_p than p_s and σ. With increasing δ_{ULi}, the observed L_p appears to slightly overestimate the true L_p, and p_s and σ are again underestimated (Fig. 3.13b). For a $\delta_{ULi} > 200\mu m$, the ULi has little additional effect on the parameter estimation. The estimation (measurement) of p_s and σ appear to be affected by ULs in a similar manner to each other, and this is similar for the ULe and ULi. The effects of ULs on the measured L_p is more marked, and do not appear to be the same for the ULe and ULi.

For an HPP curve, a ULe did not have any effect on the classically-estimated membrane parameters, because the concentration of impermeant solutes in the external solution is very small ($\pi_{ie} = 0.1$ MPa) compared to the concentration of impermeant solutes inside the cell ($\pi_i = 0.63$ MPa). A ULi had only a small effect on the classically-estimated L_p, slightly reducing it so that $\xi = 0.96$ for a $\delta_{ULi} \geq 100\mu m$. This is to be expected, since

unlike the OPP experiment using permeant solutes, diffusion in the ULs is primarily due to concentration changes at the moving membrane, and not changes in the bulk solution. Concentration changes due to the moving membrane is much smaller than that due to diffusion of permeant solutes across the membrane.

The results shown here indicate that the classically-estimated membrane parameters are strongly dependent on the thickness of the ULe and ULi. Results clearly demonstrate that if the Classical method of estimating membrane parameters is applied to real data from systems in which ULs are present, the estimated parameters will generally underestimate the true membrane parameters. This raises the question: By how much may the classically-estimated membrane parameters underestimate the actual membrane parameters? This will be explored when CPP data is fit in Chapter 4. It should be noted that the magnitude of the effects in Fig. 3.13 will change if a different starting 'true' membrane parameter is used. For example, if the true P_s is very low then the ULs will have no effect, but if the true P_s is larger than that used in Fig. 3.13 the effects of ULs will be more (see §3.1.3).

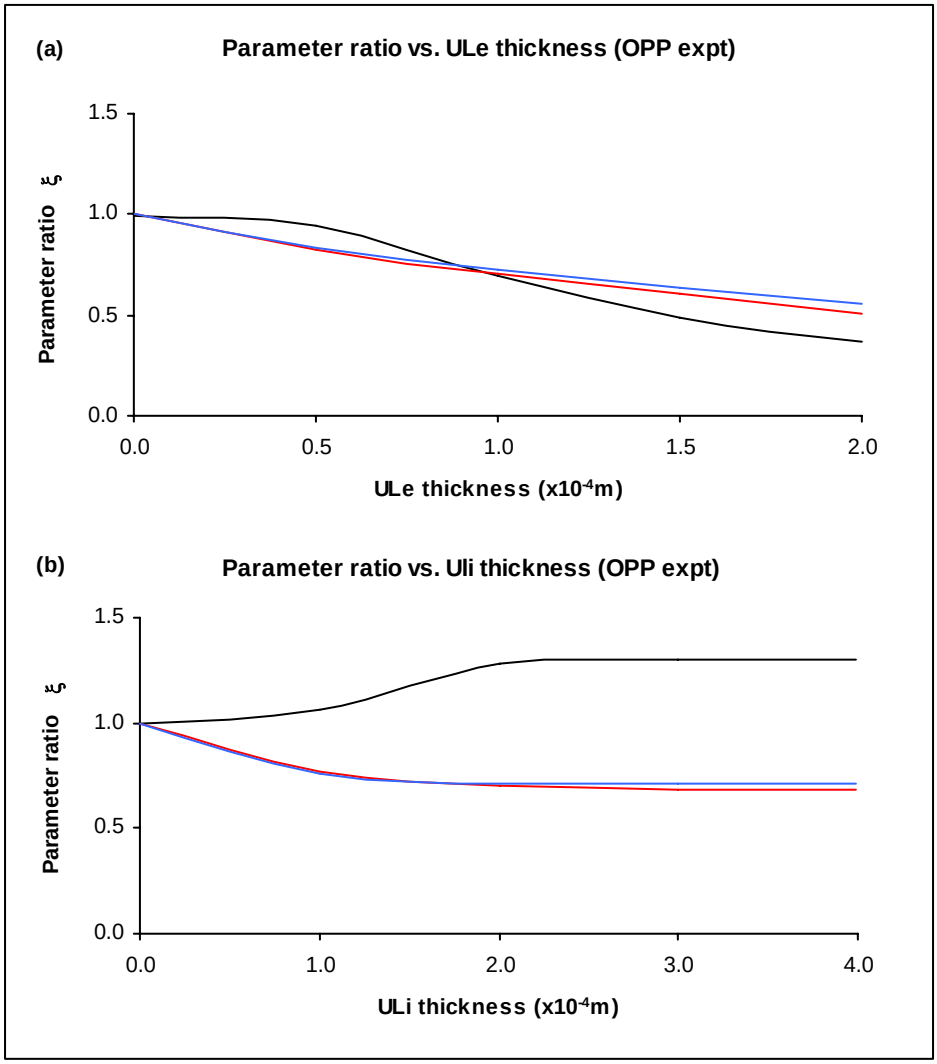

Fig. 3.13 Showing parameter ratios for simulated OPP data. L_p (——), p_s (——), and σ (——) vs. (a) ULe thickness, and (b) ULi thickness.

b) Polarity in membrane parameters

A polarity in L_p has been observed in HPP experiments and in OPP experiments with impermeant solutes (Dainty and Ginzburg, 1964a; Steudle and Zimmermann, 1974), and in OPP experiments with permeant solutes (Steudle and Tyerman, 1983). Polarity may be species-dependent, or dependent on the water flow across the membrane, as Steudle and Tyerman (1983) did not observe a polarity in L_p in HPP experiments. Polarity in L_p may also be due to the presence of ULs (Steudle and Tyerman, 1983).

To test whether the UL model predicts polarity in the membrane parameters, the model was used to predict and compare *P-t* curves for HPP experiments and for OPP experiments with permeant solutes. Simulations using positive and negative pulses of the same magnitude, using the same membrane parameters but a range of ULe and ULi thicknesses, were compared. It was found that positive and negative pulses produced *P-t* curves which are symmetric about the *t*-axis, for both HPP and OPP experiments.

In order to test the experimental findings that polarity is increased with increasing external concentration of impermeant solutes (Zimmermann & Steudle, 1978), the analysis was repeated with the external osmotic pressure increased by 2 orders of magnitude (π_{ie} = 1.0 MPa). No significant polarity in the measured parameters was predicted for either an HPP or OPP experiment.

Finally, the analysis was repeated using different values of the diffusion coefficient for the external and internal ULs ($D = 1.15 \times 10^{-9}$ m s^{-1} for the ULe; $D = 0.8 \times 10^{-9}$ m^2 s^{-1} for the ULi), and with varying UL thicknesses. Again no polarity in membrane parameters was predicted by the model.

In summary, the present model does not predict that ULs introduce a polarity into classically-estimated membrane parameters. Consequently, any polarity observed in the classically-estimated parameters when the data is fit (Chapters 4 and 5), are due to other experimental or physical conditions and not UL effects. It was pointed out in §2.2.2 that the KK equations also do not predict polarity in the membrane parameters.

c) Effects of external concentration on membrane parameters

Experiments have found that measured L_p values decrease when the external concentration of impermeant solutes is increased (Zimmermann & Steudle, 1978). In the absence of ULs the model did not predict any change in the classically-estimated parameters when external concentration was changed. However, changes were predicted in the classically-estimated parameters when ULs are present.

When the external osmotic pressure π_{ie} was varied over the range 0.01-1.0 MPa ($\pi_{ie} = CRT$) for $\delta_{ULe} = 5 \times 10^{-5}$ m and $\delta_{ULi} = 4 \times 10^{-4}$ m, the model predicted a decrease in L_p with

increased external concentration for an HPP experiment, but a non-monotonic change in L_p for an OPP experiment (Table 3.1). An influence of external concentration on L_p is expected since the ULs act to change the concentration gradient across the membrane, which would also be affected by the amount of solutes in the external solution. This behaviour is also expected by looking at the KK equations (Eq. (2.13)), which show that changing π_{ie} affects k_w (and thus L_p) through changing π_{i0} (which is an equilibrium value and thus dependent upon π_{ie}).

Table 3.1 Showing how the classically-estimated L_p changes with differing external concentration of impermeant solutes, for a negative HPP and negative OPP experiment.

π_{ie} (MPa)	L_p (x 10^6 m s^{-1} MPa^{-1})	
	Neg HPP	Neg OPP
0.01	1.92	2.11
0.05	1.91	2.30
0.1	1.91	2.28
0.5	1.88	2.14
1	1.88	1.82

d) Effects of size of perturbation pulse on membrane parameters

Increasing the size of the pressure pulse increases the magnitude of J_v, which causes a larger sweep-away effect since *dV/dt* and the changes in volume are larger (Ye *et al.* 2006). The model runs for the negative OPP and negative HPP experiments were repeated using a pressure pulse of twice the original magnitude. The classically determined parameters were calculated for a few values of δ_{ULe} and δ_{ULi} and compared with those found previously.

It was found that there were no differences in the parameter values or behaviour of the *P-t* curve due to changing the size of the pressure pulse. This is consistent with the KK equations, which exhibit a linear relationship between ΔC_{se} and P for the OPP (Eq. (2.9)), and P_1 and P for the HPP (Eq. (2.6)), when the membrane parameters and initial equilibrium conditions are kept constant.

The above results show that inclusion of ULs in the model doesn't affect the overall dynamics of the *P-t* curve, but does affect the actual values of parameters estimated using the model.

3.6.6 Effects of D on pressure dynamics, and the permeability equation

a) Influence of D on the measured membrane parameters

When the membrane parameters are kept constant and the value of D is decreased, the total permeability p_T of the system should decrease by Eq. (3.2). This behaviour was verified with the numerical UL model from simulations of OPP experiments, where D in the ULi was varied and D in the ULe ($1.15\text{x}10^{-9}$ m^2s^{-1}) and the UL thicknesses were kept constant ($\delta_{ULe} = 5\text{x}10^{-5}$ m and $\delta_{ULi} = 3.5\text{x}10^{-4}$ m). In this case p_T is the classically-estimated p_s value, i.e. the value that would be measured for the membrane p_s when ULs are assumed to be absent. Decreasing D is equivalent to increasing the UL thickness, as both slow down the diffusion of solutes. When different values of D are used for the ULi and ULe in the model, the classically-estimated parameters should change in a manner similar to those in Fig. 3.13, where the x-axis now represents decreasing D rather than increasing UL thickness. E.g. when D in the ULi is decreased, $\xi(L_p)$ should increase and $\xi(p_s)$ and $\xi(\sigma)$ should decrease. This was indeed verified by the numerical UL model (Table 3.2).

Table 3.2 Parameter ratios due to decreasing *D* in the ULi. Base value for *D* is $1.15\text{x}10^{-9}$ $m^2 s^{-1}$.

D($\text{x}10^{-9}$ m^2 s^{-1})	$\xi(L_p)$	$\xi(p_s)$	$\xi(\sigma)$
1.15	1.16	0.60	0.62
1.05	1.18	0.59	0.61
0.95	1.21	0.57	0.60
0.85	1.25	0.55	0.58
0.75	1.30	0.53	0.57
0.65	1.34	0.51	0.55
0.55	1.40	0.49	0.53
0.45	1.47	0.46	0.50

Although it was assumed that D is the same outside and inside the cell (due to the scarcity of information about D inside the cell), and equal to $D = 1.15\text{x}10^{-9}$ m^2 s^{-1} in

water, it is likely that D is less inside the cell since the cell interior is more concentrated than water and contains more suspended particles. This suggests that, in reality, the under-estimation or over-estimation of the measured parameters will be even more than that predicted by the UL model which assumes that D is the same for the ULi and ULe. If, for a particular solute, the value of D inside the cell is much less than the value in APW, then this will have a large impact on the estimated parameters. Table 3.2 shows that the parameter ratios vary significantly from those for the reference value of D = 1.15×10^{-9} m^2 s^{-1}. However, this may be different when parameters are estimated for fits to the data. This will be done in §4.8.4.

b) The permeability equation

The steady-state permeability equation (Eq. (3.2)) is sometimes used to predict the influence of ULs on the classically-estimated membrane parameters (Ye *et al.* 2006; Steudle and Frensch, 1989). Therefore, it is important to examine and compare predictions of total permeability using Eq. (3.2) with predictions using the non-steady state UL model. As mentioned above, p_T is the classically-estimated p_s. It was found that the value of $1/p_s$ predicted by Eq. (3.2) departed from the value of $1/p_s$ using the classical method of parameter estimation, by up to 30% for certain ranges of the UL thicknesses (ULe and ULi were both varied between 0-200 μm). This shows that Eq. (3.2) cannot be used to quantify the effects of ULs for systems in non-steady state. That is, estimates of p_s using Eq. (3.2) would differ from that estimated by the UL model. When the true membrane p_s was changed by 10% for a typical set of ULe and ULi values, this resulted in a 6% difference in p_T, which shows that a 30% error in the estimate of p_T would correspond to a much larger error in the estimate of the true membrane p_s.

3.7 Conclusions

A model of water and solute transport across a membrane with unstirred layers (ULs), coupling the KK equations and diffusion equations, has been described. A numerical solution using Euler's method was implemented in Matlab with provision for accommodating a number of experimental conditions.

Three approaches to implementing the UL model were discussed: one where the outer ULe and inner ULi boundaries are fixed, one where the outer ULe and inner ULi boundaries move together with the membrane, and one where all numerical grids except those immediately adjacent to the membrane are fixed. The first method is recommended since it is mathematically rigorous (in contrast to the third method) and the ULi thickness can be the entire cell volume (an advantage over the second method). Whether fixing the non-membrane UL boundaries accurately reflects the physics of UL behaviour is unimportant for modelling purposes, since the change in volume of the cell (and UL) at any one time step is small relative to the total cell volume, and all three methods gave consistent model predictions.

Simulation of an OPP relaxation curve (§3.6.3) gave concentration profiles in the ULs which were consistent with those given by the analytical solution to non-steady state diffusion through a cylinder (Crank, 1975). These are not the same as the profiles often encountered in the literature which aim to show how ULs affect the concentration near the membrane. This is because the model used in this study assumes that for an OPP perturbation the concentration in the bulk solution changes but the concentration in the ULe doesn't, so that there is a discontinuity at the outer ULe boundary. This is believed to more accurately reflect the conditions of a CPP experiment and the physical nature of a UL (a stagnant layer with primarily diffusional mixing).

An analysis of convection in the ULs revealed that this is a major component to transport in the ULs for an HPP experiment, but a small component compared to diffusion in the ULs for an OPP experiment with permeant solutes (§3.6.4). This is consistent with literature reports which have stated that ULs affect HPP experiments primarily through sweep-away effects (Ye *et al.* 2006; Hertel and Steudle, 1997; Steudle, 1993).

The effect of ULs on the relaxation curves, curve characteristics, and measured membrane parameters were examined. In Chapter 2 (§2.3.1) it was shown that a decrease in L_p results in an increased τ_w and t_m, a decrease in p_s results in an increased τ_s, and a decrease in σ results in an increased P_m. In this Chapter it was shown that the addition of ULs serve to retard the pressure response so that P_m decreases, t_m increases, and the half-times increase with increasing UL thickness (§3.6.2). This means that ULs will generally

cause the measured L_p, p_s, and σ (those determined from CPP data using the classical method of parameter estimation) to underestimate the true parameters of the membrane (§3.6.5a). Estimation of the true membrane parameters is therefore not possible without knowledge of the UL thickness. This will be demonstrated in Chapter 4 when the model is fit to CPP data by directly modifying the membrane parameters.

Another effect of the ULe on the relaxation curve is that it causes a delay in the pressure response immediately following a perturbation in the external concentration. This is because it takes time for the solutes to pass through the ULe and reach the membrane. This time-delay increases non-linearly with ULe thickness (§3.6.2a). This will be further examined in Chapter 4.

It was examined whether the model could reproduce the various parameter behaviours which have been suggested might indicate the presence of ULs (see §3.1.2), namely: a decrease in the classically-estimated parameters with increasing external solute concentration, and a polarity in the classically-estimated parameters. The UL model did not predict any polarity in the membrane parameters when the external concentration of impermeant solutes was increased, or the value of the diffusion coefficient D inside the cell was changed (§3.6.5b). (The influence of external flow rate with L_p could not be examined since the flow rate is not a component of the model.) Causes of polarity in the classically-estimated L_p reported in the literature are thus likely to be due to composite membrane effects and influences of the tonoplast, where theory predicts a polarity in L_p and p_s for membranes arranged in series (Kedem and Katchalsky, 1963c), or other physical effects of the membrane such as dehydrating one side of the membrane more than the other (Dainty and Ginzburg, 1964a; Kiyosawa and Tazawa, 1973). Evidence of polarity and other variations in the estimated parameters will be examined when the UL model is fit to data in Chapter 4.

The model predicted a decrease in L_p with increasing external solute concentration (§3.6.5c), which is consistent with the literature (Zimmermann and Steudle, 1978). However, it predicted that increasing the perturbation pulse has no effect on the measured membrane parameters (§3.6.5d), contrary to general expectations in the literature (Ye *et al.* 2006).

The above model predictions of no polarity, and of the effects of external concentration and perturbation size, are all consistent with the behaviour predicted by the KK equations. It is concluded that inclusion of ULs in the model doesn't affect the overall dynamics of the *P-t* curve, but affects the actual values of parameters estimated using the model.

The model showed that while it is likely that the value of *D* for the ULi is less than that for the ULe, this is likely to have only a small influence on the measured membrane parameters. It also showed that diffusional resistances of the membrane and ULs are not additive according to the permeability equation (Eq. (3.2)) based on Kirchoff's law of resistances in series, and therefore use of Eq. (3.3) to estimate quantitatively the influence of ULs on the estimated membrane parameters leads to large errors.

In Chapter 4, the UL model will be applied to raw CPP data collected by Dr. Helen Bramley (University of Adelaide) and Prof. Mel Tyree (USDA Forest Service).

4 Model with Unstirred Layers: Application to CPP data

4.1 Introduction

In this chapter, the UL model described in §3.2.2 is used to fit raw data collected by Dr. Helen Bramley (University of Adelaide) and Prof. Mel Tyree (USDA Forest Service). Data for several OPP and HPP experiments from different *Chara corallina* cells will be fit using the optimization method described in §2.3.3. Model validation and evaluation of the UL model, analysis of estimated parameters from the model, and a comparison with fits and predictions from the classical model, will be carried out.

The results are split into 3 sections: a) fitting one HPP and one OPP data set with the classical model, and UL model with 1 or 2 ULs, in a comparison of different UL models; b) fitting several HPP and OPP data sets (no ramp) with the classical and UL model with 2 ULs; c) fitting a few OPP data sets (with ramp) with the classical and UL model with 2 ULs. Fits and estimated parameters will be compared between the models, and between data sets from one cell (within-cell variation), and between cells (between-cell variation).

It will be shown that models with unstirred layers and without unstirred layers (classical model) can both reproduce the observed CPP relaxation curves. The models, which represent different hypotheses on the transport processes driving pressure changes in the cell, predict different sets of membrane parameters. Therefore, membrane parameters deduced from CPP data are very much dependent on the model used. This has implications on our current knowledge of membrane parameters and current methods of parameter estimation.

4.2 Description of experiments and experimental data

4.2.1 Description of CPP and conductivity experiments

Experiments were conducted by Dr. Helen Bramley and Prof. Mel Tyree at the University of Adelaide. Simultaneously with the CPP experiments, the conductivity of the external solution was measured in order to determine the time of osmotic perturbation and the time when the perturbation impacts on the cell (observed as a turgor pressure change). In addition, two methods of solution exchange (whereby a new solution completely replaces the old) were used: a) one where the new solution immediately followed the old, as in most CPP experiments, and b) one where a bubble was inserted between the old and new solutions for a more instantaneous change in solution. The bubble forces a slug movement of the new solution, where the front flattens out against the air-fluid interface and greatly reduces the duration of the solution exchange phase.

The CPP apparatus closely resembled that of Henzler *et al*. (2004). Solutions were delivered to the cell by gravity-feed from two plastic beakers 30-50cm above the *Chara* cell (Fig. 4.1). Stopcock valves at the bottom of the containers were used to control the flowrate at 16-18 cm s^{-1}, through tubing which had an inner diameter of 3 mm throughout. A second set of 3-way stopcocks (3WS) farther down the tubing were used to open and close flow from the containers and to admit air into the tubing for a distance of 10-12 cm below the stopcock. The length of the bubble ensured that the bubble passed beyond the Y-junction and clearly separated the two solutions. This differed from the apparatus used in Henzler *et al.* (2004) where only one 3WS was located at the Y-junction. The mean time of solution exchange when bubbles were present (based on 50 measurements on 4 cells) was 0.6 ± 0.1s. The mean time of solution exchange when no bubble was present was 2.3 ± 0.3s due to laminar flow mixing (Tyree, *pers. comm.*).

Artificial pond water (APW, a dilute solution of the salts Na^+, K^+, Ca^{+2} and Cl^- with a total ionic strength of ~3mM) was used as the external solution. Two Ag/AgCl electrodes were placed about 5cm apart in the vicinity of the cell.

The solution was changed from full APW to half-strength APW + 160mM EtOH in positive OPP experiments, and vice-versa in negative OPP experiments. As the electrolyte resistance of half-strength APW is half that of full APW, the timing and speed of the solution exchange could be measured by monitoring the electrical resistance and voltage change between the electrodes. In experiments without bubbles, the voltage starts changing as soon as the solution reaches the first electrode, and rises and becomes constant as it reaches and passes the second electrode (Fig. 4.2). In experiments with bubbles, the voltage rises to a maximum as the bubble reaches the second electrode, as air is now present between the electrodes and there is no current. Voltage from the conductivity measurements was recorded using the data acquisition and analysis software pCLAMP-9 (Axon Instrument Inc, Union City, CA, USA), and plotted simultaneously with the CPP voltage output from the data acquisition and analysis software Pfloek (V.1.09, provided with the CPP).

Noise from the CPP apparatus was also measured on a 14-minute period of constant turgor pressure (the plot of pressure against time gave a very low slope of -7×10^{-5}, with $R^2 = 0.0027$). The plot exhibited discrete jumps in pressure of 0.0001-0.0002 MPa, which can be taken as the measuring resolution of the CPP. The plot had an RMS of 0.0003 MPa about the mean with a maximum deviation of 0.0008 MPa from the mean. The overall measurement error in the pressure can be taken to be around 0.0005 MPa, or about 2 standard deviations.

Measurements of the bulk modulus ε were conducted prior to each course of experiments. It was verified for one set of HPP experiments that ε was the same measured at the beginning and end of the set (over a 6 minute time-period). The laboratory temperature was not measured, but could be assumed to be about 20^{o} C (Bramley, *pers. comm.*).

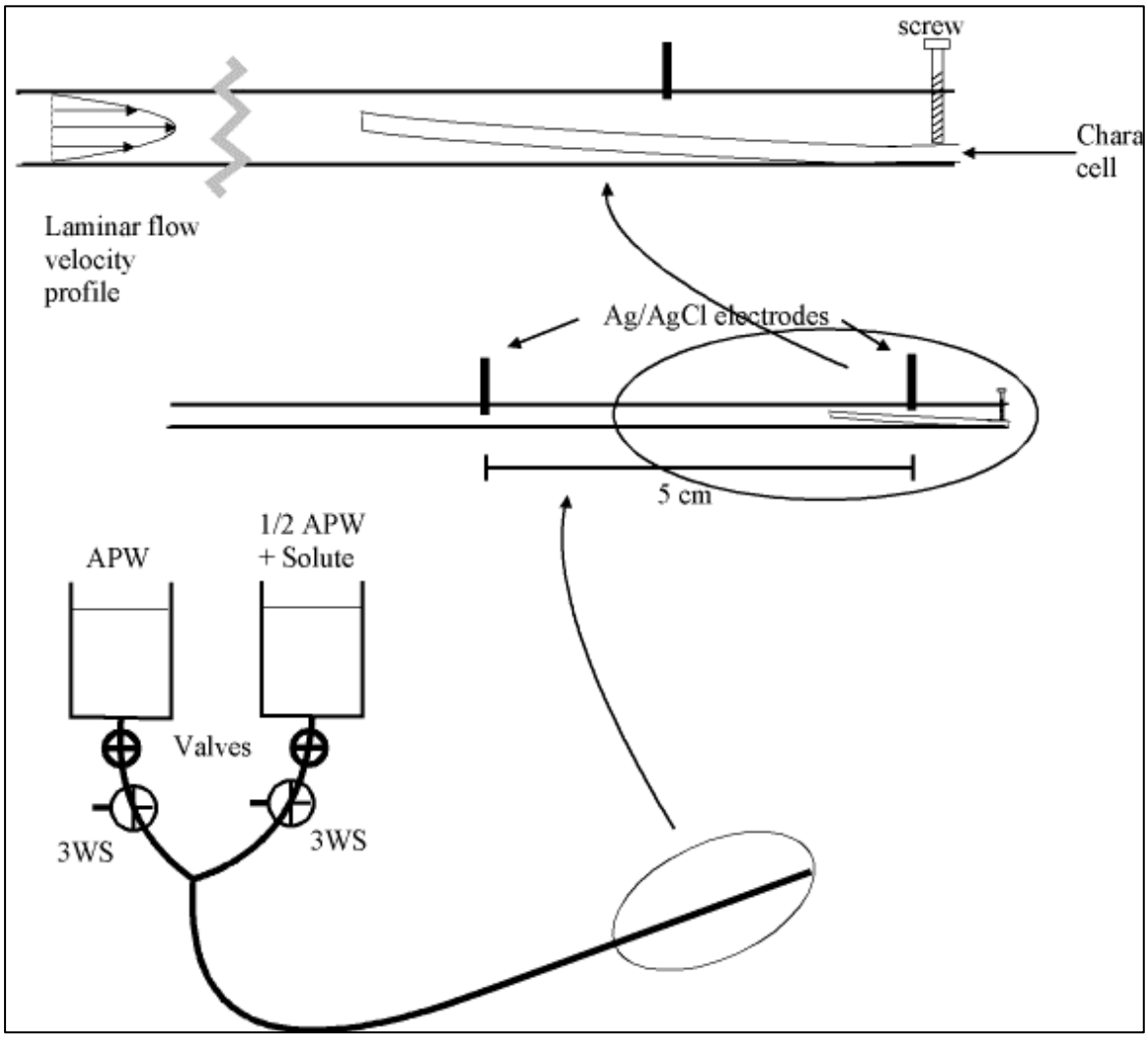

Fig. 4.1 Set-up for CPP and conductivity experiments. Showing *Chara* cell fixed in place by a plastic screw; 2 Ag/AgCl electrodes placed 5cm apart (and 1cm from the end of the tube) for monitoring change in electrolyte resistance; beakers, stopcock values and tubing for solution exchange (not drawn to scale). (Tyree, unpublished)

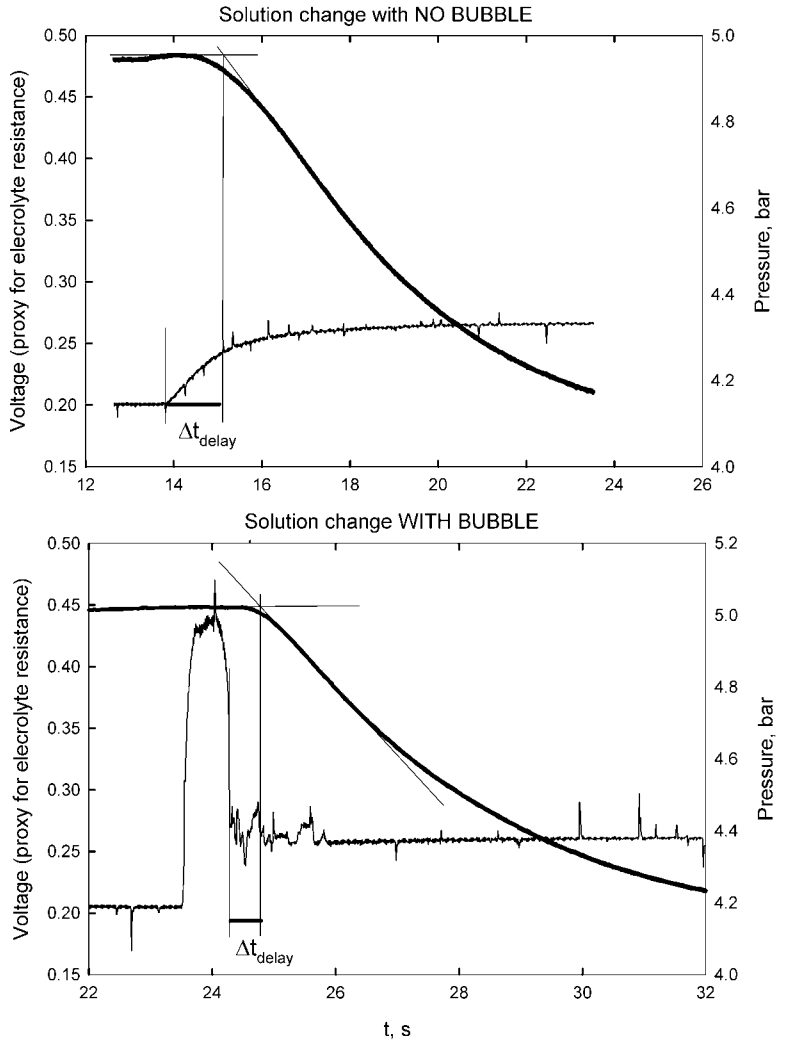

Fig. 4.2 Showing pressure (smooth black line) and conductivity measurements for OPP experiments with and without bubbles. Full APW was exchanged for ½ APW + 160mM EtOH for both experiments. Passage of a bubble can be observed (lower diagram) by a voltage rise to 0.43V and step-wise change in electrolyte resistance. (Tyree, unpublished)

4.2.2 Data collected

a) CPP data

OPP and HPP experiments were carried out on 4 different *Chara* cells (Table 4.1). Equal numbers of positive and negative pulses were carried out for each set. The cell dimensions were measured by the experimenters, but I derived values for ε using the

Pfloek software. For Cell 1 a concentration of 125mM ethanol was used for the OPP perturbations. For the other 3 cells a concentration of 160mM ethanol was used.

Table 4.1 Cell dimensions, ε values, and type of experiments conducted on 4 *Chara* cells. L = cell length, d = cell diameter, V = cell volume.

Cell	Date of expt	L (mm)	d (mm)	V (mm^3)	ε (MPa)	Experiments
1	10-2-05	21	0.930	14.3	28.4 ± 4.4*	8 OPP (4b**); 4 HPP
2	11-2-05	24	0.977	18.0	27.9 ± 4.1	10 OPP (4b); 6 HPP
3	11-2-05	45	0.791	22.1	24.6 ± 2.4	10 OPP (4b); 8 HPP
4	18-2-05	33	0.977	24.7	36.5 ± 4.2	10 OPP (6b); 12 HPP

* includes measurement and operator error
** 'nb' indicates n experiments used bubbles during the solution exchange

b) Conductivity data

From the conductivity measurements one can obtain the time-delay (time between an osmotic perturbation and when the perturbation impacts on the cell), and the exchange time (time it takes for the external solution to be completely exchanged). The time for solution exchange is the time it takes the external concentration to reach the final perturbation value, and is the ramp time mentioned in previous chapters. Individual time-delays and ramp times were recorded for each OPP experiment. An example of these data is given in Table 4.2.

The UL model simulates radial flow at any point along the cell axis, and assumes radial and axial symmetry. The time and place at which the perturbation impacts on the cell was taken to be at an axial point midway along the length of the cell. The time-delay t_D was therefore defined as the time between the solution reaching the middle of the cell and the time t_P when the cell pressure is first observed to change. For OPP experiments with a bubble, the measured time-delay (t_{Dr}) is the time between the bubble reaching the second electrode and t_P. t_D was obtained by calculating $t_D = t_{Dr} + t_2$, where t_2 is the time it takes for the solution to travel between the second electrode and the center of the cell. For OPP experiments without a bubble, t_{Dr} is the time between the solution reaching the first electrode and the cell pressure changing. t_D is obtained by calculating $t_D = t_{Dr} - t_1$, where t_1 is the time it takes for the solution to travel between the first electrode and the center of the cell.

The ramp time is the time it takes for the external concentration to reach its final perturbation value. The measured ramp time t_{Rr} (in experiments without bubbles), was the time between the solution reaching the first electrode and the time when the voltage reaches a constant value (indicating no more mixing or increase in external concentration; see top diagram in Fig. 4.2). The ramp time t_R is calculated by $t_R = t_{Rr} - t_1$, where t_1 is as defined above.

Table 4.2 Time-delay (t_D) and ramp time (t_R) data for Cell 4 of Table 4.1. N=bubble not present, Y=bubble present.

Run no.	Bubble	t_D (s)	t_R (s)
1	N	0.92	2.34
2	N	0.50	1.37
3	N	0.80	2.14
4	N	0.55	1.60
5	Y	0.56	
6	Y	0.42	
7	Y	0.69	
8	Y	0.42	
9	Y	0.62	
10	Y	0.44	

As one can see from Table 4.2, the ramp times are 2-3 times as long as the time-delays. This is because the ramp time is comprised of a transit time (the time it takes for the front of the new solution to traverse the length of the cell), and the mixing time (the time it takes for the region of partial mixing behind the front to traverse the cell, before the solution is completely replaced). For OPP experiments with a bubble, the ramp time may be considered negligible since there is no mixing time, and the transit time for the 4 cells ranged from 0.01 to 0.26 s. These are very small ramp times compared to the measured ramp times, and it can be concluded that the main component of the ramp time is the mixing time.

4.3 Analysis and use of CPP data

4.3.1 Chosen subset of CPP data

A subset of the available data was chosen for fitting (Table 4.3). In order to examine within-cell variation in parameters, and differences in parameters between fits to experiments with and without bubbles, all the data for Cell 4 was fit. Cell 4 was chosen as there were 6 smooth OPP curves with bubbles, and more available HPP data for this cell. In order to examine between-cell variation in parameters, a positive and negative OPP and HPP set was fit for Cells 2 and 3. Data for Cell 1 was not fit as it was a noisier data set.

Table 4.3 Subset of the data that will be fit by the models.

Cell	Experiments
2	4 OPP with bubble; 4 HPP
3	4 OPP with bubble; 4 HPP
4	6 OPP with bubble, 4 OPP without bubble; 10 HPP

4.3.2 Resolution of CPP data

The time resolution of the Pfloek data was about 0.02-0.2 s, giving around 3000-6000 data points for OPP experiments, and around 500-800 data points for HPP experiments. Use of all the data points in a parameter estimation via Matlab optimization runs was impractical because of excess computer runtimes (which could take an hour or more) and therefore the data was culled. To this aim, the effects of culling on parameter values estimated using the classical model were analysed. For an OPP data set with 520 points in the water phase and 2127 points in the solute phase, points in both phases were culled by selecting every i^{th} point, where i varied between 2 and 10. When the data was culled by the same amount in both water and solute phases, the parameters differed by <1% for fits between the unculled and most greatly culled data. This behaviour was verified on another OPP data set. While there was little change in the parameters, the SE's for the estimated parameters increased with

decreasing data resolution. However, the magnitude of the SE's when every 10th point was retained was found to be acceptable (Table 4.4), and it was decided to use this data resolution for all OPP data sets, i.e. every 10th data point in the pfloek output was retained during parameter estimation.

A similar analysis on two HPP data sets revealed that retaining every 10th point did not alter the estimated parameters, but did increase the SE in L_p. It was chosen to retain every 2nd point for the HPP data sets, since there are far fewer points as compared to OPP data and the optimization is still efficient. This brings the size of the culled HPP data sets down to that of the culled OPP data sets, and the SE in L_p to 0.01 x 10^{-6} m s^{-1} MPa^{-1}.

Table 4.4 Showing parameters estimated with the classical model and their standard errors, for two OPP data sets. A data resolution of 1/10th has been used, giving a total of 265 points for the negative OPP and 272 points for the positive OPP data sets.

	Negative OPP		Positive OPP	
L_p (x 10^{-6} m s^{-1} MPa^{-1})	1.30	±0.01	1.49	±0.01
p_s (x 10^{-6} m s^{-1})	3.92	±0.02	3.84	±0.02
σ	0.273	±0.001	0.262	±0.001
t_0 (s)	1.04	±0.02	0.73	±0.02

It must be noted that when a different data resolution is used between the water and solute phases in the OPP data, points in the water and solute phases are differentially weighted, which affects the estimated parameters. It was found that the estimated parameters differed by 2-8% for fits between the unculled data and most greatly culled data – where every point in one phase was retained while every 10th point in the other phase was retained. The above results show that as long as the same data resolution is used for the whole data set, there is little effect on the estimated parameters.

The time interval that resulted from using every 10th data point generally ranged between 0.5 and 1.5 s. The data could also be culled based on time intervals, e.g. retaining points every 0.5s apart. An exploration of this was not carried out.

4.3.3 Analysis of CPP equilibrium pressures

Initial and final equilibrium pressures were determined over periods of about 20s, depending on the amount of noise in the data. It was observed that the final equilibrium pressure often overshot the initial equilibrium pressure for the OPP experiments. An analysis of equilibrium values revealed a consistent pattern where P_E was slightly lower than P_0 for the negative OPP, and P_E was slightly higher than P_0 for the positive OPP (Table 4.5; Fig. 4.3a). The APW change from full to half-strength, or vice-versa, was suspected to be the cause of this overshoot. This was confirmed when OPP experiments were later conducted on another *Chara* cell without the APW change (Cell 5), as no overshooting of P_E occurred for this cell, but instead a consistent slight undershooting was observed (Table 4.5). Possible reasons for this will be outlined in a later discussion.

Table 4.5 Mean differences between initial equilibrium pressures P_0 and final equilibrium pressures P_E observed in the OPP data, for cells 2 to 5. Errors given are standard errors.

Cell	Mean P_0 - P_E values	
	Positive OPP	Negative OPP
2	-0.0020 ±0.0005	0.0028 ±0.0003
3	-0.0012 ±0.001	0.0031 ±0.0005
4	-0.0013 ±0.0006	0.0006 ±0.0008
5	0.0013 ±0.0001	-0.0014 ±0.0003

Sensitivity of cell turgor to the external concentration was also confirmed in the models, where the APW change had to be incorporated into the perturbation (initial) conditions in order to give a reasonable fit to the P_E values of the data. As shown in §2.2.2, the standard KK equations without an APW change predict that P_E returns to the original equilibrium pressure P_0, and the value of P_E is not changed by the presence of ULs (§3.6.2).

A long-term drift in the equilibrium pressures was observed for cells 2-4 (e.g. Fig. 4.3b). Cells 2 and 3 showed a downward drift, and Cell 4 showed an upward drift. No significant drift was observed for Cell 5, which may be due to it being a larger cell (volume = 31.2 mm^3) with more stable turgor pressures. It is possible that the lack of

an overshoot in P_E and long-term drift for Cell 5 are both related to the absence of an APW change, however this could not be determined from the data available.

Although P_0 was determined individually for each experiment, a constant cell volume V_0 and cell radius r_0 were used for all experiments on the one cell, corresponding to the measured values at the beginning of all the experiments. These values were not adjusted to correspond to P_0, since the corresponding changes in V_0 and r_0 are so small as to make negligible impact on the fits, which are more sensitive to the value of P_0.

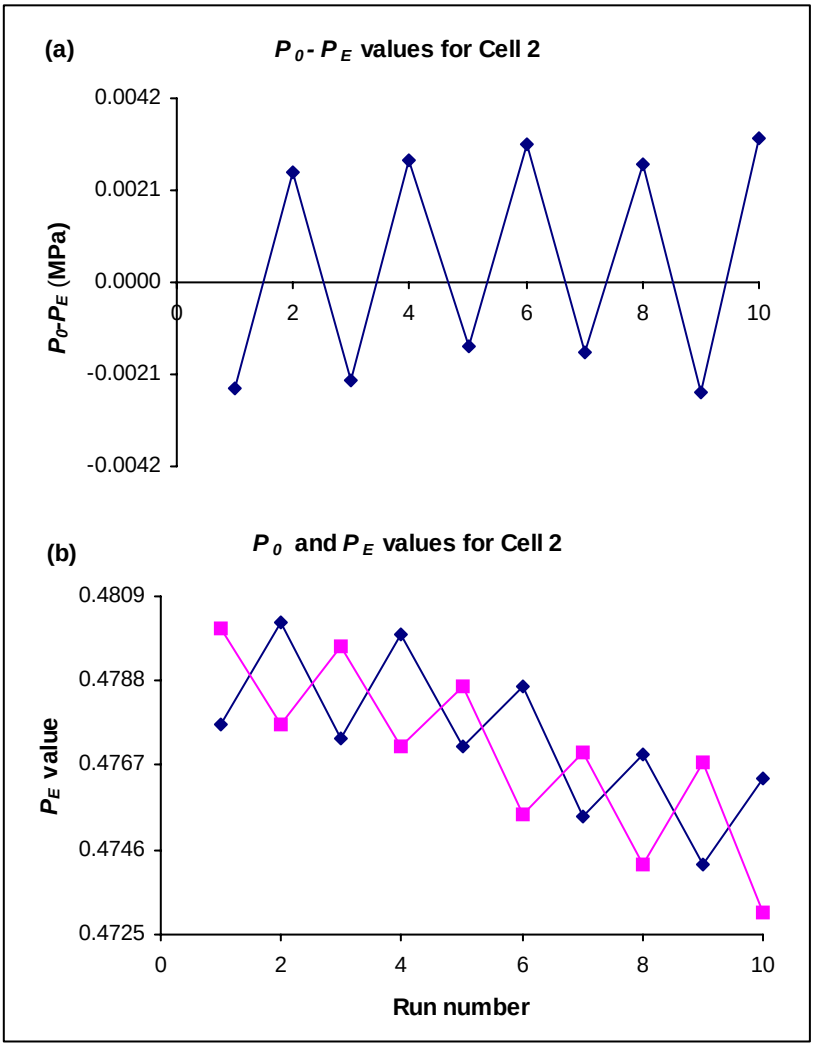

Fig. 4.3 Showing (a) differences in initial and final equilibrium pressures, and (b) a gradual downward drift in P_0 (——) and P_E (——), for OPP experiments for Cell 2.

For the HPP experiments, it is expected that $P_E < P_0$ for the positive pulses, and vice-versa for the negative pulses (§2.2.2). There was some difference in the magnitude of $P_E - P_0$ between the positive and negative pulses, however these cannot be said to be significant since the standard errors for the mean values of $P_E - P_0$ were quite high (Table 4.6). The HPP data was generally not as smooth as the OPP data, and for some data sets the equilibrium pressure would rise or drop before the perturbation so that there was uncertainty surrounding P_0. In the example in Fig. 4.4, P_0 is steady for a few seconds then rises by 0.01 MPa before the perturbation, remaining at the new value for a couple of seconds. In this case the pressure values just before the perturbation were used to calculate P_0 as they were closer to the final perturbation pressure. However, in other cases it seemed more appropriate to calculate P_0 using the pressure values a few seconds before the perturbation, depending on which value was closer to the final equilibrium pressure, which was usually quite steady.

Table 4.6 Mean differences between initial equilibrium pressures P_0 and final equilibrium pressures P_E observed in the HPP data, for Cells 2 to 4. Errors given are standard errors.

Cell	Mean $P_0 - P_E$ values (MPa)	
	Positive HPP	Negative HPP
2	-0.0005 ± 0.0003	0.0017 ± 0.0009
3	-0.0009 ± 0.0003	0.0012 ± 0.0002
4	-0.0004 ± 0.0002	0.0008 ± 0.0004

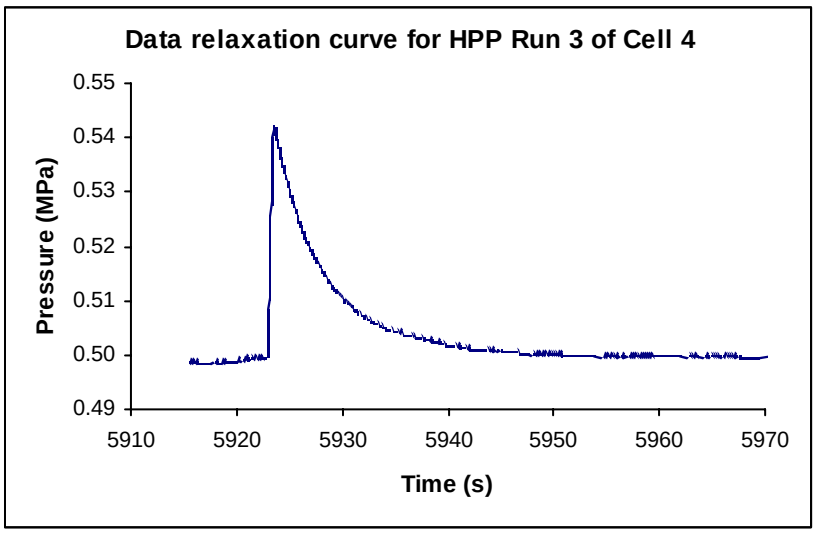

Fig. 4.4 Showing a rise in initial equilibrium pressure before the perturbation in an HPP experiment

4.3.4 Analysis of perturbation pressures in HPP data

It was observed that the "instantaneous" perturbation from P_0 to P_m in an HPP experiment typically took 0.3-0.8 s. Moreover, the region around the maximum or minimum pressure of the data and the point at which the simulations begin, is often not well-defined. In some data sets this region exhibited a kink in the data following the extremum point (e.g. Fig. 4.5a) or during the perturbation itself (e.g. Fig. 4.5b), where the pressure dynamics seemed to suddenly change. In other data sets the extremum point was slightly rounded (e.g. Fig. 4.5c). These variations may be attributed to the manual operation of the CPP, where the operator adjusts the metal rod by manually rotating a screw to inject or withdraw sap from the cell (see §1.2). These variations will have implications on fitting HPP data in §4.5.3 and §4.6. Data sets which are very noisy around the extremum were not used here.

4.4 Analysis and use of conductivity data

4.4.1 Data patterns

Variation in the measured ramp times and time-delays were different for each cell (Table 4.7). This was often due to time-delays and ramp times being shorter for the negative OPP experiments than the positive OPP experiments, particularly for cell 4. The large variation in measurements for cell 4 may be partly due to a blip in pressure just before the water phase for 4 positive OPP runs (Fig. 4.6). By disturbing the equilibrium pressure, this blip may be causing the water phase to occur later that it would otherwise, increasing the time-delay. It is thought that blips in pressure may be from switching flow on and off to change solutions, and appears to be cell-dependent occurring in extremely sensitive cells (Bramley, *pers. comm.*).

Table 4.7 Mean time-delay and ramp time measurements for each cell. Ramp times for Cell 1 were not obtained.

Cell	Time-delay (s)		Ramp time (s)
	Bubble	No bubble	
1	0.48 ± 0.07	0.55 ± 0.10	
2	0.37 ± 0.07	0.57 ± 0.12	2.01 ± 0.01
3	0.56 ± 0.03	0.73 ± 0.16	2.17 ± 0.10
4	0.52 ± 0.12	0.70 ± 0.20	1.87 ± 0.45

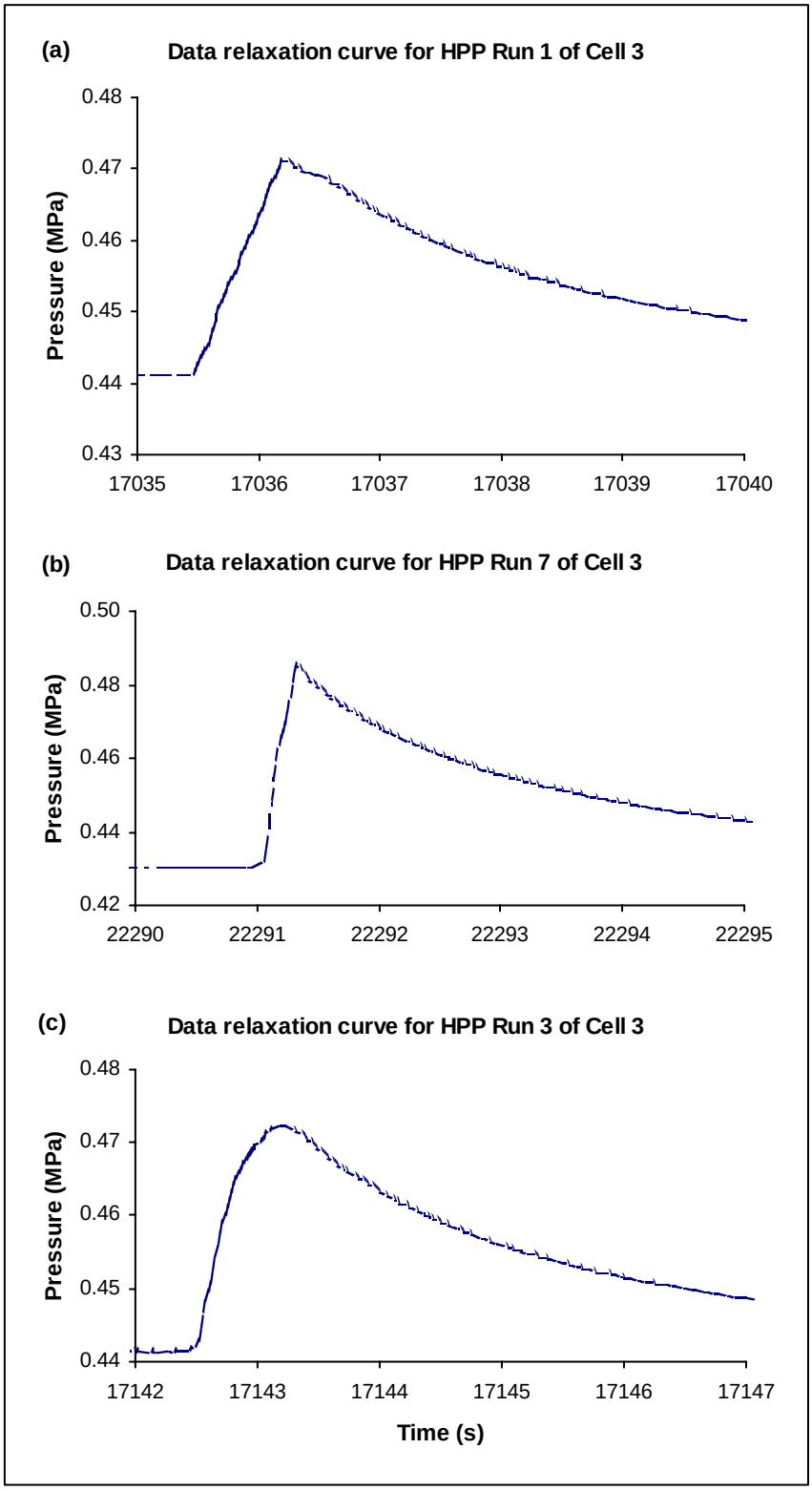

Fig. 4.5 Showing region of pressure perturbations for 3 HPP data sets from Cell 3.

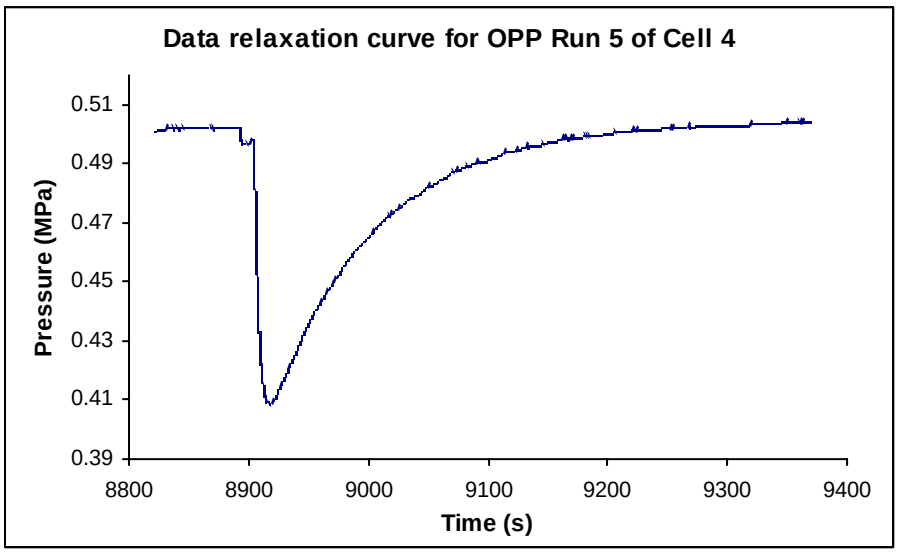

Fig. 4.6 Showing a blip in pressure before the water phase for an OPP relaxation curve.

4.4.2 Use of conductivity data

a) Time-delay measurements

The time-delay measurements for the OPP experiments were used to determine t_0, the time when the osmotic perturbation occurred. A value of t_P (the time when the cell pressure starts changing) was obtained from the unculled data by taking a linear regression of points in the first 1/3-1/2 of the water phase (see Fig. 3.8). From the time-delay t_D, we have:

$$t_0 = t_P - t_D. \qquad (4.1)$$

One may ask: does the measured time-delay give information about the ULe thickness present in an OPP experiment? In §3.6.2 it was demonstrated that, in simulated data, a relationship exists between the ULe thickness δ_{ULEsim} and the time-delay t_{Dsim}. This suggests that a relationship may also exist between the measured time-delay t_D and the ULe thickness δ_{ULE} present in an OPP experiment. If there is a consistent t_D vs. δ_{ULE} relationship, then t_D can be used to infer a value of δ_{ULE}.

Since the value of δ_{ULE} is unknown, the relationship between t_D and δ_{ULE} cannot be examined directly. It may then be asked whether the simulated data can be used instead to infer δ_{ULE} in an OPP experiment. However, this will only be possible if:

a) the simulated curve fits the initial curvature and water phase of the observed data exactly (i.e. $t_{Dsim} = t_D$)
b) the relationship between the ULe thickness and the time-delay in both observed and simulated data are consistent across different cells.

It may be shown that (a) is rarely achieved and that (b) is false, thus limiting the usefulness of t_D as a general predictive tool for the ULE thickness. To show this, the relationships between t_{Dsim} and δ_{ULEsim}, and between t_D and δ_{ULEsim}, for fits to two OPP data sets from different cells, were examined. δ_{ULEsim} in this case is used as a hypothetical proxy for δ_{ULE}. δ_{ULEsim} was fixed at different values, the data fitted by optimizing L_p, p_s, σ and t_0, and t_{Dsim} and t_D calculated. t_0 must be optimized since t_D is affected by δ_{ULEsim}, and t_P in Eq. (4.1) changes by a lesser amount than t_0 for fits to the data.

It was found that for a small range of δ_{ULEsim} values (3-7 x 10^{-5}m), the δ_{ULEsim} vs. t_D and δ_{ULEsim} vs. t_{Dsim} relationships for fits to two data sets from different cells were linear (Fig. 4.7). However, the slope of these relationships differed between δ_{ULEsim} vs. t_D and δ_{ULEsim} vs. t_{Dsim} (in each Fig. 4.7b and Fig. 4.7c), as predicted, due to differences in the slopes of the water phases between simulated and observed data. The slope of these relationships also differed between the two data sets (Fig. 4.7b & Fig. 4.7c). The δ_{ULEsim} vs. t_{Dsim} relationship for simulations where the data is not fitted but different values of δ_{ULE} were chosen and used to generate different relaxation curves (Fig. 4.7a), was linear but with a different slope again.

These results confirm that (a) and (b) above are not true and that there is no method for inferring the ULe thickness in CPP experiments from available data. Therefore, δ_{ULE} should be treated as an additional parameter to be optimized for fits using the UL model. Use of the measured time-delay was limited to determination of t_0 for OPP experiments.

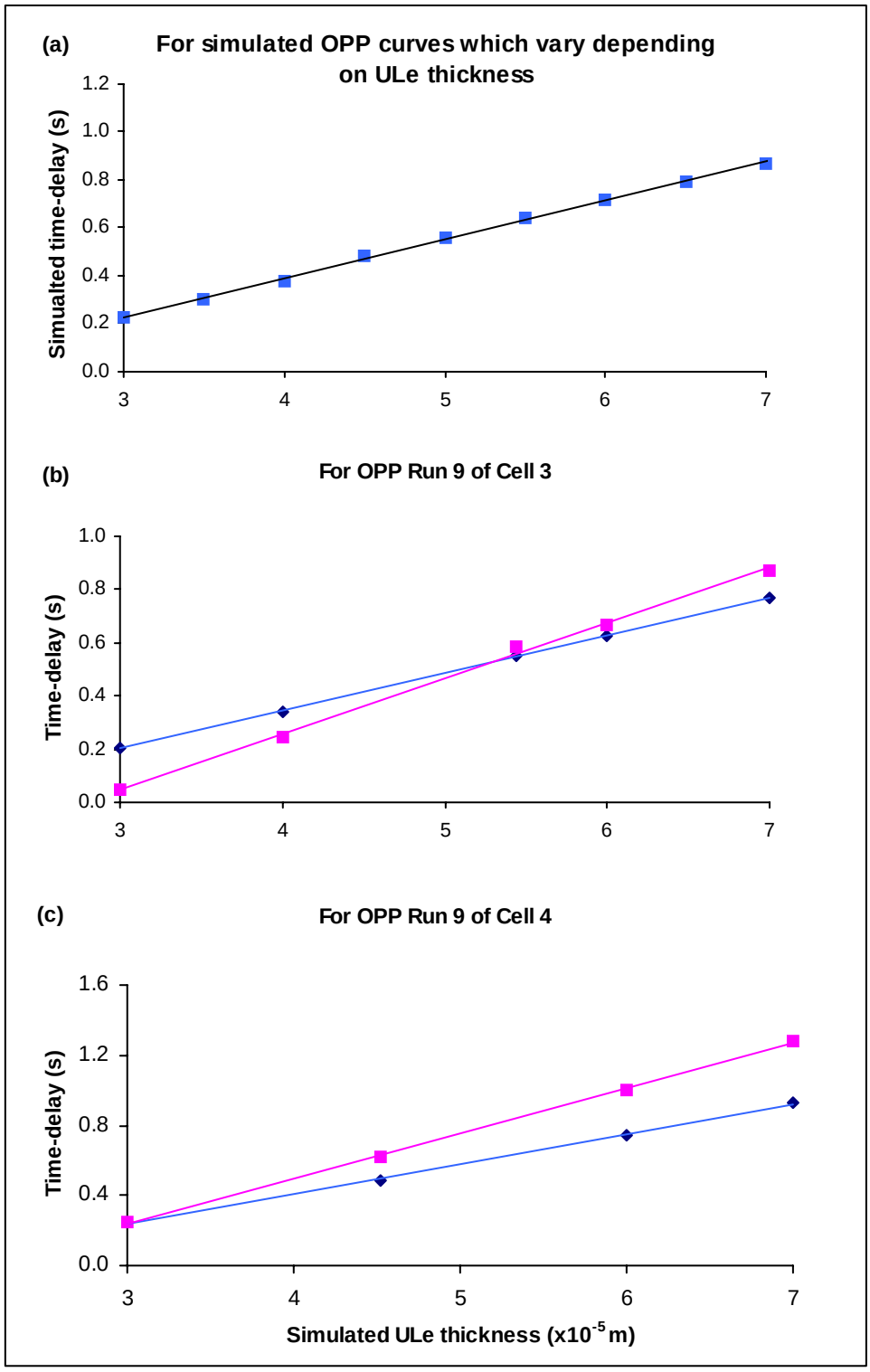

Fig. 4.7 Showing time-delay vs. ULe thickness ($\boldsymbol{\delta_{ULEsim}}$) relationships. (a) For simulated curves which change with $\boldsymbol{\delta_{ULEsim}}$. In (b) and (c), the pink line indicates $\boldsymbol{\delta_{ULEsim}}$ plotted against t_D for observed OPP data, and the blue line indicates $\boldsymbol{\delta_{ULEsim}}$ plotted against t_{Dsim} for fits to the observed OPP data.

b) Ramp time measurements

The relationship between the ramp time and time-delay was examined by imposing a ramp in the external solute concentration in simulated OPP data and calculating the time-delay from the output *P-t* curve. The model showed a correlation between the ramp time and time-delay, as expected since they are both dependent on t_0 (Fig. 4.8). However, as the main component of the ramp time is the mixing time (§4.2.2b) which may vary between runs and have no relation to t_0, this correlation would not necessarily be observed in the observed data.

When measured ramp times and time-delays were plotted for the observed data (Fig. 4.9), it was found that only cell 4 exhibited a correlation between these two factors. For cells 2 and 3 the ramp times were similar for each OPP run (Table 4.7).

Considering these patterns in the measured ramp times, the latter was not suitable for use as an input into the model. It was decided that for model fits to OPP experiments without a bubble (e.g. for Cell 4), the ramp time will be considered a free parameter to be optimized along with the membrane parameters (in a similar way that the ULe thickness was considered an additional free parameter for OPP experiments with bubbles). Since the ramp time and ULe thickness can't be simultaneously optimized due to their correlation (the ramp time is correlated with the time-delay which in turn is dependent on the ULe thickness), the ULe thickness will be fixed at average values found for fits to the OPP experiments with a bubble, and the ramp times then estimated using the model. This is because for a given cell geometry and the same external flow rate and external solution, one would expect the ULe thickness to be more or less a constant value for each cell.

There is a lack of sufficient information available on how the external concentration changes over time. The conductivity data in Fig. 4.2 suggests that the change in external concentration (or shape of the concentration exchange function) is non-linear and is not actually a ramp. Consequently, different representations for this exchange function (linear and exponential) will also be explored (see §4.7).

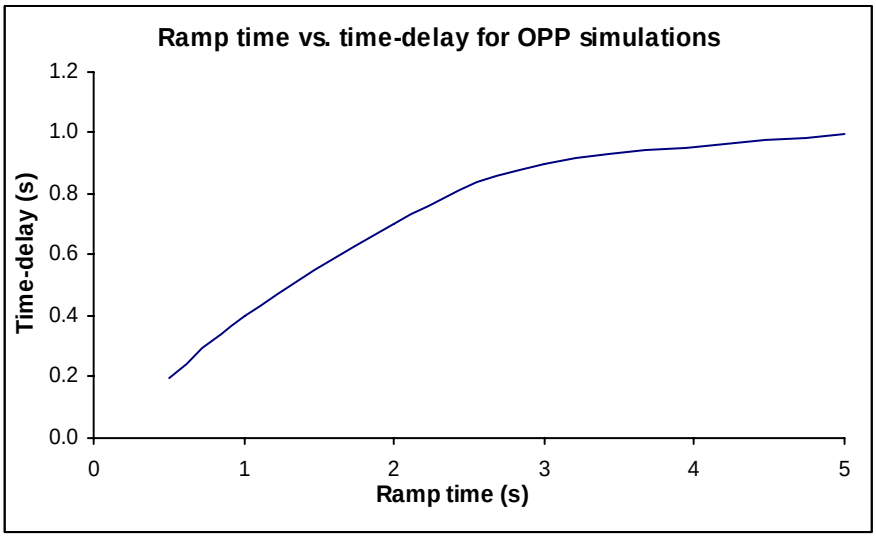

Fig. 4.8 Showing a correlation between ramp times and time-delays for simulated OPP data using the UL model.

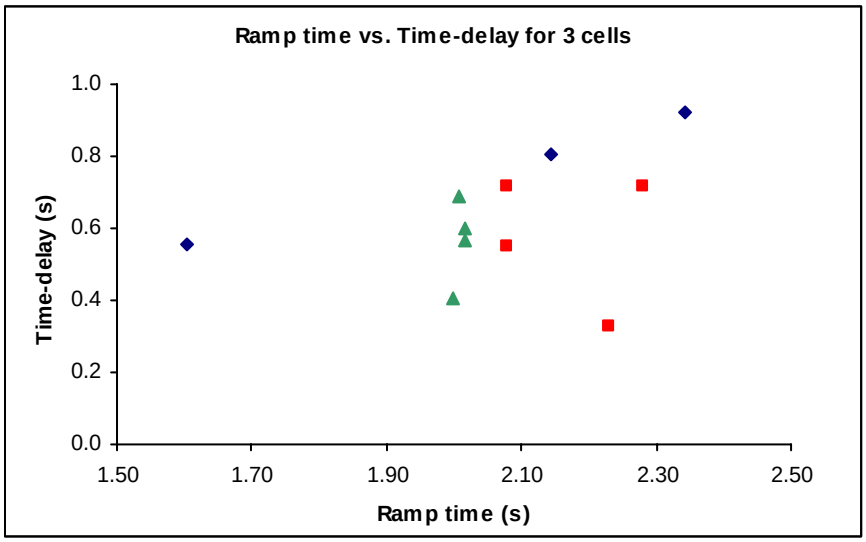

Fig. 4.9 Ramp times vs. time-delays for observed OPP data for Cell 2 (▲), Cell 3(■), and Cell 4 (♦).

4.5 Fits to data: Comparison of model options

4.5.1 Choice of model option

In order to compare influences of a ULe and ULi on the relaxation curves and estimated membrane parameters, an OPP and an HPP experiment were fit with

different model options incorporating 0, 1, or 2 ULs. It can be noted that the UL model with ULs excluded reverts to the classical model.

A runtime of 400s was used for the OPP data, and a runtime of 40s used for the HPP data. P_E was calculated using the last 20s for OPP data and the last 5s for HPP data. For all fits to subsequent data sets, the same time periods of the data and method of calculating P_E will be used, as the optimized parameters depend a little on the extent of the data fit.

As the thicknesses of the ULs are unknown, they are considered free parameters which may be optimized. However, as shown in §3.6.2 the *P-t* curve and curve characteristics change little after a certain ULi thickness (δ_{ULi}), that is for $\delta_{ULi} > 2\text{x}10^{-4}$ m the model is insensitive to δ_{ULi}. During parameter optimization the value of δ_{ULi} often fell in this range where the model is insensitive to it, which suggests that the optimum value for δ_{ULi} as determined by the model is large. However, since the model cannot optimize δ_{ULi} in this region where it is insensitive, for subsequent analyses δ_{ULi} is assigned a value instead of being optimized. As one may reasonably assume that the whole cell interior is a ULi it was chosen to fix δ_{ULi} at $3\text{x}10^{-4}$m, a value close to but not equal to the whole cell interior, since larger values have negligible impact on the pressure dynamics and estimated parameters (see §3.6.2). Where a ULe is present, δ_{ULe} was optimized.

For the OPP data, both a ULe and a ramp may contribute to the time-delay following the time of perturbation (see §2.7.3c). For the Classical model the fit to the initial points also depends on the value of t_0 (see §2.5.2). When a ULe is not present, a ramp must be included or t_0 optimized in order to fit the initial data points. The ULe thickness, t_0 and ramp time are strongly correlated, and therefore these 3 values were fit independently of each other, according to the model options in Table 4.8.
For the HPP data, a ULe has little influence on the pressure dynamics (see §3.6.2), and therefore the data was fit with and without a ULi only. It was found that, in particular for the negative pulses, the data could not be fit well unless P_E was fit in addition to L_p, as otherwise the model kept overpredicting P_E for the negative HPP. As the CPP software Pfloek also fits the HPP data by fitting P_E, fitting P_E seemed a reasonable approach to take for comparing the UL model fits to the Classical model

fits. P_E is an output of the simulation and so cannot be directly fit, but the quantity π_{ie} is determined by the experimenter and this affects P_E. If π_{i1} is the osmotic pressure in the cell at the time of perturbation, then at equilibrium $P_E = \pi_{i1} - \pi_{ie}$. Therefore to fit P_E, π_{i1} was optimised. We may assume that π_{ie} is a constant since the external solution is constantly being replaced. Model options and parameters used to fit the HPP data are shown in Table 4.8.

Table 4.8 Showing the different model options and their estimated parameters used to fit OPP and HPP data.

OPP data	Fitted parameters	HPP data	Fitted parameters
0 ULs (Classical)	L_p, p_s, σ, t_0	0 ULs (Classical)	L_p
0 ULs with ramp	L_p, p_s, σ, t_R	0 ULs (Classical)	L_p, π_{i0}
1 ULe	L_p, p_s, σ, δ_{ULe}	1 ULi	L_p
1 ULi with ramp	L_p, p_s, σ, t_R	1 ULi	L_p, π_{i0}
2 ULs	L_p, p_s, σ, δ_{ULe}		

When comparing fits, the RMS, bias and trend of the residuals will be given. The bias is the arithmetic mean residual, and indicates by how much the average residual departs from 0. The trend is the slope of a regression line through the residuals, and indicates how even the spread of the residuals are.

The temperature used in the model is 293K (20^o C). It was found that a 2 degree change in the temperature makes <1% difference to the estimated parameters, so that any slight variation in the laboratory temperature (which is usually quite constant) would have little impact on the estimated parameters. A diffusivity of $D = 1.28 \times 10^{-9}$m is used for the permeant solute ethanol.

4.5.2 Results for an OPP

The 5 model options in Table 4.8 were fit to a positive OPP experiment, OPP run 9 of Cell 3. In order to obtain a uniform distribution of residuals, it was chosen to fit P_m to within ± 0.001 MPa, which is also twice the measurement error in P. In order to

achieve this, for some fits the RMS was weighted in a window around the extremum (using a weight of 2), based on 10% of the maximum pressure change in the data. Improving the fit to the extremum was also considered important since the RMS method often fails to fit this region where there is significant noise in the data as P approaches P_E (see §2.6.2).

All 5 model options were found to give similar fits to the data. The RMS values were slightly better for the UL models, however the residuals were comparable with all having a low bias and trend (Table 4.9; Fig. 4.10). All of the fits returned the same value of P_E (as expected), which slightly over-estimated the data P_E of 0.4338 MPa by 0.001.

Table 4.9 Estimated parameters ± SE for the 5 model options (listed in Table 4.8) used to fit negative OPP data (OPP run 9 in Cell 3): 1. Classical model with optimized t_0; 2. Classical model with ramp; 3. UL model with 1 ULe; 4. UL model with 2 ULs; 5. UL model with 1 ULi and ramp.

	1. 0 ULs		2. 0 ULs with ramp		3. 1 ULe		4. 2 ULs		5. 1 ULi with ramp	
t_0 (s)	0.74	±0.012	0		0		0		0	
ramp time (s)	0		1.45	±0.03	0		0		1.49	±0.02
δ_{ULi} (x 10^{-5} m)	0		0		0		30.0		30.0	
δ_{ULe} (x 10^{-5} m)	0		0		4.88	±0.06	4.80	±0.06	0	
L_p (x 10^{-6} m s^{-1} MPa^{-1})	2.88	±0.02	2.88	±0.03	3.16	±0.04	2.33	±0.02	2.20	±0.02
p_s (x 10^{-6} m s^{-1})	3.77	±0.01	3.83	±0.01	4.37	±0.02	6.46	±0.03	5.29	±0.02
σ	0.257	±0.001	0.260	±0.001	0.299	±0.001	0.444	±0.002	0.364	±0.003
t_m (s)*	9.30		9.31		9.09		9.31		9.40	
P_m (MPa)	0.3508		0.3503		0.3501		0.3494		0.3496	
P_E (MPa)**	0.4348		0.4348		0.4348		0.4348		0.4348	
RMS (x 10^{-4} MPa)	7.26		6.94		6.55		6.14		6.01	
Bias (x 10^{-4} MPa)	3.93		4.55		3.79		3.25		2.92	
Trend (x 10^{-4} MPa s^{-1})	3.50		3.63		3.68		3.17		3.30	

* For the observed data, t_m = 9.49s, P_m = 0.3502 MPa, P_E = 0.4338 ± 0.0001 MPa.

** SE for P_E = 1x10^{-5} MPa

Relaxation curves for the 2 UL model fit to OPP run 9, Cell 3

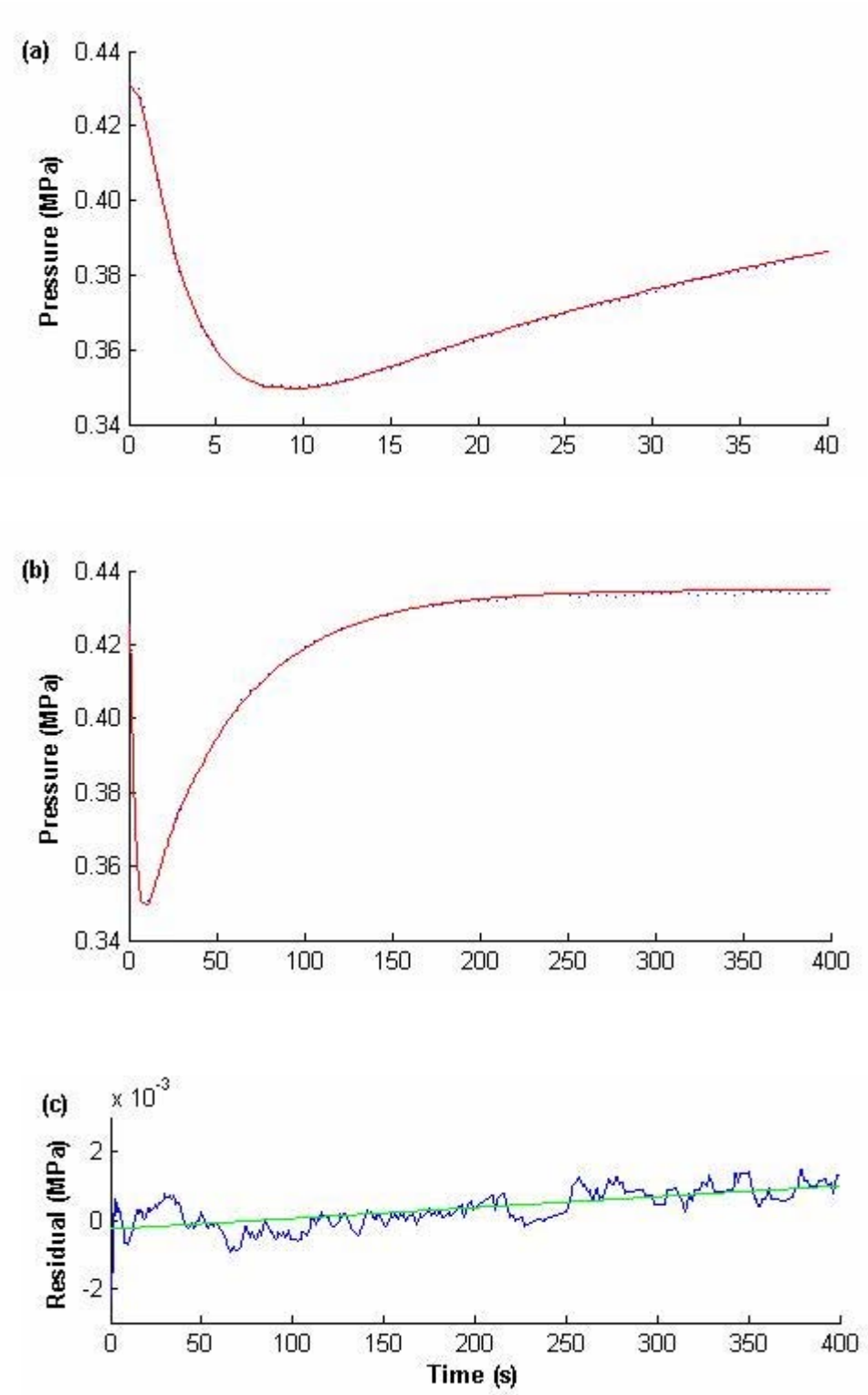

Fig. 4.10 Results from fitting the UL model with 2 ULs to OPP run 9 of cell 3, showing raw pressure data (-----) and model fit (——). (a) Showing 0-40s of the curve, (b) showing the full simulated relaxation curve, (c) showing residual plot, with trendline (——). Curves and residual patterns were very similar for all 5 model options.

Parameter values were found to be the same for the two classical model options (Table 4.9; Fig. 4.11). With the UL model, including a ULe caused all 3 membrane parameters to increase slightly, while including a ULi caused p_s and σ to increase and L_p to decrease. Changes in p_s and σ due to ULs were strongly correlated. The ULi had a far greater effect on the estimated parameters than did the ULe, and differences in the membrane parameters between the UL model and the classical model were greatest when 2 ULs were present (Fig. 4.11, Table 4.10). These results are in accordance with the parameter analysis carried out in §3.6.5a.

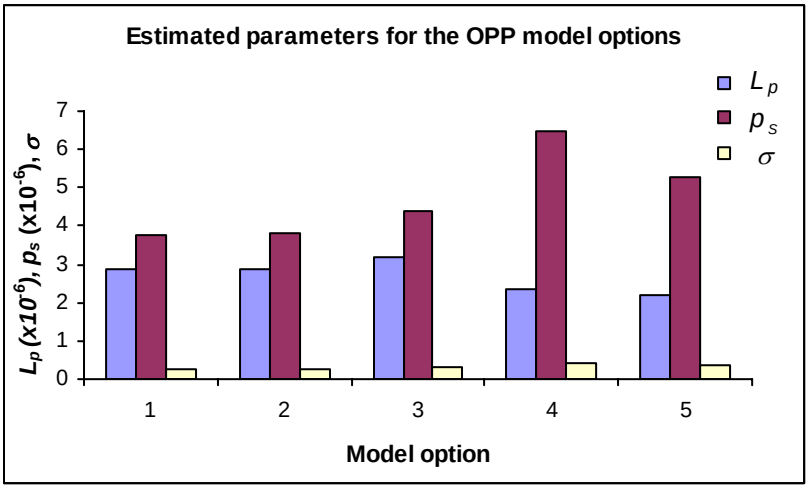

Fig. 4.11 Showing how estimated L_p, p_s and σ vary between the 5 OPP model options. Model option number refers to the model options shown in Table 4.9.

Table 4.10 Relative percentage differences in parameters estimated using the UL model and the classical model with a ramp. Percentage differences are relative to the classical model values.

	`1 Ule	2 ULs	ULi with ramp
L_p (x 10^{-6} m s^{-1} MPa^{-1})	10%	-19%	-23%
p_s (x 10^{-6} m s^{-1})	14%	69%	38%
σ	15%	71%	40%

It is interesting to observe that optimized ramp times for the 0 ULs and 1 ULi model options were similar, and optimized δ_{ULe} values for the 1 ULe and 2 ULs model options were also similar (Table 4.9). This is probably because a ULe and ramp affect

points around t=0 but a ULi does not (a ULi does not introduce a time-delay, see §3.6.2).

4.5.3 Model results for an HPP

The 4 model options for HPP data in Table 4.8 were fit to a negative HPP experiment, HPP run 8 of Cell 3. Fits using all 4 model options showed the same residual pattern (Fig. 4.12c), with differences in the magnitude of residuals (Table 4.11). It was found that for fits where π_{i1} (and therefore P_E) was optimized, RMS values were lower and fits to the shoulder of the curve (between 5-15 s) better (Table 4.11, Fig. 4.12a,b). For these fits P_E underpredicted the data P_E value of 0.4296 ± 0.0002 MPa. For fits where π_{i1} were non-optimized the data P_E was overpredicted.

Fits using the UL model fit the shoulder of the curve better than the classical model, as suggested by the lower maximum residuals (Table 4.11). L_p values were higher and RMS values lower for the UL model fits compared to those predicted by the classical model. This parameter behaviour is in accordance with the parameter analysis carried out in §3.6.5a. The relative difference in the estimated parameters between the UL and 0 ULs models, where π_{i1} was optimized, was 5%.

Table 4.11 Results from fitting the negative HPP experiment (run 8 of Cell 3), with and without a ULi, and with and without optimizing π_{i1}.

	π_{i1} non-optimized		π_{i1} optimized	
	0 ULs	1 ULi	0 ULs	1 ULi
δ_{ULi} (x 10^{-5} m)	0	30	0	30
π_{i1} (MPa)	0.4379	0.4379	0.4365 ±0.0001	0.4367 ±0.0001
L_p (x 10^{-6} m s $^{-1}$ MPa^{-1})	3.28 ±0.03	3.48 ±0.03	3.53 ±0.03	3.71 ±0.02
P_E (MPa)*	0.4303	0.4303	0.4289	0.4291
RMS (x 10^{-4} MPa)	14.13	11.75	9.57	7.63
Bias (x 10^{-4} MPa)	6.16	5.45	-1.18	-0.88
Trend (x 10^{-4} MPa s^{-1})	0.29	0.26	-0.20	-0.16
Max. residual (x 10^{-4} MPa)**	25.79	21.78	19.88	16.27

* P_E of the data was 0.4296 ± 0.0002 MPa. Standard errors for P_E are all ≤ 1x10^{-5} MPa
** Maximum residuals occurred in the shoulder of the curve (5-15 s).

The HPP fits were found to be very sensitive to the value of P_1, the perturbation pressure. In Table 4.11 the fits begin at the extremum point of the data, such that (t_0, P_1) = (t_m, P_m), but as mentioned in §4.3.4 there is some uncertainty in the value of P_m. When (t_0, P_1) was chosen to be a point about 0.1s after the extremum, lower RMS and estimated L_p values were obtained for both the classical and UL models. π_{i1} and P_E values remained the same. Results for the UL model are shown in Table 4.12 (L_p and RMS values changed by the same amount for the classical model). It is clear that changing P_1 by only 0.001 MPa may significantly affect L_p and alter the quality of the fit. This sensitivity and possible variation in the estimated L_p must be taken into account when comparing values of L_p between data sets.

Table 4.12 Comparing L_p and RMS values between 2 fits using different values of (t_0, P_1). Results are for those using the UL model with 1 ULi, with π_{i1} optimized.

P_1 (MPa)	0.3833	0.3855
L_p (x 10^{-6} m s^{-1} MPa^{-1})	3.71 ± 0.02	3.63 ± 0.02
RMS (x 10^{-4} MPa)	7.63	7.22

Although the HPP and OPP data come from experiments carried out on the same cell, the estimated L_p values between the data sets differed significantly. L_p values were higher for the HPP data even when a variation of 0.1 in L_p (due to sensitivity to P_1) is taken into account. From Table 4.9 and Table 4.11, for the classical model L_p was 3.28–3.53 x 10^{-6} m s^{-1} MPa^{-1} for the HPP data compared with 2.88 ± 0.03 x 10^{-6} m s^{-1} MPa^{-1} for the OPP data. For the models with a ULi, L_p was 3.48–3.71 x 10^{-6} m s^{-1} MPa^{-1} for the HPP data compared with 2.2–2.33 x 10^{-6} m s^{-1} MPa^{-1} for the OPP data. Refer to discussions in §4.6.2b and §4.8.3b on differences in estimated parameters between OPP and HPP experiments.

Relaxation curves for the 1 ULi model fit to HPP Run 8, Cell 3

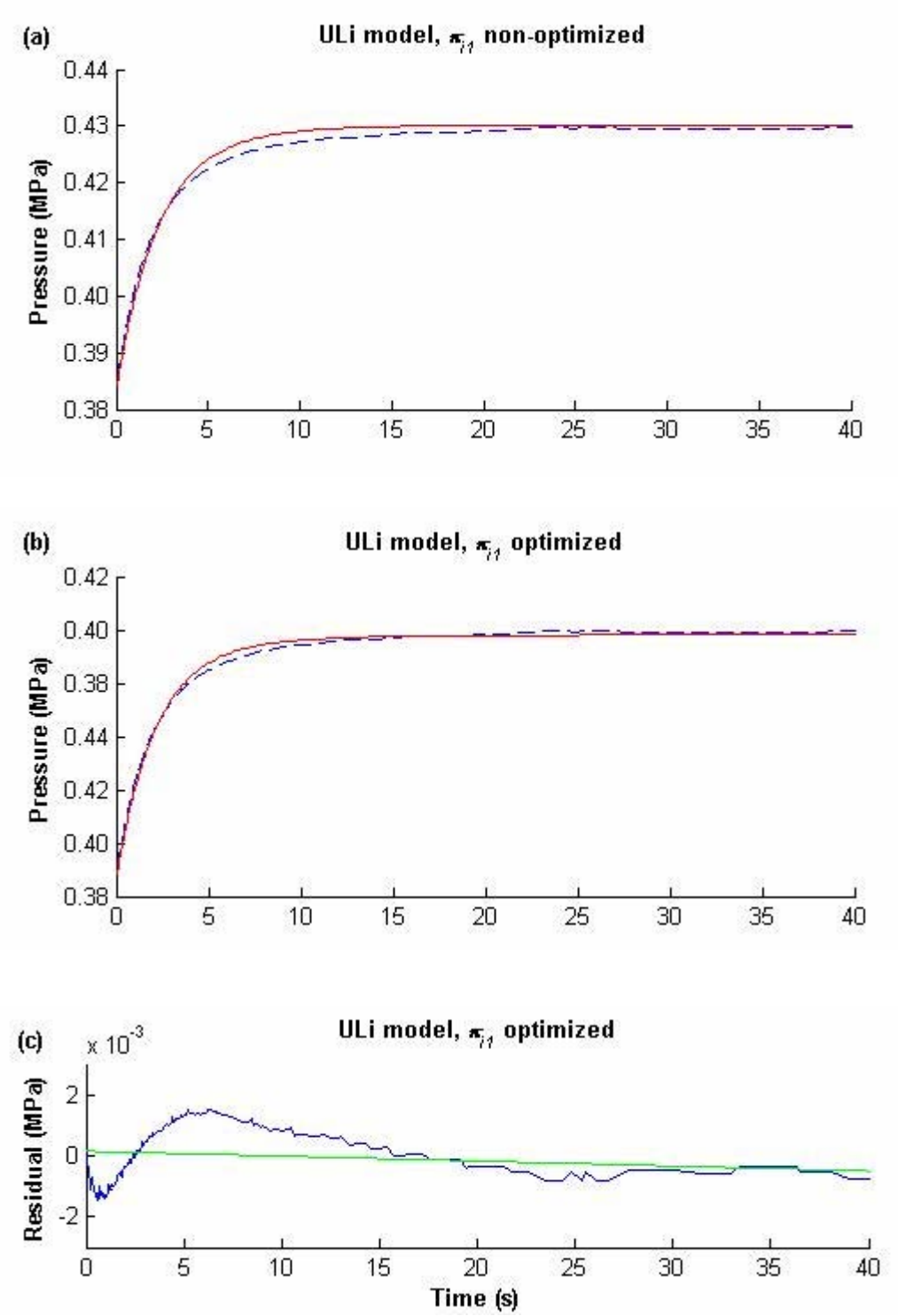

Fig. 4.12 Results from fitting the UL model with 1 ULi to a negative HPP experiment (HPP run 8 in Cell 3. (a) and (b), showing raw pressure data (-----) and model fit (——). (c), residual plot for relaxation curves in (b), with trendline (——).

4.5.4 Effects of ULs on cell pressure dynamics

The above comparison of fits using different models shows that the UL model is capable of fitting CPP data as well as or better than the Classical model, for both OPP and HPP data. If the UL model is assumed to accurately represent transport across a membrane in the presence of ULs, then the above results suggest that for an OPP, the classical method of parameter estimation (using the Classical model) may overestimate L_p by up to 19%, underestimate p_s by up to 71%, and underestimate σ by up to 73% (Table 4.10). These figures were obtained by comparing the parameters between the Classical model and the UL model with 2 ULs. For an HPP, the classical method of parameter estimation may underestimate L_p by 6%.

These differences are quite large. CPP experimenters have asserted that the ULs should have limited effect on the membrane parameters, since the time it takes for solutes to move through a UL is generally much shorter than the halftimes for the water or solute phases (Steudle and Tyerman, 1983; Hertel and Steudle, 1997). Although the experimental observation is true – the solute concentration in the ULs for an OPP experiment reaches a constant value within a few seconds compared to halftimes of around 30s (see the UL concentration profiles in Fig. 3.11) – a closer examination of the assertion is warranted. An analysis of the effects of ULs over the course of a CPP experiment can be made by plotting the difference in concentration across the membrane over time. When this was done for different model fits to OPP and HPP data (Fig. 4.13), the results clearly showed that a UL affects the concentration difference at the membrane for all time t. Thus, ULs affect the pressure dynamics for all time t.

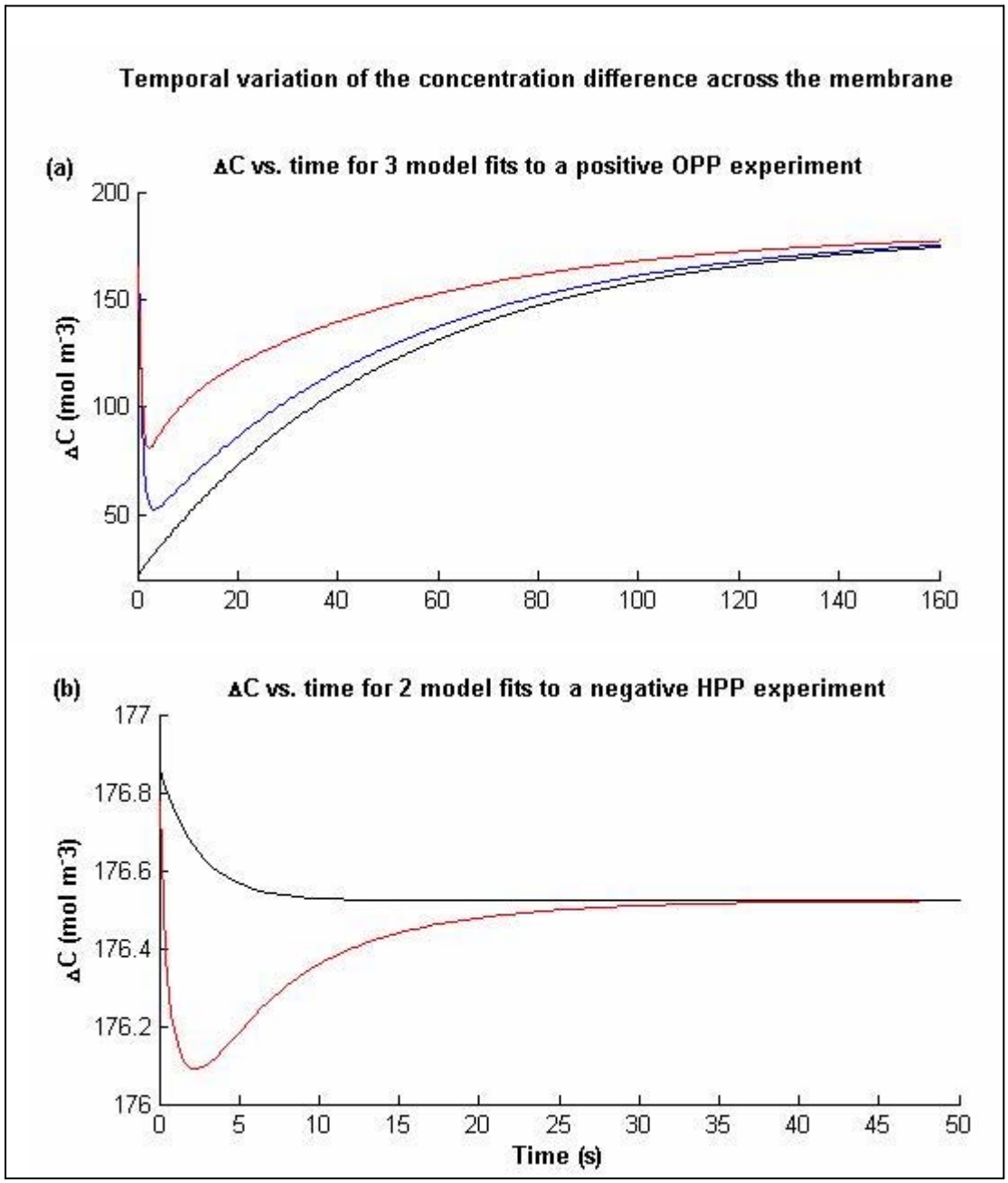

Fig. 4.13 Change in concentration across the membrane (ΔC) over time. (a) Showing fits to a positive OPP experiment (Dataset: OPP run 9, Cell 3), incorporating 0 ULs (——), 1 ULe (——), and 2 ULs (——). (b) Showing fits to a negative HPP experiment (Dataset: HPP run 8, Cell 3), incorporating 0 ULs (——), and 1 ULi (——).

The effects of ULs on the time-course of ΔC are different for HPP and OPP experiments. With ULs ΔC is biphasic for both OPP and HPP experiments (Fig. 4.13). However, for an HPP an increase in the magnitude of ΔC precedes a decrease

in the magnitude of ΔC such that the return of C to equilibrium is in an opposite direction to that when no ULs are present. This is due to the primary influence of convection in the ULs in an HPP experiment (see §3.6.4a), which acts in the opposite direction to diffusion (see §3.1.3). For an OPP experiment, diffusion dominates in the ULs (see §3.6.4b). The magnitude of ΔC for the HPP is also much smaller than that for the OPP, illustrating the smaller effect of ULs on an HPP experiment. These findings are consistent with statements in the literature regarding the primary roles of sweep-away (convection) in HPP experiments and diffusion in OPP experiments (Steudle and Tyerman, 1983).

4.5.5 Comments on optimization of the ULi thickness

Practical difficulties in optimizing the ULi thickness were explored by optimizing δ_{ULi} for an HPP fit (with π_{i1} non-optimized). Although the value of L_p was found to be the same as the fit in Table 4.8 for a fixed δ_{ULi}, the SE for δ_{ULi} was very large, with δ_{ULi} = 32.91 ± 615 x 10^{-5} m. This is indicative of the fact that small changes in δ_{ULi} make little difference to the RMS value, so that an optimum δ_{UL} cannot be achieved.

4.6 Fits to data: Estimation of parameters for 3 cells

Since in reality there are both internal and external ULs, fits to data sets in the next two sections will use the classical model (without a ramp, since a ramp makes little difference), and the UL model with 2 ULs. This will be done by first fitting OPP data from experiments with bubbles, where the ULi thickness is fixed at 3.0 x 10^{-5} m (a value larger than this makes negligible difference to the estimated parameters, see §3.6.2) and the ULe thickness is found by optimization. No ramp is included in the fits, since only a transit time is present for OPP experiments without bubbles (§4.2.2b), where the time for the solution to travel the length of the cell is at most 0.26s. A ramp time of 0.13s introduced into the models has very little effect on the pressure dynamics. Optimized parameters for the OPP fits will thus be: L_p, p_s, σ, δ_{ULe}.

Although a ULe has negligible influence on HPP experiments, for consistency a ULe will be used in model fits to HPP data, with δ_{ULe} fixed at the average value found for

the cell in the OPP fits. This is because one would expect the thickness of the ULe to be approximately the same size for each cell under the same external conditions. Optimized parameters for the HPP fits will be: L_p and π_{i1}.

In §4.6.1 results from the classical and UL model incorporating 2 ULs will be compared. The remaining sections will primarily concentrate on results obtained from the UL model, since these are considered to be more representative of the membrane parameters in *Chara*.

4.6.1 Fit results using the classical model vs. UL model

a) Predicted P-t curves

The UL model was generally found to fit the data well. For the OPP experiments, RMS values for fits using the UL model were lower than those using the classical model for all 6 data sets. On a whole the fit statistics for the UL model were better. The main regions of the relaxation curve where the UL model fits showed improvement were in the water phase and first part of the solute phase.

Table 4.13 Fit statistics for 4 OPP experiments with bubble, Cell 4. P_E' and P_m' are data equilibrium pressures and data extremum pressures respectively.

	Run 7 (pos)	Run 6 (neg)	Run 9 (pos)	Run 10 (neg)
UL model				
RMS (x10^{-4}MPa)	**6.94**	**9.64**	**7.21**	**6.94**
Bias (x10^{-4} MPa)	2.1	-3.7	2.5	-2.1
Trend (x10^{-6} MPa)	3.3	-5.7	3.7	-2.4
Largest residual (x10^{-4} MPa)	15.7	-24.2	-15.3	-18.1
$P_E - P_E'$	0.0009	-0.0020	0.0010	-0.0010
$P_m - P_m'$	-0.0004	0.0002	-0.0002	0.0004
Classical model				
RMS (x10^{-4}MPa)	**8.27**	**11.67**	**8.98**	**7.47**
Bias (x10^{-4} MPa)	2.3	-3.9	2.7	-2.6
Trend (x10^{-6} MPa)	5.1	-7.5	5.4	-3.2
Largest residual (x10^{-4} MPa)	-18.9	-34.8	-19.0	-31.0
$P_E - P_E'$	0.0010	-0.0022	0.0011	-0.0011
$P_m - P_m'$	0.0003	-0.0008	0.0005	-0.0007

Table 4.13 summarises details of fits to OPP experiments for Cell 4. The UL model fits generally had lower RMS values, residuals, and trends in the residuals than the classical model. For Run 6 P_E was markedly underpredicted, resulting in a larger magnitude (given by the RMS value), bias and trend of the residuals. This was also the case for Run 8 (not shown in Table 4.13). A contributing factor in why P_E was underpredicted for these two runs may be the comparatively small difference between the initial and final equilibrium pressures, since the change from half to full-strength APW results in a greater difference between P_0 and P_E (see §4.3.3). When APW was kept at full-strength in the model, the data was fit better with a RMS of 5.80 MPa and P_E -P_E' = 0.0006 MPa. See further discussion in §4.8.6.

For fits to OPP experiments for Cell 2, RMS values for fits using the UL model were lower than or equal to those using the classical model for 3 out of 4 data sets, and for Cell 3 the proportion was 2 out of 4 (data not shown).

For the HPP experiments, the UL model fit the data better than the classical model for all data sets fit in Cells 2-4, with consistently lower RMS values (e.g. Table 4.14). The main improvement was in the first half of the data from t_0 to the end of the shoulder of the curve. However, the shoulder of the curve usually could not be fit as well as other regions of the curve.

For Cell 4 the negative HPP data were more difficult to fit than the positive HPP data, with RMS values in the range 4.59–7.02 MPa for the 5 negative pulses compared with 3.48–4.93 MPa for the 5 positive pulses for fits with the UL model **(**Table 4.14**)**. The difference between π_{i1} and π_{i0} was also generally higher for the negative pulses in this cell, with π_{i1} - π_{i0} being in the range 0.0007–0.0015 MPa compared with <0.0006 MPa for the positive pulses. These patterns were not generally observed for Cells 2 and 3, although the Cell 2 fits also displayed a significant difference in values of π_{i1} - π_{i0} between positive and negative pulses. There seems to be no underlying reason for this difference in fits between positive and negative pulses. Differences between P_0 and P_E were not different for Cell 4 compared to the other cells (Table 4.6).

For Cell 4, experiments were carried out in two sets of 6 HPP experiments, separated by two or more OPP experiments. The nature of the fits did not seem to vary between the sets (Table 4.14).

Table 4.14 Fit statistics for 4 HPP experiments (out of 10 fit altogether), for Cell 4. P_E' is the data equilibrium pressure.

	Run 11 (pos)	Run 12 (neg)	Run 1 (pos)	Run 2 (neg)
UL model				
RMS (x10^{-4}MPa)	**4.93**	**5.06**	**3.48**	**5.98**
Bias (x10^{-4} MPa)	1.2	-0.9	0.5	-1.2
Trend (x10^{-6} MPa)	-3.7	-0.9	3.7	-2.1
Largest residual (x10^{-4} MPa)	12.8	10.9	-7.1	-10.8
$P_E - P_E'$	0.0003	-0.0003	0.0003	-0.0004
$\pi_{i1} - \pi_{i0}$	0.0005	-0.0012	-0.0002	-0.0006
Classical model				
RMS (x10^{-4}MPa)	**5.66**	**6.06**	**4.30**	**6.93**
Bias (x10^{-4} MPa)	1.4	-1.1	0.7	-1.4
Trend (x10^{-6} MPa)	-3.3	-1.6	4.5	-2.7
Largest residual (x10^{-4} MPa)	14.0	12.4	-7.5	-12.2
$P_E - P_E'$	0.0004	-0.0004	0.0004	-0.0005
$\pi_{i1} - \pi_{i0}$	0.0006	-0.0014	-4.86E-06	-0.0008

b) Estimated parameters

The parameter ratio ξ is defined as: (classically-estimated parameter)/ (parameter estimated using the UL model). It was found that for fits to the OPP experiments values of ξ were similar for each run on a given cell, but differed between cells (Table 4.15). The classically-estimated L_p was consistently greater than that predicted by the UL model, whilst the classically-estimated p_s and σ values were consistently less than that predicted by the UL model. Results suggest that for OPP experiments, the classically-estimated L_p may over-estimate the true membrane L_p by up to 50%, and the classically-estimated p_s and σ may under-estimate the true membrane p_s and σ by up to 50%.

The parameter ratio $\xi(L_p)$ for fits to the HPP experiments deviated much less from 1.0, and were similar between cells (Table 4.15). The classically-estimated L_p was consistently less than that predicted by the UL model. Results suggest that for HPP

experiments the classically-estimated L_p may under-estimate the true membrane L_p by up to 5%.

Table 4.15 Parameter ratios for OPP experiments with bubbles and HPP experiments.

	OPP expts			HPP expts		
	Cell 2	Cell 3	Cell 4	Cell 2	Cell 3	Cell 4
sample size	4	4	6	4	4	9
ξ **(L_p)**	1.49	1.25	1.25	0.97	0.95	0.97
ξ **(p_s)**	0.49	0.60	0.67			
ξ **(σ)**	0.49	0.60	0.67			

A direct comparison of these findings with those in Chapter 3 is not possible as parameter ratios were not obtained for the UL model with 2 ULs in Chapter 3. However, these findings are broadly consistent with those in §3.6.5 where, keeping in mind that the ULi has more influence on the pressure dynamics than the ULe, it was predicted that for OPP experiments the classical model is likely to underpredict p_s and σ and overpredict L_p by 30% or more (Fig. 3.13).

4.6.2 Parameter variation (UL model)

a) Within-cell variation

A previous examination of the conductivity data showed that measured time-delay values t_D vary within each cell, in particular between positive and negative pulses (Table 4.7). This suggests that the predicted δ_{ULe} would vary within each cell, which indeed was found in model fits to the data (Table 4.16) where values for δ_{ULe} varied by 0.4-1.5 x 10^{-5} m between positive and negative OPP experiments conducted on the same cell. For Cell 4, where the differences in measured time-delays between positive and negative experiments was greatest (§4.4.1), the difference in estimated δ_{ULe} values between positive and negative experiments was also greatest.

However, it is doubtful whether δ_{ULe} would in reality differ between positive and negative experiments. The pattern was also inconsistent, with δ_{ULe} larger for the positive experiments in Cells 3 and 4, and vice-versa for Cell 2 (although for the latter

the difference in δ_{ULe} was not significant). One would expect the ULe thickness to be the same for all OPP experiments on the same cell, under the same external conditions. It is probable that the variation of δ_{ULe} between positive and negative experiments is due to experimental or measurement errors. Sometimes bubbles may get stuck in the tube, affecting flow and causing variation in the time-delay (Bramley, *pers. comm.*). It is interesting, however, that the range of ULe thickness values predicted for the data are in the range of the values estimated in the literature, i.e. 30-50 μm.

Table 4.16 Estimated parameters ± SD from the UL model, for OPP experiments from Cells 2-4. *L* = cell length, *d* = cell diameter.

	Cell 2		Cell 3		Cell 4	
***L* (mm)**	24		45		33	
***d* (mm)**	9.77		7.91		9.77	
ε (MPa)	27.9		24.6		36.5	
	Pos	Neg	Pos	Neg	Pos	Neg
sample size	2	2	2	2	3	3
δ_{ULe} (x10^{-5} m)	3.05 ±0.15	3.46 ±0.29	4.89 ±0.13	4.25 ±0.00	5.01 ±0.39	3.48 ±0.06
L_p (x10^{-6} m s^{-1} MPa^{-1})	1.38 ±0.01	1.16 ±0.03	2.77 ±0.62	2.19 ±0.12	1.28 ±0.04	1.36 ±0.03
p_s (x10^{-6} m s^{-1})	7.76 ±0.19	8.93 ±0.05	6.17 ±0.42	6.22 ±0.21	4.15 ±0.04	3.88 ±0.2
σ	0.490 ±0.004	0.573 ±0.01	0.416 ±0.04	0.419 ±0.03	0.438 ±0.01	0.433 ±0.01

A difference in estimated parameters between positive and negative pulses was observed for all 3 cells (Table 4.16). However, a significant difference was only observed for Cell 2, and furthermore there was no consistent pattern in the magnitude or direction of the differences. For example, L_p for the negative pulses was less than L_p for the positive pulses for Cells 2 and 3, but vice-versa for Cell 4 (Table 4.17). The sample size of 7 positive and 7 negative OPP experiments was not sufficiently large for definitive conclusions regarding polarity in the parameters to be drawn. There were large standard deviations for the estimated L_p and p_s for Cell 3 (Table 4.16), which was due to estimated parameters for one of the positive experiments differing significantly from those for the other 3 experiments fitted for that cell. The strength and direction of the polarity also depended on the type of model fit to the data (Table 4.17).

Table 4.17 Ratios of estimated parameters from positive OPP experiments to corresponding parameters estimated from negative OPP experiments.

	Cell 2	Cell 3	Cell 4
sample size	4	4	6
UL model			
δ_{ULe}	0.88	1.15	1.44
L_p	1.19	1.27	0.93
p_s	0.87	0.99	1.07
σ	0.85	0.99	1.01
Classical model			
L_p	1.17	1.18	0.91
p_s	0.97	1.00	1.01
σ	0.94	0.99	0.96

It is possible that differences in estimated δ_{ULe} values are contributing to differences in the estimated parameters between positive and negative experiments. However, for Cell 4, where the difference in estimated δ_{ULe} values between positive and negative experiments was greatest, the difference in estimated parameters between positive and negative experiments was not more than that for Cells 2 and 3 (Table 4.16). This suggests that δ_{ULe} values are not strongly influencing the estimated parameters. This will be further examined in §4.8.1.

For the HPP data, there was also no evidence that a polarity in estimated L_p values exists. For Cell 4, where the sample size was largest, L_p was similar for positive and negative experiments (Table 4.18). Although there was a significant difference in L_p between positive and negative pulses for Cell 3, two of the data sets were difficult to fit, and the RMS values exhibited the widest range for this cell (a range of 4.5MPa).

Table 4.18 Estimated L_p ± SD from the UL model, for HPP experiments from Cells 2 to 4. L = cell length, d = cell diameter.

	Cell 2		Cell 3		Cell 4	
***L* (mm)**	24		45		33	
***d* (mm)**	9.77		7.91		9.77	
ε (MPa)	27.9		24.6		36.5	
	Pos	Neg	Pos	Neg	Pos	Neg
sample size	2	2	2	2	5	5
L_p (x10^{-6} m s^{-1} MPa^{-1})	1.56 ±0.01	1.61 ±0.04	3.47 ±0.03	3.72 ±0.12	1.49 ±0.05	1.51 ±0.05

b) Between-cell variation

For the OPP experiments, estimated membrane parameters were found to differ between cells (Table 4.19). A significant difference was observed in p_s, where the value was twice as large for Cell 2 as for Cell 4. A significant difference was also observed in L_p, where the value was almost twice as large for Cell 3 as for Cell 2.

It was observed that the average estimated ULe thickness for each cell was correlated with cell length (Table 4.19). This could be because δ_{ULe} is not constant along the length of the cell, but is thinner at the leading edge (upstream of the flow) and thickest at the trailing edge (Pedley, 1983). The model uses a constant δ_{ULe} and is effectively taking an average of the varying δ_{ULe} along the cell length. If it is assumed the maximum δ_{ULe} is reached after the same distance from the leading edge for all cells, the average δ_{ULe} would be larger for a longer cell, where the maximum δ_{ULe} would occupy a higher proportion of the cell length compared to for a shorter cell.

Table 4.19 Average estimated parameters ± SD for OPP expts, for each cell, using the UL model.

	Cell 2	Cell 3	Cell 4
Cell geometry			
***L* (mm)**	24	45	33
***d* (mm)**	9.77	7.91	9.77
ε (MPa)	27.9	24.6	36.5
sample size	4	4	6
Parameters			
δ_{ULe} (x10^{-5} m)	3.26 ±0.30	4.57 ±0.38	4.25 ±0.87
L_p (x10^{-6} m s^{-1} MPa^{-1})	1.27 ±0.13	2.48 ±0.15	1.32 ±0.06
p_s (x10^{-6} m s^{-1})	8.34 ±0.68	6.19 ±0.27	4.01 ±0.19
σ	0.532 ±0.05	0.418 ±0.03	0.436 ±0.01

Table 4.20 Average estimated L_p ± SD for HPP expts, for each cell, using the UL model.

	Cell 2	Cell 3	Cell 4
sample size	4	4	10
L_p (x10^{-6} m s^{-1} MPa^{-1})	1.58 ±0.04	3.59 ±0.16	1.50 ±0.05

For the HPP experiments, estimated L_p values were similar for Cells 2 and 4 but markedly larger for Cell 3 (Table 4.20), which is the same pattern as observed in the OPP experiments (Table 4.19).

It was observed that L_p values were 14-45% higher for the HPP experiments as compared to the OPP experiments. In the literature it has been found that L_p for HPP experiments is higher than that for OPP experiments, which has been attributed to the greater influence of the ULe on OPP experiments since the estimated L_p values were found to converge at high stirring rates (Steudle and Tyerman, 1983). It is interesting that this difference in L_p values between HPP and OPP experiments was observed in the model results here, since the model takes ULs into account so that one would expect the L_p values to be the same. Possible reasons for this will be discussed in §4.8.3b.

4.7 Fits to data: OPP experiments with ramps (UL model)

4.7.1 Exploration of exchange function

The effect of the shape of the external concentration *C(t)* of permeant solutes as a function of time (exchange function) on parameter estimation was explored by representing it as a linear ramp, and as 2 different exponential functions. If C_1 the final concentration of permeant solutes in the bulk solution after ramping, C_0 the concentration of permeant solutes in the bulk solution at t=0, and t_R the ramp time, then these functions are:

Linear function:

$$C(t) = C_0 + \frac{(C_1 - C_0)}{t_R} t\,, \quad 0 < t < t_R \tag{4.1}$$

Bounded exponential function 1:

$$C(t) = \frac{(C_1 - C_0)}{1 - e^{-1}} \left[1 - e^{-t/t_R} \right] + C_0\,, \quad 0 < t < t_R \tag{4.2}$$

Bounded exponential function 2:

$$C(t) = C_1 + (C_0 - C_1)e^{-t/t_R}, \qquad 0 < t < \infty. \tag{4.3}$$

Eqs. (4.1) & (4.2) reach the final concentration at t_R, and Eq. (4.3) reaches 2/3 of the final concentration at t_R and approaches C_1 as $t \to \infty$ (see Fig. 4.14).

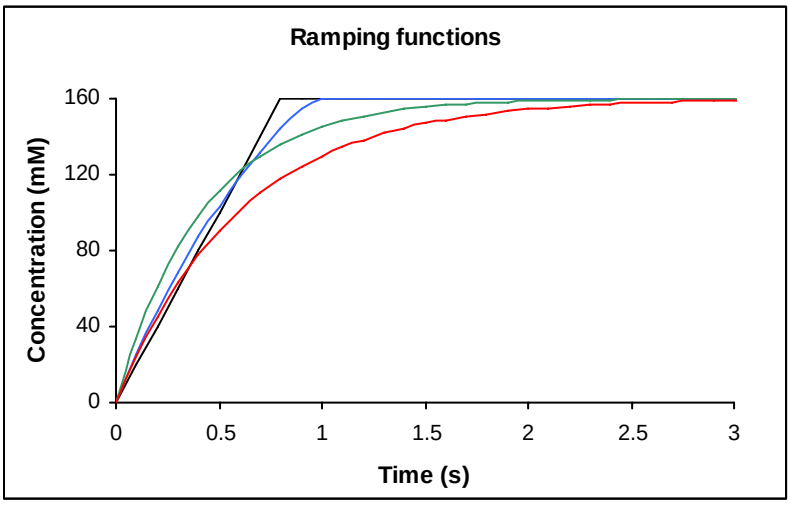

Fig. 4.14 Plots for different ramping functions, used for fits to the positive OPP experiment, Run 1 in Cell 4. Functions used: a) linear (——) with t_R = 0.8s, b) bounded exponential 1 (——) with t_R = 0.95s, c) bounded exponential 2 (——) with t_R = 0.42s, d) bounded exponential 2 (——) with t_R = 0.6s.

Membrane parameters and ramp times were optimized for one positive OPP experiment in Cell 4, using the different exchange functions. The ULe thickness δ_{ULe} was fixed at 5.03 x 10^{-5} m (the average value found for fits to positive OPP experiments with bubbles). The optimizations returned different ramp times t_R but the same membrane parameters for each of the exchange functions (Table 4.21), and optimized membrane parameters appeared to be independent of the shape of the exchange function when t_R is optimized.

Table 4.21 Optimized parameters using different exchange functions for OPP Run 1 (positive pulse) for Cell 4. Ramp times t_R were also optimized. Standard errors from optimization are similar to those in Table 4.17.

	Linear	Exponential 1	Exponential 2
t_R (s)	0.8	0.95	0.42
L_p (x10^{-6} m s^{-1} MPa^{-1})	1.20	1.20	1.21
p_s (x10^{-6} m s^{-1})	3.93	3.93	3.93
σ	0.448	0.448	0.446
RMS (MPa)	5.81	5.75	5.57

4.7.2 Influence of exchange function on membrane parameters

4 OPP data sets for Cell 4 (runs 1-4) were fit using Eq. (4.1) as the exchange function. During optimization of t_R it was found that the simulated data and RMS values were insensitive to small changes in t_R. Therefore a best t_R was found by fixing t_R at 3 or 4 different values, optimizing the membrane parameters for each t_R, and interpolating plots of t_R, L_p, p_s, and σ vs. RMS values to obtain values of t_R, L_p, p_s, and σ which corresponded to a minimum RMS. It was found that the estimated L_p and p_s were consistently lower and σ consistently higher than the corresponding values for OPP experiments with bubbles (Table 4.22). As L_p is correlated with t_R through the effect of a ULe on the water phase (§3.6.2), if a ramp time is not included at all (i.e. $t_R = 0$) the estimated L_p from OPP experiments without a bubble would be even less than that estimated from OPP experiments with a bubble (where δ_{ULe} is the same).

Table 4.22 Average optimized parameters ± SD for Cell 4, for OPP experiments with bubbles (runs 5-10) and without bubbles (runs 1-4). For experiments without bubbles, ramp times are fixed and the membrane parameters are optimized.

	Pos		Neg	
δ_{ULe} (x10^{-5} m)	5.01	±0.39	3.48	±0.06
With bubble				
sample size	3		3	
L_p (x10^{-6} m s^{-1} MPa^{-1})	1.28	±0.04	1.36	±0.03
p_s (x10^{-6} m s^{-1})	4.15	±0.04	3.88	±0.2
σ	0.438	±0.01	0.433	±0.01
Without bubble				
sample size	2		2	
t_R (s)	0.71	±0.13	0.67	±0.29
L_p (x10^{-6} m s^{-1} MPa^{-1})	1.14	±0.08	1.17	±0.04
p_s (x10^{-6} m s^{-1})	3.90	±0.04	3.87	±0.18
σ	0.443	±0.007	0.447	±0.011

The membrane parameters, however, should be the same since the experiments are all conducted on the same cell. When runs 1 and 2 were fit using Eq. (4.3) as the exchange function and t_R fixed (at some arbitrary value), the data was fit quite well and the estimated L_p values (Table 4.23) were much closer to the estimated values from OPP experiments with bubbles (Table 4.22), although p_s was still low. The improved consistency in L_p is probably because the initial slope of this exchange function is now similar to the slope of the linear function (Fig. 4.14d), at least for Run 1, and may be closer to the actual exchange function for the experiment. It is encouraging that when the voltage data in Fig. 4.2 was digitized, a bounded exponential function of the form of Eq. (4.3) fit it well, suggesting that Eq. (4.3) may be an appropriate function for representing the change in external concentration.

Table 4.23 Optimized membrane parameters using exponential function 2 for the ramp, for a positive and a negative OPP run. Ramp times t_R are fixed at approximately the averaged values for fits in Table 4.20.

	Run 1 (pos)	Run 2 (neg)
δ_{ULe} (x10^{-5} m)	5.03	3.49
t_R (s)	0.6	0.5
L_p (x10^{-6} m s^{-1} MPa^{-1})	1.27	1.29
p_s (x10^{-6} m s^{-1})	3.89	3.69
σ	0.443	0.432

The above analysis shows that knowledge of an appropriate exchange function for the data is necessary in order to estimate membrane parameters for OPP experiments without a bubble. Since the duration and shape of the exchange function may differ between experiments, a different function may be required for each experiment. The definition of the measured exchange time must also be the same as that used in the models. The measured ramp times of 1.37–2.34 s for Cell 4 (Table 4.2) are much larger than the fixed ramp times used in Table 4.22, but the measured t_R are defined as being the time it takes for the external concentration to approximately reach the final concentration, which is different from the definition of t_R in Eq. (4.3). At present, a consistent set of membrane parameters for all the OPP data for Cell 4 is not possible due to lack of knowledge about the exchange time and function.

4.8 Discussion of some predictions of the UL model

4.8.1 How estimated parameters vary with ULe thicknesses

Analysis of results from OPP experiments revealed no strong correlation between the estimated δ_{ULe} and estimated membrane parameters within each cell (Fig. 4.15). Within each cell the estimated parameters were fairly consistent. This was particularly so for Cell 4, where the estimated parameters were quite constant over a large range of δ_{ULe} values. A consistent estimate of the membrane parameters for each cell, which is independent of δ_{ULe}, is a good sign since the estimated parameters, if they are accurately reflecting those of the membrane, should be constant for a cell and not dependent on external factors.

Fig. 4.15 shows that scatter in the estimated membrane parameters for each cell was less than the variation in membrane parameters between cells. The results clearly show that membrane parameters between cells can differ significantly. For example, for Cells 2 and 3 the between-cell difference in parameters was much greater than the within-cell differences, so that they formed two separate clusters on the plot where the ranges of δ_{ULe} for each cell did not overlap.

Results from the 3 cells together may appear to show a correlation between δ_{ULe} and the membrane parameters (Fig. 4.15). However, this is largely due to the fact that results from Cells 2 and 3 occupy separate regions of the plot. There should be no reason for a correlation between δ_{ULe} and the membrane parameters, since estimation of the membrane parameters has taken δ_{ULe} into account. Data from a larger cell sample size would be unlikely to show a correlation.

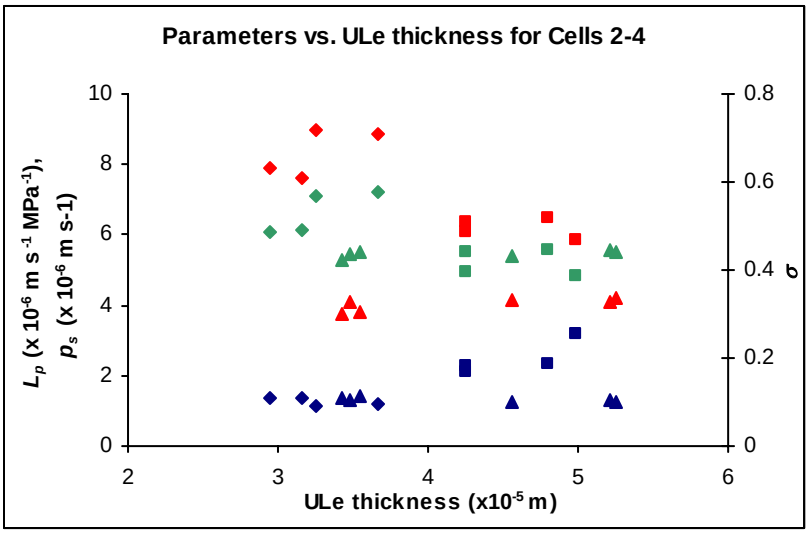

Fig. 4.15 Estimated L_p (blue), p_s (red), and σ(green) vs. estimated ULe thickness, for fits to individual OPP experiments from Cell 2 (♦), Cell 3 (■), and Cell 4 (▲).

4.8.2 Sensitivity of estimated ULe thickness to measured time-delay

In order to examine the extent to which the experimental time-delay and estimated parameters vary with the estimated ULe thickness, some individual model fits to OPP data were identified for comparison.

In §4.4.2 it was shown that a relationship generally exists between the estimated ULe thickness and the experimental time-delay. However, this relationship was not always observed in fits to OPP data. For example, in one case the experimental time-delay was the same for very different values of δ_{ULe} predicted by the model (Table 4.24). In another case, the experimental time-delays were very different but the model estimated similar values of δ_{ULe} (Table 4.25).

Table 4.24 Estimated ULe thickness and parameters ± SE for a positive and negative OPP run from Cell 3. Results are from using the UL model, and for when the experimental time-delay is the same but the estimated ULe thicknesses are different.

	Run 9 (pos)		Run 10 (neg)	
Time-delay (s)	0.58		0.58	
δ_{ULe} (x10^{-5} m)	4.80	±0.06	4.25	±0.20
L_p (x10^{-6} m s^{-1} MPa^{-1})	2.33	±0.02	2.10	±0.02
p_s (x10^{-6} m s^{-1})	6.46	±0.03	6.37	±0.07
σ	0.444	±0.002	0.442	±0.005
RMS (x10^{-4} MPa)	6.14		6.43	

Table 4.25 Estimated ULe thickness and parameters ± SE for 2 positive OPP runs from Cell 4. Results are from using the UL model, and for when the estimated ULe thicknesses are similar but the experimental time-delays are different.

	Run 5 (pos)		Run 7 (pos)	
Time-delay (s)	0.56		0.69	
δ_{ULe} (x10^{-5} m)	5.22	±0.07	5.25	±0.06
L_p (x10^{-6} m s^{-1} MPa^{-1})	1.32	±0.01	1.27	±0.01
p_s (x10^{-6} m s^{-1})	4.10	±0.01	4.18	±0.01
σ	0.444	±0.001	0.442	±0.001
RMS (x10^{-4} MPa)	5.46		6.94	

Variation in δ_{ULe} also affects all 3 membrane parameters (see Fig. 4.15; not evident from Table 4.24). It was observed that where values of δ_{ULe} were similar between runs with the same magnitude and direction of the perturbation pulse, the estimated parameters were usually quite similar (e.g. Table 4.25). However, for one case the values of δ_{ULe} were the same but a degree of variation in the membrane parameters was observed (e.g. p_s and σ in Table 4.26).

Table 4.26 Estimated ULe thickness and parameters ± SE for 2 negative OPP runs from Cell 2. Results are from using the UL model, showing the case for when the estimated ULe thicknesses are the same, the experimental time-delays are similar, but the estimated parameters quite different.

	Run 8 (neg)		Run 10 (neg)	
Time-delay (s)	0.52		0.58	
δ_{ULe} (x10^{-5} m)	4.25	±0.16	4.25	±0.20
L_p (x10^{-6} m s^{-1} MPa^{-1})	2.27	±0.02	2.10	±0.02
p_s (x10^{-6} m s^{-1})	6.07	±0.08	6.37	±0.07
σ	0.397	±0.004	0.442	±0.005
RMS (x10^{-4} MPa)	4.92		6.43	

It was suggested previously (§4.6.2a) that since the measured time-delay generally influences the estimated δ_{ULe} and perhaps the membrane parameters, the polarity observed in the estimated membrane parameters (i.e. estimated parameters sometimes differed between positive and negative pulses of the same magnitude) may not actually reflect that of the system but may be due to errors in the measured time-delay. However, results in this section show that differences in estimated parameters

between positive and negative pulses cannot solely be attributed to differences in the measured time-delay, and thus the estimated δ_{ULe} between positive and negative pulses. Tables 4.24–4.26 show that the degree of parameter variation would not necessarily be different if consistent values of t_0 and δ_{ULe} were used in the fits to OPP data. The estimated parameter values (as well as the large variation in standard errors between the fits) in Tables 4.24–4.26 show that due to some variation in parameters estimated with the model, it is necessary to estimate parameters for several experiments so that parameters can be averaged and more conclusive relationships between the parameters can be drawn.

4.8.3 Estimated L_p values

a) Sensitivity of $\mathbf{L_p}$ *to* $\mathbf{P_1}$ *in HPP expts*

Simulations of HPP data can be initialised at any observed (t,P), but is usually at the perturbation values corresponding to the extremum (t_m, P_m) of the data. It has previously been shown that there is some experimental uncertainty surrounding these values (§4.3.4), and that the estimated L_p is very sensitive to the value of the initial (perturbed) pressure P_1 used in the model (§4.5.3). Therefore the impact on the estimated L_p due to selecting a different initial (t_0, P_1) point is explored here.

The sensitivity of L_p to P_1 was analysed using the UL model to estimate the parameters for an HPP data set. L_p and π_1 were optimized for 6 different values of P_1 corresponding to value of t between 0s and 1.07s after the time t_m of extreme pressure P_m. It was found that using values of P_1 less than P_m decreases the estimated value of L_p for both positive and negative pulses (Fig. 4.16).

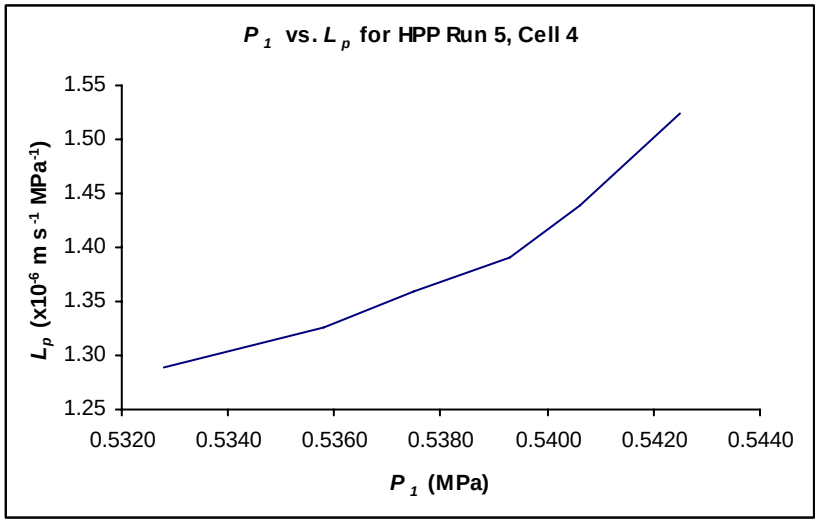

Fig. 4.16 L_p vs. P_1 for fits to HPP Run 5, Cell 4. This is a positive pulse where the maximum pressure P_m = 0.5425MPa.

In §4.6.2b it was found that estimated L_p values from HPP experiments were higher than that from OPP experiments for fits using the UL model with 2 ULs (Table 4.19 and Table 4.20). For the data set fit here, when (t_0, P_1) = (t_m, P_m) the estimated L_p was 1.52 m s^{-1} MPa^{-1}. However, when (t_0, P_1) = (t_m +1.07, 0.5328), the estimated L_p was 1.29 m s^{-1} MPa^{-1}. This value is close to the average estimated L_p for the OPP data for Cell 4 (of 1.31 m s^{-1} MPa^{-1}), and corresponds to a fit to the later regions of the observed HPP data (Fig. 4.17). One may hypothesise that L_p for both HPP and OPP experiments are in fact the same for the same cell, but that the model has trouble fitting the initial steeper region. L_p as defined by the KK equations may govern the later portion of the HPP curve and not the first 2-3 s.

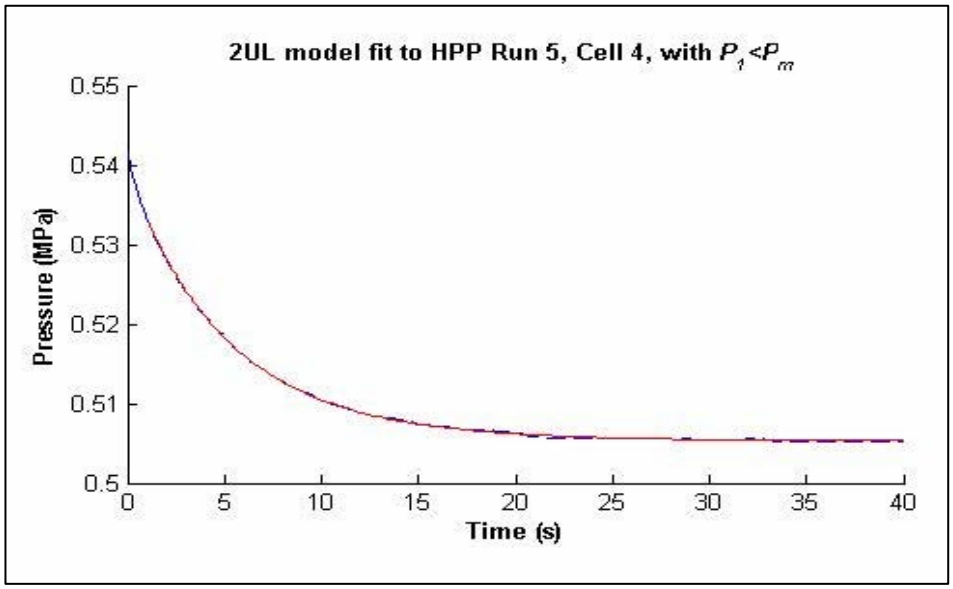

Fig. 4.17 Fit to an HPP data set using the UL model, where the fit begins at a point after (t_m, P_m,) = (0, 0.5425), namely (t_0, P_1,) = (1.07, 0.5328). Showing raw pressure data (-----) and model fit (——).

b) Differences in L_p between HPP and OPP experiments

The parameters L_p, p_s and σ, being properties of the membrane, should be constant for each cell, assuming that there are no external factors affecting the parameters such as temperature changes or leaks in the apparatus. The results above in §4.8.3a lend weight to this claim for the case of L_p. Differences observed between HPP and OPP experiments in the present study may be due to inadequacies in the model rather than a real physical difference in the parameters. Inadequacies may include:

- Limitations in the applicability of the KK equations. Evidence includes difficulties in fitting the shoulder of the HPP curve (§4.5.3, §4.6.1) and the superior fit given by a double exponential (§2.7.3a). A double exponential was also fit to an HPP curve for the data used in this chapter, and found to give a superior fit.

- Neglect of other dynamics in the experiment, such as possible pressure changes during the perturbation pulse, presence of some permeant solutes in the cell in HPP experiments (§4.8.6), influence of the tonoplast on the pressure

dynamics, and influence of different values of *D* between APW and the cytoplasm (§4.8.4)

4.8.4 Impact of different *D* values on estimated parameters

It has been assumed that the diffusion coefficient *D* for the cell interior is the same as that for APW. In fact it is likely to be less, and the extent to which values of *D* used for the ULi may impact on the estimated parameters for fits to the data, using the UL model, are examined here. This analysis differs from that in §3.6.6 in that here parameters are estimated by fitting the model to observed data.

Membrane parameters were estimated for an OPP experiment (OPP Run 8 of Cell 2) for 3 different values of *D* in the ULi (D_{ULi}), where D_{ULi} = 0.9, 1.1, and 1.28 x 10^{-9} m^2 s^{-1}. *D* for the ULe (D_{ULe}) was kept constant at 1.28 x 10^{-9} m^2 s^{-1}. It was found that the estimated membrane parameters varied significantly with D_{ULi} (Fig. 4.18). Changing D_{ULi} by 1% resulted in a 0.7% change in L_p, a 1.2% change in p_s, and a 1.2% change in σ. These results indicate that quantification of *D* for the cell interior is important in parameter estimation. Using an incorrect value of *D* for the ULi may also be a contributing factor to the finding that L_p values were higher for the HPP experiments as compared to the OPP experiments (§4.6.2b, §4.8.3b), as ULs have a greater influence on the parameter estimation in OPP experiments than HPP experiments (§4.6.1b). For OPP experiments, Fig. 4.18 reveals that a lower value of *D* for the ULi leads to a lower value of L_p, and results from the analysis in §3.6.6a suggests a monotonic decrease of L_p with decreasing *D* for the ULi. However, there appears to be no current available data on the value of *D* for the interior of *Chara*, so the actual extent of the influence of *D* for the ULi cannot be verified.

As in §3.6.6, predictions of the total permeability p_T using the permeability equation (Eq. (3.2)) were also calculated (Table 4.27). It was found that values of p_T differed significantly from that of 4.16 x 10^{-6} m^{-1} s^{-1} given by the classical model, for which $p_s = p_T$. This confirms again that Eq. (3.2) cannot be used to infer the membrane permeability p_m (= p_s) based upon an estimated value of p_T obtained using the classical model, as is a common practice in the literature. The large differences

between p_s and p_T in Table 4.27 also indicates that the permeability of the ULs are strongly limiting transport across the membrane for this cell.

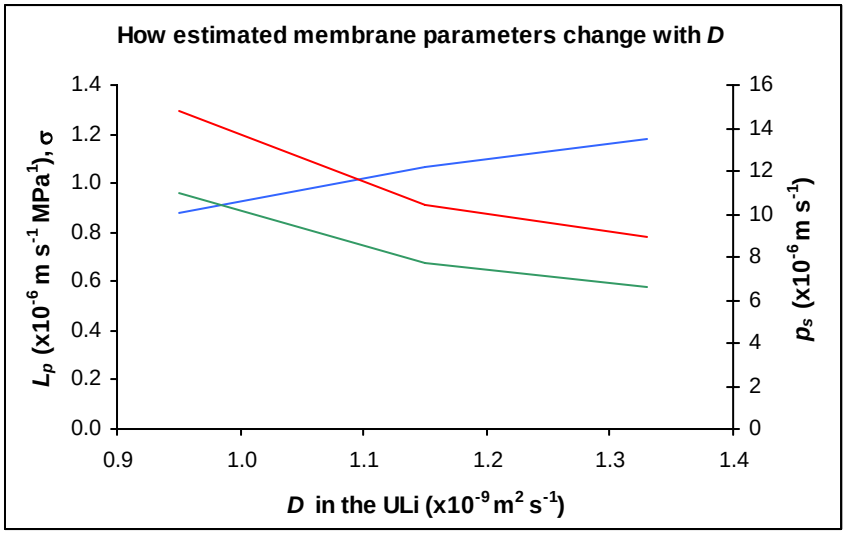

Fig. 4.18 Plots of L_p (——), p_s (——), and σ (——)vs. D in the ULi, for fits to OPP Run 8 of Cell 2.

Table 4.27 Membrane permeability p_s and total permeability p_T for 3 different values of D_{ULi}. For OPP Run 8 of Cell 2.

D_{ULi} (x10^{-9} m^2 s^{-1})	1.28	1.10	0.90
p_s (x10^{-6} m s^{-1})	8.89	10.41	14.78
p_T (x10^{-6} m s^{-1})	2.56	2.22	1.84

4.8.5 Impact of different ε values on estimated parameters

The impact of ε on estimated parameters was analysed for an HPP and OPP experiment from Cell 2, where ε was independently estimated to be 27.9 ± 4.1 MPa. Membrane parameters were estimated for the two ε values at either end of this range, using the classical and UL models. Differences between estimated parameters using ε = 27.9 MPa were calculated (Table 4.28). It was found that the value of ε impacted strongly on the estimated L_p and had negligible effect on p_s and σ. Therefore, experimental errors in ε may introduce a large error in the estimated L_p of 10-20%.

Table 4.28 Showing relative changes in estimated parameters due to using 2 different values of ε as compared to using ε = 27.9 MPa.

	OPP Run 8		HPP Run 1	
ε (MPa)	23.8	32	23.8	32
Classical model				
L_p (x10^{-6} m s^{-1} MPa^{-1})	16.92%	-12.31%	18.39%	-12.64%
p_s (x10^{-6} m s^{-1})	0.00%	0.00%		
σ	0.30%	-0.22%		
UL model				
L_p (x10^{-6} m s^{-1} MPa^{-1})	16.84%	-13.01%	18.13%	-13.74%
p_s (x10^{-6} m s^{-1})	0.33%	-0.24%		
σ	0.61%	-0.47%		

In §1.2 it was mentioned that the value of ε is not constant over time due to viscoelastic properties of the cell wall. The measured value of ε due to an 'instantaneous' volume change is generally larger than the 'stationary' value measured following a period of relaxation in the cell. Using an 'instantaneous' value of ε in the parameter estimation process may therefore introduce an error in the estimated parameters, for example an overestimation of ε may lead to an underestimation of L_p (by Eq. 2.13). If the value of ε is measured prior to HPP experiments on *Chara*, then errors in the estimated L_p from the HPP experiments resulting from the use of this value are unlikely as it was found that the measured values of ε before and after one set of HPP experiments (6 experiments over a duration of approximately 6 minutes) was the same within measurement error. HPP experiments were usually conducted immediately after the measurement of ε. However, errors in the estimated parameters from OPP experiments resulting from using an 'instantaneous' measurement of ε are more likely as the duration of the course of experiments were 1 to 2 hours. This error cannot be quantified for the present data due to a lack of available data on ε.

It was also found that the product εL_p was approximately constant between the fits to each data set, where the same model was used. In the context of the classical model, constancy of εL_p is expected because of Eq. (2.7) linking εL_p and the rate constant k_w of the water phase. As mentioned previously (§3.6.5c,d), the behaviour of the estimated parameters and variables predicted by the analytical solution to the KK equations, on which the classical model is based, seem to carry over to the UL model.

This is probably because the ULs change the concentration difference at the membrane, but not the transport processes across the membrane, which are still governed by the KK equations.

4.8.6 Equilibrium pressures

It has been mentioned that in the OPP experiments analysed in this chapter, the observed final equilibrium pressure P_E usually doesn't equal the observed initial pressure P_0 due to the APW change from full to half-strength or vice-versa (§4.3.3). Although the magnitude of P_E - P_0 differs between experiments, in most cases the classical and UL models were capable of predicting the tail of the OPP well, at least up to 400s.

In a few cases, however, the simulated data could not fit P_E or the tail of the observed data. For some data sets the best fit was obtained when the APW was not changed from full to half-strength (or vice-versa) (§4.6.1a). It is not clear what these inconsistent differences in initial and final equilibrium pressures are due to. Possible reasons (Tyree, *pers. comm.*) may be that the ethanol is affecting cell turgor dynamics by chemically or physically changing the membrane properties, or changing the osmotic pressure inside the cell due to molecular interactions with the cell contents. However, why this should vary between experiments is not clear. A more likely explanation is that the cell is reacting to the perturbations, and the reaction varies between experiments. *Chara* cells are not typically exposed to ethanol in nature, and the cells could be using active transport to get rid of the ethanol via ion channels in the membrane. Both permeant and impermeant solutes may be affected by the above disturbances to membrane properties or concentration of solutes in the cell, especially if the latter are only relatively impermeant as compared to the permeant solutes used.

It was found that following negative HPP experiments, the observed P_E is usually lower than that predicted by the models. To accommodate this, the internal concentration π_{i1} at the time of perturbation was changed, and changed for all fits to HPP data for consistency. Changes in π_{i1} may be occurring due to the presence of some permeant solutes inside the cell ("impermeant" solutes are only relatively impermeant) affecting the internal concentration at time of perturbation. If permeant

solutes present inside the cell are leaking out during perturbation, or during the course of the experiment via passive or active transport in negative HPP experiments, this would cause the equilibrium pressure to fall short of the predicted equilibrium.

Another possibility is that water exchange occurring during the perturbation (the perturbation is not strictly instantaneous) is affecting the internal concentration at time of perturbation. An examination of HPP experiments reveals that it takes about 0.5s for the pressure to rise or fall to a maximum or minimum value. During this change in pressure some water exchange would be occurring with the external medium, so that for negative HPP experiments $\pi_{i1} < \pi_{i0}$, and for positive HPP experiments $\pi_{i1} > \pi_{i0}$, rather than $\pi_{i1} = \pi_{i0}$ as is usually assumed for an instantaneous pressure change. This would cause P_E to return to a lower or higher value than that predicted by the models for a negative and positive HPP respectively.

Although it is not known whether changes in the internal concentration at time of perturbation are in fact occurring, this is considered the most likely explanation. The external concentration is constant as it is continually being replaced, and differences in the perturbation pressure P_1 used in the models do not affect the predicted P_E (§4.8.3a). However, it is also possible that ethanol from a previous OPP experiment may be left in the cell, affecting the concentration of solutes inside the cell by adding some permeant solutes to an HPP experiment.

None of the above factors, however, explains why P_E was more poorly predicted by the models for negative HPP experiments as compared to positive HPP experiments. This pattern seems to indicate an asymmetrical behaviour, or polarity in, the response of the cell to hydrostatic pressure perturbations. For a small proportion of the HPP data fit in this chapter, the choice of P_0 was unclear (see §4.3.3), and the value of P_0 used affects the fits and predicted P_E. However, when a different value of P_0 was used for a couple of these fits, the fits were not altered much so the original choice of P_0 was maintained. This uncertainty in P_0 may affect the estimated parameters for a couple of the HPP fits, but would not be the reason for general differences in fits between positive and negative experiments.

4.9 Comparison of estimated parameters with those in the literature

Estimated parameters averaged over all data sets examined in this study were compared with average parameter values in the literature. It was found that classically-estimated membrane parameters in the present study are consistent with those from Henzler *et al.* (2004) and Hertel and Steudle (1997) (compare Table 4.29 & Table 4.30).

Table 4.29 Average estimated parameters for OPP and HPP experiments, using the UL and classical models, for 3 *Chara* cells. Errors are standard deviations.

	UL model		Classical model	
	OPP	HPP	OPP	HPP
L_p (x10^{-6} m s^{-1} MPa^{-1})	1.69 ±0.68	2.23 ±1.2	2.22 ±0.78	2.14 ±1.1
p_s (x10^{-6} m s^{-1})	6.18 ±2.16		3.51 ±0.73	
σ	0.462 ±0.06		0.267 ±0.02	

Table 4.30 Average estimated parameters from existing literature, for *Chara corallina* where ethanol was used as the permeant solute. L_p is obtained from HPP experiments.

	a	b	c	d	d'
No. of cells	not stated	6	15 (p_s), 4 (σ)		
L_p (x10^{-6} m s^{-1} MPa^{-})	2.0 ±0.8	1.6 ±0.7			
p_s (x10^{-6} m s^{-1})	3.5 ±0.3	2.8 ±0.4	2.36 ±0.28	1.97 ±0.1	2.82 ±0.31
σ	0.21 ±0.02	0.36 ±0.05	0.4 ±0.06		

a Henzler *et al.* (2004)
b Hertel and Steudle (1997)
c Steudle and Tyerman (1983)
d Dainty and Ginzburg (1964c), theoretical predictions using analytical equation
d' Dainty and Ginzburg (1964c), value corrected for unstirred layers.

Dainty and Ginzburg (1964c) carried out a theoretical prediction of membrane parameters using analytical equations, and corrected for ULs by solving the diffusion equation for the planar case. They predicted p_s may be underestimated by 30% if not corrected for ULs (Table 4.31). In order to compare their results with those in this study, parameter ratios ξ of classically-estimated/ non-classically estimated parameters (Table 4.31) were calculated using the averaged parameter values in Table 4.30. These results suggest that for an OPP experiment, the classical model may over-

estimate L_p by 31% and underestimate p_s and σ by 43%. Since Dainty and Ginzburg (1964c) stated that their corrected values will "underestimate the effect of diffusion resistances on the permeability", due to their application of equations for planar geometry, the results for p_s drawn from Table 4.31 are consistent with the predictions of Dainty and Ginzburg (1964c) since the numerical model in this study solves the diffusion equation for cylindrical geometry.

Table 4.31 Parameter ratios for values in Table 4.29.

	OPP	HPP
No. of cells	3	3
ξ **(L_p)**	1.31	0.96
ξ **(p_s)**	0.57	
ξ **(σ)**	0.58	

The parameter ratios calculated for each individual cell in §4.6.1b (Table 4.15) showed that for an OPP experiment the classical model may over-estimate L_p by up to 50% and underestimate p_s and σ by up to 50%. The difference between these values and those stated in the preceding paragraph shows that while parameters averaged over a few cells indicate the extent to which classically-estimated average parameters may be affected by ULs, they do not indicate the full impact unstirred layers may have on classically-estimated parameters. This is due to the significant inter-cell variation in the estimated membrane parameters, as can be seen from the large standard deviations in Table 4.29 and Table 4.30, and the large range in estimated parameters shown in Fig. 4.15.

4.10 Conclusions

A model incorporating unstirred layers (UL model), developed in Chapter 3, was applied in this chapter to CPP data obtained by Dr. Helen Bramley and Prof. Mel Tyree. Data from 3 *Chara* cells were analysed using both a model with 2 ULs and the classical model. It was found that the UL model reproduced the observed CPP relaxation curves as well as, and often better, than the classical model. For fits to OPP data, the UL model generally improved fits to the water phase and first part of the

solute phase, and for fits to HPP data the UL model improved fits to the first half of the data, from t_0 to the end of the shoulder of the curve (§4.6.1a).

It was shown that the UL model does not just influence the first few seconds of the relaxation curves, as often assumed in the literature (Hertel and Steudle, 1997), but influences the pressure dynamics throughout the course of an HPP or OPP experiment (§4.5.4).

It was found that estimated parameters differed significantly between the UL and classical models. Parameters estimated using the UL model, being a more accurate model, can be viewed as being closer to the true values for the membrane. Compared to these, the classical model underestimated p_s and σ by up to 50% and overestimated L_p by up to 50%. For the HPP experiments, the classical model underestimated L_p by up to 5% (§4.6.1b).

The UL model also gave estimates for the ULe thickness δ_{ULe} in OPP experiments in the range of 30-50 µm. One would expect δ_{ULe} to be the same between positive and negative OPP experiments conducted on the same cell. However, estimated values for δ_{ULe} varied by 4-15 µm between positive and negative OPP experiments conducted on the same cell. This pattern was observed for all 3 cells (§4.6.2a) and was partly dependent on the extent to which the measured time-delay differed between positive and negative pulses (§4.6.2a, §4.8.2). It is considered that apparent differences in δ_{ULe} between positive and negative experiments are likely to be due to measurement errors, and to a greater extent differences in pressure dynamics between experiments (§4.8.2).

Some difference was observed in estimated parameters between fits to positive and negative OPP data from the same cell. However, definitive conclusions could not be drawn about the presence or absence of polarity in the parameters, since the direction and magnitude of the polarity was inconsistent between the cells, and the sample size was small. A polarity in L_p was also not observed in fits to HPP data. Although there was some difference in L_p between positive and negative experiments for two of the cells, a difference was absent for Cell 4 where the sample size was largest. This is also interesting considering that for Cell 4 fits to negative HPP data were worse than fits to

positive HPP data, which seems to suggest some asymmetry (polarity) in the pressure dynamics (§4.6.21a). However, it is unclear what this asymmetry may be due to (§4.8.6).

Differences were found in estimated L_p values between OPP and HPP experiments, where L_p for HPP experiments were 14-45% higher than the L_p for OPP experiments (§4.6.2a). However, it is possible that the L_p values are the same, but difficulties in fitting the first 2-3 s of the HPP data and in determining initial conditions for HPP simulations may be causing a difference in L_p between HPP and OPP experiments (§4.8.3). A larger sample size is again required for more conclusive results. In addition, more accurate HPP data could be obtained by using a mechanical system for adjusting the metal rod in the CPP. This would likely remove some of the variation observed during the HPP perturbations.

In OPP experiments where a bubble is not used to separate the old and new external solutions, the exchange time must be included as this affects the estimated parameters. However, the solution exchange acts over a different time scale to unstirred layers, i.e. only during the first few seconds of a relaxation. Optimization of the exchange time is not recommended, as changes in the relaxation curve are not very sensitive to small changes in it. Optimized parameters also appear to be independent of the form of the exchange function used, but are affected by the duration. Therefore, it is recommended that the exchange time is fixed in the model, based on a known exchange function. However, as this information is currently not available, it was difficult to compare estimated parameters between OPP experiments where a bubble is present during the solution changeover to OPP experiments where a bubble is not present.

Estimated membrane parameters between cells were found to differ by as much as a factor of 2 (§4.6.2b, Fig. 4.15). The intra-cell variation in estimated parameters was less than the inter-cell variation, and within each cell the estimated parameters were fairly consistent (§4.8.1, Fig. 4.15). This suggests that the UL model is predicting the membrane parameters well, and these should be consistent within a cell as they are intrinsic properties of the membrane. Some correlation of δ_{ULe} with cell length was also observed (§4.6.2b).

Studies elsewhere in the literature have also found significant inter-cell variation in estimated membrane parameters (§4.9). It is well established that a wide range of L_p values exist in plant cells, and that this probably reflects a property of the membranes (Maurel, 1997). Averaging estimated parameters over all cells leads to different conclusions regarding the extent to which ULs influence estimated parameters, as compared to averaging estimated parameters within each cell. This must be noted when comparing results from studies which aim to evaluate the impact of ULs on estimated parameters, where parameters are usually averaged across cells, with results from the present study.

Estimated parameters were shown to be sensitive to the value of the diffusivity D for the cell interior (§4.8.4). It was shown that the value of D used for the internal UL can significantly affect the membrane parameters estimated using the numerical model. Simulations in Chapter 3 suggest that using a value of D for the ULi which is nearer to the actual value may result in an even greater difference between the estimated parameters using the UL and classical models, particularly for L_p (§3.6.6a). In addition it was shown that estimated parameters are sensitive to the value of the elastic modulus ε of the membrane (§4.8.5). These factors must be considered when comparing estimated parameters between experiments. However, a present lack of data on the likely range of D and ε values for *Chara* means that the impact of these factors on the estimated parameters cannot be fully explored.

Hertel and Steudle (1997) have found that there is also a strong correlation between temperature and L_p in *Chara* over a temperature range of 10-35°C, and the effects of temperature on the estimated L_p using the UL model could be explored in future studies. The temperature was not changed during the CPP experiments from which data was obtained, however the UL model was used to show that a 2 degree change in temperature in the model made <1% difference to the estimated parameters.

Predictions of the total permeability using the equation analagous to Kirchoff's laws for electrical resistances in series (Eq. (3.2) were examined (§4.8.4). A large difference was found between the membrane parameters estimated using the UL model and the total permeability predicted by this equation. This shows that ULs are

strongly limiting transport across the membrane. Predictions of total permeability from this equation also differed significantly from the total permeability predicted by the classical model, showing that predictions using this equation and the classical model cannot be compared.

The results in this chapter are based on an examination of a small set of experimental data. Despite this, the analysis has produced interesting results. Further, it has highlighted what additional details about the experimental system are required for a more definitive estimation of membrane parameters. These include:

a) Direct and accurate measurement of the time of perturbation in an OPP experiment. This affects the estimation of the ULe thickness, and can be obtained from simultaneous recording of changes in cell pressure and conductivity of the external solution. These data, although recorded, were not made available for the present study.

b) Information about how the external concentration changes during an osmotic perturbation. Estimation of the membrane parameters and the ULe thickness in OPP experiments where a bubble is not present in the solution changeover, is problematic without knowledge of the exchange function. This has meant that in the present study only results from OPP experiments with a bubble could be compared.

c) More knowledge of what is happening during the pressure perturbation in HPP experiments. Changes in the concentration or pressure during this phase affect the model inputs and hence the estimated parameters, and may be an important missing element in the model. This can be mediated to an extent by adjusting the initial conditions in the model, i.e. values of P and C at $t=t_1$. However, it is important to understand the realistic physical processes in order to know what appropriate changes to make in the model. A mechanical system for adjusting the metal rod in the CPP would also provide for more accurate HPP data, and is recommended for future studies.

d) Better replication to enable more conclusive results of within-cell and between-cell variation in membrane parameters to be drawn. More CPP data would also remove the influence of other variables such as differences in equilibrium pressures between the beginning and end of an OPP experiment (§4.3.3, §4.8.6), and drifts in equilibrium pressures over the course of a few OPP experiments, by fitting only those experiments for which these variations do not occur.

5 Conclusion

5.1 Overview of implications of UL model

A model of pressure dynamics during a CPP experiment has been developed and applied. This model incorporates unstirred layers (ULs), in contrast to the classical model traditionally used to estimate membrane parameters from CPP experiments. It was found that the UL model was able to reproduce the observed CPP relaxation curves better than the classical model. Membrane parameters estimated with the two models differ significantly, and this study proposes that the classically-estimated parameters (i.e. estimated using the classical model) are not a true representation of the membrane parameters. Rather, the UL model developed in this study is a more accurate and comprehensive representation of transport across a cell membrane in CPP experiments, and parameters estimated by this model are likely to be nearer to the true membrane parameters. Results from applying the model suggest that the classical model may underestimate p_s and σ and overestimate L_p in an OPP experiment by up to 50%, and underestimate L_p in an HPP experiment by up to 5% (§4.6.1b).

The ability of the classical model to reproduce observed pressure relaxations does not negate the presence of ULs. While both models can be made to fit the data, differences in the model fits are subtle and important. The classical model, for instance, does not reproduce the initial curvature in the OPP data following the osmotic perturbation. It fits the water phase only by adjusting the time of perturbation t_0, which must be later than the actual t_0 (§2.5.2). The UL model, by contrast, automatically reproduces the initial curvature in the OPP data (Fig. 3.6; Fig. 4.10). In HPP experiments, the UL model consistently fits the shoulder of the data curve more closely than the classical model (§4.6.1a).

This study has unequivocally shown that ULs are an important factor in cell pressure dynamics, and impact on all parts of the OPP and HPP relaxation curves. ULs should be included in all models used to fit CPP data as they have a significant impact on the

estimated membrane parameters. With the exception of Tyree *et al.* (2005), no process-based model including ULs has been developed to model transport across a cell membrane in a CPP experiment. The UL model developed here thus provides a better and alternative model for membrane parameter estimation.

Although this model includes ULs in a realistic manner, other features of cells that affect pressure dynamics have not been included, e.g. influences of the tonoplast on water and solute transport, and pressure dynamics during the period of an HPP perturbation. However, the model does provide a means for estimating membrane parameters more accurately. Further, the study highlights that current experimental protocols, methods of parameter estimation, and how unstirred layers are treated in the literature, must be re-assessed. The study shows that membrane parameters for *Chara* given in the literature are not the true values for the membrane.

5.2 Critique of current methods for dealing with unstirred layer effects on estimated parameters

A brief review of how ULs have been considered in the CPP literature was given in §3.1.4a. In this section, claims in the literature will be addressed in detail, in light of the findings of this study.

a) Claim that ULs take a while to form during a relaxation, and have little influence during certain periods

It has been suggested (Henzler and Steudle, 2000) that internal and external ULs take a while to form during a relaxation, and that through the process of internal diffusion the thickness of ULs increase over time during the solute phase of a CPP experiment. It has been claimed (Hertel and Steudle, 1997) that if experiments are conducted when ULs have not reached their maximum thickness, e.g. if membrane parameters such as σ are measured at times before the internal unstirred layer has completely formed, the effects of ULs would be less and the measurement of membrane parameters would be relatively unaffected by ULs).

These suggestions, however, are inconsistent with the concept and definition of an unstirred layer. A ULe forms as a result of fluid flowing past a solid body, in this case a cell (Barry and Diamond, 1984). The ULe would be well-established within the first few seconds of switching on the flow in a CPP experiment, and remain at a constant thickness as long as the external solution is flowing at a constant rate. Since equilibrium is established prior to any experiment, a ULe would already be at its maximum thickness during an experiment. The ULi would also not change in thickness since there is little stirring within the cell and no outside forces acting on it. Since water is incompressible, and cell sap and APW are mostly water, fluid flowing into the cell would not disturb the bulk of the cell solution but merely add to the cell volume by flowing into the region near the membrane (§3.2.2). See §A.4 in appendix for further comments.

b) Claim that a ULe only affects the initial few seconds

It has been suggested (Hertel and Steudle, 1997) that effects of external ULs should be negligible if the time it takes for solutes to traverse the ULe is small compared to the halftime of the solute phase. For example, it has been stated that for an external UL of no more than 50μm, the effect of external ULs should not be significant since a solute molecule would take a couple of seconds to diffuse from the bulk solution to the membrane surface, which is much smaller than the half-times of 15-100 s required for the equilibration of solutes.

The results of this thesis do not support this suggestion. A behavioural analysis of the UL model has shown that ULs affect both the pressure dynamics in these few seconds following the perturbation and also the concentration difference at the membrane (which drives cell pressure dynamics) for the entire course of an HPP and OPP experiment (§3.6.2, §3.6.3, §4.5.4). Furthermore, if the exchange time of the external solution (up to 3s) is not taken into consideration, an additional error is introduced in the estimation of membrane parameters since the exchange time affects the relaxation curves (§4.7). The influence of the exchange time on CPP experiments does not seem to have been fully explored in the literature, where it appears no bubbles have been used to separate new and old solutions during the solution changeover.

c) Claim that sweep-away effects in HPP experiments should be negligible due to small volume flows

It has been suggested (Hertel and Steudle, 1997; Zimmermann and Steudle, 1974a) that sweep-away effects in HPP experiments should be small or negligible because the amount of water moved across the membrane is small. However, the UL model in this thesis has shown that sweep-away effects in HPP experiments can affect the estimated membrane parameters by up to 5% (§4.6.1b). While this may be a small effect in some circumstances, the effects of ULs should nevertheless not be discounted in general.

d) Claim that fitting the solute phase by a single exponential shows effects of ULs in OPP experiments are small

It has been suggested that the influence of ULs in OPP experiments should be evident from their effects on relaxation curves. For example, Hertel and Steudle (1997) have stated that the ULi could be a few hundred micrometers thick, but that the effects of a ULi on OPP experiments would be insubstantial since otherwise rate constants measured during the solute phase would decrease continuously during the formation of the internal unstirred layer. This implies that it should not be possible to determine a single rate constant (determined from fitting a single exponential) for the solute phase. This conclusion is reinforced by Henzler and Steudle (2000) who state that "solute phases could be nicely fitted by a single exponential which would not be true in the presence of a limitation by diffusion within the cell."

Results of this thesis, however, do not support this suggestion. It has been shown that the classical and the unstirred layer models fit the solute phase of the relaxation curve equally well (§4.5.2). The presence of ULs do not change the fundamental shape of the curve, and the solute phase remains essentially an exponential decay with a different time constant to that for the classical model.

e) Claim that KK equations correct for ULs

Some papers in the literature (Steudle and Tyerman, 1983; Henzler and Steudle, 1995; Hertel and Steudle, 1997) claim to have corrected for unstirred layers in their parameter estimation. This claim rests on the argument that Eq. (2.16) corrects for solute flow and unstirred layers because the term [$\exp(p_s A_0 t_m / V_0)$] in the equation reduces $\Delta\pi_{se}$ to the true value across the membrane, thereby incorporating the effects of ULs on t_{min} and p_s .

However, Eq. (2.16) is obtained from the analytical solution to the KK equations at the point (t_m, P_m). It has been shown here that the KK equations by themselves do not incorporate effects of ULs, as evidenced by the fact that the classical model based on the KK equations estimates very different parameters to that of the UL model. Steudle and Tyerman (1983), Henzler and Steudle (1995), and Hertel and Steudle (1997) applied the classical model and used the bulk concentration values in the KK equations. Eq. (2.16) is simply a more accurate determination of σ in relation to a previous equation used to determine σ (Eq. (4) in Tyerman and Steudle, 1982) which applies for slowly permeating solutes only.

f) Claim that steady-state equations can be used to estimate the ULe thickness and its influence on membrane parameters

Some papers in the literature (Steudle and Tyerman, 1983; Ye *et al.* 2006) have applied steady state equations to determine the effects of external unstirred layers on HPP experiments. The following steady state equation has often been used, which relates the solute concentration at the membrane (C_m) to that in the bulk solution (C_b) (Dainty, 1963):

$$C_m = C_b \exp\left(-\frac{J_V \delta_{ULe}}{D}\right). \qquad (5.1)$$

It has been assumed that a ULe in an HPP experiment is formed by water extruded instantaneously from the cell (Steudle and Tyerman, 1983; Ye *et al.* 2006). Based upon the maximum change in the cell radius and volume during the relaxation, the maximum thickness δ_{ULe} of the ULe has been estimated to be 0.2-0.3 μm. Eq. (5.1)

has then been applied to estimate that the effects of sweep away due to ULs would be small, e.g. “less than a 0.7% reduction of the driving force” (Steudle and Tyerman, 1983). Dainty (1963) also used Eq. (5.1) to estimate that for δ_{ULe} = 10μm the assumed driving force (and measured L_p) would be 2% less than the true driving force (and membrane L_p).

Although sweep away (due to convection) arises due to movement of the cell membrane and changes in volume of the cell (§3.2.2), this thesis suggests that the above method of estimating δ_{ULe} cannot be applied, and that emphasis should not be put upon quantitative estimates resulting from Eq. (5.1). In regards to the first point, it was mentioned in (b) above that a ULe does not form due to fluid flowing across the cell membrane but forms due to fluid flowing past the cell, which establishes a ULe prior to a CPP perturbation. In regards to the second point, even if the value of δ_{ULe} is known, the use of Eq. (5.1) as a quantitative measure of the influence of a ULe should be cautioned against, as a relaxation is time-dependent. Steady state equations can only provide “best guesses” for effects of unstirred layers and cannot truly or fully quantify their effects.

g) Claim that the steady state permeability equation gives an upper bound to the thickness and contribution of ULs

The permeability equation (Eq. (3.2)) is another steady state equation that is sometimes used to quantify the effects of ULs on the membrane parameters. Ye *et al.* (2006) obtained rate constants k_s from the slope of semilog plots of the solute phase, used Eq. (2.10) to determine the total permeability p_T, and then used Eq. (3.2) to estimate a maximum ULi thickness. To do this, they assumed that the membrane is not limiting transport, i.e. that p_s in Eq. (3.2) is large. Thereafter, they appear to put back the estimated ULi thickness into Eq. (3.2) to estimate the membrane permeability and thus the contribution of ULs (by calculating the resulting difference between the membrane and total permeabilities).

Results of this thesis do not support the use of Eq. (3.2) for estimating effects of ULs on membrane parameters. It was demonstrated that the permeability equation (Eq. (3.2)) relating the membrane permeability to the total permeability across the membrane-UL system cannot be used to correct for ULs in the classical model (see

§3.6.6b, §4.84). It was also shown that predictions based on the steady-state permeability equation and the non-steady state UL model do not agree. Furthermore, the assumption in Ye *et al.* (2006) that the value of p_s is very large so that $1/p_s \rightarrow 0$ corresponds to a totally different system, where a membrane is not present in the region of diffusion. Both transport at the membrane and in the ULs govern transport across the system, and both are essential to the pressure dynamics.

In actual fact, the application of Eq. (3.2) to the conditions of a CPP experiment is inappropriate. As $a \rightarrow 0$, which corresponds to the entire internal region of the cell being unstirred, the term containing a goes to infinity which is non-sensical. This arises from the inadequate internal boundary condition which itself arises from the assumption of steady state, whereas in reality $C=f(t)$ at the internal boundary $r=a$ (see §A.3 for derivation). Eq. (3.2), therefore, cannot be applied to determine bounds for UL thicknesses or limits for the contribution of ULs.

h) Claim that variation in membrane permeability values reflect a small influence of ULs

In the literature, measured p_s values have been found to range over 2 orders of magnitude for different solutes which have similar values of the diffusion coefficient D (Henzler and Steudle, 2000). It has been suggested that this shows that membrane transport is not controlled by diffusion in the ULs but is dominated by the membrane permeability; otherwise p_s values should all be similar due to the similar values of D (*ibid.* 2000). It has also been found that the permeability of heavy water is strongly affected by blocking water channels, from which it has been concluded that ULs are not significantly affecting solute transport and the measured permeability largely reflects that of the membrane (Hertel and Steudle, 1997).

Results of this thesis do not support these views. The converse of the above scenario suggests that if p_s of the membrane is changed by using different solutes or blocking water channels, and ULs are strongly influencing transport, changes in p_s will not be evident in the pressure dynamics. However, it has been shown using the UL model that if the membrane permeability is changed, the observed pressure dynamics will change, and so will the classically-estimated parameters. ULs do not make the membrane permeability irrelevant to the transport processes, which the above

suggestions imply, but act in conjunction with transport through the membrane. The KK equations still govern transport across the membrane in the presence of ULs, which is evident from the fact that the relationship between parameters and variables predicted by the KK equations still hold in the presence of ULs (see §3.6.5d; §4.8.5). This thesis has shown that internal ULs may significantly limit transport across the membrane, while significantly affecting the estimated membrane parameters.

i) Claim that agreement between parameter estimates based on different experimental techniques implies that ULs have a low impact in CPP experiments

It has sometimes been suggested (Henzler and Steudle, 2000; Zimmermann and Steudle, 1978) that agreement between estimated parameters using the CPP, and results from other experimental techniques conducted by Dainty and Ginzburg (1964c,d), show that ULs in CPP experiments probably have a low impact.

This thesis proposes that this comparison is not an accurate one. Dainty and Ginzburg (1964c) used equations which apply to the planar case only, which has been shown to underestimate the impact of ULs on estimated parameters (§4.9). Also, in one paper (Steudle and Zimmermann, 1974) a correction for unstirred layers (based on steady state equations) was necessary to bring values of σ into closer agreement with Dainty and Ginzburg (1964c).

In summary, this thesis suggests that a process-based model incorporating unstirred layers is the only means by which effects of ULs on estimated parameters can be quantified. In the absence of this, analysis of the potential effects of ULs are largely guesses based on analogies, assumptions, and application of equations which do not strictly apply to the system being studied. This thesis has demonstrated that the effects of ULs in CPP experiments can be subtle, such that a significant influence of ULs on the concentration difference at the membrane during the course of an experiment cannot be observed from relaxation curves.

5.3 Some results from the UL model in relation to the literature

It was summarised in §3.1.2 that some evidence in the literature show that effects of ULs include a polarity in L_p, an increase in L_p with external flow rate, and a decrease in L_p with increasing external solute concentration. Polarity is where the estimated L_p is different between positive and negative pulses of the same magnitude.

The extent to which an observed polarity in L_p is due to either properties of the membrane or to unstirred layer effects has been a subject of much debate (Steudle, 1993; Dainty, 1963). Polarity in L_p has been found to increase at higher external concentrations (Steudle and Zimmermann, 1974), suggesting an influence of ULs due to sweep-away effects (Dainty and Ginzburg, 1964a). However, Dainty and Ginzburg (1964a) have concluded that an absence of sweep-away effects would not result in an absence of observed polarity, and polarity in L_p may be largely an intrinsic property of the membrane (plasmalemma) in some *Characeae* species due to a differential dehydration of the membrane (Dainty and Ginzburg, 1964a; Kiyosawa and Tazawa, 1973). It is also possible that polarity arises due to combined effects of the tonoplast and the plasmalemma, i.e. is due to a composite membrane (Zimmermann and Steudle, 1978; Kedem and Katchalsky, 1963c).

Use of the present UL model to estimate membrane parameters may potentially help resolve whether and by how much the presence of ULs contribute to observed polarity in the membrane parameters. It was shown (§3.6.5b) that the presence of an UL does not induce polarity in the parameters. Since the model explicitly takes the influence of ULs on the estimated parameters into account, any polarity in the parameters must therefore be due to other factors affecting the cell pressure dynamics and not ULs. When the UL model was applied to observed data, the present study found no evidence of polarity in L_p in HPP experiments (§4.6.2a), and some but no conclusive evidence of polarity in membrane parameters for OPP experiments (§4.6.2a). The former result is in agreement with results of Steudle and Tyerman (1983) who did not observe polarity in L_p for HPP experiments in *Chara corallina*, although Steudle and Tyerman (1983) observed polarity in L_p for OPP experiments (with permeant solutes).

Unfortunately, due to the small sample size, polarity in membrane parameters could not be fully explored in the present study.

The UL model could be used to determine whether changes in the estimated parameters due to differing external solute concentrations or external flow rates are influenced by ULs. Unfortunately, these variables were not changed in the experiments analysed here. However, it was shown that the UL model predicts the classically-estimated L_p from HPP experiments will decrease marginally with increasing external concentration (§3.6.5c), and that the classically-estimated L_p from OPP experiments will be more affected by increasing the external concentration.

A difference in the classically-estimated L_p between HPP and OPP experiments observed in the literature (and confirmed in the present study) is considered by CPP experimenters to be due to effects of a ULe. In the literature it has been found that in OPP experiments with ethanol as the permeating solute, L_p reached a saturation level for flow rates above 25 cm s^{-1} where its value was similar to L_p in HPP experiments (Steudle and Tyerman, 1983). This observation suggests that the ULe thickness for OPP experiments at higher flow rates has been reduced significantly, since a ULe has little effect on L_p in HPP experiments. The difference in L_p between HPP and OPP experiments found using the UL model is therefore surprising, since this takes effects of ULs on the estimated parameters explicitly into account. However, the difference may be due to inadequacies of the model in fitting the initial 2-3 s of HPP data (§4.8.3a,b).

5.4 Suggestions for, and comments on, the parameter estimation process

Here an outline of the parameter estimation process carried out in this study is given, together with important things to consider when fitting CPP data and estimating parameters.

5.4.1 OPP experiments

a) Importance of initial conditions

The observed final equilibrium pressure (P_E) in OPP experiments is not always well predicted by the models. This is because P_E for OPP experiments often differs from the initial value P_0, where theory predicts they should be the same when the external osmotic pressure π_{se} is constant (§2.2.2, §3.6.2). Therefore the degree to which the tail of the observed OPP data is fitted by the model depends very much on the value of P_0 used in the model. If π_{se} is not constant throughout the experiment, the predicted P_E will differ from P_0, but not necessarily by the amount observed in the data (§4.3.3, §4.5.1a).

Therefore, model predictions are very sensitive to values of P_0 and π_{se} used in the model, and it is important that these values are accurate and consistent with experimental data. P_0 must be determined individually for each cell, but the initial cell volume V_0 and cell radius r_0 need not be since the pressure dynamics are not so sensitive to these, and the same values of V_0 and r_0 can be used for all OPP experiments on the same cell (§4.3.3). If the values of P_0 and π_{se} are accurate but P_E is not well predicted, some other factor in the experiment must be affecting the pressure dynamics which is not included in the model. In particular, drifts in equilibrium pressure for a series of experiments on the same cell (§4.3.3) would affect model predictions of OPP data. This was the case for the 3 cells examined in Chapter 4.

It is important to use an accurate value for the time of osmotic perturbation t_0. As there is a correlation between the experimental time-delay and the estimated ULe thickness, accurate estimation of the ULe thickness depends upon how accurately t_0 can be determined (§4.4.2, §4.6.2a). t_0 should be able to be determined accurately by simultaneously recording the cell pressure change and conductivity of the external solution, and plotting these on the same time-axis. The error from the application of t_0 will then be confined to how it is used in the model, which assumes that t_0 is when the solution front reaches the middle of the cell.

b) Incorporation and estimation of unstirred layers and exchange times

Both internal (ULi) and external (ULe) unstirred layers should be included in the model, since both are present in the physical system. Inclusion of one UL alone is meaningless, as each UL has a different and significant effect on the estimated parameters (§4.5.2). The internal UL thickness δ_{ULi} is assumed to equal the whole cell interior, but can be fixed at $3x10^{-4}$ m since larger values have negligible impact on the pressure dynamics and estimated parameters (§3.6.2).

The external ULe thickness δ_{ULe} can be estimated by optimising δ_{ULe} along with the membrane parameters L_p, p_s and σ for OPP experiments where a bubble is used to separate the new and old solutions. Applying the model to estimate δ_{ULe} is self-consistent with the data (§4.4.2), and is a better method than using an experimental time-delay to determine a value of δ_{ULe} to use in the model. The time-delay vs. δ_{ULe} relationship varies between cells and is subject to measurement errors in the time-delay, and cannot be used as a general predictive tool for estimating δ_{ULe}.

Parameter estimation using OPP experiments where a bubble is not used to separate the new and old solutions, is more difficult. In this case the exchange time of the external solution must be incorporated into the model, but it is not possible to use the model to predict both δ_{ULe} and the exchange time, since these are correlated (§2.7.3c, §4.4.2). Predictions of δ_{ULe} are best obtained from OPP experiments where a bubble is present, as the exchange time is much smaller and can be ignored (§4.6). The predicted values of δ_{ULe} obtained from these experiments on the same cell can then be used as fixed values when the model is fit to OPP experiments where a bubble is not present (§4.4.2b). The exchange time of the external solution can then be optimized together with the 3 membrane parameters (§4.4.2b). However, this would not give consistent or accurate predictions of the membrane parameters unless the exchange function appropriate for each OPP experiment is known and obtained from experimental data. If this information is available, the exchange could be explicitly included in the model instead and δ_{ULe} optimized.

At present, not enough experimental data are available on the exchange times in OPP experiments. In the present study, it was found that estimated parameters for OPP

experiments where a bubble is present, compared to those for OPP experiments where a bubble is not present, differ significantly (§4.7.2). It is therefore suggested that a bubble always be used in the solution exchange in OPP experiments. The exchange time can then be removed from the estimation process. Since CPP experimenters do not routinely do this, their estimated parameters would not properly reflect the true membrane parameters because effects of the exchange time on them cannot be quantified.

5.4.2 HPP experiments

The final equilibrium pressure P_E in HPP experiments also cannot always be well predicted by the models. The predicted P_E for HPP experiments depends on the perturbation values used in the model, namely the hydrostatic perturbation pressure P_1 and the osmotic pressure π_{i1} in the cell at time of perturbation. There is experimental uncertainty in these values as the perturbation is not instantaneous, and detailed knowledge of the processes affecting the cell during the perturbation is lacking (§4.3.4).

It is recommended, therefore, that π_{i1} be optimized together with L_p to obtain the best fit to the data. This does not give a more consistent L_p, but significantly improves the fits (§4.5.1) to the *P*-*t* curve. There should also be some flexibility in choosing an appropriate P_1, and datasets which exhibit a lot of noise around the perturbed pressure should not be used for parameter estimation. Although a point after the perturbation pressure can be used for (t_1, P_1), using a point too far after the perturbation pressure greatly affects the estimated parameters, because the time interval of the data used is different (§4.8.3a). Therefore these estimated parameters cannot be compared with those for other data sets.

The external osmotic concentration π_{ie} should be a constant for all HPP experiments. However, one should also be aware that errors in the value of π_{ie} used in the model will affect the quality of model fits to the data.

A ULe has little influence on an HPP experiment (§3.6.2), and therefore δ_{ULe} cannot be estimated by fitting to HPP data. HPP data can be simulated by incorporating a

ULi only. However, because a δ_{ULe} is present, it is recommended that both a ULe and a ULi be incorporated when fitting HPP data. The average δ_{ULe} obtained from fits to OPP data on the same cell should be used for the HPP data, because δ_{ULe} should be the same for the two types of experiment.

5.4.3 Comparison of fits and determination of best fit

It is best to use the same CPP runtimes when estimating parameters and comparing fits between experiments, as estimated parameters are dependent on the quality of the fit, which is in turn dependent on the temporal range of the data used. Where the same quantity is determined for observed and simulated data (e.g. calculation of P_E), the same method based on the same number of points should be used in both cases. An adequate sample size of at least 5 positive and 5 negative experiments is also recommended for each experiment type (HPP or OPP).

Minimization of the root-mean-square error (RMS) of the residuals is a simple, objective means of fitting CPP data. Goodness-of-fit is best measured by analysing residuals between observed and simulated data. Calculation of the RMS, bias in residuals, trend in residuals, largest residual, residual in P_E, and residual in the extreme pressure P_m, give a comprehensive set of values by which fits can be compared (§4.5.1, §4.5.2, §4.6.1a). To obtain a uniform distribution of residuals it is suggested fitting P_m to within ± 0.001 MPa, which can be done by weighting the RMS error around the extremum, using a window based on 10% of the maximum pressure change in the data. A weight of 2-3 is sufficient.

5.4.4 Other recommendations

It is recommended that the temperature of the apparatus be monitored and maintained at a constant temperature to within ± 2˚C, as temperature affects the estimated parameters (§4.10).

5.5 Suggestions for further research

This study has been a preliminary investigation of the impact of ULs on parameter estimation using data obtained from CPP experiments. In this section some suggestions for further research are made based on the findings of this study. Further research is required for validation of the UL model, examination of the model behaviour, and for more conclusive results regarding the presence of and reasons for parameter variation in the UL model.

5.5.1 Experiments

a) Exchange times

A more consistent and precise measurement of the exchange time (or ramp time if the exchange function is linear) of the external solution is required. This is necessary for parameter estimation in OPP experiments where bubbles are not used during the solution changeover. It was shown that the exchange time affects the estimated parameters by a significant amount (§4.7); however the exchange time is rarely considered in CPP experiments. Determining the influence of the exchange time on the estimated parameters is therefore important as it would reveal to what extent parameters estimated in previous studies may be inaccurate due to neglect of the exchange time.

It is unclear from the data used in the present study if the exchange time usually varies or is usually consistent between experiments. Exchange times varied greatly for Cell 4 where there was a strong relationship between the time-delay and the exchange time, but for Cells 2 and 3 the exchange times were quite consistent between experiments and independent of the time-delay (§4.4.2b). It is recommended that the exchange time of the external solution be recorded for each experiment, and a function fitted to the conductivity data to give an exchange function for input into the model.

b) External flow rates

External flow rates should be varied, in a range similar to that used in Steudle and Tyerman (1983) of between 5 and 44 cm^{-1}. This will physically change the ULe thickness and allow the examination of the impact of different ULe thicknesses on

parameters estimated for a single cell. This will be an important validation of the UL model because it takes the influence of ULs into account, and hence the estimated parameters for a single cell should be consistent and independent of the ULe thickness. If differences in the estimated L_p between HPP and OPP experiments change depending on stirring rates, this would suggest that some other factor in the pressure dynamics are changing due to higher stirring rates, or more likely, that the UL model is not adequately taking the effects of ULs into account.

c) External concentration

It is suggested that experiments be conducted where the external concentration is varied. On the basis of the behavioural analysis of the UL model (§3.6.5c), this is expected to change the estimated L_p since the external concentration affects the rate constant governing water flow across the membrane in the KK equations. Many CPP experimenters have observed a change in the classically-estimated L_p with external concentration, which they consider to be largely due to sweep-away in the ULs (Zimmermann and Steudle, 1978). It would be worthwhile to see if and how L_p estimated with the UL model differs from this, as it may help decide if there really is a change in L_p with concentration, or evaluate the contribution of ULs to this observation.

d) OPP experiments with impermeant solutes

It is suggested that experiments be conducted for OPP experiments using impermeant solutes, where estimated values of L_p could be compared with those from HPP experiments. This may suggest reasons for the differences in the non-classically estimated L_p between HPP and OPP experiments, since the relaxation curves for OPP experiments using impermeant solutes are similar to that for HPP experiments (i.e. monophasic, see §2.2.2). Differences in the polarity in L_p found between OPP experiments using impermeant and permeant solutes have also been observed (Steudle and Tyerman, 1983), and it would be interesting to see if polarity in the non-classically estimated L_p gives similar results. OPP experiments with impermeant solutes should also be conducted using different external flow rates (as in (b) above).

e) Using different solutes

OPP experiments should also be conducted using a wide range of different solutes which might have differing permeabilities across the membrane. This will allow an examination of whether the observed variations and differences in the estimated membrane parameters for ethanol agree with those observed for other solutes. This will also reveal whether the quality of fits to the data depend on the solute used, and by how much differences between the classically-estimated and non-classically estimated parameters vary depending on the solute used. ULs are expected to have more effect on the classically-estimated parameters for rapidly permeating solutes, i.e. those with a higher p_s (§3.1.3).

Furthermore, these experiments will provide information about the solute-dependence of the parameters, i.e. how p_s and σ change with the solute used, whether L_p changes with the solute used (it is not expected to change on the basis of the present study), and how the parameters are correlated. This will further differentiate effects of the membrane from effects of the solute on p_s and σ, which are solute and membrane dependent.

f) HPP experiment with the cell in still water

It is suggested that an HPP experiment be conducted where the cell sits in still water, and the concentration of the external solution monitored for any change due to leaking of cell contents into the solution. This could be done by monitoring changes in conductivity of the external solution during an HPP experiment, including the period of the perturbation. These experiments may provide a clue as to whether the internal concentration of impermeant solutes in the cell is changing during an HPP experiment (§4.8.6). They may also provide information to help resolve the asymmetrical pressure dynamics between positive and negative HPP pulses, where it was found that negative HPP pulses were in general more difficult to fit with the UL model (§4.6.1a, §4.8.6).

g) Experiments without an APW change

The change from full to half-strength APW (or vice-versa) in an OPP experiment results in a distinct difference between the initial and final equilibrium pressures (§4.3.3). At times this difference was much lower than expected, so that the tail of the

data could not be fit well (§4.5.1, §4.8.6). At the time of this study, the experimenters (Bramley and Tyree) were making preparations to conduct OPP experiments with mannitol added to the external solution during the change from full to half-strength APW, so that the concentration of impermeant solutes in APW remains the same but the conductivity of the external solution can still be measured. This will result in smaller and hopefully more consistent differences between initial and final equilibrium pressures, which can be fitted more consistently by the model.

h) Diffusivity coefficient **D** *for the interior of* **Chara**

If possible, experiments should be conducted to measure the value of D for typical test solutes and impermeant ions in the interior of *Chara*. This would contribute to the accuracy of the estimated parameters using the numerical model, since the value of D can significantly affect the parameters (§3.6.6a, §4.8.4). It is not known at present how this could be done. However, Nitsche *et al.* (2004) has estimated the diffusivity of 3 dyes in cytoplasm, and found that the value for D in cytoplasm was 12-68% lower (depending on the dye) than the value for D in water, at a temperature of 25°C. This suggests that the value of D in *Chara* for typical test solutes used in CPP experiments may be affected to a similar degree (although the vacuole occupies most of the volume of a *Chara* cell it comprises a solution of the same osmolality as the cytoplasm, see §2.1.1).

i) Time-dependence of **ε**

It was shown in §4.8.5 that it is important to determine the elastic modulus ε of the membrane as accurately as possible, as its value contributes significantly to the error in L_p. It was also discussed in §4.8.5 that the measured value of ε changes over time and this may introduce an error into the estimated membrane parameters. It is recommended that in future experiments, ε be measured a few times during a series of CPP experiments (which include OPP experiments), so that the extent to which ε changes over time for CPP experiments on *Chara* can be quantified. This would allow the impact of time-variable behaviour of ε on the estimated membrane parameters to be estimated.

5.5.2 UL models

Results from this study suggest that an important process is missing in the UL models for HPP experiments. In general, the shoulder of the HPP curve could not be fitted by either the UL or classical models, and negative HPP experiments were generally more difficult to fit than positive HPP experiments (§4.6.1a, §4.8.6). However, a double exponential function gave a remarkably good fit to HPP relaxation curves (§2.7.3a). As the solution to the KK equations for OPP experiments in the presence of permeant solutes is a double exponential function (Eq. (2.9) in §2.2.2), it is suggested that the UL model be extended to allow for the possibility of a small amount of permeant solutes in an HPP experiment. This would involve solving the KK equations for an OPP experiment (with permeant solutes) with perturbation conditions for an HPP. It is also suggested that changes during the HPP perturbation be modelled explicitly. Apart from potentially fitting the data better and providing more accurate parameter estimation, these model extensions may help determine the reasons why L_p for HPP experiments appear to be higher than those for OPP experiments using the UL model. Or, the L_p values may end up being the same.

If it is possible to obtain an estimate of D inside the cell for the test solutes used in this thesis, then the UL model should be applied to fit experimental data using different D values inside the cell, for both HPP and OPP experiments. Alternatively, further numerical research could be done by treating D inside the cell as an additional free parameter which could be optimized in model fits using the UL model under different assumptions. For example, it could be assumed that the value of L_p obtained from OPP and HPP experiments are the same, or the parameters obtained from positive and negative pulses are the same, and the numerical model then run to optimize the value of D inside the cell. If the numerical model can fit the data well using a reasonable value of D for the ULi, then it could be concluded that uncertainty in D may be a key factor contributing to some of the patterns observed in this thesis.

Reducing the data resolution by selecting CPP data at regular time intervals rather than at every so many points should be examined (§4.3.2). It was found that RMS values were insensitive to small changes in the exchange time (§4.7). This may have been due to having relatively few points in the period of the exchange time, as a

consequence of culling the data. Selecting the data based at regular time intervals may give more points for the initial few seconds of the data, thus allowing for better optimization of the exchange time for fits to OPP experiments without bubbles. It may also give more points during the periods when the pressure is changing most rapidly, e.g. in the water phase and around the extremum during an OPP relaxation, which would be desirable and may enable the RMS method to fit the model to the data without weighting these points.

The UL model could also be extended to 3 dimensions by including axial flow and axial variation in the external concentration. Appropriate scaling could be used to develop an expression for how the thickness of the ULe changes with axial distance along the cell (see Pedley, 1983). This extension would allow for more accurate representation of the exchange function, and hence a more realistic consideration of the temporal impact of the osmotic perturbation on the cell. However, the added complexity will make the model very numerically intensive, and hence difficult to optimize for parameter estimation.

The model can be extended and applied to data from root pressure probe (RPP) experiments. Although the composite nature of the root has been considered (Steudle, 2000), the RPP apparatus and method of parameter estimation is similar to that for the CPP, and is based upon a model of the root as a two-compartment system (Steudle, 1994; Steudle, 1993; Steudle and Frensch, 1989). Estimated membrane parameters for roots may therefore also be in error due to ignoring effects of unstirred layers. Many roots have a similar length and diameter to *Chara* and should have an external UL of a similar thickness when placed in the pressure probe (Tyree *et al.* 2005). However, in roots the endodermis is usually considered to be the main barrier to transport, and therefore the entire region external to the endodermis (i.e. the cortex plus the region external to the root) may be considered an unstirred layer (Steudle and Frensch, 1989). Unstirred layers in roots may therefore have a more significant impact on the estimated membrane parameters for the root system (Tyree *et al.* 2005). In other studies on roots, the CPP and RPP have been used in conjunction to measure membrane parameters in the cortical cells and for the entire root (Frensch *et al.* 1996; Zhu and Steudle, 1991; Steudle and Jeschke, 1983), and for these studies effects of ULs on both the CPP and RPP data must be considered. The root system is a very

complex composite membrane system with elements in series and parallel, and conclusions about membrane parameters drawn from pressure probe experiments may be subject to alternative interpretations (Tyree, 2003).

The UL model may be extended to include active transport, following the theory of Kedem and Katchalsky (1963a), and the examples of Fiscus (1975) and Dalton *et al.* (1975) who developed models of water and solute transport through plant roots. The presence of active transport may contribute to observed nonlinear behaviour between the volume flux and pressure gradients (Fiscus, 1975), and similarly to ULs may cause the classically-estimated L_p to change with the external flow rate or applied pressure (see §3.1.2a). An active transport component can be introduced into the membrane transport equations in the CPP models, to assess what impact this has on the cell pressure dynamics.

The UL model may also be extended and applied to research on aquaporins (water channels), where membrane parameters estimated using CPP experiments are used to infer the pathways of water and solutes through the membrane, and the selectivity of water channels to water (Henzler and Steudle, 1995; Hertel and Steudle, 1997; Niemietz and Tyerman, 1997; Maurel, 1997; Zhang and Tyerman, 1999; Ye *et al.* 2004). In §2.7.3a of this thesis it was found that a double exponential function fit some HPP data better than the single exponential function from using the classical model. It would be interesting to apply the classical and UL models to experiments on *Chara* cells which involve the blocking of aquaporins, which may shed light on the relative hydraulic conductivities of the tonoplast and the plasma membrane (e.g. similar to CPP experiments carried out on wheat root cells in Zhang and Tyerman, 1999). However, research in this area requires further theoretical exploration on the applicability and implementation of the KK equations to composite membranes where elements are in parallel (Curry *et al.* 2001), before appropriate numerical models can be developed.

5.6 Final comments

This study has shown that a numerical process-based model aids in qualifying and quantifying the impact of ULs on relaxation curves and estimated parameters. Hertel and Steudle (1997) have commented that to help them reach conclusive results, they require that “effects of internal unstirred layers be eliminated” but “this, however, is hard to carry out experimentally”. A model which explicitly takes ULs into account during parameter estimation can take into account effects of ULs on the estimated parameters so that the estimated values are truly characteristic of the membrane. It is not only a useful tool, but a necessary tool for experimentalists attempting to determine the membrane parameters of cells.

This study has revealed the limitations of the classical and UL models, pointed out what experimental information is needed for more accurate parameter estimation, and the potential error in current estimates of membrane parameters where ULs are not properly taken into account. From the results of this study, it is suggested that the current parameter estimation process based on the classical model should be abandoned, and replaced by a model which incorporates ULs. Many equations and methods currently used to quantify or infer the impact of ULs on the estimated parameters are wrong and should also be abandoned.

Further experimental data is required for a thorough analysis of the effects of ULs on estimated membrane parameters, and for a more accurate estimation of membrane parameters and ULe thicknesses. At present, estimated parameters depend on experimental values such as the time the pressure perturbation is made, the shape and duration of the external exchange function, and whether one assumes that the UL thickness is the same for all experiments on the one cell. Further development of the UL model is also recommended, in conjunction with further knowledge of the physical processes occurring in the cells during CPP experiments.

With further development and application, the UL model developed in this study can be a valuable tool for shedding light on some observed membrane parameter behaviour, such as differences in estimated parameters between positive and negative pulses, between HPP and OPP experiments, and effects of external concentration on

estimated parameters. With further research a comprehensive analysis of the quantitative effects of ULs can be achieved.

6 References

Ames, W.F. (1977) *Numerical Methods for Partial Differential Equations*, New York: Academic Press.

Barry, P.H. and Diamond, J.M. (1984) Effects of unstirred layers on membrane phenomena. *Physiological Reviews* **64**, 763-872.

Bevington, P.R. (1969) *Data Reduction and Error Analysis for the Physical Sciences*, New York: McGraw-Hill Book Company.

Crank, J. (1975) *The Mathematics of Diffusion*, London: Oxford University Press.

Curry, M.R., Shachar-Hill, B. and Hill, A.E. (2001) Single water channels of aquaporin-I do not obey the Kedem-Katchalsky equations. *Journal of membrane biology* **181**, 115-123.

Dainty, J. (1963) Water relations of plant cells. *Advances in Botanical Research* **1** , 279-326.

Dainty, J. (1976) Water relations of plant cells. *Transport in plants II: Part A Cells, Encyclopedia of Plant Physiology* **2**, 12-35.

Dainty, J. and Ginzburg, B.Z. (1963) Irreversible thermodynamics and frictional models of membrane processes, with particular reference to the cell membrane. *Journal of Theoretical Biology* **5**, 256-265.

Dainty, J. and Ginzburg, B.Z. (1964a) The measurement of hydraulic conductivity (osmotic permeability to water) of internodal characean cells by means of transcellular osmosis. *Biochimica Et Biophysica Acta* **79**, 102-111.

Dainty, J. and Ginzburg, B.Z. (1964b) The permeability of the cell membranes of *Nitella Translucens* to urea, and the effect of high concentrations of sucrose on this permeability. *Biochimica Et Biophysica Acta* **79**, 112-121.

Dainty, J. and Ginzburg, B.Z. (1964c) The permeability of the protoplasts of *Chara Australis* and *Nitella Translucens* to methanol, ethanol and isopropanol. *Biochimica Et Biophysica Acta* **79**, 122-128.

Dainty, J. and Ginzburg, B.Z. (1964d) The reflection coefficient of plant cell membranes for certain solutes. *Biochimica Et Biophysica Acta* **79**, 129-137.

Dainty, J. and Hope, A.B. (1959) The water permeability of cells of *Chara australis*. *Australian Journal of Biological Sciences* **12**, 136-145.

Dalton, E.N., Raats, P.A.C. and Gardner, W.R. (1975) Simultaneous uptake of water and solutes by plant roots. *Agronomy Journal* **67**, 334-9.

Devireddy, R.V. (2005) Predicted permeability parmaeters of human ovarian tissue cells to various cryoprotectants and water. *Molecular reproduction and development* **70**, 333-343.

Dworecki, K., Kosztolowicz, T., Mrowczynski, S. and Wasik, S. (2000) Time evolution of near membrane layers. *European Journal of Physics E* **3**, 389-394.

Dworecki, K., Wasik, S. and Slezak, A. (2003) Temporal and spatial structure of the concentration boundary layers in a membrane system. *Physica A* **326**, 360-369.

Fiscus, E.L. (1975) The interaction between osmotic and pressure-induced water flow in plant roots. *Plant Physiology* **55**, 917-922.

Frensch, J., Hsiao, T.C. and Steudle, E. (1996) Water and solute transport along developing maize roots. *Planta* **198**, 348-355.

Heidecker, M., Mimietz, S., Wegner, L.-H. and Zimmermann, U. (2003) Structural peculiarities dominate the turgor pressure response of the marine alga *Valonia utricularis* upon osmotic challenges. *Journal of Membrane Biology* **192**, 123-139.

Henzler, T. and Steudle, E. (1995) Reversible closing of water channels in Chara internodes provides evidence for a composite transport model of the plasma membrane. *Journal of Experimental Botany* **46**, 199-209.

Henzler, T. and Steudle, E. (2000) Transport and metabolic degradation of hydrogen peroxide in *Chara corallina:* model calculations and measurements with the pressure probe suggest transport of H_2O_2 across water channnels. *Journal of Experimental Botany* **51**, 2053-2066.

Henzler, T., Ye, Q. and Steudle, E. (2004) Oxidative gating of water channels (aquaporins) in Chara by hydroxyl radicals. *Plant, Cell and Environment* **27**, 1184-1195.

Hertel, A. and Steudle, E. (1997) The function of water channels in *Chara:* The temperature dependence of water and solute flows provides evidence for composite membrane transport and for a slippage of small organic solutes across water channels. *Planta* **202**, 324-335.

Husken, D., Steudle, E. and Zimmermann, U. (1978) Pressure probe technique for measuring water relations of cells in higher plants. *Plant Physiology* **61**, 158-163.

Kargol, A. (2001) A mechanistic model of transport processes in porous membranes generated by osmotic and hydrostatic pressure. *Journal of Membrane Science* **191**, 61-69.

Kargol, A., Przestalski, M. and Kargol, M. (2005) A study of porous structure of cellular membranes in human erythrocytes. *Cryobiology* **50**, 332-337.

Kargol, A. (2000) Modified Kedem-Katchalsky equations and their applications. *Journal of Membrane Science* **174**, 43-53.

Kargol, M. and Kargol, A. (2003) Mechanistic equations for membrane substance transport and their identity with Kedem-Katchalsky equations. *Biophysical Chemistry* **103**, 117-127.

Kargol, M. and Kargol, A. (2000) Membrane transport generated by the osmotic and hydrostatic pressure. Correlation relation for parameters L, ref coeff, perm. *Journal of Biological Physics* **26**, 307-320.

Katchalsky, A. and Curran, P.F. (1967) *Nonequilibrium Thermodynamics in Biophysics*, Cambridge, Massachusetts: Harvard Uni Press.

Kedem, O. and Katchalsky, A. (1963a) Permeability of composite membranes, Part 1 - Electric current, volume flow and flow of solute through membranes. *Transactions of the Faraday Society* **59**, 1918-1930.

Kedem, O. and Katchalsky, A. (1963b) Permeability of composite membranes, Part 2 - Parallel Elements. *Transactions of the Faraday Society* **59**, 1931-1940.

Kedem, O. and Katchalsky, A. (1963c) Permeability of composite membranes, Part 3 - Series Array of Elements. *Transactions of the Faraday Society* **59**, 1941-1953.

Kedem, O. and Katchalsky, A. (1961) A physical interpretation of the phenomenological coefficients of membrane permeability. *Journal of General Physiology* **45**, 143-179.

Kiyosawa, K. and Tazawa, M. (1977) Hydraulic conductivity of tonoplast-free *Chara* cells. *Journal of Membrane Biology* **37**, 157-166.

Kiyosawa, K. and Tazawa, M. (1973) Rectification characteristics of *Nitella* membranes in respect to water permeability. *Protoplasma* **78**, 203-214.

Maurel, C. (1997) Aquaporins and water permeabiilty of plant membranes. *Annual Reviews of Plant Physiology and Plant Molecular Biology* **48**, 399-429.

Molz, F.J. and Ferrier, J.M. (1982) Mathematical treatment of water movement in plant cells and tissue: a review. *Plant, Cell and Environment* **5**, 191-206.

Murphy, R. (1999) A modified two-compartment model of the root: response to a pressure clamp. *Plant, Cell and Environment* **22**, 875-881.

Murphy, R. and Smith, J.A.C. (1998) Determination of cell water-relation paramters using the pressure probe: extended theory and practice of the pressure-clamp technique. *Plant, Cell and Environment* **21**, 637-657.

Niemietz, C.M. and Tyerman, S.D. (1997) Characterization of water channels in wheat root membrane vesicles. *Plant Physiology* **115**, 561-567.

Nitsche, J.M., Chang, H.-C., Weber, P.A. and Nicholson, B.J. (2004) A transient diffusion model yields unitary gap junctional permeabilities from images of cell-to-cell flurorescent dye transfer between *Xenopus* oocytes. *Biophysical Journal* **86**, 2058-2077.

Ortega, J.K.E. (1993) Pressure probe methods to measure transpiration in single cells . In: Smith, J.A.C. and Griffiths, H. (Eds.) *Water Deficits*, pp. 73-86. UK: Bios Scientific Publishers]

Pedley, T.J. (1983) Calculation of unstirred layer thickness in membrane transport experiments: a survey. *Quarterly Review of Biophysics* **16**, 115-150.

Peterson, C.A. (1988) Exodermal Casparian bands; their significance for ion uptake by roots. *Physiologia Plantarum* **72**, 2-04-208.

Raven, P.H., Evert, R.F. and Eichhorn, S.E. (1992) *Biology of Plants*, New York: Worth Publishers, Inc.

Steudle, E. (1993) Pressure probe techniques: basic principles and application to studies of water and solute relations at the cell, tissue, and organ level. In: Smith, J.A.C. and Griffiths, H. (Eds.) *Water Deficits: Plant Responses from Cell to Community*, pp. 5-36. U.K: Bios Scientific Publishers.

Steudle, E. (1997) Water transport across plant tissue: role of water channels. *Biology of the Cell* **89**, 259-273.

Steudle, E. (1994) Water transport across roots. *Plant and Soil* **167**, 79-90.

Steudle, E. (2000) Water uptake by plants roots: an integration of views. *Plant and Soil* **226**, 45-56.

Steudle, E., Ferrier, J.M. and Dainty, J. (1982) Measurements of the volumetric and transverse elastic extensibilities of *Chara corallina* internodes by combining the external force and pressure probe techniques. *Canadian Journal of Botany* **60**, 1503-1511.

Steudle, E. and Frensch, J. (1989) Osmotic responses of maize roots. *Planta* **177**, 281-295.

Steudle, E. and Jeschke, W.D. (1983) Water transport in barley roots. *Planta* **158**, 237-248.

Steudle, E., Oren, R. and Schulze, E.D. (1987) Water transport in maize roots. *Plant Physiology* **84**, 1220-1232.

Steudle, E. and Tyerman, S.D. (1983) Determination of permeability coefficients, reflection coefficients, and hydraulic conductivity of Chara corallina using the pressure probe: effects of solute concentration. *Journal of Membrane Biology* **75**, 85-96.

Steudle, E. and Zimmermann, U. (1974) Determination of the hydraulic conductivity and of reflection coefficients in *Nitella Flexilis* by means of direct cell-turgor pressure measurements. *Biochimica et Biophysica Acta* **332**, 399-412.

Steudle, E., Zimmermann, U. and Luttge, U. (1977) Effect of turgor pressure and cell size on the wall elasticity of plant cells. *Plant Physiology* **59**, 285-289.

Tomos, D. (2000) The plant cell pressure probe. *Biotechnology Letters* **22**, 437-442.

Tyerman, S. (1982) Water relations of seagrasses. Stationary volumetric elastic modulus and osmotic pressure of the leaf cells of *Halophila ovalis, Zostera capricorni*, and *Posidonia australis. Plant Physiology* **69**, 957-965.

Tyerman, S. and Steudle, E. (1984) Determination of solute permeability in *Chara* internodes by a turgor minimum method (effects of external pH). *Plant Physiology* **74**, 464-468.

Tyerman, S.D. and Steudle, E. (1982) Comparison between osmotic and hydrostatic water flows in a higher plant cell: determination of hydraulic conductivities and reflection coefficients in isolated epidermis of Tradescantia virginiana. *Australian Journal of Plant Physiology* **9**, 461-79.

Tyree, M.T. (2003) Hydraulic Properties of Roots. In: de Kroon, H. and Visser, E.J.W.E. (Eds.) *Root Ecology*, pp. 125-150. Berlin Heidelberg: Springer-Verlag.

Tyree, M.T., Fischer, R.R. and Dainty, J. (1974) A quantitative investigation of symplasmic transport in *Chara corallina* II. The symplasmic transport of chloride. *Canadian Journal of Botany* **52**, 1325-1334.

Tyree, M.T., Koh, S. and Sands, P. (2005) The determination of membrane transport parameters with the cell pressure probe: theory suggests that unstirred layers have significant impact. *Plant, Cell and Environment* **28**, 1475-1486.

Verkman, A.S. (2000) Water permeability measurement in living cells and complex tissues. *Journal of Membrane Biology* **173**, 73-87.

Wendler, S. and Zimmermann, U. (1985a) Compartment analysis of plant cells by means of turgor pressure relaxation: I. Theoretical considerations. *Journal of Membrane Biology* **85**, 121-132.

Wendler, S. and Zimmermann, U. (1985b) Compartment analysis of plant cells by means of turgor pressure relaxation: II. Experimental results on Chara corallina. *Journal of membrane biology* **85**, 133-142.

Ye, Q., Wiera, B. and Steudle, E. (2004) A cohesion/ tension mechanism explains the gating of water channels (aquaporins) in Chara internodes by high concentration. *Journal of Experimental Botany* **55**, 449-461.

Ye, Q., Yangmin, K. and Steudle, E. (2006) A re-examination of the minor role of unstirred layers during the measurement of transport coefficients of *Chara corallina* internodes with the cell pressure probe . *Plant, Cell and Environment* **29**, 964-980.

Young, H.D. (1962) *Statistical Treatment of Experimental Data*, U.S.A: McGraw-Hill Book Co.

Zemansky, M.W. and Dittman, R.H. (1981) *Heat and Thermodynamics*, Singapore: McGraw-Hill Book Co.

Zhang, W. and Tyerman, S.D. (1999) Inhibition of water channels by $HgCl_2$ in intact wheat root cells. *Plant Physiology* **120**, 849-857.

Zhu, G.L. and Steudle, E. (1991) Water transport across Maize roots - simultaneous measurement of flows at the cell and root level by double pressure probe technique. *Plant Physiology* **95**, 305-315.

Zimmermann, U. and Husken, D. (1979) Theoretical and experimental exclusion of errors in the determination of the elasticity and water transport parameters of plant cells by the pressure probe technique. *Plant Physiology* **64**, 18-24.

Zimmermann, U. and Steudle, E. (1974b) Hydraulic conductivity and volumetric elastic modulus in giant algal cells: pressure- and volume- dependence. In: Zimmermann, U. and Dainty, J. (Eds.) *Membrane Transport in Plants*, Berlin: Springer-Verlag.

Zimmermann, U. and Steudle, E. (1978) Physical aspects of water relations of plant cells. *Advances in Botanical Research* **6**, 45-117.

Zimmermann, U. and Steudle, E. (1974a) The pressure-dependence of the hydraulic conductivity, the membrane resistance and membrane potential during turgor pressure regulation in *Valonia utricularis*. *Journal of Membrane Biology* **16**, 331-352.

A Appendices

A.1 Fitting the data using curve characteristics

In §2.3 two methods of parameter estimation were applied with the classical model. One is the classical method, where the estimated membrane parameters L_p, p_s, and σ are obtained from curve characteristics of the data by applying appropriate analytical equations (§2.3.3). The other is the RMS method, where membrane parameters are estimated using least-squares optimization (§2.3.3).

With the UL model, where no analytical equations are available to solve for pressure vs. time, the RMS method was used to estimate the membrane parameters. However, the parameters can also be estimated using curve characteristics, where the relaxation curves are fit with the following criteria: t_m, P_m, and τ_s of the simulated OPP data must agree with t_m, P_m, *and* τ_s of the observed OPP data to within a certain degree of accuracy, and τ_w and P_E of the simulated HPP data must agree with τ_w and P_E of the observed HPP data to within a certain degree of accuracy. The logic behind this is that if the simulated curves begin at the same P value, reach the same maximum or minimum value, rise or fall at the same rate, and finish at the same P value as the observed curves, the simulated data should fit the observed data well.

The process of fitting involves finding empirical relationships between the membrane parameters and curve characteristics. This is done by using the model to generate data using known parameters and UL thicknesses, determining the curve characteristics from the data, and finding an equation which relates the membrane parameters and the curve characteristics. The parameters are then optimized so that the curve characteristics of the simulated and observed data agree. This method, like the RMS method, can fit the data very well and is the method of fitting used in Tyree *et al.* (2005).

A.2 Derivation of stability criteria for Euler's method for finite differences

The stability condition for a numerical solution of the diffusion equation using Euler's method is easiest to derive for cartesian coordinates, where the diffusion equation is:

$$\frac{\partial C}{\partial t} = D\frac{\partial^2 C}{\partial x^2} \quad . \tag{A.1}$$

In finite difference notation, Taylor's expansion of C as a function of t, to first order, gives:

$$C_j^{k+1} = C_j^k + \Delta t \frac{\partial C}{\partial t};$$

$$\frac{\partial C}{\partial t} = \frac{C_j^{k+1} - C_j^k}{\Delta t} \tag{A.2}$$

where j represents a spatial step and k represents a temporal step.

Taylor's expansion of C as a function of x, to second order, gives:

$$C_{j+1}^k = C_j^k + \Delta x \frac{\partial C}{\partial x} + \frac{\Delta x^2}{2}\frac{\partial^2 C}{\partial x^2}$$

$$C_{j-1}^k = C_j^k - \Delta x \frac{\partial C}{\partial x} + \frac{\Delta x^2}{2}\frac{\partial^2 C}{\partial x^2}$$

which upon addition results in

$$C_{j+1}^k + C_{j-1}^k = 2C_j^k + \Delta x^2 \frac{\partial^2 C}{\partial x^2}$$

$$\frac{\partial^2 C}{\partial x^2} = \frac{C_{j+1}^k - 2C_j^k + C_{j-1}^k}{\Delta x^2}. \tag{A.3}$$

Putting (A.2) and (A.3) into (A.1) gives

$$\frac{C_j^{k+1} - C_j^k}{\Delta t} = D\frac{C_{j+1}^k - 2C_j^k + C_{j-1}^k}{\Delta x^2}$$

$$C_j^{k+1} = C_j^k + \alpha(C_{j+1}^k - 2C_j^k + C_{j-1}^k) \quad , \qquad \text{(A.4)}$$

where $\alpha = \dfrac{D\Delta t}{\Delta x^2}$.

(A.4) is Euler's finite-difference method for the solution of the diffusion equation. Using a Fourier stability analysis, an initial condition is represented by the sinusoid

$$C_j^k = A^k e^{ij\Delta x}$$

where *A* is some function of *t*, and *i* is the complex number $\sqrt{-1}$.

Substituting into (A.4) gives

$$\begin{aligned} A^{k+1}e^{ij\Delta x} &= A^k e^{ij\Delta x} + \alpha A^k (e^{i(j+1)\Delta x} - 2e^{ij\Delta x} + e^{i(j-1)\Delta x}) \\ A^{k+1} &= A^k[1 + \alpha(e^{i\Delta x} + e^{-i\Delta x} - 2)] \\ &= A^k[1 + \alpha(2\cos\Delta x - 2)] \ . \end{aligned}$$

For stable convergence to a solution, it is required that

$$\left|\frac{A^{k+1}}{A^k}\right| < 1$$

$$\Rightarrow \left|1 + 2\alpha(\cos\Delta x - 1)\right| < 1$$
$$\Rightarrow \left|1 - 4\alpha\sin^2(\Delta x/2)\right| < 1$$

using a trigonometric identity. We then have

$$-1 < 1 - 4\alpha\sin^2(\Delta x/2) < 1$$
$$\Rightarrow 4\alpha\sin^2(\Delta x/2) < 2$$
$$\Rightarrow \alpha < 1/2.$$

$$\therefore \frac{D\Delta t}{\Delta x^2} < 1/2 \ .$$

A.3 Derivation of permeability equation (for cylindrical geometry)

Fick's second law for the steady state diffusion equation in cylindrical coordinates,

$$\frac{\partial}{\partial r}\left(rD\frac{\partial C}{\partial r}\right) = 0\,, \tag{A.5}$$

has the solution

$$C = A + B \ln r\ , \tag{A.6}$$

where A and B are constants, C is the solute concentration, r is the radius from the center of the cell, and D is the diffusivity coefficient (Crank, 1975).

Let the system by comprised of 2 unstirred layer (UL) regions separated by a cell membrane (assumed to have an infinitesimal thickness) located at $r=R$. The boundary of the inner UL is located at $r=a$, where $a<R$, and the boundary of the outer UL is located at $r=b$, where $b>R$. Region 1 is the area inside the cell for which $0<r<R$, and region 2 is the area outside the cell for which $r>R$. C_1 is the concentration in region 1, and C_2 is the concentration in region 2.

From Eq. (A.6), we have

$$\frac{\partial C}{\partial r} = \frac{B}{r}\,.$$

From Fick's first law for diffusion (Eq. (3.1)), it follows that for the solute flux J_s:

$$J_s(r) = -D\frac{\partial C}{\partial r} = -D\frac{B}{r}\,. \tag{A.7}$$

$J_s(R)$ at the membrane is also given by the expressions

$$\begin{aligned} J_s(R) &= p_m(C_1(R) - C_2(R)) \\ &= p_T(C_1(a) - C_2(b)) \end{aligned} \tag{A.8}$$

where p_m is the permeability of the membrane, and p_T is the measured permeability based on using the bulk concentration values. From Eq. (A.7) & Eq. (A.8),

$$\frac{1}{p_T} = \frac{C_1(a) - C_2(b)}{J_s(R)} = -C_1(a)\frac{R}{D_1B_1} + C_2(b)\frac{R}{D_2B_2} \tag{A.9}$$

$$\frac{1}{p_m} = \frac{C_1(R) - C_2(R)}{J_s(R)} = -C_1(R)\frac{R}{D_1B_1} + C_2(R)\frac{R}{D_2B_2}. \tag{A.10}$$

Combining Eq. (A.9) and Eq. (A.10), and using Eq. (A.6),

$$\begin{aligned}\frac{1}{p_T} - \frac{1}{p_m} &= \frac{1}{J_s(R)}[C_1(a) - C_2(b) - C_1(R) + C_2(R)] \\ &= -\frac{R}{D_1B_1}(A_1 + B_1\ln a - A_1 - B_1\ln R) + \frac{R}{D_2B_2}(A_2 + B_2\ln b - A_2 - B_2\ln R) \\ &= -\frac{R}{D_1}(\ln a - \ln R) + -\frac{R}{D_2}(\ln b - \ln R)\end{aligned}$$

$$\therefore \frac{1}{p_T} = \frac{1}{p_m} + \frac{R}{D_1}\ln\left(\frac{R}{a}\right) + \frac{R}{D_2}\ln\left(\frac{b}{R}\right) . \tag{A.11}$$

This equation expresses the total permeability across the system in terms of the membrane permeability and the permeability in the ULs. If $D_1 = D_2$, Eq. (A.11) reduces to

$$\frac{1}{p_T} = \frac{1}{p_m} + \frac{R}{D}\ln\left(\frac{b}{a}\right) . \tag{A.12}$$

Eq. (A.12) applies for steady-state only. For non-steady state *A* and *B* (determined from the boundary conditions at $r=a$ and $r=b$) are not constants, since the boundary conditions are: $C=f(t)$ at $r=a$ and $C=C_0$ at $r=b$ where C_0 is a constant. Eq. (A.12) reduces to Eq. (A.15) for sufficiently thin ULs.

A.4 Operational definition of the UL thickness

The view that the UL thickness changes during diffusion probably arises from an incorrect usage and interpretation of a definition of the UL thickness given in the literature. For planar geometry, an *operational* definition of the UL thickness δ is given by (Barry and Diamond, 1984; Pedley, 1983; Dainty, 1963):

$$\frac{C_b - C_m}{\delta} = \left.\frac{\partial C}{\partial r}\right|_m , \tag{A.13}$$

where C_b is the concentration in the bulk solution, C_m the concentration at the membrane, and r the radius from the center of the cell. Eq. (A.13) estimates δ based on the concentration gradient at the membrane (see Pedley, 1983), and gives a linear concentration distribution in the ULs. Fig. A.1 shows a typical diagram given in the literature of how ULs affect the concentration difference at the membrane, which also shows how δ is defined by Eq. (A.13).

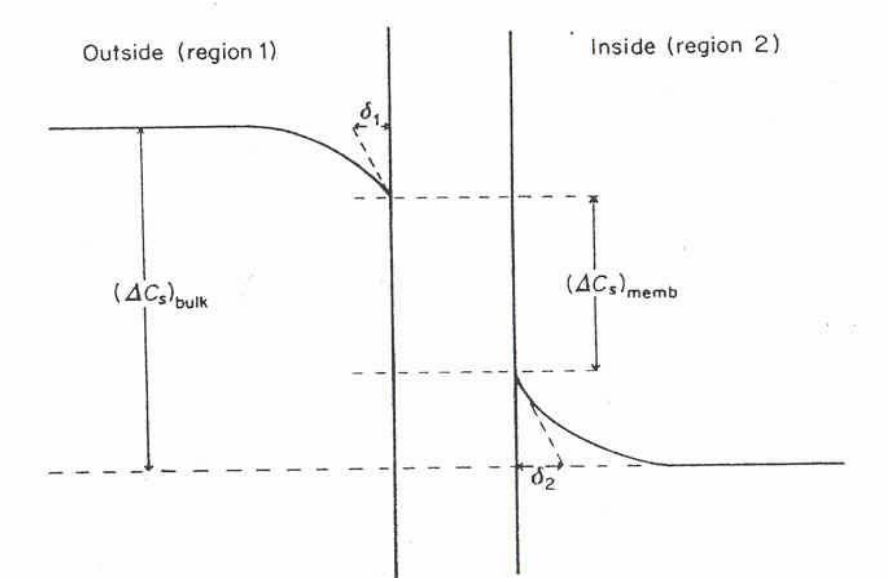

Fig A.1 Showing how ULs are expected to affect the concentration difference at membrane, and how δ is often defined (Dainty, 1963).

The definition of δ by Eq. (A.13) may be valid for a system in steady-state. However, if Eq. (A.13) is applied to a system in non-steady state, as diffusion proceeds the concentration gradient at the membrane decreases, and correspondingly δ will change. However, an unstirred layer does not change thickness as diffusion proceeds. It is important to realise that Eq. (A.13) and Fig. A.1 do not reflect the actual behaviour of ULs. As Dainty (1963) points out, δ given by Eq. (A.13) is "not the actual thickness but rather an operational thickness. "

Incidentally, δ as defined by Eq. (A.13) can be related to the permeability p_δ in the UL by:

$$J_s(r) = D\left.\frac{\partial C}{\partial r}\right|_m = \frac{D(C_b - C_m)}{\delta}$$

$$\Rightarrow p_\delta = \frac{D}{\delta} \quad , \tag{A.14}$$

since $J_s(r) = p_\delta(C_b - C_m)$, where J_s is the solute flux in the UL due to diffusion only, and D = coefficient of diffusivity of the solute in the UL (Dainty, 1963; Barry and Diamond, 1984). Eq. (A.14) suggests that the UL may be considered to be a type of membrane with a permeability inversely proportional to the UL thickness (Dainty, 1963), and leads to the permeability equation based on Kirchoff's law of resistances in series for the planar case:

$$\frac{1}{p_T} = \frac{1}{p_m} + \frac{\delta_1}{D_1} + \frac{\delta_2}{D_2} \tag{A.15}$$

(Dainty, 1963).

Clearly, Eq. (A.15) only holds if the system is in steady state, so that the concentration gradient in Eq. (A.5) is a constant and the concentration profiles are linear. Eq. (A.15), like Eqs. (A.13) and (A.14), does not reflect the actual behaviour of ULs or give information on the actual UL thickness. This is a commonly used unstirred layer model, which, as Pedley (1983) notes, "is not to be taken literally."

A.5 List of acronyms and symbols

Table A.1 List of acronyms

Acronym	Meaning
CPP	cell pressure probe
HPP	hydrostatic pressure pulse
OPP	osmotic pressure pulse
UL	unstirred layer
ULi	internal unstirred layer
ULe	external unstirred layer
APW	artificial pond water
KK	Kedem-Katchalsky
RMS	root mean square
SE	standard error
3WS	3-way stopcock
EtOH	ethanol

Table A.2 List of frequently used symbols

Symbol	Units	Definition
J_v	m s^{-1}	volume flux density
J_s	mol m^{-2} s^{-1}	solute flux density
J	mol m^{-2} s^{-1}	radial flux
t	s	time
v	mol m^{-2} sec^{-1}	radial flow velocity
P	MPa	hydrostatic (turgor) pressure of cell
P_E	MPa	equilibrium pressure
π	MPa	osmotic pressure
π_i	MPa	osmotic pressure due to impermeable solutes
π_s	MPa	osmotic pressure due to permeable solutes
n_s	mol (M)	number of mol of permeable solutes in cell
C	mol m^{-3}	solute concentration
C_i	mol m^{-3}	concentration of impermeable solutes in cell
C_s	mol m^{-3}	concentration of permeable solutes in cell
C_{ie}	mol m^{-3}	concentration of impermeable solutes in bulk solution
C_{se}	mol m^{-3}	concentration of impermeable solutes in bulk solution

$\overline{C_s}$	mol m^{-3}	average concentration of permeable solutes across membrane
L_p	m s^{-1} MPa^{-1}	hydraulic conductivity of membrane
σ	dimensionless	reflection coefficient of membrane
p_s	m s^{-1}	solute permeability coefficient of membrane
R_g	MPa mol^{-1} K^{-1}	universal (ideal) gas constant
T	K	absolute temperature
ε	MPa	bulk elastic modulus
D	m^2 s^{-1}	diffusion coefficient
D_{ULi} (or D_1)	m^2 s^{-1}	diffusion coefficient inside cell
D_{ULe} (or D_2)	m^2 s^{-1}	diffusion coefficient outside cell
ξ	dimensionless	parameter ratio
p_m	m s^{-1}	true solute permeability of membrane
p_T	m s^{-1}	measured (total) solute permeability of membrane, which includes effects of ULs
A	m^2	surface area of cell
V	m^3	cell volume
L	m	cell length
d	m	cell diameter
r	m	radial distance from center of cell
R	m	cell radius
a	m	radial distance to boundary of internal unstirred layer
b	m	radial distance to boundary of external unstirred layer
δ_{UL}	m	unstirred layer thickness
δ_{ULi}	m	thickness of internal unstirred layer
δ_{ULe}	m	thickness of external unstirred layer
t_0	s	time at which perturbation pulse occurs
P_0	MPa	initial equilibrium pressure in cell
V_0	m^3	initial cell volume at equilibrium
A_0	m^2	initial cell surface area at equilibrium
π_{i0}	MPa	initial cell osmotic pressure (due to impermeable solutes) at equilibrium
C_0	mol m^{-3}	solute concentration in bulk solution
P_1	MPa	cell pressure at t_0 in an HPP
π_{i1}	MPa	osmotic pressure inside the cell (due to impermeable solutes) at t_0 in an HPP
t_P	s	time at which cell pressure starts changing
t_D	s	time-delay
t_R	s	ramp time
τ_w	s	halftime of pressure relaxation in an HPP or in the water phase of an OPP
τ_s	s	halftime of solute phase
k_s	MPa	rate constant for solute phase
k_w	s	rate constant for water phase

P_{min}	MPa	minimum value of P
P_{max}	MPa	maximum value of P
P_m	MPa	P_{min} or P_{max}
t_{min}	s	value for t at which P_{min} is reached
t_{max}	s	value for t at which P_{max} is reached
t_m	s	t_{min} or t_{max}